

ISSN: 2067-3809



ACTA TECHNICA CORVINIENSIS – Bulletin of Engineering

Tome XIII [2020]
Fascicule 3
[July–September]



Editura POLITEHNICA

ACTA TECHNICA CORVINIENSIS

Bulletin of Engineering



Edited by:

UNIVERSITY POLITEHNICA TIMISOARA



with kindly supported by:

THE GENERAL ASSOCIATION OF ROMANIAN ENGINEERS (AGIR)
– branch of HUNEDOARA



Editor / Technical preparation / Cover design:

Assoc. Prof. Eng. KISS Imre, PhD.
UNIVERSITY POLITEHNICA TIMISOARA,
FACULTY OF ENGINEERING HUNEDOARA

Commenced publication year:
2008

ACTA TECHNICA CORVINIENSIS

Bulletin of Engineering

ASSOCIATE EDITORS and REGIONAL COLLABORATORS

MANAGER & CHAIRMAN

ROMANIA  **Imre KISS**, University Politehnica TIMISOARA, Faculty of Engineering HUNEDOARA, Department of Engineering & Management, General Association of Romanian Engineers (AGIR) – branch HUNEDOARA

EDITORS from:

ROMANIA 
Dragoș UȚU, University Politehnica TIMIȘOARA – TIMIȘOARA
Vasile ALEXA, University Politehnica TIMIȘOARA – HUNEDOARA
Sorin Aurel RAȚIU, University Politehnica TIMIȘOARA – HUNEDOARA
Vasile George CIOATĂ, University Politehnica TIMIȘOARA – HUNEDOARA
Simona DZIȚAC, University of Oradea – ORADEA
Valentin VLĂDUȚ, Institute of Research-Development for Machines & Installations – BUCUREȘTI
Dan Ludovic LEMLE, University Politehnica TIMIȘOARA – HUNEDOARA
Emanoil LINUL, University Politehnica TIMIȘOARA – TIMIȘOARA
Virgil STOICA, University Politehnica TIMIȘOARA – TIMIȘOARA
Sorin Ștefan BIRIȘ, University Politehnica BUCUREȘTI – BUCUREȘTI
Mihai G. MATACHE, Institute of Research-Development for Machines & Installations – BUCUREȘTI


REGIONAL EDITORS from:

SLOVAKIA 
Juraj ŠPALEK, University of ŽILINA – ŽILINA
Peter KOŠTÁL, Slovak University of Technology in BRATISLAVA – TRNAVA
Tibor KRENICKÝ, Technical University of KOŠICE – PREŠOV
Beata HRICOVÁ, Technical University of KOŠICE – KOŠICE
Peter KRIŽAN, Slovak University of Technology in BRATISLAVA – BRATISLAVA

HUNGARY 
Tamás HARTVÁNYI, Széchenyi István University – GYŐR
Arpád FERENCZ, Pallasz Athéné University – KECSKEMÉT
József SÁROSI, University of SZEGED – SZEGED
Attila BARCZI, Szent István University – GÖDÖLLŐ
György KOVÁCS, University of MISKOLC – MISKOLC
Zsolt Csaba JOHANYÁK, John von Neumann University – KECSKEMÉT
Gergely DEZSÓ, College of NYÍREGYHÁZA – NYÍREGYHÁZA
Krisztián LAMÁR, Óbuda University BUDAPEST – BUDAPEST
Loránt KOVÁCS, Pallasz Athéné University – KECSKEMÉT
Valeria NAGY, University of SZEGED – SZEGED
Sándor BESZÉDES, University of SZEGED – SZEGED
Csaba Imre HENCZ, Széchenyi István University – GYŐR
Zoltán András NAGY, Széchenyi István University – GYŐR
László GOGOLÁK, University of SZEGED – SZEGED

SERBIA 
Zoran ANIŠIĆ, University of NOVI SAD – NOVI SAD
Milan RACKOV, University of NOVI SAD – NOVI SAD
Igor FÜRSTNER, SUBOTICA Tech – SUBOTICA
Eleonora DESNICA, University of NOVI SAD – ZRENJANIN
Blaža STOJANOVIĆ, University of KRAGUJEVAC – KRAGUJEVAC
Aleksander MILTENOVIC, University of NIŠ – NIŠ
Milan BANIC, University of NIŠ – NIŠ
Slobodan STEFANOVIĆ, Graduate School of Applied Professional Studies – VRANJE
Sinisa BIKIĆ, University of NOVI SAD – NOVI SAD
Masa BUKUROV, University of NOVI SAD – NOVI SAD
Ana LANGOVIC MILICEVIC, University of KRAGUJEVAC – VRNJAČKA BANJA
Imre NEMEDI, SUBOTICA Tech – SUBOTICA
Živko PAVLOVIĆ, University of NOVI SAD – NOVI SAD

CROATIA 
Gordana BARIC, University of ZAGREB – ZAGREB
Goran DUKIC, University of ZAGREB – ZAGREB

BULGARIA 
Krasimir Ivanov TUJAROV, “Angel Kanchev” University of ROUSSE – ROUSSE
Ognyan ALIPIEV, “Angel Kanchev” University of ROUSSE – ROUSSE
Ivanka ZHELEVA, “Angel Kanchev” University of ROUSSE – ROUSSE
Atanas ATANASOV, “Angel Kanchev” University of ROUSSE – ROUSSE

BOSNIA &
HERZEGOVINA



Tihomir LATINOVIĆ, University in BANJA LUKA – BANJA LUKA
Sabahudin JASAREVIC, University of ZENICA – ZENICA
Šefket GOLETIĆ, University of ZENICA – ZENICA

POLAND



Jarosław ZUBRZYCKI, LUBLIN University of Technology – LUBLIN
Maciej BIELECKI, Technical University of LODZ – LODZ
Bożena GAJDZIK, The Silesian University of Technology – KATOWICE

TURKEY



Önder KABAŞ, Akdeniz University – KONYAAALTI/Antalya

CHINA



Yiwen JIANG, Military Economic Academy – WUHAN

SPAIN



César GARCÍA HERNÁNDEZ, University of ZARAGOZA – ZARAGOZA

GREECE



Apostolos TSAGARIS, Alexander Technological Educational Institute of THESSALONIKI – THESSALONIKI
Panagiotis KYRATSI, Western Macedonia University of Applied Sciences – KOZANI



The Editor and editorial board members do not receive any remuneration. These positions are voluntary. The members of the Editorial Board may serve as scientific reviewers.

We are very pleased to inform that our journal **ACTA TECHNICA CORVINIENSIS – Bulletin of Engineering** is going to complete its ten years of publication successfully. In a very short period it has acquired global presence and scholars from all over the world have taken it with great enthusiasm. We are extremely grateful and heartily acknowledge the kind of support and encouragement from you.

ACTA TECHNICA CORVINIENSIS – Bulletin of Engineering seeking qualified researchers as members of the editorial team. Like our other journals, **ACTA TECHNICA CORVINIENSIS – Bulletin of Engineering** will serve as a great resource for researchers and students across the globe. We ask you to support this initiative by joining our editorial team. If you are interested in serving as a member of the editorial team, kindly send us your resume to redactie@fih.upt.ro.



ACTA TECHNICA CORVINIENSIS – Bulletin of Engineering
ISSN: 2067-3809
copyright © University POLITEHNICA Timisoara,
Faculty of Engineering Hunedoara,
5, Revolutiei, 331128, Hunedoara, ROMANIA
<http://acta.fih.upt.ro>

INTERNATIONAL SCIENTIFIC COMMITTEE MEMBERS and SCIENTIFIC REVIEWERS


MANAGER & CHAIRMAN

ROMANIA  **Imre KISS**, University Politehnica TIMISOARA, Faculty of Engineering HUNEDOARA, Department of Engineering & Management, General Association of Romanian Engineers (AGIR) – branch HUNEDOARA

INTERNATIONAL SCIENTIFIC COMMITTEE MEMBERS & SCIENTIFIC REVIEWERS from:

ROMANIA 
Viorel–Aurel ȘERBAN, University Politehnica TIMIȘOARA – TIMIȘOARA
Teodor HEPUȚ, University Politehnica TIMIȘOARA – HUNEDOARA
Mircea BEJAN, Technical University of CLUJ-NAPOCA – CLUJ-NAPOCA
Liviu MIHON, University Politehnica TIMIȘOARA – TIMIȘOARA
Ilare BORDEAȘU, University Politehnica TIMIȘOARA – TIMIȘOARA
Liviu MARȘAVIA, University Politehnica TIMIȘOARA – TIMIȘOARA
Ioan VIDA-SIMITI, Technical University of CLUJ-NAPOCA – CLUJ-NAPOCA
Csaba GYENGE, Technical University of CLUJ-NAPOCA – CLUJ-NAPOCA
Sava IANICI, “Eftimie Murgu” University of REȘIȚA – REȘIȚA
Ioan SZÁVA, “Transilvania” University of BRASOV – BRASOV
Sorin VLASE, “Transilvania” University of BRASOV – BRASOV
Horatiu TEODORESCU DRĂGHICESCU, “Transilvania” University of BRASOV – BRASOV
Maria Luminița SCUTARU, “Transilvania” University of BRASOV – BRASOV
Iulian RIPOȘAN, University Politehnica BUCUREȘTI – BUCUREȘTI
Ioan DZITAC, Agora University of ORADEA – ORADEA
Carmen ALIC, University Politehnica TIMIȘOARA – HUNEDOARA

SLOVAKIA 
Štefan NIZNIK, Technical University of KOŠICE – KOŠICE
Karol VELIŠEK, Slovak University of Technology BRATISLAVA – TRNAVA
Juraj ŠPALEK, University of ŽILINA – ŽILINA
Ervin LUMNITZER, Technical University of KOŠICE – KOŠICE
Miroslav BADIDA, Technical University of KOŠICE – KOŠICE
Milan DADO, University of ŽILINA – ŽILINA
Lubomir ŠOOŠ, Slovak University of Technology in BRATISLAVA – BRATISLAVA
Miroslav VEREŠ, Slovak University of Technology in BRATISLAVA – BRATISLAVA
Milan SAGA, University of ŽILINA – ŽILINA
Imrich KISS, Institute of Economic & Environmental Security – KOŠICE
Vladimir MODRAK, Technical University of KOSICE – PRESOV
Michal HAVRILA, Technical University of KOSICE – PRESOV

CROATIA 
Dražan KOZAK, Josip Juraj Strossmayer University of OSIJEK – SLAVONKI BROD
Predrag COSIC, University of ZAGREB – ZAGREB
Milan KLJAJIN, Josip Juraj Strossmayer University of OSIJEK – SLAVONKI BROD
Miroslav CAR, University of ZAGREB – ZAGREB
Antun STOIC, Josip Juraj Strossmayer University of OSIJEK – SLAVONKI BROD
Ivo ALFIREVIC, University of ZAGREB – ZAGREB

HUNGARY 
Imre DEKÁNY, University of SZEGED – SZEGED
Béla ILLÉS, University of MISKOLC – MISKOLC
Imre RUDAS, Óbuda University of BUDAPEST – BUDAPEST
Tamás KISS, University of SZEGED – SZEGED
Cecilia HODÚR, University of SZEGED – SZEGED
Arpád FERENCZ, Pallasz Athéné University – KECSKEMÉT
Imre TIMÁR, University of Pannonia – VESZPRÉM
Kristóf KOVÁCS, University of Pannonia – VESZPRÉM
Károly JÁRMAI, University of MISKOLC – MISKOLC
Gyula MESTER, University of SZEGED – SZEGED
Ádám DÖBRÖCZÖNI, University of MISKOLC – MISKOLC
György SZEIDL, University of MISKOLC – MISKOLC
Miklós TISZA, University of MISKOLC – MISKOLC
Attila BARCZI, Szent István University – GÖDÖLLŐ
István BIRÓ, University of SZEGED – SZEGED
József GÁL, University of SZEGED – SZEGED
Ferenc FARKAS, University of SZEGED – SZEGED
Géza HUSI, University of DEBRECEN – DEBRECEN
Ferenc SZIGETI, College of NYÍREGYHÁZA – NYÍREGYHÁZA

GREECE Nicolaos VAXEVANIDIS, University of THESSALY – VOLOS



BULGARIA Kliment Blagoev HADJOV, University of Chemical Technology and Metallurgy – SOFIA
Nikolay MIHAILOV, “Anghel Kanchev” University of ROUSSE – ROUSSE
Krassimir GEORGIEV, Institute of Mechanics, Bulgarian Academy of Sciences – SOFIA
Stefan STEFANOV, University of Food Technologies – PLOVDIV



SERBIA Sinisa KUZMANOVIC, University of NOVI SAD – NOVI SAD
Zoran ANIŠIĆ, University of NOVI SAD – NOVI SAD
Mirjana VOJINOVIĆ MILORADOV, University of NOVI SAD – NOVI SAD
Miroslav PLANČAK, University of NOVI SAD – NOVI SAD
Milosav GEORGIJEVIC, University of NOVI SAD – NOVI SAD
Vojislav MILTENOVIC, University of NIŠ – NIŠ
Miomir JOVANOVIC, University of NIŠ – NIŠ
Vidosav MAJSTOROVIC, University of BELGRADE – BELGRAD
Predrag DAŠIĆ, Production Engineering and Computer Science – TRSTENIK
Lidija MANČIĆ, Institute of Technical Sciences of Serbian Academy of Sciences & Arts – BELGRAD



ITALY Alessandro GASPARETTO, University of UDINE – UDINE
Alessandro RUGGIERO, University of SALERNO– SALERNO
Adolfo SENATORE, University of SALERNO– SALERNO
Enrico LORENZINI, University of BOLOGNA – BOLOGNA



BOSNIA & HERZEGOVINA Tihomir LATINOVIC, University of BANJA LUKA – BANJA LUKA
Safet BRDAREVIĆ, University of ZENICA – ZENICA
Ranko ANTUNOVIC, University of EAST SARAJEVO – East SARAJEVO
Isak KARABEGOVIĆ, University of BIHAĆ – BIHAĆ
Zorana TANASIC, University of BANJA LUKA – BANJA LUKA



MACEDONIA Valentina GECEVSKA, University “St. Cyril and Methodius” SKOPJE – SKOPJE
Zoran PANDILOV, University “St. Cyril and Methodius” SKOPJE – SKOPJE
Robert MINOVSKI, University “St. Cyril and Methodius” SKOPJE – SKOPJE



PORTUGAL João Paulo DAVIM, University of AVEIRO – AVEIRO
Paulo BÁRTOLO, Polytechnique Institute – LEIRIA
José MENDES MACHADO, University of MINHO – GUIMARÃES



SLOVENIA Janez GRUM, University of LJUBLJANA – LJUBLJANA
Štefan BOJNEC, University of Primorska – KOPER



POLAND Leszek DOBRZANSKI, Silesian University of Technology – GLIWICE
Stanisław LEGUTKO, Polytechnic University – POZNAN
Andrzej WYCISLIK, Silesian University of Technology – KATOWICE
Antoni ŚWIĆ, University of Technology – LUBLIN
Marian Marek JANCZAREK, University of Technology – LUBLIN
Michał WIECZOROWSKI, POZNAN University of Technology – POZNAN
Jarosław ZUBRZYCKI, LUBLIN University of Technology – LUBLIN
Aleksander SŁADKOWSKI, Silesian University of Technology – KATOWICE



AUSTRIA Branko KATALINIC, VIENNA University of Technology – VIENNA



ARGENTINA Gregorio PERICHINSKY, University of BUENOS AIRES – BUENOS AIRES
Atilio GALLITELLI, Institute of Technology – BUENOS AIRES
Carlos F. MOSQUERA, University of BUENOS AIRES – BUENOS AIRES
Elizabeth Myriam JIMENEZ REY, University of BUENOS AIRES – BUENOS AIRES
Arturo Carlos SERVETTO, University of BUENOS AIRES – BUENOS AIRES



SPAIN Patricio FRANCO, Universidad Politecnica of CARTAGENA – CARTAGENA
Luis Norberto LOPEZ De LACALLE, University of Basque Country – BILBAO
Aitzol Lamikiz MENTXAKA, University of Basque Country – BILBAO
Carolina Senabre BLANES, Universidad Miguel Hernández – ELCHE





CUBA Norge I. COELLO MACHADO, Universidad Central “Marta Abreu” LAS VILLAS – SANTA CLARA
José Roberto Marty DELGADO, Universidad Central “Marta Abreu” LAS VILLAS – SANTA CLARA



INDIA Sugata SANYAL, Tata Consultancy Services – MUMBAI
Siby ABRAHAM, University of MUMBAI – MUMBAI



TURKEY Ali Naci CELIK, Abant Izzet Baysal University – BOLU
Önder KABAŞ, Akdeniz University –KONYAAALI/Antalya



ISRAEL Abraham TAL, University TEL-AVIV, Space & Remote Sensing Division – TEL-AVIV
Amnon EINAV, University TEL-AVIV, Space & Remote Sensing Division – TEL-AVIV



LITHUANIA Egidijus ŠARAUSKIS, Aleksandras Stulginskis University – KAUNAS
Zita KRIAUCIŪNIENĖ, Experimental Station of Aleksandras Stulginskis University – KAUNAS



FINLAND Antti Samuli KORHONEN, University of Technology – HELSINKI
Pentti KARJALAINEN, University of OULU – OULU



NORWAY Trygve THOMESSEN, Norwegian University of Science and Technology – TRONDHEIM
Gábor SZIEBIG, Narvik University College – NARVIK
Terje Kristofer LIEN, Norwegian University of Science and Technology – TRONDHEIM
Bjoern SOLVANG, Narvik University College – NARVIK



UKRAINE Sergiy G. DZHURA, Donetsk National Technical University – DONETSK
Alexander N. MIKHAILOV, DONETSK National Technical University – DONETSK
Heorhiy SULYM, Ivan Franko National University of LVIV – LVIV
Yevhen CHAPLYA, Ukrainian National Academy of Sciences – LVIV
Vitalii IVANOV, Sumy State University – SUMY



SWEEDEN Ingvar L. SVENSSON, JÖNKÖPING University – JÖNKÖPING



USA David HUI, University of NEW ORLEANS – NEW ORLEANS



The Scientific Committee members and Reviewers do not receive any remuneration. These positions are voluntary. We are extremely grateful and heartily acknowledge the kind of support and encouragement from all contributors and all collaborators!

ACTA TECHNICA CORVINIENSIS – Bulletin of Engineering is dedicated to publishing material of the highest engineering interest, and to this end we have assembled a distinguished Editorial Board and Scientific Committee of academics, professors and researchers.

ACTA TECHNICA CORVINIENSIS – Bulletin of Engineering publishes invited review papers covering the full spectrum of engineering. The reviews, both experimental and theoretical, provide general background information as well as a critical assessment on topics in a state of flux. We are primarily interested in those contributions which bring new insights, and papers will be selected on the basis of the importance of the new knowledge they provide.

ACTA TECHNICA CORVINIENSIS – Bulletin of Engineering encourages the submission of comments on papers published particularly in our journal. The journal publishes articles focused on topics of current interest within the scope of the journal and coordinated by invited guest editors. Interested authors are invited to contact one of the Editors for further details.

ACTA TECHNICA CORVINIENSIS – Bulletin of Engineering accept for publication unpublished manuscripts on the understanding that the same manuscript is not under simultaneous consideration of other journals. Publication of a part of the data as the abstract of conference proceedings is exempted.

Manuscripts submitted (original articles, technical notes, brief communications and case studies) will be subject to peer review by the members of the Editorial Board or by qualified outside reviewers. Only papers of high scientific quality will be accepted for publication. Manuscripts are accepted for review only when they report unpublished work that is not being considered for publication elsewhere.

The evaluated paper may be recommended for:

- **Acceptance without any changes** – in that case the authors will be asked to send the paper electronically in the required .doc format according to authors' instructions;
- **Acceptance with minor changes** – if the authors follow the conditions imposed by referees the paper will be sent in the required .doc format;
- **Acceptance with major changes** – if the authors follow completely the conditions imposed by referees the paper will be sent in the required .doc format;
- **Rejection** – in that case the reasons for rejection will be transmitted to authors along with some suggestions for future improvements (if that will be considered necessary).

The manuscript accepted for publication will be published in the next issue of **ACTA TECHNICA CORVINIENSIS – Bulletin of Engineering** after the acceptance date.

All rights are reserved by **ACTA TECHNICA CORVINIENSIS – Bulletin of Engineering**. The publication, reproduction or dissemination of the published paper is permitted only be written consent of one of the Managing Editors.

All the authors and the corresponding author in particular take the responsibility to ensure that the text of the article does not contain portions copied from any other published material which amounts to plagiarism. We also request the authors to familiarize themselves with the good publication ethics principles before finalizing their manuscripts



ACTA TECHNICA CORVINIENSIS – Bulletin of Engineering
ISSN: 2067-3809
copyright © University POLITEHNICA Timisoara,
Faculty of Engineering Hunedoara,
5, Revolutiei, 331128, Hunedoara, ROMANIA
<http://acta.fih.upt.ro>

TABLE of CONTENTS

1.	Mustefa JIBRIL, Tesfabirhan SHOGA – ETHIOPIA H _∞ AND M- SYNTHESIS DESIGN OF QUARTER CAR ACTIVE SUSPENSION SYSTEM	13
2.	Petar ČISAR, Sanja MARAVIĆ ČISAR – SERBIA DEVELOPMENT CONCEPTS OF VIRTUAL REALITY SOFTWARE	23
3.	D.A. KAMBLE, Nihal SHAIKH – INDIA DESIGN AND DEVELOPMENT OF SEAT (SOLDIER) AGAINST MINE BLAST IMPACT	31
4.	Zoran PANDILOV – Republic of MACEDONIA OPTIMIZING THE CONTOURING ACCURACY OF CNC MILLING MACHINE WITH DOUBLE BALL BAR TEST	37
5.	S.K. SHINDE, R.M. MORE – INDIA FAULTS FINDING ANALYZER OF WEB APPLICATIONS	43
6.	Miodrag MILČIĆ, Dragan MILČIĆ, Nataša ZDRAVKOVIĆ – SERBIA EXPERIMENTAL INVESTIGATION OF FRICTION STIR WELDING OF 2024 ALUMINIUM ALLOYS JOINTS TESTING	47
7.	Susarla Venkata Ananta Rama SASTRY – INDIA SURFACE ASSIMILATION OF COPPER (CU ²⁺) FROM WASTE WATER USING MANGO PEEL POWDER (MPP)	51
8.	Mustefa JIBRIL, Eliyas Alemayehu TADESE – ETHIOPIA H ₂ OPTIMAL AND M-SYNTHESIS DESIGN OF QUARTER CAR ACTIVE SUSPENSION SYSTEM	55
9.	Tihomir S. LATINOVIC, Mladen M. TODIC, Dorian NEDELICU, Cristian P. BARZ – BOSNIA & HERZEGOVINA / ROMANIA IMPROVING THE SAFETY OF RAILWAY FROM BASIC START-STOP TO THE INTELLIGENT SYSTEM	59
10.	Ancuța N. JURCO, Liviu I. SCURTU – ROMANIA GEOMETRICAL DESIGN AND CRASH SIMULATION OF A SHOCK ABSORBER	63
11.	Slobodanka BOLJANOVIĆ, Stevan MAKSIMOVIĆ, Strain POSAVLJAK – SERBIA / BOSNIA & HERZEGOVINA ANALYSIS OF TWO SYMMETRIC CRACKS AT A HOLE UNDER CYCLIC LOADING	67
12.	Milena ĆOSIĆ, Slobodanka BOLJANOVIĆ – SERBIA CHARACTERIZATION OF THE STRUCTURAL CHANGES OF Al18SiCuMg ALLOY DURING THE RHEOCASTING PROCESS	71
13.	G.K. GIRISHA, S.L. PINJARE – INDIA IMPLEMENTATION OF NOVEL ALGORITHM FOR AUDITORY COMPENSATION IN HEARING AIDS USING STFT ALGORITHM	75
14.	Srinivasa GK GOWDA, Sunil JACOB – INDIA NETWORK MOBILE TOPOLOGY IMPACT QOS IN MULTI-SERVICE MANET	79
15.	Srbislav ALEKSANDROVIĆ, Đjordje MILOSAVLJEVIĆ – SERBIA ACCURACY OF PURE COPPER FLOW CURVES DETERMINATION IN COMPRESSION TESTS	87

16.	Petar S. DJEKIC, Biljana MILUTINOVIC – SERBIA STUDY OF APPLICATION OF WASTE GLASS POWDER IN VIRGIN RUBBER BLENDS	91
17.	Meenakshi A. THALOR – INDIA ANALYSIS OF DIFFERENT DRIFT DETECTION TECHNIQUES ON DATA STREAM	95
18.	Nikola PETROVIĆ, Bojan KRSTIĆ, Jelena PETROVIĆ – SERBIA EVALUATION OF FREIGHT TRANSPORT MODES BASED ON EXTERNAL COSTS	99
19.	Stefan ĐURIĆ, Bogdan NEDIĆ, Slobodan MALBAŠIĆ, Jelena BARALIĆ – SERBIA APPLICATION OF NEW TECHNOLOGIES FOR DEMILITARIZATION ORDONANCE IN ORDER TO PROTECT ENVIRONMENT	103
20.	Babatope Abimbola OLUFEMI, Rachael Aniedi ESSIEN – NIGERIA PRODUCTION OF BIOLUBRICANTS FROM NEEM SEED OIL CATALYZED BY CALCIUM OXIDE FROM SNAIL SHELL	107
21.	Susarla Venkata Ananta Rama SASTRY – INDIA STUDIES ON ADSORPTION OF ACETIC ACID FROM AQUEOUS SOLUTION BY USING LEAVES OF MANILKARA ZAPOTA	115
22.	Mladen TODIC, Ostoja MILETIC, Said PAŠALIĆ – BOSNIA & HERZEGOVINA ZONE OF THE STRESS AND OF THE STRAINS WHEN BENDING LAMINARY COMPOSITES	119
23.	Victor Viorel SAFTA, Bianca-Ştefania ZĂBAVĂ, Viviana CIUCĂ – ROMANIA HIGH EFFICIENCY GAS HEATING SYSTEMS – A REVIEW	123
24.	Iulia GĂGEANU, Petru CÂRDEI, Gheorghe VOICU – ROMANIA EXPERIMENTAL RESEARCHES ON THE EVOLUTION OF THE LENGTH OF FIR TREE SAWDUST PELLETS	129
25.	Sakshi SINGH, Suresh KUMAR – INDIA THE TIMES OF CYBER ATTACKS	133
***	MANUSCRIPT PREPARATION – GENERAL GUIDELINES	139

The **ACTA TECHNICA CORVINIENSIS – Bulletin of Engineering, Tome XIII [2020], Fascicule 3 [July–September]** includes original papers submitted to the Editorial Board, directly by authors or by the regional collaborators of the Journal.



Also, the **ACTA TECHNICA CORVINIENSIS – Bulletin of Engineering, Tome XIII [2020], Fascicule 3 [July–September]**, includes scientific papers presented in the sections of:

- **DEMI 2019 – The 14th International Conference on Accomplishments in Mechanical and Industrial Engineering**, organized by Faculty of Mechanical Engineering, University of Banja Luka, BOSNIA & HERZEGOVINA, co-organized by Faculty of Mechanical Engineering, University of Niš, SERBIA, Faculty of Mechanical Engineering Podgorica, University of Montenegro, MONTENEGRO and Faculty of Engineering Hunedoara, University Politehnica Timisoara, ROMANIA, in Banja Luka, BOSNIA & HERZEGOVINA, 24–25 May 2019. The current identification numbers of the selected papers are the #6, #11–12, #15–16, #18–19 and #22, according to the present contents list.
- **ICAS 2020 – The International Conference on Applied Sciences**, organized by University Politehnica Timisoara – Faculty of Engineering Hunedoara (ROMANIA) and University of Banja Luka, Faculty of Mechanical Engineering Banja Luka (BOSNIA & HERZEGOVINA), in cooperation with Academy of Romanian Scientists (ROMANIA), Ministry for Scientific and Technological Development, Higher Education and Information Society of the Republic of Srpska (BOSNIA & HERZEGOVINA), Academy of Sciences and Arts of the Republic of Srpska (BOSNIA & HERZEGOVINA), Academy of Technical Sciences of Romania – Timisoara Branch (ROMANIA), General Association of Romanian Engineers – Hunedoara Branch (ROMANIA) and Association Universitaria Hunedoara (ROMANIA), in Hunedoara, ROMANIA, 20–22 May, 2020. The current identification number of the selected paper is the #9, according to the present contents list.
- **ISB–INMA TEH' 2019 – International Symposium (Agricultural and Mechanical Engineering)**, organized by Politehnica University of Bucharest – Faculty of Biotechnical Systems Engineering (ISB), National Institute of Research–Development for Machines and Installations Designed to Agriculture and Food Industry (INMA Bucharest), Romanian Agricultural Mechanical Engineers Society (SIMAR), National Research & Development Institute for Food Bioresources (IBA Bucharest), National Institute for Research and Development in Environmental Protection (INCDPM), Research-Development Institute for Plant Protection (ICDPP), Research and Development Institute for Processing and Marketing of the Horticultural Products (HORTING), Hydraulics and Pneumatics Research Institute (INOE 2000 IHP) and “Food for Life Technological Platform”, in Bucharest, ROMANIA, between 31 October – 1 November, 2019.



ACTA TECHNICA CORVINIENSIS – Bulletin of Engineering

ISSN: 2067–3809

copyright © University POLITEHNICA Timisoara,

Faculty of Engineering Hunedoara,

5, Revolutiei, 331128, Hunedoara, ROMANIA

<http://acta.fih.upt.ro>

Fascicule 3

[July – September]

t o m e

[2020] XIII

ACTA Technica CORVINIENSIS
BULLETIN OF ENGINEERING



ACTA TECHNICA CORVINIENSIS – Bulletin of Engineering

ISSN: 2067-3809

copyright © University POLITEHNICA Timisoara,

Faculty of Engineering Hunedoara,

5, Revolutiei, 331128, Hunedoara, ROMANIA

<http://acta.fih.upt.ro>

¹Mustefa JIBRIL, ²Tesfabirhan SHOGA

H_{∞} AND μ - SYNTHESIS DESIGN OF QUARTER CAR ACTIVE SUSPENSION SYSTEM

¹Department of Electrical & Computer Engineering, DireDawa Institute of Technology, DireDawa, ETHIOPIA

²Department of Electrical & Computer Engineering, Jimma Institute of Technology, Jimma, ETHIOPIA

Abstract: To improve the road handling and passenger comfort of a vehicle, a suspension system is provided. An active suspension system is considered to be better than the passive suspension system. In this paper, 2 degrees of freedom of a linear quarter car active suspension system is designed, which is subject to different disturbances on the road. Since the parametric uncertainty in the spring, the shock absorber, mass and the actuator has been considered, robust control is used. In this paper, H_{∞} and μ - synthesis controllers are used to improve the driving comfort and the ability to drive the car on the road. For the analysis of the time domain, using a MATLAB script program and performed a test using four disturbance inputs of the road (bump, random, sinusoidal and harmonic) for the suspension deflection, the acceleration of the body and the body travel for the active suspension with the H_{∞} controller and active suspension with μ - synthesis controller and the comparative simulation and reference results demonstrate the effectiveness of the presented active suspension system with μ - synthesis controller.

Keywords: Quarter car active suspension system, H_{∞} controller, μ - synthesis controller, Robust controller

INTRODUCTION

At present, the world's leading automotive companies and research institutions have invested considerable human and material resources to develop a cost-effective vehicle suspension system, in order to be widely used in the vehicle. The main aim of suspension system

is to isolate a vehicle body from road irregularities in order to maximize passenger ride comfort and retain continuous road wheel contact in order to provide road holding. Many studies have shown that the vibrations caused by irregular road surfaces have an energy-draining effect on drivers, affecting their physical and mental health [1]. Demands for better ride comfort and controllability of road vehicles like passenger cars has motivated to develop new type of suspension systems like active and semi active suspension systems. These electronically controlled suspension systems can potentially improve the ride comfort as well as the road handling of the vehicle. An active suspension system has the capability to adjust itself continuously to changing road conditions. By changing its character to respond to varying road conditions, active suspension offers superior handling, road feel, responsiveness and safety.

An active suspension system has the ability to continuously adjust to changing road conditions. By changing its character to respond to different road conditions, the active suspension offers superior handling, road feel, responsiveness and safety.

Active suspension systems dynamically respond to changes in the road profile because of their ability to supply energy that can be used to produce relative motion between the body and wheel. Typically, the active suspension systems include sensors to measure suspension variables such as body velocity,

suspension displacement, and wheel velocity and wheel and body acceleration. An active suspension is one in which the passive components are augmented by actuators that supply additional forces. These additional forces are determined by a feedback control law using data from sensors attached to the vehicle.

The existing active suspension system is inefficient if there are changes in parameter of the system or of actuator, then controlling the suspension system becomes a big problem.

Therefore H_{∞} and μ - synthesis control technique are used. H_{∞} and μ - synthesis control effectively suppresses the vehicle vibrations in the sensitive frequency range of the human body. The desired robust performance and robust stability are achieved in the closed loop system for a quarter vehicle model in the presence of structured uncertainties.

MATHEMATICAL MODELS

— Active Suspension System Mathematical Model

The mathematical model of the following subsection are only discussing the amount of force created by the active suspension. Active suspensions allow the designer to balance these objectives using hydraulic actuator which is driven by a motor between the chassis and wheel assembly. The actuator force f_s applied between the body and wheel assembly is represents the active component of the suspension system.

Most of the researchers choose to utility quarter vehicle dynamic shock model when they hubs on the vehicle body vertical vibration caused by the capacity of pavement roughness. Although quarter vehicle dynamic vibration configuration has not included the entire vehicle geometrical information, and it cannot

research the vehicle pitching angle shock and roll angle vibration.

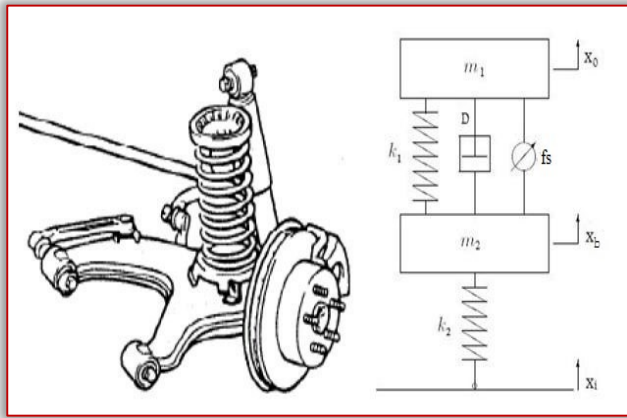


Figure 1: Quarter model of active suspension system with actuating force f_s between sprung and unsprung mass.

Figure 1 shows a vehicle quarter model of active suspension system. The mass m_1 (in kilograms) represents the car chassis (body) and the mass m_2 (in kilograms) represents the wheel assembly. The spring K_1 and damper D represent the passive spring and shock absorber placed between the car body and the wheel assembly. The spring K_2 models the compressibility of the pneumatic tire. The variables x_0 , x_b and x_i (all in meters) are the body travel, wheel travel, and road disturbance, respectively. The actuator force f_s (in kiloNewtons) applied between the body and wheel assembly is controlled by feedback and represents the active component of the suspension system.

From this model, we can analyze the vehicle suspension system dynamics as a linear system model and establish two degrees of freedom motion differential equations will be as follow:

$$m_1 \ddot{x}_0(t) + D[\dot{x}_0(t) - \dot{x}_2(t)] + k_1[x_0(t) - x_2(t)] = u$$

$$m_2 \ddot{x}_2(t) - D[\dot{x}_0(t) - \dot{x}_2(t)] + k_1[x_2(t) - x_0(t)] + k_2[x_2(t) - x_i(t)] = -u$$

We can set:

$$x_1 = x_2(t), x_2 = x_0(t), x_3 = \dot{x}_2(t), x_4 = \dot{x}_0(t)$$

The system state space equation can be express as:

$$\frac{dX}{dt} = AX + BU \quad (1)$$

In this equation, state variable matrixes are:

$$X = (x_1 \quad x_2 \quad x_3 \quad x_4)^T \quad (2)$$

Constant matrixes A and B are shown as below:

$$A = \begin{pmatrix} 0 & 0 & 1 & 0 \\ 0 & 0 & 0 & 1 \\ -\frac{k_1 + k_2}{m_2} & \frac{k_1}{m_2} & -\frac{D}{m_2} & \frac{D}{m_2} \\ \frac{k_1}{m_1} & -\frac{k_1}{m_1} & \frac{D}{m_1} & -\frac{D}{m_1} \end{pmatrix}$$

$$B = \begin{pmatrix} 0 & 0 \\ 0 & 0 \\ \frac{k_2}{m_2} & \frac{1}{m_2} \\ 0 & -\frac{1}{m_1} \end{pmatrix}$$

The system input variable matrix will be:

$$U = (x_1(t) \quad u)^T$$

The vehicle suspension system output matrix equation will be:

$$Y = CX + DU$$

In above equation, the output variable matrix Y will be:

$$Y = (k_2[x_1(t) - x_2(t)] \quad \ddot{x}_0(t) \quad x_0(t))$$

Y will also express as the following equation:

$$Y = (k_2[x_1(t) - x_2(t)] \quad \ddot{x}_0(t) \quad x_0(t))$$

Constant matrixes C and D will be shown as below:

$$C = \begin{pmatrix} -k_2 & 0 & 0 & 0 \\ \frac{k_1}{m_1} & -\frac{k_1}{m_1} & \frac{D}{m_1} & -\frac{D}{m_1} \\ 0 & 1 & 0 & 0 \end{pmatrix}$$

$$D = \begin{pmatrix} k_2 & 0 \\ 0 & -\frac{1}{m_1} \\ 0 & 0 \end{pmatrix}$$

—Hydraulic Actuator System Mathematical Model

The hydraulic actuator consists of a variable stroke hydraulic pump and a fixed stroke hydraulic motor as shown in the below Figure 2. The device accepts a linear displacement (stroke length) input and delivers an angular displacement. The pump and motor attached with the wheel assembly and this arrangement attached with the car chassis through a metal chain. When a sudden road disturbance enters to the pump, high pressure oil will enter to the motor and the motor control the displacement between the wheel assembly and the car chassis.

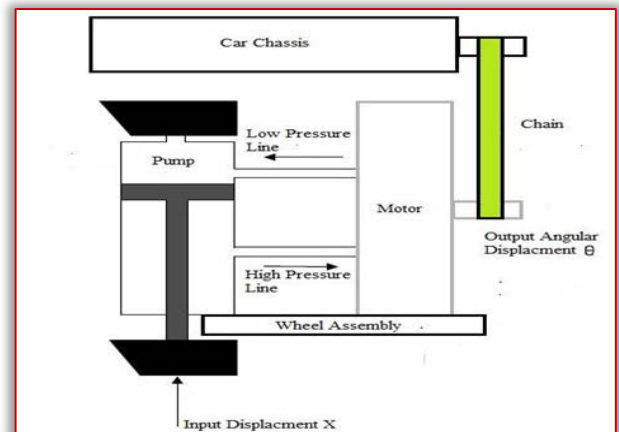


Figure 2: Hydraulic actuator block diagram

The hydraulic motor is controlled by the amount of oil delivered by the pump. By mechanically changing the pump stroke, the oil delivered by the pump is controlled. Like in a DC generator and dc motor, there is no essential difference between hydraulic pump and motor. In a pump the input is mechanical power and output is hydraulic power and in a motor, it is vice versa.

Let

q_p Rate at which the oil flows from the pump

q_m Oil flow rate through the motor

q Leakage flow rate

q_c Compressibility flow rate

x Input stroke length

θ Output angular displacement of motor

P Pressure drop across motor

The rate at which the oil flow from the pump is proportional to stroke speed, i.e. $q_p \propto \frac{dx}{dt}$.

Oil flow rate from-the pump,

$$q_p = K_p \frac{dx}{dt} \quad (3)$$

where

K_p = Ratio of rate of oil flow to unit stroke angle.

The rate of oil flow through the motor is proportional to motor speed, i.e. $q_m \propto \frac{d\theta}{dt}$.

Oil flow rate through motor,

$$q_m = K_m \frac{d\theta}{dt} \quad (4)$$

where

K_m = Motor displacement constant.

All the oil from the pump does not flow through the motor in the proper channels. Due to back pressure in the motor, a slices of the shape flow from the pump leaks back past the pistons of motor and pump. The back pressure is the importance that is built up by the hydraulic flow to overcome the hostility of free movement offered by load on motor shaft.

It is usually assumed that the leakage flow is proportional to motor pressure, i.e. $q_i \propto P$.

Leakage flow rate,

$$q_i = K_i P \quad (5)$$

where

K_i = constant.

The back pressure built up by the motor not only causes leakage flow in the motor and pump but oil in the lines to compress. Volume compressibility flow is essentially proportional to pressure and therefore the tariff of flow is proportional to the rate of innovations

of pressure, i.e. $q_c \propto \frac{dP}{dt}$

Compressibility flow rate,

$$q_c = K_c \frac{dP}{dt} \quad (6)$$

where

K_c = Coefficient of compressibility.

The rate at which the oil flows from the pump is given by sum of oil flow tariff through the motor, leak flow rate and compressibility flow rate.

$$q_p = q_m + q_i + q_c$$

Substituting eqn. (3), (4), (5) and (6) from above equations, we get

$$K_p \frac{dx}{dt} = K_m \frac{d\theta}{dt} + K_i P + K_c \frac{dP}{dt} \quad (7)$$

The torque T_m developed by the motor is proportional to pressure drop and balances load torque.

Hydraulic motor torque,

$$T_m = K_t P \quad (8)$$

where

K_t is motor torque constant.

If the load is assumed to consist of moment of inertia J and viscous friction with coefficient B ,

Then

Load Torque

$$T_l = J \frac{d^2\theta}{dt^2} + B \frac{d\theta}{dt} \quad (9)$$

$$\text{Hydraulic power input} = q_m P \quad (10)$$

Substituting eqn. (4) into eqn. (10), we get

$$\text{Hydraulic power input} = K_m \frac{d\theta}{dt} P \quad (11)$$

$$\text{Mechanical power output} = T_m \frac{d\theta}{dt} \quad (12)$$

Substituting eqn. (8) into eqn. (12), we get

$$\text{Mechanical power output} = K_t P \frac{d\theta}{dt} \quad (13)$$

If hydraulic motor losses are neglected or included as a part of load, then the hydraulic motor input is equal to mechanical power output of hydraulic motor.

$$K_m \frac{d\theta}{dt} P = K_t P \frac{d\theta}{dt} \quad (14)$$

From equation (14), it is clear that $K_m = K_t$.

Hence we can write

$$T_m = K_t P = K_m P$$

Since the motor torque equals load torque, $T_m = T_l$

$$K_m P = J \frac{d^2\theta}{dt^2} + B \frac{d\theta}{dt} \quad (15)$$

$$P = \frac{J}{K_m} \frac{d^2\theta}{dt^2} + \frac{B}{K_m} \frac{d\theta}{dt} \quad (16)$$

Differentiating equation (16) w.r.t time, we get

$$\frac{dP}{dt} = \frac{J}{K_m} \frac{d^3\theta}{dt^3} + \frac{B}{K_m} \frac{d^2\theta}{dt^2} \quad (17)$$

Substituting for P and dP/dt to eqn.(7), we get,

$$K_p \frac{dx}{dt} = K_m \frac{d\theta}{dt} + K_i \left[\frac{J}{K_m} \frac{d^2\theta}{dt^2} + \frac{B}{K_m} \frac{d\theta}{dt} \right] + K_c \left[\frac{J}{K_m} \frac{d^3\theta}{dt^3} + \frac{B}{K_m} \frac{d^2\theta}{dt^2} \right] \quad (18)$$

Taking Laplace transform with zero initial conditions, we get,

$$\frac{\theta(s)}{X(s)} = \frac{K_p}{\left[\frac{K_c J}{K_m} s^2 + \left[\frac{K_i J + K_c B}{K_m} \right] s + \frac{K_m^2 + K_i B}{K_m} \right]} \quad (19)$$

In hydraulic systems, normally $K_m \ll K_c$, therefore, Put $K_c = 0$ in above equation.

$$\frac{\theta(s)}{X(s)} = \frac{K_p}{\left[\frac{K_i J}{K_m} s + \frac{K_m^2 + K_i B}{K_m} \right]} = \frac{K}{(\tau s + 1)} \quad (20)$$

where

$$K = \frac{K_p}{\frac{K_m^2 + K_i B}{K_m}} \text{ and } \tau = \frac{K_i J}{K_m^2 + K_i B}$$

$$K_p = 1$$

$$K_m = 4$$

where: $K_i = -3$

$$B = 4$$

$$J = 16.67$$

The value of K and τ is $K=1$ and $\tau = 1/50$

The transfer function of the hydraulic actuator is

$$\frac{\theta(s)}{X(s)} = \frac{1}{\frac{1}{50}s + 1}$$

ROAD PROFILES

— Bump Road Disturbance

Bump road disturbance is a basic input to research the suspension system. It simulated a very intense force for a very short time, such as a vehicle drive through a speed hump. This road disturbance has a maximum height of 5 cm as shown in Figure 3.

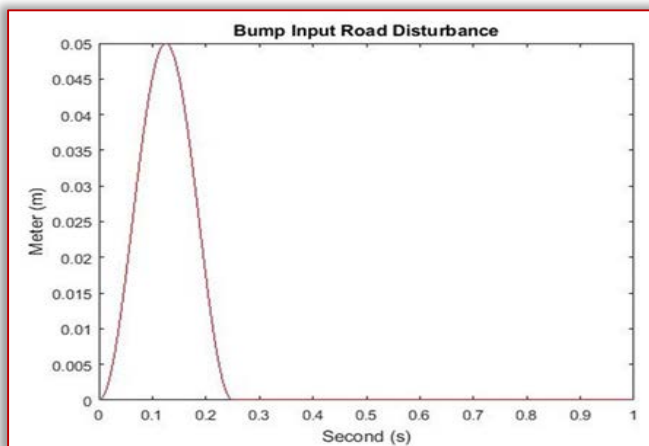


Figure 3: Bump road disturbance

— Random Road Disturbance

Numerous researches shows that it is necessary to test a car to a random road disturbance to check the spring and damper respond quickly and correctly. The random road disturbance has a maximum height of 15 cm and minimum height of -15 cm as shown in Figure 4.

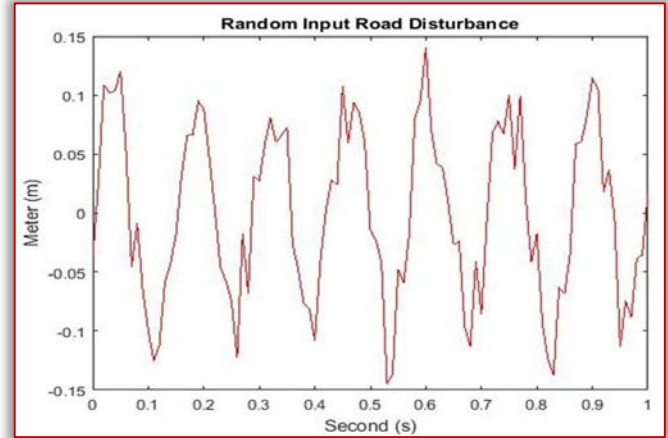


Figure 4: Random road disturbance

— Sine Pavement Road Disturbance

Sine wave input signal can be used to simulate periodic pavement fluctuations. It can test the vehicle suspension system elastic resilience ability while the car experiences a periodic wave pavement. Sine input pavement test is made by every automotive industries before a new vehicle drives on road. The sine pavement road disturbance has a height of -10 cm to 10 cm as shown in Figure 5.

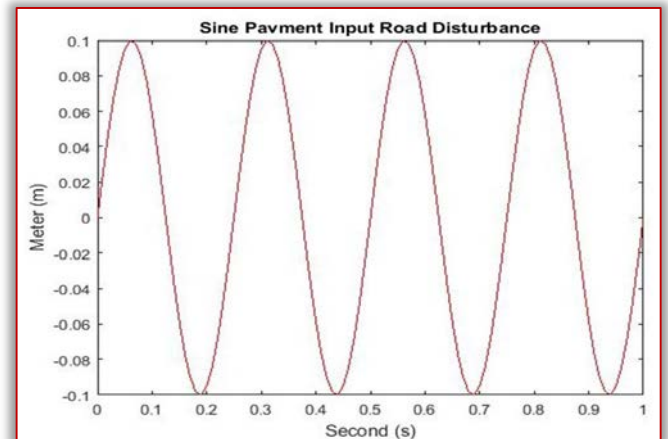


Figure 5: Sine pavement road disturbance

— Harmonic Road Disturbance

Numerous researches show that when the vehicle speed is constant, harmonic road profile may be usually used in the simulation to verify the stability and capability of the designed control system, besides the system response status.

The harmonic road disturbance model is shown in Figure 6 with a maximum height of 5cm and a minimum height of -5cm.

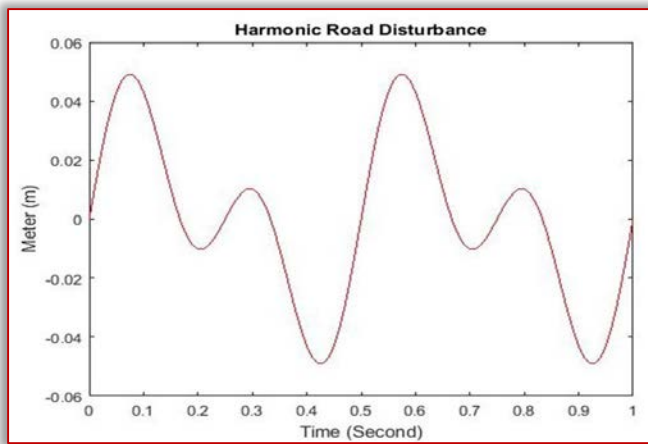


Figure 6: Harmonic road disturbance

WEIGHTING FUNCTIONS

It is required that in the H^∞ framework to use weighting functions to reconciliation different performance objectives. The performance goal of a feedback system can be usually determined in terms of requirements on the sensitivity functions and/or complementary sensitivity functions or in terms of some other closed loop transfer functions. The odds of occupying weighted performance in multivariable system design is firstly, some part of a vector signal are usually more important than others, secondly, measuring each signal will not be in the same unit. For instance, some part of the output error signal may be measured in terms of length, and others may be measured in terms of voltage. Therefore, weighting functions play an essential rule to type these part comparable. The weighting functions are discussed below.

The weighting function W_{act} is used to limit the magnitude and frequency content of the active control force signal. Choosing

$$W_{act} = \frac{80}{11} \frac{s + 60}{s + 600}$$

W_{x1} and W_{x1-x3} are used to keep the car deflection and the suspension deflection small over the desired range. The car body deflection W_{x1} is given as

$$W_{x1} = \frac{508.1}{s + 56.55}$$

The suspension deflection is used via weighting function W_{x1-x3} . The weighting function is given as

$$W_{x1-x3} = \frac{15}{0.2s + 1}$$

THE PROPOSED CONTROLLER DESIGN

The design of active suspension system to provide passenger comfort and road handling is developed using H^∞ and μ -synthesis controllers design. In the active suspension system, the proposed controllers design included the hydraulic actuator dynamics. In order to account for the difference between the actuator model and the actual actuator dynamics, a

first order model of the actuator dynamics as well as an uncertainty model have been used. The main aim of the controller design is to minimize suspension deflection, body acceleration and body travel of the system. Synthesis method is used to design the proposed controllers by achieving the performance objective via minimizing the weighted transfer function norm. The active suspension system with H^∞ and μ -synthesis controllers with hydraulic motor actuator system interconnections block diagram is shown in Figure 7.

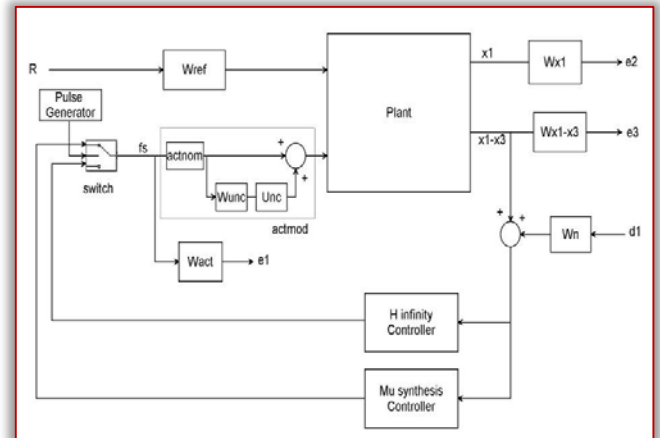


Figure 7: Active suspension system with H^∞ and μ -synthesis controllers system interconnections block diagram

In Figure 7 plant represents the quarter car suspension model, H^∞ controller is a controller which is designed by H^∞ approach. e_1 , e_2 and e_3 are the first, second and third outputs after influencing weighting functions.

A μ -synthesis controller is synthesized using D-K iteration. The D-K iteration method is an approximation to synthesis that attempts to synthesize the controller. There is two control input the road disturbance signal and the active control force. There are three measurement output signals, the suspension deflection, car body acceleration and car body travel. The pulse generator switches between the two systems in μ seconds. In practice, the suspension deflection can be measured by acoustic or radar transmitter/receiver, while the velocity is typically obtained by integrating the acceleration which is measured using accelerometer.

There are two purposes for the weighted functions norm: for a given norm, there will be a direct comparison for different performance objectives and they are used for knowing the frequency information incorporated into the analysis. The output or feedback signal y is

$$y = ((x_1 - x_3) + d_1 \times W_n)$$

The controller's acts on the y signal to produce the active control force signal. The W_n block modelled

the sensor noise in the channel. W_n is given a sensor noise of 0.05m.

$$W_n = 0.05$$

W_n is used to model the noise of the displacement sensor. The magnitude of the road disturbance is scaled using the weight W_{ref} . Let us assume the maximum road disturbance is 0.1m which means

$$W_{ref} = 0.1$$

RESULT AND DISCUSSION

To ensure that our controller design achieves the desired objective, the closed loop active suspension system is simulated with the following parameter values as shown in Table 1.

Table 1: Parameters of quarter vehicle model

Model parameters	symbol	symbol Values
Vehicle body mass	m 1	300 Kg
Wheel assembly mass	m 2	40 Kg
Suspension stiffness	k 1	15,000 N/m
Tyre stiffness	k 2	150,000 N/m
Suspension damping	D	1000 N-s/m

—Active Suspension System Control Targets Simulation Output Specifications

Each active suspension system control targets (body travel, body acceleration and suspension deflection) has its own output specifications while the vehicle in motion.

The body travel output should be the minimum vertical amplitude because the passenger must not feel the road disturbance while the vehicle in motion. In an ideal suspension system, the body travel vertical amplitude is zero.

The body acceleration output should be the minimum vertical acceleration because the passenger must not feel the sudden vertical acceleration while the vehicle hits the road disturbance. In an ideal suspension system, the vertical velocity is constant.

The suspension deflection output should be the same as the road disturbance input because if it is above or below the road disturbance input, it will affect the body travel output.

—Time Domain Comparison of the Active Suspension System with H_∞ and μ - synthesis Controllers

In this subsection, we simulate the active suspension system with H_∞ controller and active suspension system with μ - synthesis controller for suspension deflection, body acceleration and body travel using bump, random, sine pavement and harmonic road disturbances.

» Simulation of a Bump Road Disturbance

The simulation for a bump input road disturbance is shown below. In this simulation, we simulate active

suspension system with H_∞ controller and active suspension system with μ - synthesis controller for suspension deflection, body acceleration and body travel.

The body travel, body acceleration and suspension deflection simulation output is shown in Figure 8, Figure 9 and Figure 10 respectively for a bump road disturbance.

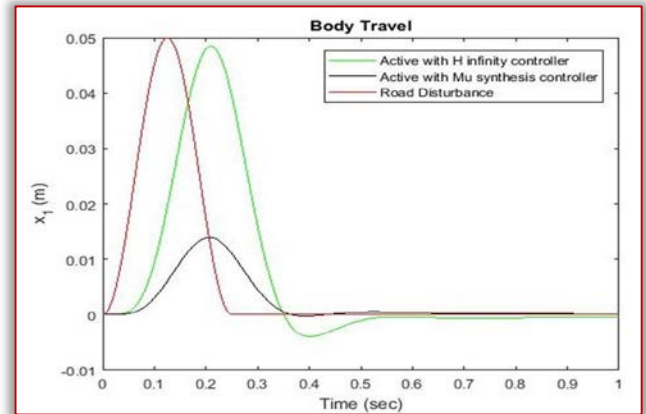


Figure 8: Body travel for bump road disturbance

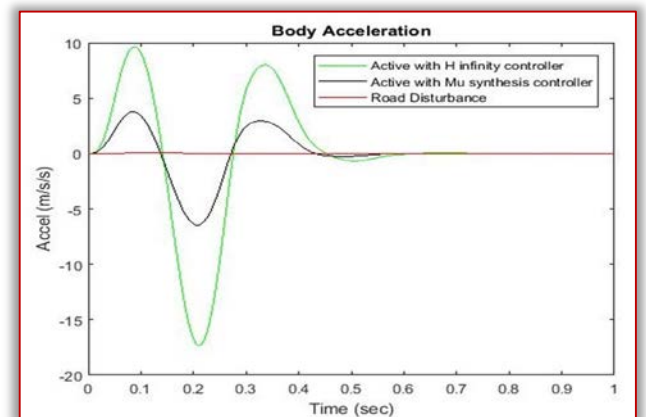


Figure 9: Body acceleration for bump road disturbance

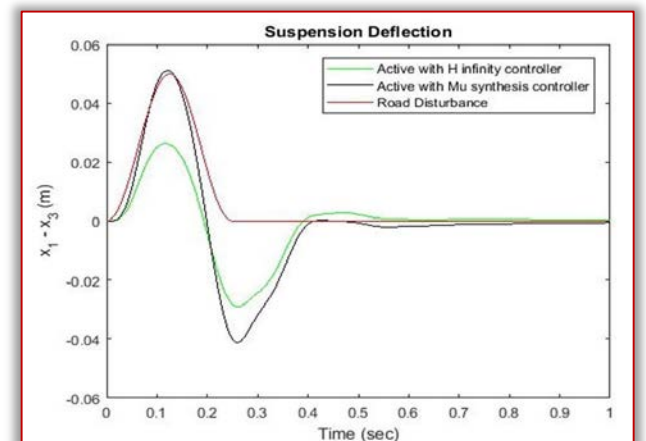


Figure 10: Suspension deflection for bump road disturbance

» Simulation of a Random Road Disturbance

The simulation for a random input road disturbance is shown below. In this simulation, we simulate active suspension system with H_∞ controller and active

suspension system with μ - synthesis controller for suspension deflection, body acceleration and body travel.

The body travel, body acceleration and suspension deflection simulation output is shown in Figure 11, Figure 12 and Figure 13 respectively for a random road disturbance.

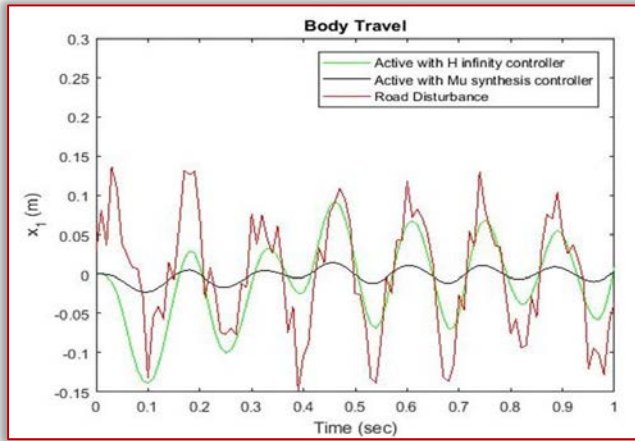


Figure 11: Body travel for random road disturbance

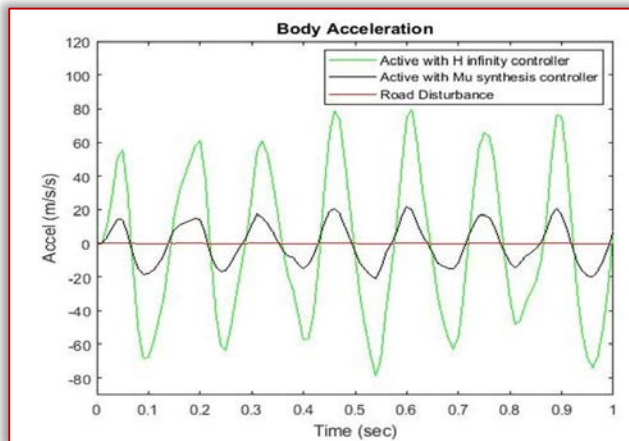


Figure 12: Body acceleration for random road disturbance

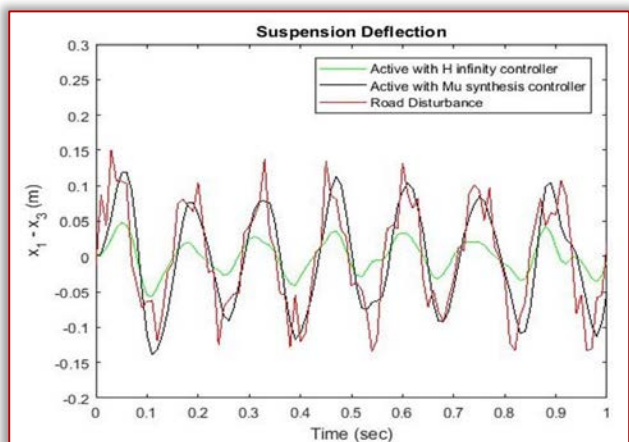


Figure 13: Suspension deflection for random road disturbance

» Simulation of a Sine Pavement Input Road Disturbance

The simulation for a sine pavement input road disturbance is shown below. In this simulation, we simulate active suspension system with H_∞ controller and active suspension system with μ - synthesis controller for suspension deflection, body acceleration and body travel.

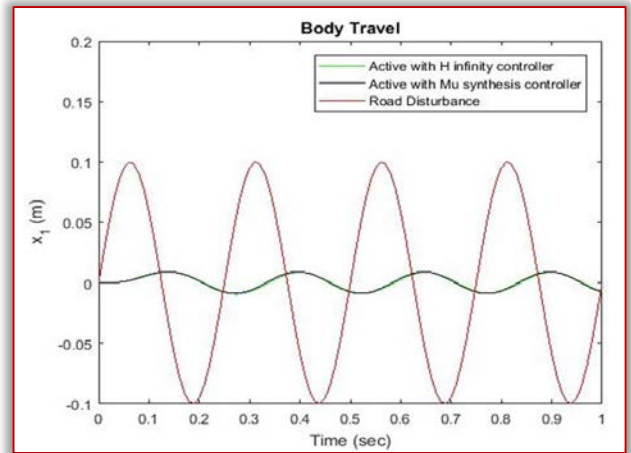


Figure 14: Body travel for sine input pavement road disturbance

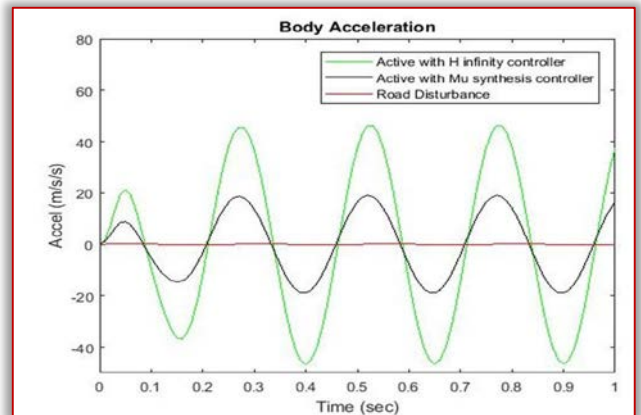


Figure 15: Body acceleration for sine input pavement road disturbance

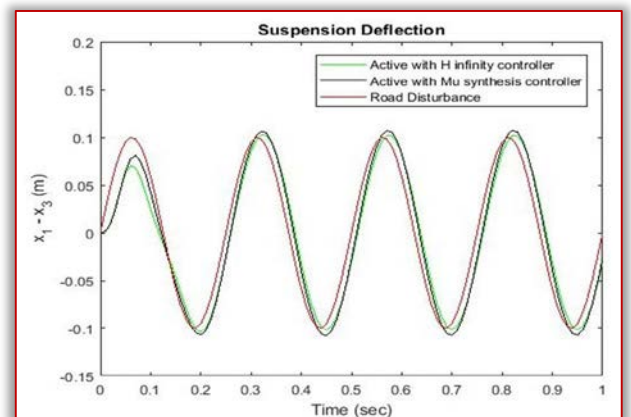


Figure 16: Suspension deflection for sine input pavement road disturbance

The body travel, body acceleration and suspension deflection simulation output is shown in Figure 14, Figure 15 and Figure 16 respectively for a sine pavement road disturbance.

» **Simulation of a Harmonic Road Disturbance**

The simulation for a harmonic input road disturbance is shown below. In this simulation, we simulate active suspension system with H^∞ controller and active suspension system with μ -synthesis controller for suspension deflection, body acceleration and body travel.

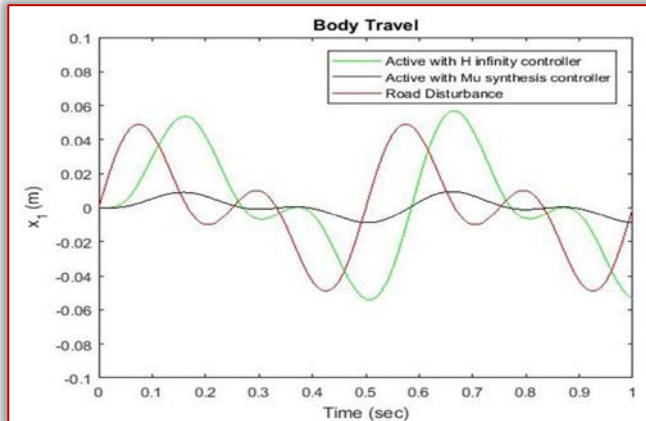


Figure 17: Body travel for harmonic road disturbance

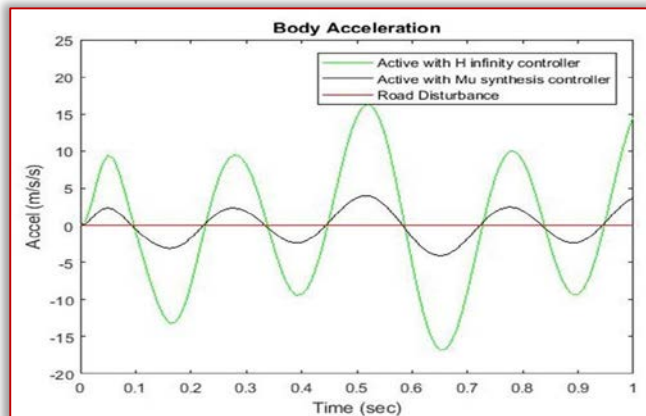


Figure 18: Body acceleration for harmonic road disturbance

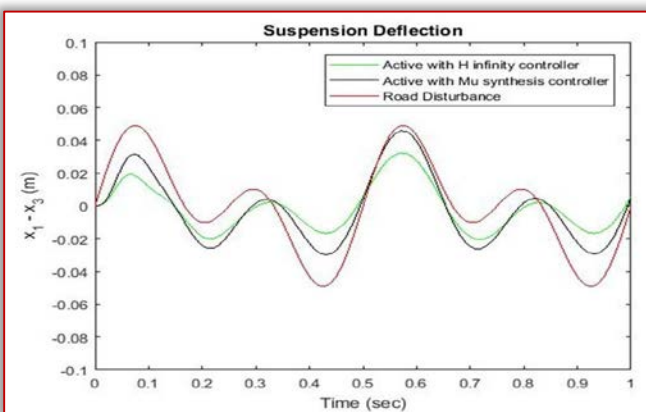


Figure 19: Suspension deflection for harmonic road disturbance

The body travel, body acceleration and suspension deflection simulation output is shown in Figure 17, Figure 18 and Figure 19 respectively for a harmonic road disturbance.

— **Frequency Domain Comparison of the Active Suspension System with H^∞ and μ -synthesis Controllers**

The frequency domain analysis of the active suspension system with H^∞ controller and active suspension system with μ -synthesis controller to body travel, body acceleration and suspension deflection is presented below.

» **Body Travel**

The bode plot comparison of the active suspension system with H^∞ controller and active suspension system with μ -synthesis controller for body travel is shown in Figure 20 below.

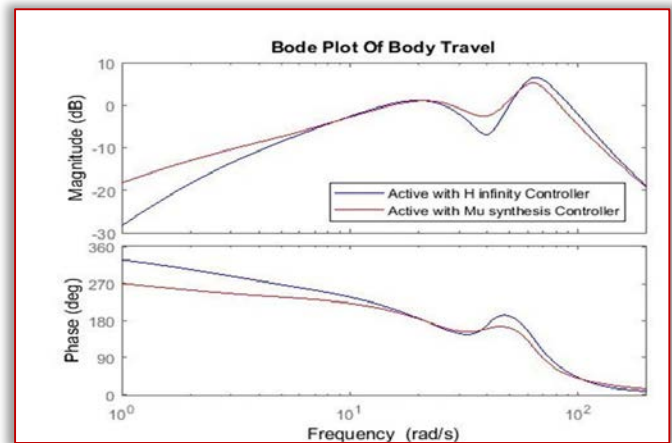


Figure 20: Bode plot of body travel

— **Body Acceleration**

The bode plot comparison of the active suspension system with H^∞ controller and active suspension system with μ -synthesis controller for body acceleration is shown in Figure 21 below.

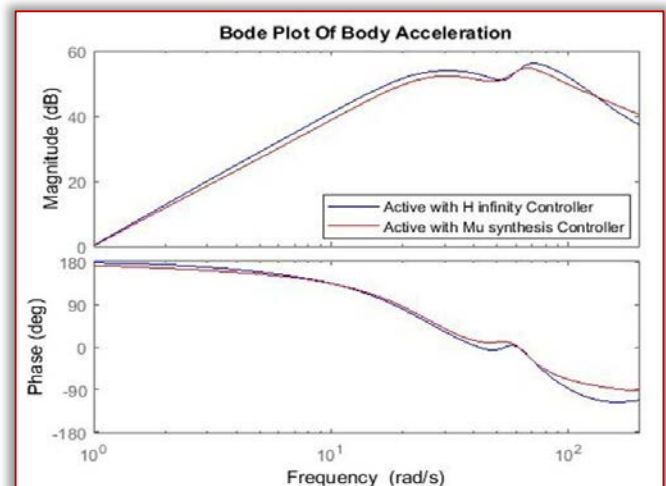


Figure 21: Bode plot of body acceleration

» **Suspension Deflection**

The bode plot of the active suspension system with H^∞ controller and active suspension system with μ - synthesis controller for suspension deflection is shown in Figure 22 bellow.

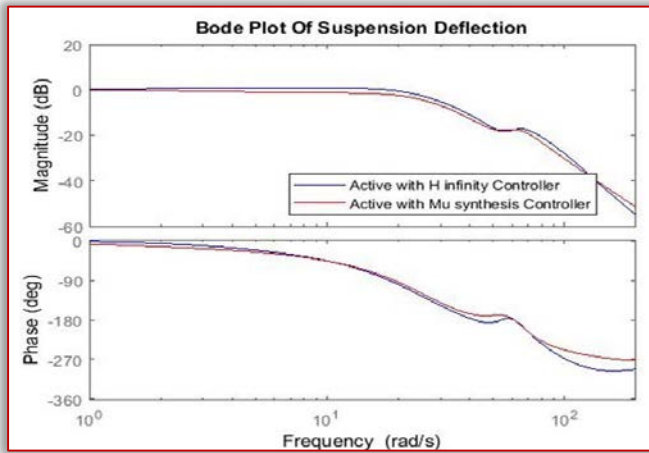


Figure 22: Bode plot of Suspension deflection

— **Frequency Domain Comparison Result of Active Suspension System with H^∞ and μ - synthesis Controllers**

While in motion, human body is more prone to the possessions of shock in the frequency cord of 10–20 Hz. Figures 20, Figure 21 and Figure 22 shows the frequency feedback plot of suspension deflection, body acceleration and body travel of robust H-infinity and robust Mu-synthesis technique. From the result, it is evident that there exist two natural frequency which can be classified as lower frequency and higher frequency.

At higher frequency, the active controller with mu-synthesis controller shows a good response, whereas, at lower frequency, both the active controller with H infinity and mu-synthesis controllers is more effective is suppressing the vibration.

Comparing all the results, it is clear that at higher frequency, the active controller with mu-synthesis controller shows a good response and both H infinity and mu-synthesis controller has best performance in controlling the shock at low frequency region.

— **Numerical Values of the Simulation Outputs**

The numerical values of the simulation output for the control targets body travel, body acceleration and suspension deflection for the four road disturbances is shown in Table 2, Table 3 and Table 4 bellow.

Table 2: Numerical values of the body travel simulation output

No	Systems	Bump	Random	Sine	Harmonic
1	Road Profile	0.05m	0.15m	0.1m	0.05m
2	H^∞	0.049m	0.09m	0.01m	0.055m
3	μ - synthesis	0.013m	0.01m	0.01m	0.011m

Table 2 shows us the active suspension system with μ - synthesis controller have the minimum body travel amplitude in the random road disturbance and the active suspension system with μ - synthesis controller shows the best performance in the random road profile.

Table 3: Numerical values of the body acceleration simulation output

No	Systems	Bump	Random	Sine	Harmonic
1	Road Profile	1 m/s ²	5 m/s ²	2 m/s ²	1 m/s ²
2	H^∞	10 m/s ²	80 m/s ²	45 m/s ²	16 m/s ²
3	μ - synthesis	4 m/s ²	20 m/s ²	18 m/s ²	3 m/s ²
8	H^∞ Loop Shaping	5.5 m/s ²	40 m/s ²	30 m/s ²	15 m/s ²

Table 3 shows us the active suspension system with μ - synthesis controller have the minimum body acceleration amplitude in the harmonic road disturbance and the active suspension system with μ - synthesis controller shows the best performance in the harmonic road profile.

Table 4: Numerical values of the suspension deflection simulation output

No	Systems	Bump	Random	Sine	Harmonic
1	Road Profile	0.05m	0.14m	0.1m	0.05m
2	H^∞	0.022m	0.05m	0.1m	0.03m
3	μ - synthesis	0.05m	0.14m	0.1m	0.05m

Table 4 shows us the active suspension system with μ - synthesis controller have the suspension deflection amplitude the same as the road disturbance input in all the four road disturbances and the active suspension system with μ - synthesis controller shows the best performance in all the four road disturbances.

CONCLUSIONS

In this paper, H^∞ controller and μ - synthesis controllers are successfully designed using MATLAB/Script for quarter car active suspension system.

The design of a MATLAB script that represents the active suspension system with H^∞ controller and μ - synthesis controller have been done and tasted with bump, sine input pavement, random and harmonic road disturbances for body travel, body acceleration and suspension deflection.

The comparison of the time and frequency domain of the active suspension system with H^∞ controller and μ - synthesis controller for the body travel, body acceleration and suspension deflection have been analyzed.

In the time domain analysis, we have tested the two systems with bump, sine input pavement, harmonic and random road disturbances and the comparative simulation and reference results prove the effectiveness of the presented active suspension with μ - synthesis controller.

In the frequency domain analysis, the results shows that at higher frequency, the active suspension system with μ - synthesis controller shows a good response and at low frequency region, both the active suspension system with H_{∞} controller and the active suspension system with μ - synthesis controller has best performance in controlling the vibration.

Finally the comparative simulation and reference results prove the effectiveness of the presented active suspension with μ - synthesis controller and it achieves the passenger comfort and road handling criteria that needed to make the active suspension system is the best suspension system.

Acknowledgment

First and foremost, I would like to express my deepest thanks and gratitude to Dr. Parashante and Mr. Tesfabirhan for their invaluable advices, encouragement, continuous guidance and caring support during my journal preparation.

Last but not least, I am always indebted to my brother, Taha Jibril, my sister, Nejat Jibril and my family members for their endless support and love throughout these years. They gave me additional motivation and determination during my journal preparation.

References

- [1] Gang Wang, Zhijin Zhou, Design and Implementation of H_{∞} Miscellaneous Information Feedback Control for Vehicle Suspension System, Shock and Vibration Volume, ID 3736402, 15 pages, 2019.
- [2] Peter Benner, Tim Mitchell, Faster and More Accurate Computation of the H_{∞} Norm via Optimization, Society for Industrial and Applied Mathematics, Vol. 40, No. 5, pp. A3609-A3635, 2018.
- [3] J. Marzbanrad, N. Zahabi, H_{∞} Active Control of a Vehicle Suspension System Exited by Harmonic and Random Roads, Journal of Mechanics and Mechanical Engineering, Vol. 21, No. 1, pp 171-180, 2017.
- [4] Kruczek Ales, Stribrsky Antonin, Automotive active suspension – case study on H-infinity control, Recent Researches in Automatic Control, 2017.
- [5] Wang Chun Yan, Deng K, Robust Control for Active Suspension System Under Steering Condition, Science China Press, Springer-Verlag Berlin, Heidelberg, 2017.
- [6] Katerina Hyniova, One-Quarter-Car Active Suspension Model Verification, ITM Web of Conferences 9, 03003, 2017.
- [7] Abdoljalil Addeha, Abolfazl Ebrahimi, Optimal Design of Robust Controller for Active Car Suspension System Using Bee's Algorithm, Journal of Computational Research Progress in Applied Science & Engineering, ©PEARL publication, 2016.
- [8] Nouby M Ghazaly, Abdel-Nasser Sharkawy, H_{∞} Control of Active Suspension System for a Quarter

- Car Model, International Journal of Vehicle Structures and Systems, 2016.
- [9] Ales Kruczek, Antonin Stribrsky, H_{∞} Control of Automotive Active Suspension with Linear Motor, MŁMT project no. LN00B073 - Josef Bodek's Research Center of Combustion Engines and Automobiles, 2016.
- [10] Gaurav Kumar Sinha, Vibration Control of Car Suspension System Using Different Controllers, International Journal of Advance Reseach in Science and Engineering, Vol. No.6, Issue No.4, April, 2016.
- [11] Katerina Hyniova, On Testing of Vehicle Active Suspension Robust Control on An One-Quarter-Car Test Stand, International Journal of Mechanical Engineering, Volume 1, 2016.
- [12] Narinder Singh, Himanshu Chhabra, Robust Control of Vehicle Active Suspension System, International Journal of Control and Automation Vol. 9, No. 4 (2016), pp. 149-160.
- [13] Panshuo Li, James Lam, Kie Chung Cheung, Experimental Investigation of Active Disturbance Rejection Control for Vehicle Suspension Design, International Journal of Theoretical and Applied Mechanics, Volume 1, 2016.



ACTA TECHNICA CORVINIENSIS – Bulletin of Engineering
ISSN: 2067-3809

copyright © University POLITEHNICA Timisoara,
Faculty of Engineering Hunedoara,
5, Revolutiei, 331128, Hunedoara, ROMANIA
<http://acta.fih.upt.ro>

¹Petar ČISAR, ²Sanja MARAVIĆ ČISAR

DEVELOPMENT CONCEPTS OF VIRTUAL REALITY SOFTWARE

¹University of Criminal Investigation and Police Studies, Cara Dušana 196, 11080 Zemun–Belgrade, SERBIA

²Subotica Tech, Department of Informatics, Marka Oreškovića 16, 24000 Subotica, SERBIA

Abstract: The evolution of appropriate hardware and software platforms has resulted in intensive increase in such applications that have placed their action in the virtual world. This enables users a special experience – the experience of virtual reality (VR). The software for developing VR is in many ways specific and demanding. Having in mind its great diversity, this paper gives an overview of categorizations, general characteristics and evaluation methods. In addition, general principles of VR software development are especially elaborated, with an emphasis on creating and testing games.
Keywords: virtual reality, software, development, evaluation, game, testing

INTRODUCTION

Virtual reality (VR) is a completely three-dimensional (3D) environment created by a combination of appropriate software and hardware. This software immerses the user into the 3D environment, giving him the ability to interact with the virtual world in about a realistic way [1].

A few steps are required to create a good VR experience. The virtual world is created by software developers and then rendered in a way that users can interact with the objects. Headsets help provide users the illusion of being completely immersed in the 3D environment. These 3D objects tend to respond to changes in the user's movement and the interactions simulate those in the real world. Some additional devices, such as data gloves, can also simulate human senses (for instance, touch).

Speaking of computer reality types, it is needed to make a clear difference between augmented reality (AR) and VR. Both AR and VR shape the way we see the world around us. But they do it differently [2]. The main difference between virtual and augmented reality is that virtual reality creates a whole new space in which user becomes involved, while augmented reality adds artificial objects to the real world [3, 4]. Software for creating VR is specific, with a large number of features [5]:

- Content management – Numerous tools allow upload either raw 3D content, which will later be changed into a VR code or existing VR content onto the device with the ability to manage and store data.
- Editing content – The great part of VR software has editing capabilities. Users can edit raw 3D or existing VR content. Some editing features have drag-and-drop capability, which implies that users can edit their content with relatively modest previous programming experience.
- Hardware – software integration – Any VR application must integrate with adequate devices that supports planned virtual experiences. These

devices are usually headsets, but can also be something else.

- Cooperation – VR tools allow multiple users to access applications remotely so they can cooperate in real time. While cooperating, users are able to interact on the same things simultaneously.
- Analytics – Some VR applications enable analytical opportunities. It allows better understanding the behaviour of audiences accessing the VR content.

VR SOFTWARE CATEGORIES

With regard to the purpose, there are various categories of VR software:

- (a) Content management systems (CMS) – A CMS is used to collect, store and analyse all VR content in a centralized location. As VR continues to evolve, these tools will become increasingly important looking to manage and organize all virtual content. Users may upload 360-degree videos and images directly onto these platforms and edit them there. These tools allow publishing VR content directly from the platform. Many of these solutions also offer reporting and analytics, so users may better understand the behaviour of the audiences accessing the content. This software gives users the possibility to create consistency among VR experiences, ensuring brand specificity or actual regulations.

Software in this category must have the following characteristics: allowing 360-degree images and video to be uploaded onto the system, offering drag-and-drop editing capabilities, managing all created content within the platform and publishing created VR experiences.

- (b) Development software – VR is about creating a virtual and immersive environment to replace the real world. Development software is used to create native applications, typically for computers with Windows operating system. VR software development kits (SDK) provide the necessary environment to design, create and test VR experiences.

(c) Game engine software – A game engine provides developers with the framework for creating a VR video game experience [6]. A VR game engine often contains a virtual reality SDK. These tools enable developers to create and edit 3D characters and fully immersive experiences. VR game engines help developers focus on creating a product for the end user instead of wasting efforts on tying all elements of a gaming system together. VR game engines are very similar to general game engines, but are unique in that they support VR operating systems and hardware either directly or through an API (Application Programming Interface) [7]. Using VR game engines, developers can create games for various devices (for example, game consoles and smart phones). Some VR game engines can also create augmented reality experiences [8].

Software in this category must have the following characteristics: creation of custom VR video game experiences [9], creation and editing of immersive 3D experiences and integration with hardware that supports VR (mobile phones or headsets).

(d) Social platforms – These platforms allow cooperation in virtual reality from remote locations. They enable users to meet up in the same virtual space and communicate with each other (speech and text).

VR social platforms offer users the ability to choose and edit figures representing a particular person (avatars) as well as selected environments to host a virtual meet up. These meet ups can range from collaborating in a virtual conference room to viewing a presentation together. VR social platforms should allow users to develop virtual spaces to fit their specific needs [10], typically done so with a SDK. These solutions may also make easier recording and playback of virtual meetings.

Software in this category must have the following characteristics: allowing selection of a figure to represent them, enabling users to select and edit environments to host meet ups, providing the ability to communicate with other participants and allowing participation in a given activity together.

(e) Training simulator software – VR training simulators can be used in almost any area in an immersive virtual environment. These tools should not be confused with augmented reality training simulators, which provide training simulations through integrating digitally-created 3D images into the real world [11]. Giving users these experiences allows practicing and developing the skills that may be necessary in certain high-stress professions. However, the use of these tools can include industries, like aviation and transportation. Some of VR training

simulators may also have SDK functionalities (developers can customize the simulator platform to fit their specific needs).

Software in this category must have the following characteristics: creation of specific virtual reality experiences, allowing upload of relevant content directly to headsets, supporting customized content (specific to business) and provide reporting on performance.

(f) Visualization software – VR data visualization software allows users to experience aggregated data. Data visualization enables to get analytics presented visually so they may fully understand what the data is communicating. VR data visualization is used across multiple industries, allowing working with real-time data. Also, it allows users to display large amounts of data. Bringing VR into data analytics enables simultaneous cooperation on work.

Software in this category must have the following characteristics: allowing multiple users to simultaneously work on data, enabling visualization in a completely virtual environment, data editing in real time and integration with devices.

VR SYSTEM SOFTWARE

VR system software is a collection of tools and software for designing, developing and maintaining virtual environments and appropriate databases where the information is stored. The tools can be generally classified into modelling and development tools.

Modelling tools – There are many modelling tools available for designing objects and environments. The most common ones are Unity, Google VR, 3ds Max, Maya etc.

Development tools – VR is a complex and integrative technology that borrows from many other technologies, such as real-time 3D graphics, tracking technology, sound processing and haptic technology, therefore software development flexibility and real time interaction is needed. Starting the development of a VR application from the basic codes (in C/C++/C#, Java, OpenGL etc.) requires a large amount of work and time. Such system reliability is usually low, therefore, development tools are used.

Detailed analysis is needed in choosing VR development tools due to the difference in flexibility of software packages as related to input model, interface compatibility, file format, animation characteristics, collision detection, supported I/O devices and support community.

Development tools used in VR content creation include virtual world authoring tools, VR toolkits / SDKs and APIs. But it is not uncommon to determine that some APIs are in fact toolkits (OpenGL Optimizer and Java 3D API).

EVALUATION OF VE (VIRTUAL ENVIRONMENT)

Evaluation of VR systems is mostly focused on testing its usability [12]. VR functionalities fall in two main groups:

a) navigation and exploration

b) interaction and manipulation of 3D virtual objects

It is very important to understand user needs and behaviours in order to adapt and improve VR products. To do so, systematic methods have been developed to evaluate and enhance usability issues:

- # Heuristic evaluation – includes methods and techniques of problem solving, learning and discovery based on experience.
- # Guerrilla testing – a fast and cheap method of capturing feedbacks that involves a user experience (UX) specialist asking questions about specific areas of application. What makes this testing unique is that participants are not engaged in advance.
- # In-person (test coordinator is physically in the same room as participants) and remote testing (via the internet)
- # VR analytics (numerical analytics that give data around particular actions – how many total views per scene, how many hotspots initiated, etc.) and heat maps (a visual representation of where users are looking)

In the context of a virtual, and in order to evaluate the realized environment, the following heuristics can be identified [13]:

- # Natural engagement – User – VE interaction should be as close as possible to the real world. The efficacy of this heuristic will depend on the need for naturalness and the sense of presence and engagement.
- # Compatibility with the task and domain – The behaviour of objects should correlate as closely as possible to the expectation of real objects.
- # Natural expression of action – The presence in the VE should allow the user to move and act in a natural way and not restrict usual physical actions. This characteristic may be restricted by the used device.
- # Close coordination of user action and representation – Response time between user action and update of the displayed situation should be less than 100–150 ms to avoid motion sickness problem (very individual value) [14].
- # Realistic feedback – The result of actions should be immediately visible and in accordance with the laws of physics and the user's expectations.
- # Realistic view of scenes – The visual look of the virtual scenes should match to the user's perception, and the viewpoint change (by head movement) should be rendered without delay.

- # Navigation and orientation possibilities – The users need to be able to know where they are currently and return to starting positions.
- # Clear entry and exit points – Entering and exiting ways (points) from a virtual world should be clearly explained.
- # Design compromises – In situations of design compromises, they should be consistent and clearly marked (e.g. power adjustments in navigation).
- # Learning abilities – Active objects should be marked and if necessary contain additional explanations to provide learning of VEs.
- # Clear turn-taking – Where system action occurs it should be clearly signalled and rules defined for turn-taking.
- # Sense of presence – The perception of engagement and moving in a virtual world should be as natural as possible [15].

GENERAL DEVELOPMENT PRINCIPLES

During the development phase, certain guidelines must be followed for the final product to be satisfactory and to pass the specific tests. These guidelines can be divided into five categories: compatibility, functionality, graphics and performance, security and user interaction.

- # *Compatibility* ensures that the application remains compatible with libraries and that the developer takes care of recommended hardware specifications.
- # *Functionality* ensures that the application works within actual standards. For example, single player games must be paused when the player takes off the head-mounted display (HMD) or returns to the menu. Also, the application must not draw frames or accept input. In addition, the player must not remain stuck in the application. For example, the login screen must have an option to create an account. If the application requires the Internet and it is not available, the user must be informed of that. The application must not lose recorded user data.
- # *Graphics and performance* are very important in VR applications. If the graphics is poor or the application is slow, it can be uncomfortable for the user and can feel nauseous. The application has to run at 60 fps (frames per second) constantly. Otherwise the user will feel uneasy. Also, the application must work without freezing and cracking. After starting, the scene must appear within several seconds, otherwise a loading screen should be provided. CPU and GPU (Central & Graphics Processing Unit) must be used most efficiently.
- # *Security* relates to the protection of privacy and the integrity of software and user data. The application

must require a minimum number of permissions to function. If some information is sent to an external service, the user must be informed about it.

- # *User interaction* must be in accordance with known standards. For example, Back and Home buttons must always do the same. If the application requires a controller, the user must be informed about that. If the controller is supported, the user must have the option to choose between controller and touch pad. Also, the application must detect whether the controller is on the left or right side.

DEVELOPMENT ENVIRONMENT

There are several ways to develop VR applications, so they can be divided into the following groups: native development, game development tools and web browsers.

- # Native development includes drivers and software libraries that are used in conjunction with an operating system, such as Win32 libraries for C++ applications and Java libraries for Android. VR devices have an SDK for platform-dependent development and interface to access device elements. There is a need to develop low-level elements, like rendering of graphics or physics within the environment. Native application development is the most flexible and optimized, but takes a lot of time especially if we want to cover a larger number of platforms. Because of this, most developers use completed development environments.

- # Game development tools serve as a middleware, which means they have implemented lower development elements. It is an integrated development environment (IDE), primarily for video game development, allowing creation of application using higher programming languages. Due to their characteristics, video game making tools have become the basis not only for video games but also for other types of 3D applications. The tool provides export to multiple platforms, has a built-in visualizer for 2D and 3D graphics, a drive to simulate basic physical laws, sound processing, embedded animation, artificial intelligence (AI), networking and more. The most famous commercial game engine tools for rapid application development are: Unity 3D (C#, Boo, UnityScript), Unreal Engine 4 (C++), CryEngine 3 (Lua), Blender (Windows, Mac OS, Linux), Unity 4 and 5 (C# Mono and JavaScript), Amazon Lumberyard (C++, Lua), CopperCube (JavaScript) and others. Most commercial tools can be downloaded for free for educational purposes or for the development of start-up projects. The companies behind specific tools give access to the source code to their users for a fee or for free. Regarding the open source solutions, there are:

libGDX (Java), Torque 3D, Urho3D (C++), OGRE (Open Source 3D Graphics Engine) and others. The source code for these tools can be downloaded from the GitHub platform.

- # Web browsers involve the development of multi-platform applications using HTML5, WebGL and JavaScript technologies [16]. An example is developing applications using the WebGL (web graphics libraries) based JavaScript 3D libraries Three.js or Babylon.js. VR-enabled web browsers are Google Chrome VR and Mozilla Firefox Nightly. Google and Mozilla joined resources on developing a new standard for VR called WebVR, whose JavaScript API allows access to a web browser through a VR device. In addition, there is a domain-specific language and an A-Frame tool for WebGL-based applications. It was written by Mozilla and is open source project.

GAME DEVELOPMENT

Due to the popularity of games among younger population, game development gradually takes up more space in the VR software domain. In order to achieve the best player effect, several criteria must be met during game development.

- (1) *Optimization* – There are various suggestions that can help optimize games. One of them is static batching. All objects in a scene that do not move can be marked as static and will then be plotted as a single object. It's even better if these objects use the same material, as each draw on the scene makes one draw call.

Good level design can significantly optimize the game. For example, if a player moves from room to room, it is not good to load all the rooms at the beginning, but to load them when the player enters. The downside is that more memory would then be used when loading each object. Therefore, it is best to separate the rooms by levels and load them asynchronously as needed from the code. Asynchronous level loading is very useful if the game has multiple levels. If the level is loaded classically (without asynchronous loading), the game will freeze until the next level is loaded.

Pre-rendering of light is very important not only in VR games. All static objects can be turned off real-time shadows and then pre-render the light. This creates a fixed texture with shadows that is rendered static (as an image) instead of "live" shadows that are drawn in each frame.

- (2) *Moving* – Moving is a very important factor that determines player's satisfaction. If there is some moving in the game, it must be as close to natural as possible. Otherwise, player feels nausea (VR disease). It occurs because the body of the player is static in the real world, while moving in the virtual world. It is best to avoid moving, unless it imitates the true moving of the player, as it may affect the vestibular system (balance system).

In classic one-person games, nausea often occurs, so it's best to avoid them. However, if the developer chooses this type of game, it is best to test the moving with as many users as possible. One solution to FPS (First-Person Shooter) play is to make constant static visual references such as the cockpit, cabin or interior of a car.

A popular method of moving is the fade / blinking eye transition. The player moves from one position to another by darkening the camera quickly to give the user only dark in front of their eyes. Then the camera moves to a new position and the dark colour disappears. This is one of the pleasant and easiest ways to move players.

(3) *Player interaction* – Depending on the VR model, the game itself, and the player's choice, controls can be made from the HMD or from the controller. Both the device and the controller have a touch pad that can be clicked or dragged. The drag is detected in four directions up (forward), down (back), left and right.

Some games also have gaze control that works as follows: when a player looks at an object that is predefined for interaction, a circle appears and fills up for a second or two (depends on the developer) and then registers as if it were a player clicked. If the player takes his eyes off the object while filling the circle, the circle is removed and the timer is reset.

(4) *User interface and experience (UI/UX)* – When creating a user interface for VR games, there are approaches to consider that are not used in classic games. There are four types of UIs commonly used: non-diegetic, diegetic, spatial and meta.

For ordinary non-VR games, the interface is all over the screen and is called HUD (Heads Up Display). It's a non-diegetic interface, an interface that is not within the world but makes sense for the player as a spectator of the game [17]. These are usually player energy, health, score, etc. The term diegetic is taken from the film industry where non-diegetic sound is background music in a movie or TV program and a diegetic sound would be some conversation. An example of a non-diegetic interface can be seen in the figure below.

A spatial or spatial user interface would be an interface located within the game world itself. This may be the main menu or some auxiliary menu in the game. With this interface it is very important to pay attention to the distance from the user. If it is too close, the user will strain their eyes, and if it is too far it will seem as if the focus is on the horizon. It is best to position the interface a few meters away from the user, and scale the images and text to be visible and easy to read.



Figure 1. Non-diegetic interface (insert from Horizon Zero Dawn)



Figure 2. Spatial interface (insert from Splinter Cell: Blacklist)

An alternative to a spatial interface is to place the interface elements in the environment itself – diegetic interface [18]. It can be a real clock on the wall, a TV, a computer, a mobile phone or even a screen on a futuristic rifle. An example of a diegetic user interface can be seen in the following figure – elements that follow an object in the scene. A good example is the energy of the enemy on stage.



Figure 3. Diegetic interface (insert from Steel Battalion)
Meta interfaces are similar to non-diegetic interfaces. Meta interface is the effect of displaying a scene that is not part of the VR world (e.g. change of colours if the user loses energy). A good example is Call of Duty

– there is no health bar, but when the player is low on health, the screen would be overlay with blood to show that he is wounded. Meta UIs are usually represented two dimensionally.

All these types of UIs can also be combined in same game.

USABILITY TESTING OF VR APPLICATIONS

Usability is a quality attribute that indicates the ease of use of a certain application. Usability tests consist of short sessions where participants interact with the application on a specific environment, while an expert team observes, records and measures the course of that interaction. In VR domain, the essence of this is session-based exploratory testing, i.e. exploring through the application in order to find and achieve what was planned, in a fixed time period [19]. Usability tests should be performed at the right time – when the prototypes and the application are finished. It is highly recommended that the testers perform a heuristic test before the users are given the devices. The reason is that there are many issues that can be detected in this phase and fixed before the usability test [20].

For testing purposes, two factors can be identified:

—Participants – A reasonable number of test participants is at least five. This enables to get a collection of different opinions. The profile of the user has to match the target audience of the application. It is important to know the skills, VR experience and the interests of the potential participants. Different levels of expertise can be required for making the session more interesting and effective.

—Technical assumptions – It is necessary to have technical equipments like headsets and adequate devices to generate virtual reality of satisfactory quality.

Minimal hardware assumptions:

Accessories – controllers, earphones

Computer (recommended requirements): Intel i5–4590 (equivalent or greater), NVIDIA GTX 970 or AMD R9 2900 (or greater), 8 GB RAM (or more), HDMI 1.3 and 3x USB 3.0 plus 1x USB 2.0, Windows 7 64-bit (or greater)

Headset (supported by computer) Oculus Rift, HTC Vive (PC/Mac), console (PlayStation VR (PS4)) or smartphone (Google (Android/iOS), Samsung Gear VR)

As for the application, there are some general aspects to pay attention when testing (test criteria):

User interaction with the VR interface – Moving across different spaces inside the application.

Execution of flows – Test the application for what is not supposed to do (analysis of border cases in order to maximize coverage), ensure every requirement is covered.

Functionality works expectedly – Isolation from the real world, real world does not interrupt the experience, immersion is achieved completely (360-degree view, user feels sensations).

CONCLUSIONS

In the future, it can be expected that VR will continue to evolve primarily because of the great interest of companies and the user community. Virtual and augmented reality devices are popular among VR developers. Big companies are currently controlling the VR technology market. Applications are most accessible on desktop and mobile devices. The WebVR and UI/UX standards are being actively developed. New interdisciplinary fields have been created that link VR with education, medicine, film, construction, sales and the automotive industry. VR applications can be developed using popular programming languages and tools that do not require significant financial investment from the users. The ability to develop different types of VR applications can lead to major changes in the implementation of information technology. Applying best practices and standards can lead to a quality VR experience.

VR games are very popular form of software. In the course of their development, in addition to the general ones, more criteria need to be met in order to achieve fully immersive experiences. For this it is also necessary to fulfil demanding hardware and software assumptions, as well as specific testing methodology.

Literature

- [1] T. Parisi: Learning Virtual Reality, O'Reilly Media, 2015
- [2] P. Tiefenbacher, N.H. Lehment, G. Rigoll: Augmented Reality Evaluation: A Concept Utilizing Virtual Reality, International Conference on Virtual, Augmented and Mixed Reality VAMR 2014, pp. 226–236.
- [3] A. Amer, P. Peralez: Affordable Altered Perspectives Making Augmented and Virtual Reality Technology Accessible, Global Humanitarian Technology Conference (GHTC) IEEE, 2014
- [4] R. Azuma: A survey of augmented reality, Presence 6(4), 1997, pp. 355–385.
- [5] T. Mazuryk, M. Gervautz: Virtual reality history, applications, technology and future, Technical Report TR-186-2-96-06, 1996
- [6] B. Cowan, B. Kapralos: An Overview of Serious Game Engines and Frameworks, Recent Advances in Technologies for Inclusive Well-Being, Volume 119, Series Intelligent Systems Reference Library, February 2017, pp. 15–38.
- [7] C. Cruz-Neira, M. Fernandez, C. Portales: Virtual Reality and Games, Multimodal Technologies and Interaction, 2018
- [8] M. Lanham: Augmented Reality Game Development, Packt Publishing, 2017
- [9] P. Bouvier, F. De Sorbier, P. Chaudeyrac, V. Biri: Cross-benefits between virtual reality and games,

- Computer Games Multimedia and Allied Technology Conference, 2008
- [10] K.M. Stanney, R.R. Mourant, R.S. Kennedy: Human Factors Issues in Virtual Environments: A Review of the Literature, Presence, Vol. 7, No. 4, August 1998, pp. 327–351.
- [11] E. Ragan, C. Wilkes, D.A. Bowman, T. Hollerer: Simulation of augmented reality systems in purely virtual environments, In: Proc. VR, IEEE, 2009, pp. 287–288.
- [12] T. Marsh: Evaluation of virtual reality systems for usability, Proceeding CHI '99, Extended Abstracts on Human Factors in Computing Systems, pp. 61–62.
- [13] A. Sutcliffe, B. Gault: Heuristic evaluation of virtual reality applications, Interacting with Computers 16, 2004, Elsevier, pp. 831–849.
- [14] K. Norman: Evaluation of Virtual Reality Games: Simulator Sickness and Human Factors, GHItaly@AVI, 2018
- [15] A. Sutcliffe, K.D. Kaur: Evaluating the usability of virtual reality user interfaces, Behaviour and Information Technology, 19(6), November 2000, pp. 415 – 426.
- [16] T. Pant, S. Neelakantam: Learning Web-based Virtual Reality: Build and Deploy Web-based Virtual Reality Technology, Apress, 2017
- [17] I. Iacovides, A.L. Cox, R. Kennedy, P. Cairns: Removing the HUD: The impact of non-diegetic game elements and expertise on player involvement, Conference: 2015 Annual Symposium on Computer-Human Interaction in Play (CHI PLAY '15), 2015
- [18] P. Salomoni, C. Prandi, M. Rocchetti, L. Casanova, L. Marchetti, G. Marfia: Diegetic user interfaces for virtual environments with HMDs: a user experience study with Oculus Rift, Journal on Multimodal User Interfaces, January 2017, pp. 1 – 12.
- [19] BlazeMeter,
<https://www.blazemeter.com/blog/user-testing-of-virtual-reality-applications/>
- [20] P. Dias, A. Pimentel, C. Ferreira, F. van Huussen, J.–W. Baggerman, P. van der Horst, J. Madeira, R. Bidarra, B.S. Santos: Usability in virtual and augmented environments: A qualitative and quantitative study, Proceedings of SPIE – The International Society for Optical Engineering, 2007



ACTA TECHNICA CORVINIENSIS – Bulletin of Engineering
ISSN: 2067-3809
copyright © University POLITEHNICA Timisoara,
Faculty of Engineering Hunedoara,
5, Revolutiei, 331128, Hunedoara, ROMANIA
<http://acta.fih.upt.ro>

Fascicule 3

[July – September]

t o m e

[2020] XIII

ACTA Technica CORVINIENSIS
BULLETIN OF ENGINEERING



ACTA TECHNICA CORVINIENSIS – Bulletin of Engineering
ISSN: 2067-3809

copyright © University POLITEHNICA Timisoara,
Faculty of Engineering Hunedoara,
5, Revolutiei, 331128, Hunedoara, ROMANIA
<http://acta.fih.upt.ro>

¹D.A. KAMBLE, ²Nihal SHAIKH

DESIGN AND DEVELOPMENT OF SEAT (SOLDIER) AGAINST MINE BLAST IMPACT

¹Faculty Vishwakarma Institute of Information Technology Pune, INDIA

²Postgraduate Research scholar Vishwakarma Institute of Information Technology Pune, INDIA

Abstract: Explosive devices are serious threats for armoured vehicles and occupants. Following detonation of a high explosive, blast loads, which are transferred through shock waves to the vehicle hull, might potentially cause severe injuries on the body parts. The soldiers are extensively exposed to the opponent's activities while the troop carriers in service more and more frequently do not provide sufficient protection of the crew. The detonation of these threats creates high intensity blast waves that were transmitted to the occupant through vehicle structures and seats. Minimizing the occupant's casualty can be achieved by properly dissipating the shock waves exerted to the vehicle. The aim of this study was to verify the mine blast resistance of the prototype wheeled vehicle according to STANG 4569 as well as various position of seats and TNT blast. The study was contribute to the understanding of numerical simulation for dynamic response of human dummies seated in armoured vehicles subjected to land mine by comparing the performance of Hybrid-III 50th percentile ATD in numerical simulation with that of the standard set by NATO (USA) organization. Therefore, force and acceleration data were collected from critical body parts; tibia, pelvis, lumber spine, upper neck, and head of the mannequin in blast testing. The numerical simulations were performed in LS-DYNA using SPH blast loading method. The study used a model of the body of a soldier in the form of a Hybrid III 50th Dummy. From the results it was found that the seating position and charge position plays a significant role in reduction of the shock response towards the finite element dummy model.

Keywords: LS-DYNA, TNT, Blast Loading, Occupant Safety, Hybrid-III Anthropomorphic Test Device, Seating Position, Charge Position, SPH Method

INTRODUCTION

Typical land mines weights approximately 6 kg and during its detonation, the explosive releases large impulses that could deform and its shrapnel can penetrate the vehicle structures. The impulse generated from the explosion transfers to the occupant through mediums that are connected to the occupants such as the floor sections and seats. This type loading must be attenuated to a certain value and if failed, fatalities may occur to occupants.

The factors that can be used to attenuate the shock waves are studied. The three factors studies are the finite element dummy model seating height, explosive weight placement and the Hopkinson-Cranz blast scaling. First, a capsule was designed for the dummy placement [1]. Improvised Explosive Devices (IEDs), along with other types of roadside bombs and trinitrotoluene charge explosion (TNT) have accounted for over 60% of American combat casualties in Iraq.

In Afghanistan, the numbers are worse, with explosives accounting for 77% of field injuries and IEDs specifically accounting for 38% of all injuries and 32% of death [3]. Undercarriage landmine blast cause a significant threat to occupant safety in armoured personnel carriers. The blast wave interaction with armoured plates in the undercarriage is an important factor in the design process. Experimental studies provide valuable insight to the performance of armoured vehicles subjected to landmine blast. Some measures of performance

include the resistance of the undercarriage against tearing of the armour plates, failure of the structural welds, and high accelerations of the footrest plate used by the occupants. Landmine blast experiments that involve the testing of the full vehicle are costly and time consuming, while numerical simulations provide a faster alternative to measure the vehicle performance under blast loads.



Figure 1. Acceleration and Pressure measurement of critical part of human body

The blast resistant under carriage armour design is an iterative process that is shaped by the successive use of numerical simulations. There are two major approaches for modelling blast loads.

The first approach involves the use of empirical equations obtained from blast experiments. This is referred to as the CONWEP method (CONventional

WEaPons). This technique is suitable for simulating structural members directly exposed to the blast wave, without any obstructions or shadowing effects.

The second approach is the Smooth Particle Hydrodynamic (SPH) technique that requires the modelling of the surrounding air with a volumetric mesh around the target structure. It allows the application of the Navier Stokes fluid dynamics equations for simulating the blast wave propagation. Mine blast testing of armoured vehicles provides valuable insight into dynamic response of the body hull and makes possible to reveal weaknesses and strengths of the main structure under blast loading. According to NATO AEP-55 standardization agreement, vehicle integrity shall be protected and injury level of occupant inside the vehicle should be no more than the given values for specific points on human body in a blast test. For this purpose, mannequins are utilized to do the occupant safety evaluation in both blast testing and numerical simulations.

While some research has been carried out on the blast mitigating systems for armoured vehicles, there is very little scientific understanding of responses of occupants in vehicles under blast loading [5]. The research was carried out to verify explosion resistance over a prototype vehicle LBPV (Light Bullet Proof Vehicle) class in accordance with the level STANAG 4569. The second priority was to identify the load in the most injury-endangered parts of the body, e.g. tibia, pelvis, lumber spine, upper neck, and head of the soldier.

The principal aim of this paper is to contribute to the understanding of numerical simulation for dynamic response of human dummies seated in armoured vehicles subjected to land mine. Many techniques and materials have been proposed in the literature to mitigate the blast pressure and energy, but only two techniques are predominantly used at present for minimising the acceleration imparted to the vehicle compartments resulting from explosion of land mines. In the first, the occupants are separated from the vehicle floor using roof hanging and wall mounted seats. In second, specially designed energy absorbing seats, circular tubes, square tubes, frusta, struts, honeycombs, and sandwich plates are used to decrease the loads acting on the occupants.

Some other techniques such as the thin walled cylinder, upward convex hull and polyurea coating were also reported for mitigating the acceleration but no experimental study has been reported on acceleration mitigation using foam. The charge was placed at various position and checked the effect on the crew seated on seat.

LITERATURE REVIEW

Khalis S. et al. [1] Described that Explosion from an anti-tank mines or improvised explosive devices are

recognized as one of the lethal threat towards occupants inside an armored vehicle. In this paper, three factors such as occupant seating height, charge weight placement and the Hopkinson-Cran z blast scaling were studied using numerical simulations. Design of experiment (DOE) was utilized to determine the ranks and interactions between each factor from the most influential on the results to the least affects towards the results. From the results it was found that the seating position plays a significant role in reduction of the shock response towards the finite element dummy model.

Adam M. et al. [3] with casualties mounting overseas due to Improvised Explosive Devices (IEDs) and other roadside bombs, improving the safety of armoured vehicles for service personnel overseas is of paramount importance. The hypothesis is that through the manipulation of the mass ratio, stiffness and damping properties of a dual-hull system, the safety of current Mine Resistant Ambush Protected (MRAP) vehicles can be greatly improved.

The results show that, in comparison to the standard single-hull vehicle, the dual-hull vehicle reduces head injury criteria by 95.7%, neck compression by 78.3%, chest acceleration by 97.5% and leg forces by an average of 97%. Further work should focus on developing a realistic structural interface between the hulls and evaluating it using simulation, followed by fabrication and testing of limited test articles and full-vehicle systems.

Edyta K. et al. [4] studied to elaborate identification method of crew overload as a result of trinitrotoluene charge explosion under the military wheeled vehicle. The aim of this research was to verify the mine blast resistance of the prototype wheeled vehicle according to STANG 4569 as well as the anti-explosive seat. Within the work, the original methodology was elaborated along with a prototype research statement. This article presents some results of the experimental research, thanks to which there is a possibility to estimate the crew's lives being endangered in an explosion through the measurement of acceleration as well as the pressure on the chest, head and internal organs.

Atil E. et al. [5] described that Explosive devices are serious threats for armored vehicles and occupants. The objective of this paper is to contribute to the understanding of numerical simulation for dynamic response of human dummies seated in armored vehicles subjected to land mine by comparing the performance of Hybrid-III 50th percentile ATD in numerical simulation with that of full-scale blast testing.

Therefore, force and acceleration data were collected from critical body parts; tibia, pelvis, lumber spine, upper neck, and head of the mannequin in blast testing. Those data were compared with numerical

simulation results. The numerical simulations were performed in LS-DYNA using CONWEP blast loading method. It was found that the numerical simulation results are in accord with those obtained from blast testing.

Steps adopted in modelling

- (1) Acceleration in response to blasts originating from the bottom of Mine-Resistant Ambush-Protected (MRAP) vehicles must be lessened if there is to be any useful change to protect vehicle's occupants.
- (2) We had assembled these seat to the floor, side wall and hanging to the roof of the vehicle. Also in this study we vary the position of the mine blast along with varying weight of ammunition like 6 Kg, 10 Kg, 20Kg, 40Kg TNT etc.
- (3) In the numerical tests, there was determined behaviour of the carrier structure and tests dummies during explosion of an explosive charge placed on the bottom side of the vehicle.
- (4) A hemispherical shape of a charge was adopted for calculations. Due to a significant distance of the charge from the vehicle as well as simple geometry of the carrier side, `LOAD_BLAST_ENHANCED` procedure implemented in LS-DYNA system was used to generate a pressure wave representing the structure loading.
- (5) The analysis will be carried on LS-DYNA V-R11.0 (SPH) with CONWEP method.
- (6) We have to optimize best arrangement of seat structure with minimum shock to the soldier body.

METHODOLOGY ADOPTED FOR ANALYSIS

—Modelling of vehicle

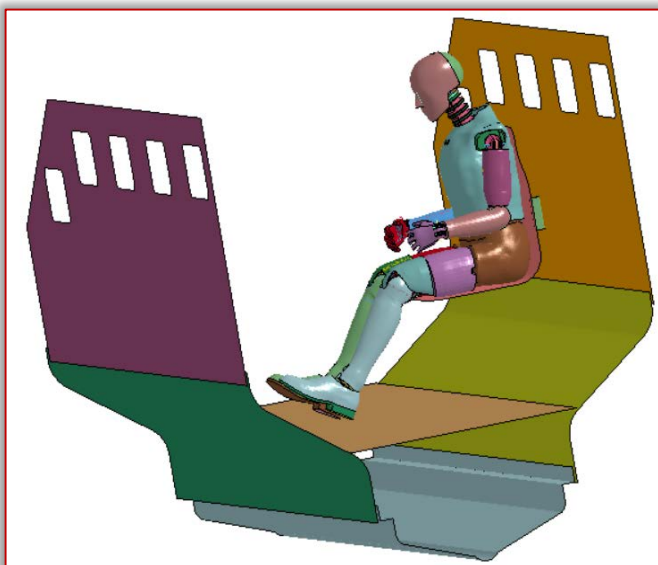


Figure 2. Modelling of Vehicle

—Blast Loading Method and Conditions

The detonation of an explosive charge releases blast energy resulting in disturbances in the surrounding

air, which grows into a blast wave system led by a shock front. This physical phenomenon can be simulated through two essential techniques in the commercial finite element method, LS-DYNA; CONWEP and Smoothed Particle Hydrodynamic (SPH). The first method calculates conventional blast loading effects on structures from the equations and curves.

To adequately collect force and acceleration data from body members of the Hybrid III dummy inside the vehicle subjected to land mine explosion, the calculation should continue at least 200 milliseconds. For TNT, Hemispherical Shape was used. The radius of TNT was 25 mm and placed 300 mm below hull.

—Finite Element modelling

Finite element model involves vehicle body, hull and power pack components as well as structural parts and seat mechanism. Hull plates and hull subsystem parts were modelled using BelytschoTsay shell elements with two integration points.

Seat mechanism consists of seat frame, seat belts, cushion, and main plate tension apparatus. Seat frame, belts and tension apparatus were modelled with shell formulation, while cushion was generated using hexahedral solid elements.

The entire model consists of 339,638 shell elements and 62,178 solid elements. LSTC's rigid Hybrid-III 50th percentile dummy was preferred as a mannequin due to its compatibility with blast simulation models. Figure 5 illustrates finite element modelling details of the entire vehicle and Hybrid III test dummy as well as detonation point.



Figure 3. Hybrid-III 50th percentile dummy

—Material Model

Energy absorbing capability is a fundamental property of a cushion material. The fact that cushion could absorb respectable shock energy, which is transmitted from structural parts of vehicle to the seat mechanism during mine blast has a direct impact on the magnitudes of the acceleration and force acting on the human body.

In the experiment, the ability of cushion in absorbing energy is obtained by measuring hysteresis, which is demonstrated by the area between load deformation curves for loading and unloading conditions through MAT_FOAM keyword function.

The TNT equivalence may depend on a number of parameters such as charge size, scaled distance, detonation speed, Chapman-Jouguet pressure; and for a given explosive the pressure and the impulse calculations may require different TNT equivalence values.

Therefore, it is difficult to handle non-TNT types of explosives with the CONWEP approach. In contrast, the SPH method allows the adjustment of material properties and the equation of state parameters for various non-TNT explosives. The keyword for TNT is HIGH_EXPLOSIVE_BURN.

The material model was used for the armour and mild steel structures in the vehicle model by activating *MAT_PIECEWISE_LINEAR_PLASTICITY material function.

— **Contact Algorithm**

*CONTACT_AUTOMATIC_NODE_TO_SURFACE function was assigned for the contact between Hull of the vehicle and blast wave. *CONTACT_AUTOMATIC_GENERAL function was thus selected for the contact between seat components and human dummy. Another possible contact interference might take place between seat frame and cushion. To prevent this, *CONTACT_NODES_TO_SURFACE keyword function was adopted. Also contact between various parts of vehicle structure used as *CONTACT_TIED_SURFACE_TO_SURFACE.

— **High Explosive (EOS)**

The evaluation of the explosive after ignition is described by the Jones-Wilkins-Lee (JWL) equation of state, defined with the keyword *EOS_JWL in the LS-Dynacode. The JWL equation of state defines the pressure as a function of the relative volume V and initial internal energy per volume E0 as given in (2)

$$p = A[1 - W / (R1 * V)] * e^{-(R1 * V)} + B[1 - W / (R2 * V)] * e^{-(R2 * V)} + [(W * E0) / V]$$

The input parameters are represented by A, B, R1, R2, W, and E0. A and B have dimensions of pressure, while the dimensionless parameters are R1, R2, and W. E0 represents the initial internal energy.

The volumetric ratio is expressed by $V = (v / v_0)$, where v_0 is the initial volume. The exponential terms are the high-pressures small-volume terms, and usually the user chooses $R1, R2 \sim = 4$ to make the two terms important indifferent regions.

Table 1. JWL equation of state parameters for TNT

ρ_0 (kg/m ³)	D (m/s)	PCJ (GPa)	E0/V (GPa)	
1630	6930	21.0	7.0	
A (GPa)	B (GPa)	R1	R2	W
371.213	3.231	4.15	0.95	0.3

— **Boundary and loading conditions**

There are no constraints, because in the event of blast the vehicle is globally displaced. Only condition is that the vehicle is blasted against gravity/self-weight of the vehicle, so gravity is included.

The unladed weight of the vehicle is 4000 kg and along with load it will goes to 5000 kg. It is applied at centre of gravity of the vehicle along with gravity.

The loading curve is deduced for the loading caused by the blast of 6 kg TNT charge as per STANAG 4569 Level II.

The transient load of duration of few milliseconds due to the blast of the charge.

— **Convergence Study**

Analyses were carried out for different element sizes by gradually increasing the number of elements until convergence occurs. Convergence was found to occur at around 4,00,000 elements as shown in Figure 4. Sizing of the element is decided based on possible high stress locations.

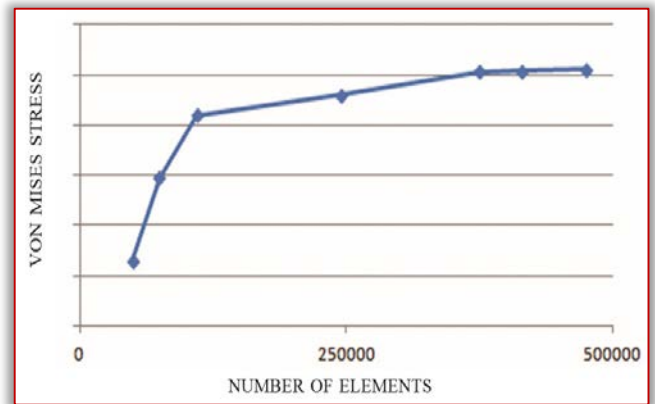


Figure 4. Mesh Convergence study

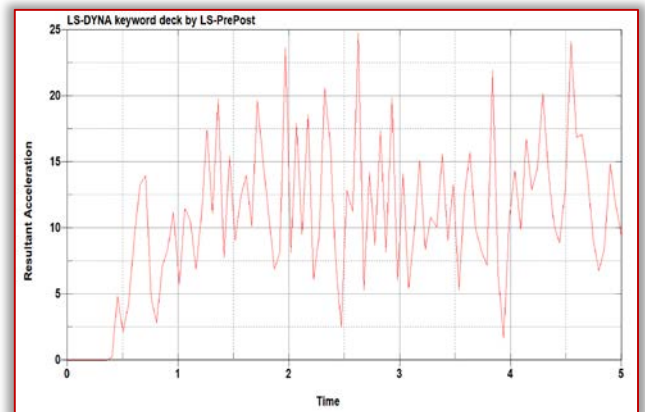


Figure 5. Nodal acceleration at seat

A great deal of attention is given to those components that are located between the inner and the outer vehicle floor. These components reduce the impact by their vary mass.

The finite element model of the armoured vehicle and hinges are modelled with shell element.

CONCLUSION & DISCUSSIONS

A number of approaches to the numerical assessment of the influence on the occupant of a vehicle under a mine blast have been shown in this report. A numerical simulation of a finite element dummy response when subjected to blast loading was modelled and verified.

The result shows that the position of blast and arrangement of seat greater impact on dummy. The interaction between two factors that is significant to the simulation results are the interaction between seating arrangement and charge position factors. Identifying these significant factors is important so that any improvement to reduce the blast acceleration could be done according to these factors and the improvement would yield better results.

References

- [1] Khalis Suhaimi, M.S. Risby, K.S. Tan, Victor Feisal Knight. “Simulation on the shock response of vehicle occupant subjected to underbelly blast loading”, in The International Conference on Computational Science, 2014.
- [2] Edyta Krzystała, Arkadiusz Mężyk, Sławomir Kciuk. “Minimisation of the explosion shock wave load onto the occupants inside the vehicle during trinitrotoluene charge blast”, in International Journal of Injury Control and Safety Promotion, 2014.
- [3] Atıl Erdik, “Investigation of dynamic response of a mannequin in a vehicle exposed to land mine blast”, in Sakarya University Journal of Science, 2019.
- [4] Zdzisław Hryciów, Grzegorz Sławiński. “Investigation of armoured personnel carrier crew subjected to impact load”, in AIP Conference Proceedings, 2019.
- [5] Agnieszka Mackiewicz, Grzegorz Sławiński, Tadeusz Niezgoda, Romuald Będziński. “Numerical analysis of the risk of neck injuries caused by ied explosion under the vehicle in military environments”, 2016.
- [6] Inderpal Singh Sandhu, Murugan Thangadurai, Prashant S. Alegaonkar, D.R. Saroha. “Mitigation of blast induced acceleration using open cell natural rubber and synthetic foam”, in Defence Science Journal, Vol. 69, 2019.
- [7] A. Erdik, S. A. Kilic1, N. Kilic, S. Bedir. “Numerical simulation of armored vehicles subjected to undercarriage landmine blasts”, 2015.
- [8] Alon Brill, Boaz Cohen, Paul A. Du Boi. “Simulation of a mine blast effect on the occupants of an APC”, in 6th European LS-DYNA Users’ Conference.
- [9] Sanjit Mahajan, R. Muralidharan. “Simulation of an armoured vehicle for blast loading”, in Defence Science Journal, Vol. 67, 2017.



ACTA TECHNICA CORVINIENSIS – Bulletin of Engineering
ISSN: 2067-3809
copyright © University POLITEHNICA Timisoara,
Faculty of Engineering Hunedoara,
5, Revolutiei, 331128, Hunedoara, ROMANIA
<http://acta.fih.upt.ro>

Fascicule 3

[July – September]

t o m e

[2020] XIII

ACTA Technica **CORVINIENSIS**
BULLETIN OF ENGINEERING



ACTA TECHNICA CORVINIENSIS – Bulletin of Engineering

ISSN: 2067-3809

copyright © University POLITEHNICA Timisoara,

Faculty of Engineering Hunedoara,

5, Revolutiei, 331128, Hunedoara, ROMANIA

<http://acta.fih.upt.ro>

¹Zoran PANDILOV

OPTIMIZING THE CONTOURING ACCURACY OF CNC MILLING MACHINE WITH DOUBLE BALL BAR TEST

¹Institute of Production Engineering and Management, Faculty of Mechanical Engineering, SS. Cyril and Methodius University in Skopje, Skopje, Republic of MACEDONIA

Abstract: In recent years, an instrumentation circular profile tests has been specified to assess the contouring accuracy of CNC machine tools. Such an instrumentation type test is the Double Ball Bar (DBB) test. In this paper, the influence of the position loop gain and mismatch of position loop gains for different machine axes are effectively studied. This work outlines a practical procedure for determining the position loop gain of the control system in order to minimize the resulting contouring errors.

Keywords: contouring accuracy, CNC machine, Double Ball Bar (DBB) test

INTRODUCTION

The contouring performance of CNC machine tool can be established by assessing its ability to move along a specified profile by the simultaneous movement of two or more axes.

When CNC machine tools are used for contouring applications, especially where high feed rates are used, significant dynamic errors can be introduced by the characteristics of the CNC controller and servo feed drive system. The assessment of such dynamic errors in CNC machines has traditionally been undertaken by machining a standard circular test piece. Such a test piece is outlined in some of the national machine tool standards American [1], British [2], where the circular profile is produced by the simultaneous motion of two linear axes.

An alternative approach to the machining test, specified in British and US machine tool standards, is emulation by instrumentation techniques of the circle test ISO 230-4 [3].

Such an instrument type test is Double Ball Bar (DBB) test. Bryan [4] first developed the Double Ball Bar (DBB) method to inspect CNC machines contouring behavior.

Although instrumentation techniques generally check the machine in no-load condition, they offer certain advantages over cutting conditions. In particular, tools and test specimens are not consumed and the time consumed in metrologising the test piece after machining is eliminated.

THE CONTISURE DOUBLE BALL BAR (DBB) HARDWARE AND SOFTWARE SYSTEM

On the market there are several commercially available Double Ball Bar (DBB) systems. The CONTISURE Double Ball Bar (DBB) system is developed by Burdekin [5,6].

The CONTISURE Double Ball Bar (DBB) system is shown schematically in figure 1.

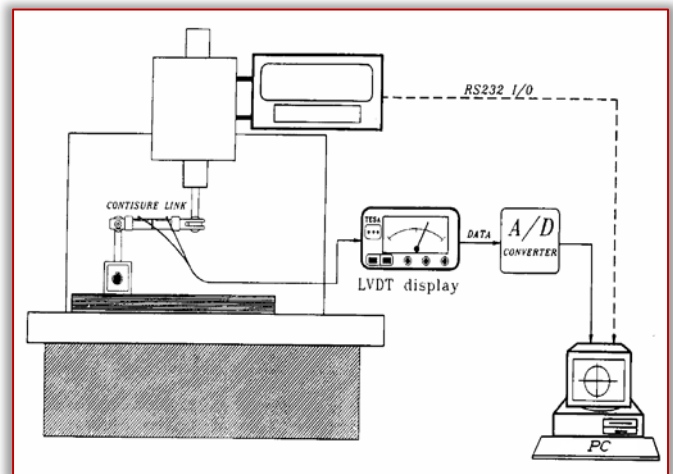


Figure 1. CONTISURE Double Ball Bar (DBB) system hardware set-up on CNC milling machine

The system comprises two high precision reference spheres, rigidly mounted at the spindle and table positions. A transducer link of carbon fiber construction and containing two precision transducers is located kinematically between the two reference spheres.

These two transducers contact directly onto the two spheres, and the summation of their outputs represents the change in distance of the two reference spheres, as the machine performs a circular contouring operation. The absolute distance between the two spheres can be established by setting the transducer link against a calibrated setting block. This feature, which is unique to the CONTISURE Double Ball Bar (DBB) system, ensures the complete traceability of data to be maintained.

The data acquisition and analysis software offer the user a complete flexibility. The number of sampled data points can be selected, up to a maximum of 12000 per 360 degrees scan. An analysis in the form of least squares best fit circles, can also be performed on data obtained for 360 degrees scans as well as for partial arcs. This feature eliminates the need for

precise set-up of the sphere datum with respect to the programmed circle.

It is also essential that the start and end points of the circular contour should be selected, so that these do not coincide with the axis reversal points. The reason for this is that significant lost motion errors may occur at these points, and additional transients errors, resulting from the servo control system, may not be detected. In this respect the software is completely flexible and enables the start and end points to be freely selected. A start position of 22 degrees from the X-axis was therefore used for all tests.

The approach to the start point of the circular profile should, if possible, be representative of that used under practical machining conditions. The software therefore assumes a tangential approach to the start and exit points on the profile.

INFLUENCE OF THE POSITION LOOP GAIN AND MISMATCH OF THE POSITION LOOP GAINS FOR DIFFERENT MACHINE AXES ON OPTIMIZING THE CONTOURING ACCURACY OF CNC MILLING MACHINE

One of the most important factors which influences the dynamical behavior of the feed drives for CNC machine tools is position loop gain or Kv factor. Tracking or following error depends on the magnitude of the Kv-factor. In multi-axis contouring the following errors along the different axes may cause form deviations of the machined contours. Generally, position loop gain Kv should be high for faster system response and higher accuracy, but the maximum allowable gains are limited due to undesirable oscillatory responses at high gains and low damping factor which produce significant transient errors and accuracy started to decrease again. Usually Kv factor is set up by the machine tool manufacturer

But the question is whether the set-up value of the Kv-factor is always optimal? Generally, contouring error of circular contour, according [7-12], could be analytically approximately calculated with following equations:

$$ec = \left| R \cdot \left[1 - \sqrt{1 + \frac{1}{2} \cdot \left(\frac{v}{60 \cdot R \cdot Kv} \right)^2} \right] \left[1 + \frac{1}{(1-a)^2} - \frac{60 \cdot a \cdot R \cdot Kv}{v \cdot (1-a)} \right] \right| \cdot 10^3 \mu\text{m} \quad (1)$$

where: ec-maximal contouring error from the nominal radius μm , R-radius of the circle mm, v-feed rate mm/min, Kv-position loop gain s^{-1} , a-mismatch of position loop gains for different machine axes ($a = (Kvx - Kvy) / Kvx$ and $Kvx = Kv$, Kvx -X axis position loop gain s^{-1} , Kvy -Y axis position loop gain s^{-1}).

If $Kvx = Kvy$, $a = 0$ and equation (1) is transformed in:

$$ec = \left| R \cdot \left[1 - \sqrt{1 + \left(\frac{v}{60 \cdot R \cdot Kv} \right)^2} \right] \right| \cdot 10^3 \mu\text{m} \quad (2)$$

Similar equations are given in [13,14]. These equations do not take into consideration the influence of nonlinear phenomena, such as lost motion, stick motion and stick-slip, etc. on the magnitude of the contouring errors [15,16,17,18,19,20], which can cause a significant difference between theoretically calculated and experimentally obtained results (see table 1 and table 2).

Experimental contouring measurements with CONTISURE Double Ball Bar (DBB) test equipment have been undertaken on a FGS32 CNC milling machine with HEIDENHANN 355 TNC controller, in order to illustrate a methodology which could generally be applied to any CNC machine. Only two sets of axes have been considered (X and Y). The same procedure can be repeated for other axes. A relatively short link of 150 mm was used for all tests.

In the tests the feedrate was constant $v = 600 \text{ mm/min}$, radius of the circle was $R = 150 \text{ mm}$, mismatch of position loop gains for different machine axes was $a = 0$ and the Kv factor in the controller was changed in the range of 4 s^{-1} to 130 s^{-1} . The tests were done in two directions clockwise (CW) and counterclockwise (anticlockwise) (CCW). The results of tests are given in table 1.

From Table 1 it is obvious that optimal experimental value for Kv factor is 100 s^{-1} . Kv factor set up by the machine manufacturer, was 28.3 s^{-1} .

We can see that increasing position loop gain Kv in the range of 4 to 100 s^{-1} decreases maximal contour deviation from nominal radius. Also we can see that the values for Kv in the range of 110 to 130 s^{-1} increase contouring error. This can be explained by the fact that transient errors become dominant. Further analyses shows that with increasing the position loop gain from 28.3 to 100 s^{-1} the maximal contouring deviation decreases from 19.6 (CW)/22.2 (CCW) μm to 10.2 (CW)/10.2 (CCW) μm . Figures 2-5 show graphically some results of the experiments. In reference [21-23] an analytical equation for estimating position loop gain Kv is given:

$$Kv = \frac{1}{4D^2 \cdot \left(\frac{2D_e}{\omega_e} + \frac{2D_m}{\omega_m} + \frac{T}{2} \right)} \quad (3)$$

where D-position loop damping, ω_e -nominal angular frequency of the feed drive electrical parts s^{-1} , D_e -damping of the feed drive electrical parts, ω_m -nominal angular frequency of the mechanical transmission elements s^{-1} , D_m -damping of the

mechanical transmission elements and T-sampling period s.

Table 1. Influence of the position loop gain Kv on the magnitude of maximal contouring error from the nominal radius

Kv s ⁻¹	4	6	8	10
ec μm (CW) experimentally	46.8	39.5	38.3	32.2
ec μm (CCW) experimentally	50.7	45.5	37.5	35.2
ec μm analytically with eq. (2)	20.8	9.26	5.21	3.33
Kv s ⁻¹	20	28.3	30	40
ec μm (CW) experimentally	20.7	19.6	16.5	14.7
ec μm (CCW) experimentally	25.2	22.2	20.3	17.8
ec μm analytically with eq. (2)	0.83	0.42	0.37	0.21
Kv s ⁻¹	50	60	70	80
ec μm (CW) experimentally	13.6	12.1	11.1	10.8
ec μm (CCW) experimentally	13.3	12.4	10.8	10.7
ec μm analytically with eq. (2)	0.13	0.09	0.07	0.05
Kv s ⁻¹	90	100	110	120
ec μm (CW) experimentally	10.5	10.2	10.3	10.4
ec μm (CCW) experimentally	10.4	10.2	10.4	10.5
ec μm analytically with eq. (2)	0.04	0.033	0.028	0.023
Kv s ⁻¹	130			
ec μm (CW) experimentally	10.5			
ec μm (CCW) experimentally	10.6			
ec μm analytically with eq. (2)	0.02			

Position loop damping of $D=0.707$ is preferable according [24-31]. That is the value, which gives minimal contouring errors. Other numerical values of the examined system are: $\omega_e=1000\text{ s}^{-1}$, $D_e=0.7$, $\omega_m=663\text{ s}^{-1}$, $D_m=0.17$, and $T=0.006\text{ s}$. With the substitution in the equation (3) the position loop gain value $Kv=106.35\text{ s}^{-1}$ is calculated.

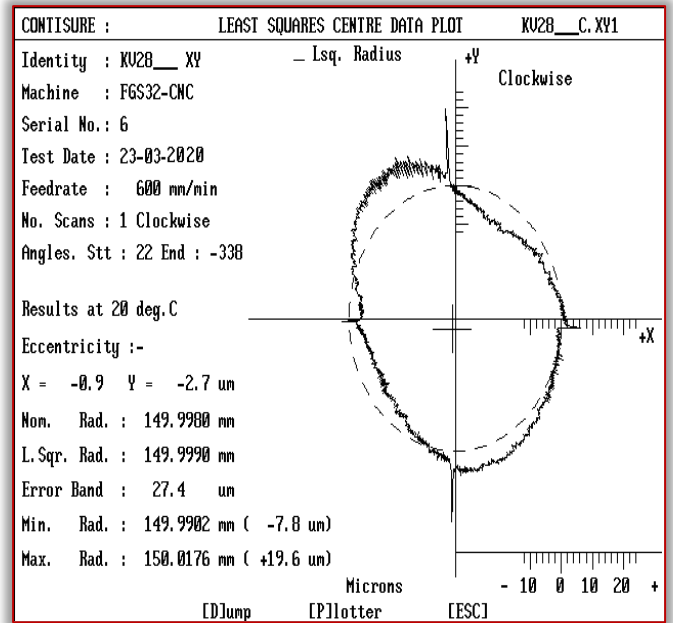


Figure 2. Polar diagram of the results of a measured circular test (feedrate $v=600\text{ mm/min}$, radius of the circle $R=150\text{ mm}$, position loop gain $Kv=28.3\text{ s}^{-1}$, $a=0$, clockwise direction).

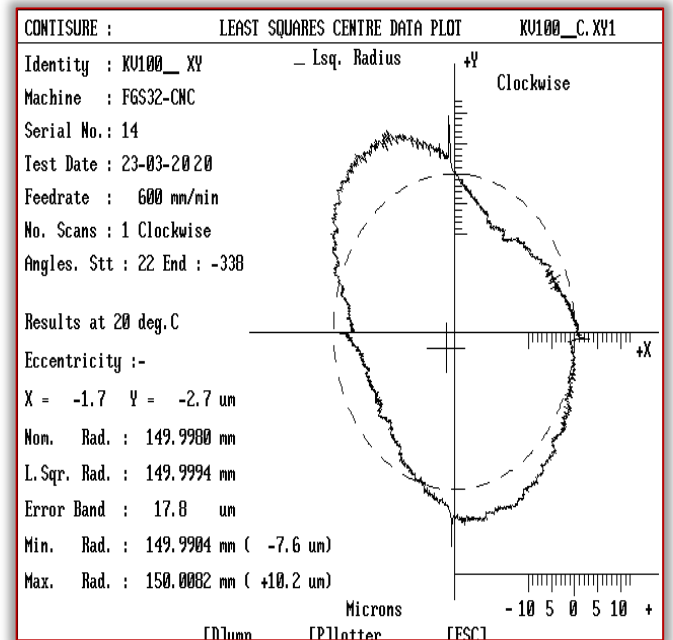


Figure 3. Polar diagram of the results of a measured circular test (feedrate $v=600\text{ mm/min}$, radius of the circle $R=150\text{ mm}$, position loop gain $Kv=100\text{ s}^{-1}$, $a=0$, clockwise direction)

The experimentally tuned value of Kv-factor on the examined machine tool axis was $Kv=100\text{ s}^{-1}$. The difference between analytically calculated and experimentally obtained value of Kv-factor is around 6.35%, which is acceptable for practical application.

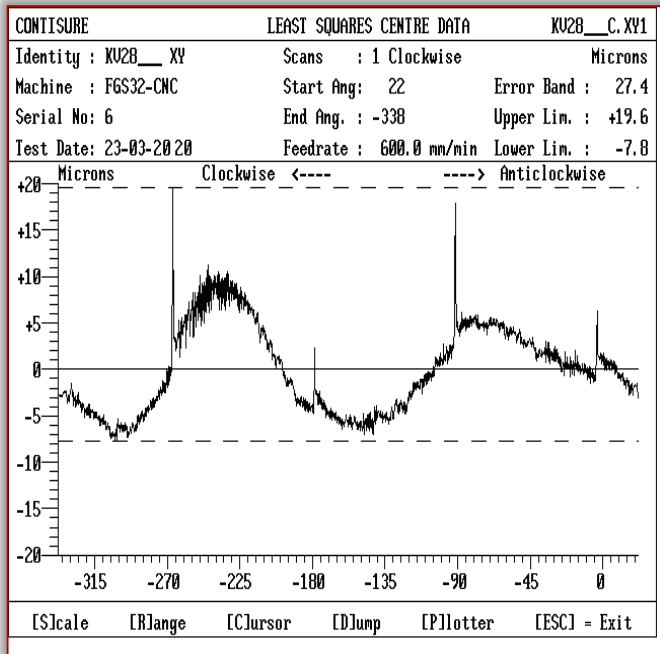


Figure 4. Linear diagram of the results of a measured circular test (feedrate $v=600$ mm/min, radius of the circle $R=150$ mm, position loop gain $Kv=28.3$ s⁻¹, $a=0$, clockwise direction)

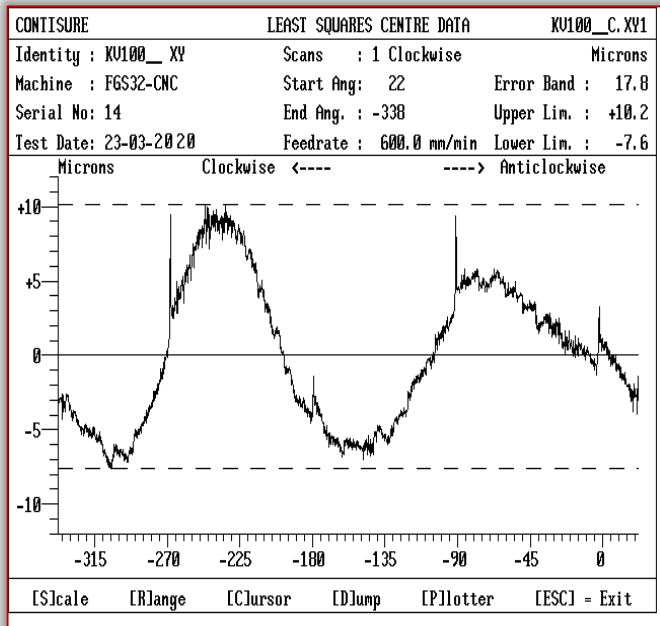


Figure 5. Linear diagram of the results of a measured circular test (feedrate $v=600$ mm/min, radius of the circle $R=150$ mm, position loop gain $Kv=100$ s⁻¹, $a=0$, clockwise direction)

Another parameter, which influences the contouring accuracy is the mismatch of position loop, gains for different machine axes. This will result in an elliptical contour path with the major axes lying ± 45 degrees, depending upon the direction of the scan, and increasing the contouring errors.

The results of the experiments with mismatching position loop gains $a = \frac{K_{vx} - K_{vy}}{K_{vx}} \cdot 100$ % are given in table 2. ($K_{vx}=30$ s⁻¹, $R=150$ mm and $v=600$ mm/min are constant.)

Table 2. Influence of the mismatching of the position loop gains on the magnitude of maximal contouring error from the nominal radius ec

a %	0	1	2	3
ec μ m (CW) experimentally	14.5	17.8	17.9	18.3
ec μ m (CCW) experimentally	16.5	19.7	19.9	20.3
ec μ m analytically with eq. (1)	0	0.47	1.32	2.19
a %	4	5	6	7
ec μ m (CW) experimentally	18.9	19.1	19.3	19.7
ec μ m (CCW) experimentally	20.9	22.5	23.1	23.3
ec μ m analytically with eq. (1)	3.08	3.99	4.92	5.87
a %	8	9	10	20
ec μ m (CW) experimentally	20.2	20.7	22.1	38.7
ec μ m (CCW) experimentally	25.4	27.5	29.4	52.9
ec μ m analytically with eq. (1)	6.84	7.83	8.84	20.34
a %	30	40	50	
ec μ m (CW) experimentally	69.5	113.2	170.9	
ec μ m (CCW) experimentally	85.6	128.4	186.2	
ec μ m analytically with eq. (1)	35.12	54.81	82.35	

It is obvious that with increasing the mismatch of position loop gains of the axes, the contouring error rises up. The best case is when the position loop gains are identical ($a=0$). Figures 6 and 7 show the results of circular test when the difference between position loop gains for X and Y axes is $a=20\%$.

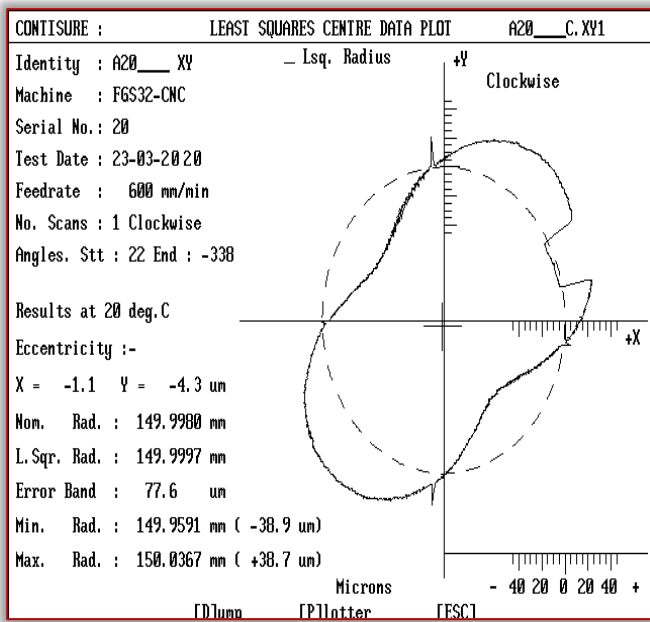


Figure 6. Polar diagram of the results of the measured circular tests with gains mismatched $a=20\%$ (clockwise direction, feedrate $v=600$ mm/min, radius of the circle $R=150$ mm, position loop gains $K_{vx}=30$ s⁻¹ and $K_{vy}=24$ s⁻¹)

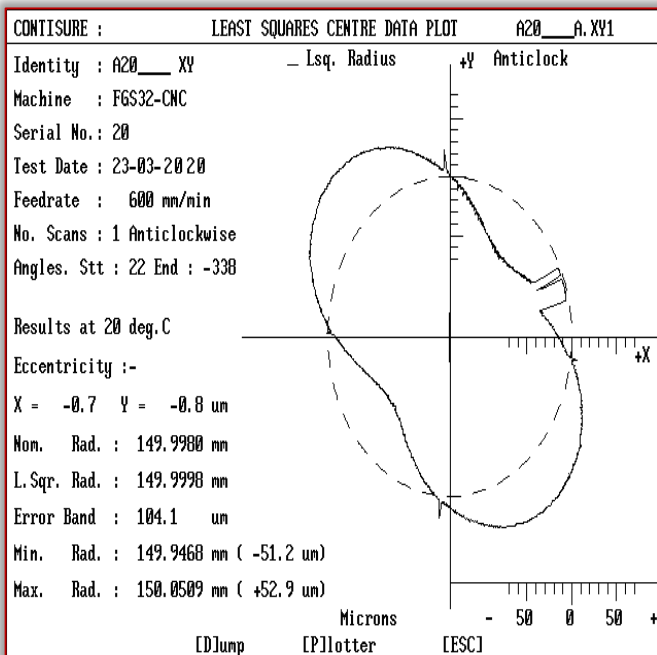


Figure 7. Polar diagram of the results of the measured circular tests with gains mismatched $a=20\%$ (anticlockwise direction, feedrate $v=600$ mm/min, radius of the circle $R=150$ mm, position loop gains $K_{vx}=30$ s⁻¹ and $K_{vy}=24$ s⁻¹)

CONCLUSION

The work has shown that the contouring errors in CNC machine tool can be minimized by appropriate selection of position loop gain in the controller. Criteria used in establishing the optimum K_v value

was minimization of maximal contouring deviation from nominal radius.

The test methodology with CONTISURE Double Ball Bar (DBB) system, demonstrated on FGS32 CNC milling machine with HEIDENHANN controller, offers a general approach for experimental determining of a position loop gain.

It was shown that the best results in contouring accuracy are provided when the position loop gains for the two axes are identical.

References

- [1] ANSI-ASME 85.54, 1991, Methods for performance evaluation of computer numerically controlled machining centers
- [2] British Standards Institution, BS 4656-30, 1992, Accuracy of machine tools and methods of test. Part 30. Specification for machining centers and computer numerically controlled milling machines, horizontal and vertical spindle types
- [3] ISO 230-4, 2005, Test code for machine tools — Part 4: Circular tests for numerically controlled machine tools
- [4] Bryan B. J., 1982, A simple method for testing measuring machines and machine tools, Part 1: principle and applications, Precision Engineering, Vol.4, No. 2, pp. 61-69
- [5] Burdekin M., Park J., 1988, Contisure-a computer aided system for assessing the contouring accuracy of NC machine tools, Proceedings of 27th International MATADOR Conference, pp.197-203, Manchester, UK, April 1988
- [6] Burdekin M., Jywe W., 1991, Application of Contisure for the Verification of the Contouring Performance of Precision Machines, Proceedings of the 6th international Precision Engineering Seminar, pp.106-123, Braunschweig, Germany, 1991
- [7] Andreev G. I., 1981, The main qualities required of electric feed drives for NC machine tools, Soviet Engineering Research, Vol.1, No.1, pp.59-62
- [8] Ghaffari A., Ulsoy A. G., 2015, Dynamic contour error estimation and feedback modification for high-precision contouring, IEEE/ASME Transactions on Mechatronics
- [9] Lacerda H.B., Belo E.M., 2000, A modified contour error controller for a high speed XY table, Journal of the Brazilian Society of Mechanical Sciences, Vol.22, n.3, Campinas 2000
- [10] Zhu Li Min, Zhao Huan, Ding Han, 2013, Real-time contouring error estimation for multi-axis motion systems using the second-order approximation, International Journal of Machine Tools and Manufacture, Volume 68, May 2013, pp. 75-80
- [11] Shi R., Lou Y., Shao Y., Li J and Chen H., 2016, A novel contouring error estimation for position-loop cross-coupled control of biaxial servo systems, 2016 IEEE/RSJ International Conference on Intelligent Robots and Systems (IROS), Daejeon, 2016, pp. 2197-2202, doi: 10.1109/ IROS.2016.7759344.
- [12] Bearee, R., Barre, P. & Bloch, S., 2004, Influence of High-Speed Machine Tool Control Parameters on the

- Contouring Accuracy. Application to Linear and Circular Interpolation, Journal of Intelligent and Robotic Systems, Vol. 40, pp.321–342 (2004).
- [13] Weck M., Ye G., 1990, Sharp Corner Tracking Using the IKF Control Strategy, Annals of the CIRP, Vol.39/1/1990, pp.437-441.
- [14] Weck M., 2006, Machine Tools and Machinig Systems, Volume 3, Mechatronics Systems: Feed Drives and Process Diagnosis, Springer, (In German)
- [15] Hayama S., Ito M., Ootake N., Fujita J., Kurokawa T., Kakino Y., 1996, A Study of the Generation Mechanism and the Compensation for the Exponential-Type Lost Motion for Feed Drive System of NC Machine Tools, International Journal of the Japan Society of Precision Engineering, Vol.30, No.1, March 1996, pp.51-52
- [16] Sato R., 2012, Generation Mechanism of Quadrant Glitches and Compensation for it in Feed Drive Systems of NC Machine Tools, International Journal of Automation Technology, Vol.6, No.2, pp. 154-162, 2012
- [17] Shiba K, Hayama S, Hamamura M., 2004, Lost motion correction system and lost motion correction method for numerical control machine tool -US Patent 6,701,212 B2, 2004
- [18] Shi Shengy, Lin Jing, Wang Xiufeng, Xu Xiaoqiang, 2015, Analysis of the transient backlash error in CNC machine tools with closed loops, International Journal of Machine Tools and Manufacture, Volume 93, June 2015, pp. 49-60
- [19] Yeh S., Su H., 2011, Development of friction identification methods for feed drives of CNC machine tools, Intternational Journal of Advanced Manufacturing Technolnology, Vol.52, pp.263–278 (2011)
- [20] Mei Xuesong, Tsutsumi Masaomi, TaoTao, Sun Nuogang, 2004, Study on the compensation of error by stick-slip for high-precision table, International Journal of Machine Tools and Manufacture, Volume 44, Issue 5, April 2004, pp. 503-510
- [21] Zirn Oliver, 2008, Machine Tool Analysis – Modelling, Simulation and Control of Machine Tool Manipulators, A Habilitation Thesis, Department of Mechanical & Process Engineering ETH Zürich, May 2008
- [22] Gross Hans, Wiegartner Georg, Hamann Jens, 2001, Electrical Feed Drives in Automation: Basics, Computation, Dimensioning, John Wiley & Sons, Inc., USA
- [23] Pandilov Z., Dukovski V., 2014. Analytical Determination of the CNC Machines High-Speed Feed Drives Position Loop Gain. Applied Mechanics and Materials Vol.555, pp.505–510
- [24] Altintas Y., Verl A., Brecher C., Uriarte L., Pritschow G., Machine tool feed drives, CIRP Annals, Volume 60, Issue 2, 2011, pp. 779-796
- [25] Bullock B. T., Younkin W. G., 1995, Bode diagrams analyze servosystems, Machine Design, February 9, 1995, pp.49-54
- [26] Koren Y., Lo C. C., 1992, Advanced Controllers for Feed Drives, Annals of the CIRP Vol.41/2/1992, pp.689-698.
- [27] Smith A.D., 1999, Wide bandwidth control of high-speed milling machine feed drives, Dissertation, University of Florida, USA, 1999
- [28] Soucek P., 2004, Servo mechanisms for machine tools, CVUT, Prague, (In Czech)
- [29] Weck M., Krueger P., Brecher C., 2001, Limits for controller settings with electric linear direct drives, International Journal of Machine Tools and Manufacture, Vol. 41, pp.65-88
- [30] Younkin W.G., 1996, Industrial Servo Control Systems: Fundamentals and Applications, Marcel Dekker Inc.
- [31] Kamalzadeh A., Erkokmaz K., 2007, Compensation of Axial Vibrations in Ball Screw Drives, CIRP Annals, Volume 56, Issue 1, 2007, pp.373-378



ACTA TECHNICA CORVINIENSIS – Bulletin of Engineering
ISSN: 2067-3809
copyright © University POLITEHNICA Timisoara,
Faculty of Engineering Hunedoara,
5, Revolutiei, 331128, Hunedoara, ROMANIA
<http://acta.fih.upt.ro>

¹S.K. SHINDE, ²R.M. MORE

FAULTS FINDING ANALYZER OF WEB APPLICATIONS

¹Vidya Pratishthan's Kamalnayan Bajaj Institute of Engg. & Technology, Baramati, Dist. Pune, INDIA

²Shree Datta Polytechnic, Shirol, INDIA

Abstract: Web text and dynamically generated web pages exist common errors, and they seriously affect the usability of Web applications. Current tools to webpage validation cannot manage the dynamically created pages that are ever-present in today's Internet. The proposed tool takes source code files as information sources. It removes HTML, ASP tags and logic codes from extracted files. Then the proposed tool discovers HTML faults and execution faults from these extracted files. The method used to make test cases automatically runs the tests taking constraints from the resource database on inputs and reduces the requirements on inputs to failing tests so that the resulting defect reports are small and important in finding the faults. Our proposed tool implements the technique for Web technologies such as PHP, C#, ASP.net. The tool makes test inputs for a Web application, controls the application for crashes, and confirms that the output conforms to the HTML specification. The proposed tool is to act as a testing tool to find faults from all LOC (line-of-code) in web applications. Comparatively more advanced tools find faults during the rendering process, so it uses line coverage so less as compared to the proposed tool.

Keywords: Faults, Bug Finder, basic validator, Web Applications, failures

INTRODUCTION

Powerful test creation tools, such as DART [1], Cute [2], and EXE [3], make tests by executing an application on input values and then building additional input values by solving symbolic conditions obtained from exercised control paths. Such approaches have not been studied in the domain of web applications, which pose special challenges due to the dynamism of the coding languages, the advantage of implicit parameters, their use of persistent state, and their designs of user interaction. The offered work continues dynamic test generation to the area of web applications that dynamically create web pages during execution, which are typically given to the user in a browser. Web development languages including server-side web programming languages such as PHP, ASP.net, and C# are used as input in the proposed work [4].

Our goal is to find two classes of failures in web applications: execution crashes that show as errors or warnings during the process execution, and HTML failures that happen when the application allows twisted HTML. Execution flops may occur, for example, when a web form calls an irregular function or reads a missing file. Some HTML code includes an error warning, and execution of the application may be suspended, depending on the hardness of the fault. If the input contains not syntactically well-formed HTML, then the proposed tool generates output containing HTML faults. HTML faults are generally not as notable as execution faults because Web browsers are intended to provide some degree of malformedness in HTML, but they are unacceptable for several reasons. The first and most critical is that browsers' attempts to compensate for malformed web pages may lead to crashes and security vulnerabilities. Second, standard HTML performs faster. Third,

deformed HTML is less portable across browsers and is vulnerable to breaking or watching apart when displayed by untested browser versions. Fourth, a browser force succeeds in presenting only part of a malformed webpage, while silently discarding important information. Fifth, search engines may have trouble indexing deformed pages [13].

Web developers widely know the importance of creating error-free HTML. HTML validators are used to control many websites. However, HTML validator can only point out problems in HTML pages and are by them incompetent of finding faults in applications that generate HTML pages. Checking dynamic Web applications requires checking that the application creates a valid HTML page on every possible execution path. In practice, even professionally developed and thoroughly tested applications often include multiple faults. So, this tool has implemented using symbolic execution to find faults in web applications. This scheme continues dynamic test creation to the area of web applications that dynamically create the HTML pages throughout execution, which offer to the user in a browser.

LITERATURE REVIEW

The main strength of DART is that testing is often performed completely automatically on any program that compiles – there's no got to write any driver or harness code. During testing, DART detects standard errors like program crashes, assertion violations, and non-termination. Preliminary experiments to unit test several samples of C programs are very encouraging. [1]

In unit testing, a program was divided into units of collection of methods. A piece of the unit can try by creating contributions for solitary section work. The entry method may contain pointer contentions, in which case the contributions to the unit are memory

graphs. The paper talks about the issue of mechanizing unit testing with memory charts as sources of info. The methodology utilized expands on before work consolidating representative and reliable execution, and all the more explicitly, utilizing such a request to produce test contributions to investigate all plausible execution ways. CUTE [2] is a variation on the DART approach.[2]

EXE is a valuable bug-discovering system that automatically creates inputs that crash genuine code. EXE utilizes secure, piece level precise representative execution to discover significant mistakes in code and naturally create inputs that can hit these faults [3]

Fuzz testing is a valuable method for discovering security vulnerabilities in programming. Customarily, fluff testing devices apply irregular transformations to very much framed contributions of a program and test the different qualities. Paper introduces an option white box fuzz testing approach motivated by ongoing advances in symbolic execution and dynamic test generation. Their methodology records a genuine keep running of the program under test on very much framed information, emblematically assesses the recorded follow, and assembles limitations on sources of info catching how the program utilizes these. The gathered requirements are then invalidated one by one and unraveled with a limitation solver, creating new information sources that activity diverse control ways in the program [9].

PROPOSED WORK

The system architecture is the conceptual model that defines the structure and behavior of the system. An architecture description is a precise representation of a system. System architecture represents the structure of system components, external visibility of those components, and their relationships between them. The language used for architecture description is called the architectural description language.

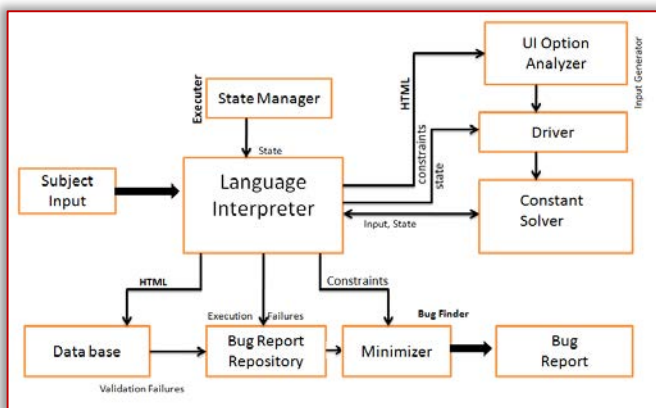


Figure 1: The Proposed system for finding faults in websites

The proposed tool is to implement our technique for Web Technology. This module consists of the following major components, input generator, executor, and bug finder illustrated in Figure 1.

— The executor is responsible for executing a web programming script with a given input in a given state. The executor contains two subcomponents:

- The Language Interpreter is a language interpreter that we modify to propagate and record path constraints and positional information associated with the output. This positional knowledge use to determine which failures are likely to be symptoms of the same fault.
- The State Manager restores the given case of the environment (database, session, and cookies) before the execution and stores the new environment next to the execution.

— The Input Generator implements the algorithm described below. The Input Generator contains the following subcomponents:

- The User Interface Analyzer examines the HTML code output of each execution to change the interactive user choices into new inputs to execute.
- The Driver generates new path checks from the checks found during the execution.
- The Constraint Solver computes an task of values to input parameters that satisfy a given path checks.

—The Bug Finder practices an oracle to find HTML failures, stores all bug reports, and finds the minimal requirements on the input parameters for each bug report. The Bug Finder has the following subcomponents:

- The database stores the HTML faults in the output of the program.
- The Bug Report database stores HTML and execution faults report found during all executions.
- The Input Minimizer determines, for an assigned bug report, the shortest path constraint on the input parameters that results in inputs producing the same failure as in the report.

EXPERIMENTAL SETUP

This module program has implemented using C#.net. The experiment is carried out by different input datasets and analyzing output with the dataset in the Windows 7 operating system. We have taken four datasets implemented using PHP server-side scripting language.

Table 1 shows a time practiced for the detection of faults by the existing tools and time needed for the detection of faults for the proposed tool. The proposed tool takes less time for the detection of execution and HTML faults present in the web applications as compared to the existing tools.

Table 1: Time required to process input

Input	Time (in seconds) required to process	
	Proposed System	Existing System
timeclock	210	425
Phpbb2	195	420
Phpsysinfo[17]	300	720
Synthetic Website Dataset 1	256	505*
Synthetic Website Dataset 2	350	680*

* Indicates expected values for time requirement to find faults generated by existing systems.

As a shown in table 1 above, execution time reduced to 50% averagely due to system executes line of code sequentially. In case of existing systems, generate input dynamically hence time required to execute LOC is high. Also LOC for existing system is below the 50% while proposed system used more than 90% except scripting (Java Script, VB Script)

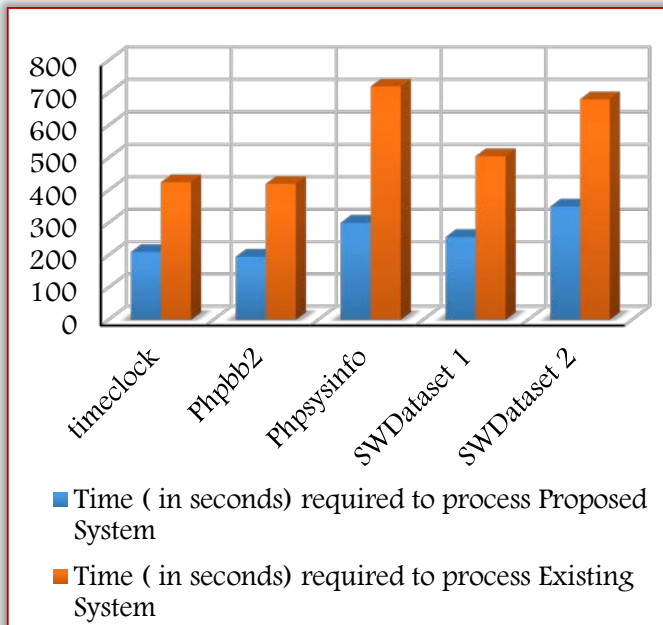


Figure 2: Time Required Comparison

Figure 2 shows some faults detected by the proposed tool and the existing tool.

Table 2: Error detection

Input	No of errors detected	
	Proposed System	Existing System
timeclock	395	387
Phpbb2	35	30
Phpsysinfo[17]	17	9
Synthetic Website Dataset 1	158	151*
Synthetic Website Dataset 2	60	54*

* Indicates expected values for errors generated by existing systems.

Table 2 shows better performance by the proposed system to find faults in respective datasets.

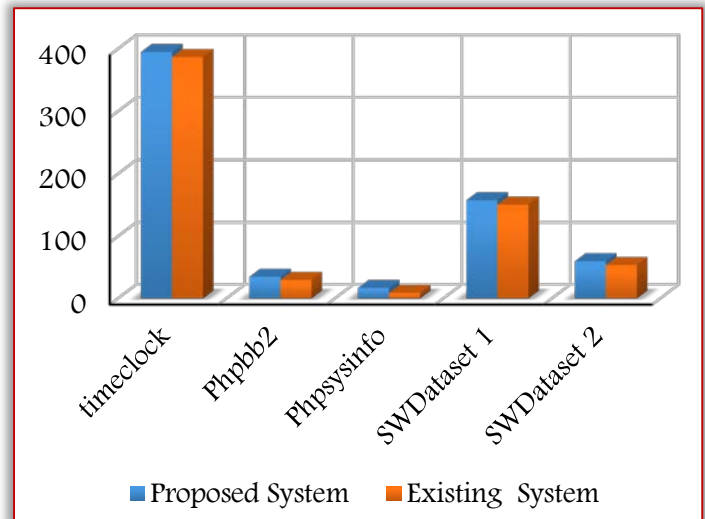


Figure 3: Error Detection Comparison

Table 3: LOC coverage

Input	LOC coverage (%)	
	Proposed System	Existing System
timeclock	94	26.8
Phpbb2	92	31.7
Phpsysinfo[17]	91	56.2
Synthetic Website Dataset 1	96	52*
Synthetic Website Dataset 2	90	54*

* Indicates expected values for LOC (line of code) coverage generated by existing systems.

Table 3 shows excellent LOC coverage by the proposed system with compare to existing system.

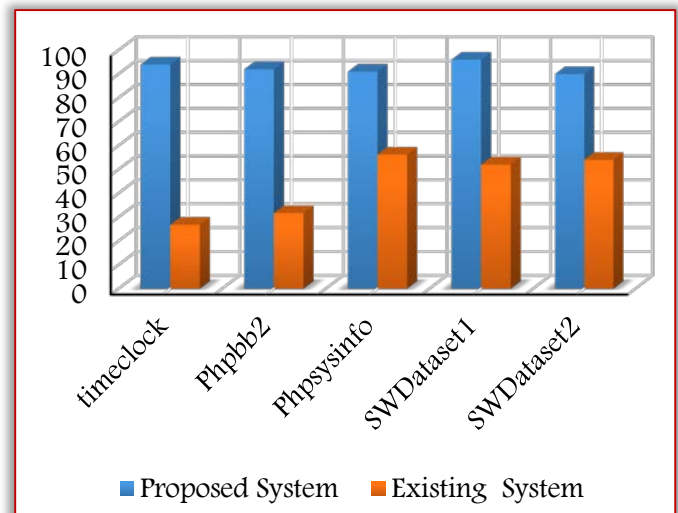


Figure 4: LOC coverage

CONCLUSION

We have introduced a technique for finding faults in web applications implemented in PHP and C#.net technology. This tool is to give a new approach to detecting HTML and execution faults. This tool has utilized the dynamic inputs to check the fault events and perform an automated examination to decrease

the extent of the fault prompting inputs. The previous tools, for example, Apollo, randomized systems, identify the faults from static applications of PHP. However, our tool detects static, dynamic bugs as well as HTML errors present in web applications implemented in PHP as well as C#.net.

The proposed tool detects HTML errors and execution errors in less time as compared to the existing tools. The accuracy of error detection of this tool is better than that of the existing tool. Hence, the precision of the web applications has improved by a proposed system.

The proposed tool is to act as a testing tool to find faults from all LOC (line-of-code) in web applications. More advanced tools find faults during rendering process, so line coverage is less but this tool is act as testing tool, so line coverage is more compare to other tools.

References

- [1] Godefroid, Klarlund N, and Sen K, “DART: Directed Automated Random Testing,” Proc. ACM SIGPLAN Conf. Programming Language Design and Implementation, pp. 213-223, 2005.
- [2] Sen K, Marinov D, and Agha G, “CUTE: A Concolic Unit Testing Engine for C,” Proc. ACM SIGSOFT Int’l Symp. Foundations of Software Eng., pp. 263-272, 2005.
- [3] Cadar C, Ganesh V, Pawlowski P M, Dill D L, and Engler D.R., “EXE: Automatically Generating Input of Death,” Proc. Conf. Computer and Comm. Security, pp. 322-335, 2006.
- [4] Artzi S, Kie zun A, Dolby J, Tip F, Dig D, Paradkar, “Finding Bugs in Web Applications Using Dynamic Test Generation and Explicit-State Model Checking” IEEE Trans. on Software Engg. Vol. 36, NO. 4, July/Aug 2010
- [5] Shinde S K, Joshi S D.,Kaushik D K., “Fault-Tolerant System for Dynamic Web Applications”, IJEDR, volume 3 issue 1, (2015), pp. 489-494.
- [6] Holzmann G J, “The Model Checker SPIN,” Software Eng., vol. 23, no. 5, pp. 279-295, 1997.
- [7] Benedikt M, Freire J, and Godefroid P, "VeriWeb: Automatically Testing Dynamic Web Sites," Proc. Intel Conf. World Wide Web, 2002.
- [8] Clause J and Orso A, "Penumbra: Automatically Identifying Failure-Relevant Inputs Using Dynamic Tainting," Proc. Intel Symp. Software Testing and Analysis, 2009.
- [9] Godefroid P, Levin M Y, and Molnar D, “Automated Whitebox Fuzz Testing,” Proc. Network Distributed Security Symp., pp. 151-166, 2008
- [10] Cleve H and Zeller A, "Locating Causes of Program Failures," Proc. Intel Conf. Software Eng., pp. 342-351, 2005.
- [11] Misherghi G and Su Z, "HDD: Hierarchical Delta Debugging," Proc. Intel Conf. Software Eng., pp. 142-151, 2006.
- [12] Csallner C, Tillmann N, and Smaragdakis Y, "DySy: Dynamic Symbolic Execution for Invariant Inference," Proc. Intel Conf. Software Eng., pp. 281-290, 2008.
- [13] Zoufaly F, "Web Standards and Search Engine Optimization (SEO)—Does Google Care About the Quality of Your Markup?" 2008.
- [14] Shinde S K, Joshi S D, “Iterative Code Reviews System For Detecting And Correcting Faults From Software Code Documents” IJARET Volume 5, Issue 11, November (2014), pp. 61-67
- [15] Minamide Y, "Static Approximation of Dynamically Generated Web Pages," Proc. Intel Conf. World Wide Web, 2005.
- [16] Shinde S K, Joshi S D, “Schema Inference & Data Extraction from Templated Web Pages”, IEEE, International conference on Pervasive Computing (ICPC) 2015, Sinhgad College of Engineering, Pune, 10.1109/PERVASIVE.2015.7087084, Jan.2015 pp. 1-6
- [17] Shinde S K, Joshi S D, “Web Based Requirement Elicitation Tool” (IJARCET) Volume 4 Issue 9, September 2015 pp. 3719-3722



ACTA TECHNICA CORVINIENSIS – Bulletin of Engineering
ISSN: 2067-3809

copyright © University POLITEHNICA Timisoara,
Faculty of Engineering Hunedoara,
5, Revolutiei, 331128, Hunedoara, ROMANIA
<http://acta.fih.upt.ro>

¹Miodrag MILČIĆ, ²Dragan MILČIĆ, ³Nataša ZDRAVKOVIĆ

EXPERIMENTAL INVESTIGATION OF FRICTION STIR WELDING OF 2024 ALUMINIUM ALLOYS JOINTS TESTING

¹Faculty of Mechanical Engineering in Nis, SERBIA

Abstract: Friction stir welding is a process of welding metals in a solid state, and it is routinely already used for joining metals that can not be welded by conventional fusion welding processes. A typical material that is almost unresponsive to conventional fusion welding procedures is the aluminum alloy AA2024 which has a wide application in the aviation industry. A study was conducted to study the influence of welding parameters on the mechanical properties of the FSW welded joint. An optimized tool was used for friction stir welding. There are welded plates of thickness of 6 mm. The following welding parameters were used: the tool rotational speed was constant and amounted to 750 rpm, and the welding speed was changed to 73, 116.150 mm / min. Welded joints are obtained without the presence of errors and with an acceptable flat surface of the compound.

Keywords: Friction stir welding (FSW), Aluminum AA2024 alloy, rotation speed, welding speed, mechanical properties

INTRODUCTION

Friction stir welding (FSW) was invented at The Welding Institute (TWI) of UK in 1991 as a solid-state joining technique, and it was initially applied to aluminum alloys [1]. The principle of obtaining inseparable joints by welding with friction stir welding is shown in the Figure 1.

The tool geometry plays an important role in material flow and in turn decides the traverse rate at which FSW can be carried out. A FSW tool has two basic functions: localized heating, and material flow. In initial stage of the tool plunge, the heating results primarily from the friction between pin and workpiece. The tool is plunged till the shoulder touches the workpiece. The friction between the shoulder and the workpiece results in the biggest component of heating.

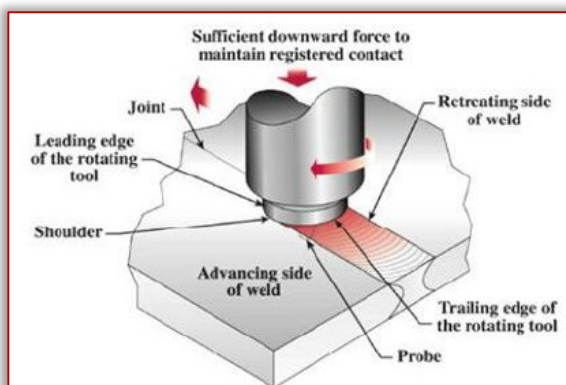


Figure 1. Illustrated scheme of friction stir welding

There have been a number of reports [2–5] highlighting the microstructural changes due to plastic deformation and frictional heat associated with FSW. Mechanical failure of the welds can take place in the SZ, TMAZ, or HAZ region depending on the amount of energy input which is controlled by the welding parameters such as rotational and travel speed [5]. Since the material flow behavior is

predominantly influenced by the material properties such as yield strength, ductility and hardness of the base metal, tool design, and FSW process parameters, the dependence of weld microstructure on process parameters differs in different aluminum alloys for a given tool design.

The main goal of this research is analyse the FSW parameters on the structural and mechanical properties FSW butt joint of aluminium alloy EN AW 2024–T351.

EXPERIMENTAL WORK

The experiment was aimed to find the influence of input kinematic parameters such as welding speed (v) and tool rotation speed (n) on metallurgical and mechanical characteristics of welded joints. Base material was aluminium alloy EN AW 2024–T351. Chemical composition of experimental plates is provided in Table 1 and mechanical properties in Table 2 [3].

Table 1. Chemical composition of AA 2024–T351

Chemical composition	Cu	Mg	Mn	Fe	Si	Zn	Ti
wt. %	4,70	1,56	0,65	0,17	0,046	0,11	0,032

Table 2. Mechanical properties of AA 2024–T351

Yield strength R_{ch} (MPa)	Ultimate tensile strength R_m (MPa)	Elongation A_5 (%)	Hardness HV
370	481	17.9	137

They are experimentally welded plates measuring 500 mm×65 mm×6 mm. The both sides of the welding plates are machined on the grinder at a thickness of 6 mm. When welding under the welding part, the base plate was made of austenitic steel. A milling machine was used for welding. The weld length was approximately 400 mm.

Figure 2 shows a machine and Figure 3 tool used for butt joint FSW.

Experimental Investigation of Friction Stir Welding Of 2024 Aluminium Alloys Joints Testing.



Figure 2. Machine for FSW welding

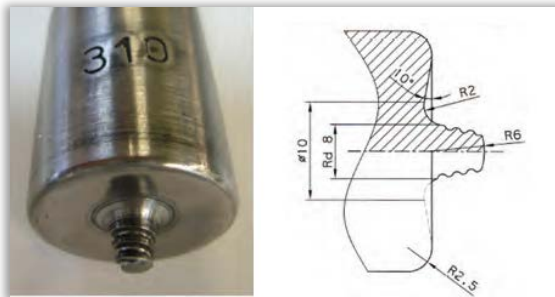


Figure 3. Fabricated FSW tools

Welding was made in accordance with the plan matrix of experiment, with variations in tool rotation speed (n) and welding speed (v), Table 3.

Table 3. Friction stir welding parameters

Sample	Rotation speed n (rpm)	Welding speed v (mm/min)	Ratio n/v (rev/mm)
A – I	750	73	10,27
B – II		116	6,47
C – III		150	5

After the welding process was completed, welds were tested. For that purpose, visual control was performed, on the weld face and root of the seam, as well as the radiographic control of samples. No defects were detected (visually, touch or magnifier).

After the welding process was completed, welds were tested. For that purpose, visual control was performed, on the weld face and root of the seam, as well as the radiographic control of samples. No defects were detected (visually, touch or magnifier).

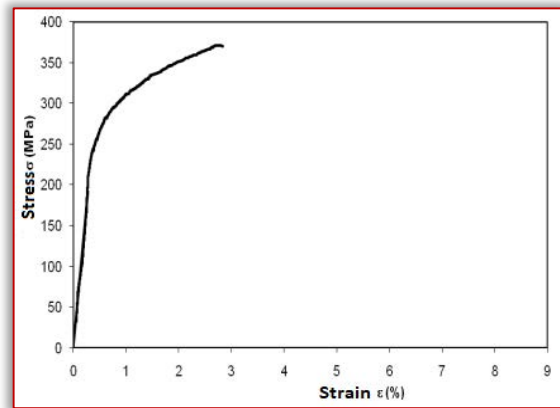
RESULTS AND DISCUSSIONS

Room-temperature tensile tests were carried out at a strain rate of $3.3 \times 10^{-3} \text{ s}^{-1}$ on ASTM E8M transverse tensile specimens. In order to assess the reproducibility, 2 specimens were tested and average value was reported.

Tensile testing was performed for all tree FSW joints. The tensile testing results FSW joints are given in Table 4. Among the tree FSW parameters studied, i.e., at 750/73, 750/116 and 750/150 rpm/(mm/min), the average tensile yield strength and ultimate tensile strength.

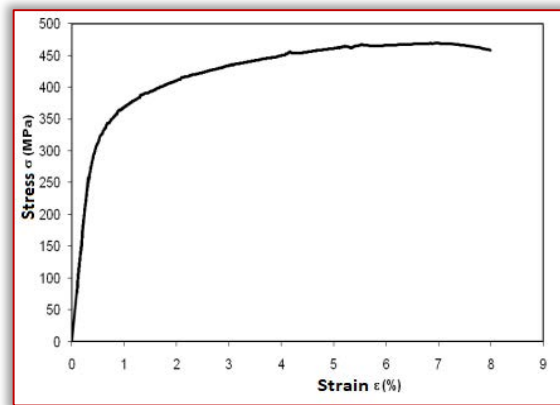
Table 4. Tensile testing results

A-I



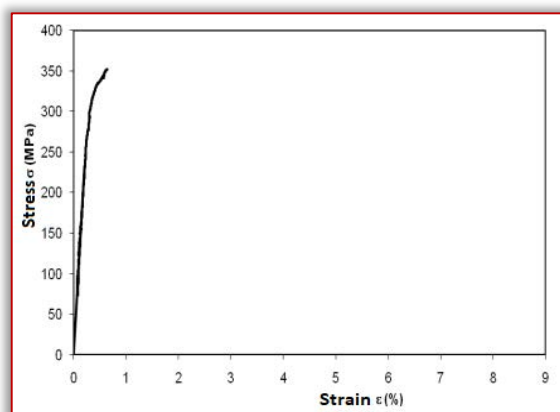
$R_{p0,2} = 281,9 \text{ MPa}$
 $R_m = 371,00 \text{ MPa}$
 $Z = 2,29\%$

B-II



$R_{p0,2} = 330,9 \text{ MPa}$
 $R_m = 469,06 \text{ MPa}$
 $Z = 7,43\%$

C-III



$R_{p0,2} = 337,6 \text{ MPa}$
 $R_m = 352,03 \text{ MPa}$
 $Z = 0,33\%$

This variation of tensile strength with rotational speeds for a given traverse speed appears to be linked to the energy of the welds. Joint efficiency as high as 97% of base metal could be achieved at 750/116 rpm/(mm/min). The highest ductility of the welded

joint is achieved with the welding parameters 750/116 and is 7,2%.

The highest ductility of the welded joint is achieved with the welding parameters 750/116 and is 7%.

Bend testing was carried out according to EN 910 with joint centered over the mandrel. The bending specimens were tested using face and root side of the joint in tension.

The results of three-point bending test results FSW joints are given in Figure 4. The welded FSW joint has poor bending characteristics. Comparing the obtained bending test results, the largest bend angle to the first cracking phenomenon is for welding parameters 750/116 and amounts to 42°.

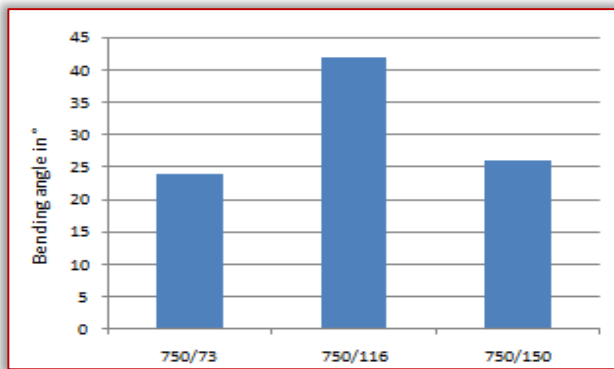


Figure 4. Results of three-point bending test

Vickers hardness measurement was conducted perpendicular to the welding direction, at cross section of weld joint, using digitally controlled hardness test machine (HVS-1000) applying 9.807 N force for 15 s. The hardness profiles were obtained along 3 horizontal and 63 vertical directions.

Figure 5 shows hardness distribution across the welded joint at different applied rotation speed (n) and welding speed (v).

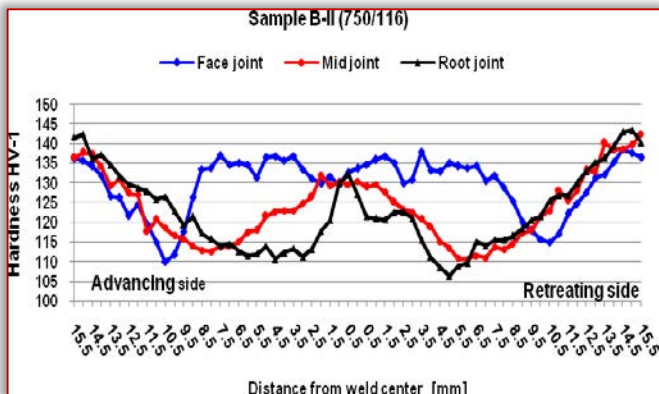


Figure 5. Hardness distribution across the welded joint for sample B-II (750/116)

Comparing the hardness distribution for the welding parameter 750/150, 750/116 and 750/73, it is noted that the hardness of the sample A-I in the stir region is uniform across the entire height (Figure 6).

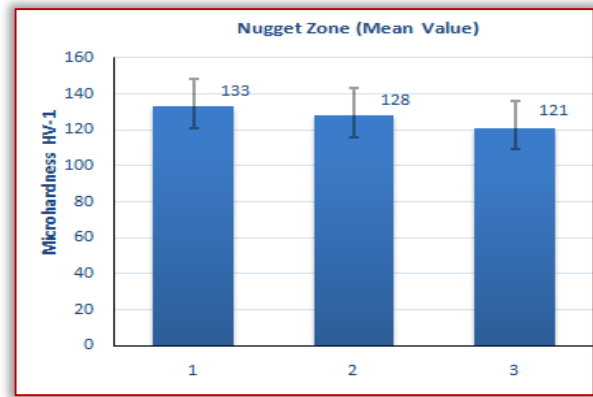


Figure 6. Microhardness results at different processing conditions (1-750/73; 2-750/116; 3-750/150) Bars the mean HV value in the NZ (error bars maximum and minimum HV in the same zone)

Charpy impact tests are carried out at room temperature using instrumented impact pendulum. The pendulum is equipped with load cells positioned on a striker edge. The impact energy values were measured in three points of the notch and that: in the weld center, the notch on the advancing side in the 4 mm position from the weld center (+4), and the notch on the side retreating at the 4 mm position from the weld center (-4).

The Charpy impact tests results FSW joints are given in Table 5. For all welded samples, the maximum impact energy values are measured for the score on the advancing side. The best characteristics of impact toughness have a welded pattern with welding parameters 750/116 (B+4) and a impact energy of 8.5 J and a impact toughness of 21.3 J / cm².

Table 5. Results of impact toughness

	KV / J/cm ²	E / J	E _i / J	E _p / J
OM	19.5	7.8	3	4.8
A-S	12.62	5,05	1.64	3.41
A+4	17.1	6.8	3	3.8
A-4	13.6	5.5	2.1	3.4
B-S	12.62	6.7	1.7	5
B+4	21.3	8.5	3.2	5.3
B-4	11.1	4.5	1.4	3.1
C-S	14.2	5.7	2.4	3.3
C+4	20.7	8.3	3.1	5.2
C-4	12.8	5.1	1.9	3.2

A – 750/73; B – 750/116; C – 750/150

CONCLUSIONS

On the basis of examinations performed, given results of the experiment and their comparison, the following conclusions can be provided:

Relation between the number of revolutions of tools n velocity of welding v directly influences the value of the fracture toughness and energy which is required for initiation and propagation of the crack;

The asymmetry of the welded joint and changes in metallurgical transformations occurring around the pin and under the shoulder of the tool during its combined moving, influence the value of impact strength in various areas of the welded joint;

Profile of distribution and allocation of micro hardness depends on the level of temperature and plastic deformation which is highest under the tool shoulder and around the pin;

This investigation points out that weld joint B–II (welded by 750/116 rpm/(mm/min)) achieves better properties and microstructure than weld joint A–I and C–III (welded by 750/73 and 750/150 rpm/(mm/min)).

Note:

This paper is based on the paper presented at DEMI 2019 – The 14th International Conference on Accomplishments in Mechanical and Industrial Engineering, organized by Faculty of Mechanical Engineering, University of Banja Luka, BOSNIA & HERZEGOVINA, co-organized by Faculty of Mechanical Engineering, University of Niš, SERBIA, Faculty of Mechanical Engineering Podgorica, University of Montenegro, MONTENEGRO and Faculty of Engineering Hunedoara, University Politehnica Timisoara, ROMANIA, in Banja Luka, BOSNIA & HERZEGOVINA, 24–25 May 2019.

References

- [1] Thomas, W. M., Nicholas, E. D., Needham J C, Murch M G, Temple-Smith P, Dawes C J 1991 Friction stir butt welding, GB Patent No. 9125978.8, International patent application No. PCT/GB92/02203.
- [2] Gupta, R. K., Das, H., Pal, T. K. (2012). Influence of Processing Parameters on Induced Energy, Mechanical and Corrosion Properties of FSW Butt Joint of 7475 AA, JMEPEG 21, p.1645–1654.
- [3] Su, J. Q., Nelson, T. W., Mishra, R., Mahoney, M. (2003). Microstructural Investigation of Friction Stir Welded 7050–T651 alloy, Acta Mater., 51, p. 713–729.
- [4] Ma, Z. Y., Mishra, R. S. (2005). Friction stir welding and processing, Materials science and engineering, vol. 1, no. 1, p. 1–78.
- [5] Zimmer, S., Langlois, L., Laye, J., Bigot, R. (2010). Experimental investigation of the influence of the FSW plunge processing parameters on the maximum generated force and torque, The International Journal of Advanced Manufacturing Technology 47, p. 201–215.



ACTA TECHNICA CORVINIENSIS – Bulletin of Engineering
ISSN: 2067-3809

copyright © University POLITEHNICA Timisoara,
Faculty of Engineering Hunedoara,
5, Revolutiei, 331128, Hunedoara, ROMANIA
<http://acta.fih.upt.ro>

¹Susarla Venkata Ananta Rama SASTRY

SURFACE ASSIMILATION OF COPPER (Cu²⁺) FROM WASTE WATER USING MANGO PEEL POWDER (MPP)

¹Department of Chemical Engineering, MVGR College of Engineering (A), Vizianagaram, Andhra Pradesh, INDIA

Abstract: Copper is a heavy metal and a pollutant from industries such as fungicides, pesticides, electrical appliances manufacturing industries and products containing copper. These industries discharge pollutants through water which contains copper metal. This has adverse effect on many creatures which damages kidneys, nervous system and liver. The main aim is to study the removal of copper as it is a heavy metal and a pollutant from industries. Experimentation on the adsorption of Cu²⁺ from waste water using Mango Peel Powder (MPP) was conducted to study different parameters such as contact time (20, 40, 60 minutes), concentration (0.05, 0.1, 0.15, 0.2 ppm) and altering adsorbent (MPP) weight (1, 2 gm). Adsorption studies were made on changing three parameters contact time, concentration and weight of adsorbent. Refractive Index method is used to calculate the percentage recovery of copper for a fixed time of contact and changing concentration by maintaining equal weight of adsorbent. The same procedure was repeated changing time of contact and weight of adsorbent (Mango Peel Powder).

Keywords: adsorption, Copper (Cu²⁺), mango peel powder, refractive index

INTRODUCTION

The heavy metal ions such as Pb(II), Cu(II), Zn(II), Hg(II), Cr(VI) and As(V) primarily come from industrial effluents in the aqueous environment. These metal ions present in water causes numerous poisonous effects on the human health and environment. The extended half-life of heavy metal ions and their non-biodegradability causes a buildup of metal ions in the living organisms, causing various diseases such as nervous system damage, poisoning, and cancer. Presence of heavy metals in the water causes various health issues such as damaging of kidneys, nervous system and liver. The elimination of heavy metals from wastewater and water is essential for environment protection and public health. The pollutants are released into water bodies through different ways. They can be released from wastewater treatment facilities, industrial effluents, refineries etc. So, it is very important to remove the excess heavy metals from water to safeguard public health and environment [1-3]. The important toxic metals i.e. Copper, Nickel, Zinc and Lead find their way to the water bodies through the waste waters. Heavy metals can accumulate in the environment elements such as food chain, and thus may pose a significant threat to human beings. Copper, in small amounts, plays a vital role as a cofactor in a variety of essential enzymes required for homeostasis, growth and development in humans. The natural concentration of Cu is about 50 ppm in soil, 4-10 µg/L in water (usually bound to organic materials) and 18-45 µg/g in the human liver (dry weight), but excessively high doses of Cu, introduced by the ingestion of food or water with excessive Cu content, may result in a variety of symptoms and illnesses [4-6]. While these primarily affect the liver, in the form of cirrhosis, they may also

result in general weakness, lethargy and anorexia. Copper enters the environment primarily through chemical-related industries such as metal plating and cleaning. Consequently, it is necessary to clean wastewater by eliminating its heavy metal content by using proficient methods. There are a variety of methods existing for the elimination toxic metals from the water such as Reverse osmosis, Ion-exchange, Membrane separation and Precipitation etc. Apart from these, other cheap adsorbents have been studied, mainly by using bio-adsorbents, such as chitosan and algae. Still the experiments performed in fixed-bed offered incomplete results. Bentonite clays are extensively used as barriers to evade underground and subsoil landfill water pollution by leaching of heavy metals. Considering the easy operational conditions and simplicity, adsorption and the retention of copper ions from aqueous solutions by Mango Peel Powder (MPP) is studied in this work [7-9].

MATERIALS AND METHODS

—Preparation of Adsorbent (Mango Peel Powder)

The peels of different types of mangoes were collected and they were dried under sunlight for nearly three weeks at a temperature of 27-32°C. After drying, the adsorbent was crumbled into fine particles and finally the size of the particles obtained as 0.074 mm diameter using the sieve of 200 mesh.

—Preparation of CuSO₄.5H₂O Stock solution

Solutions of copper ions of different concentrations (0.05, 0.1, 0.15, 0.2 mg/lit) were prepared from a stock solution of CuSO₄.5H₂O. The pH was adjusted with 0.1 NaOH or H₂SO₄.

—Preparation of Calibration Chart

Take 4 conical flasks and wash them clean using distilled water. Add 100ml distilled water to each of

the conical flask. Add 5,10,15,20 grams of $\text{CuSO}_4 \cdot 5\text{H}_2\text{O}$ to each of the flask. Swirl the solutions in flasks until the solutions gets uniformity. Using Refractive Index (RI) meter find RI for each solution present in flasks. Plot graph for Weight of copper in $\text{CuSO}_4 \cdot 5\text{H}_2\text{O}$ vs. RI [10-11]. This plot is considered as Calibration chart (Table 1 & Figure 1).

Table 1: Calibration chart

Vol. of water added (ml)	Wt.of $\text{CuSO}_4 \cdot 5\text{H}_2\text{O}$ (gm)	Wt. of Cu (gm)	R.I
100	1	0.254505	1.3651
100	2	0.509011	1.3702
100	3	0.763516	1.3785
100	4	1.018022	1.3858
100	5	1.272527	1.3898
100	10	2.5448	1.3923
100	15	3.8173	1.3989
100	20	5.0897	1.4026

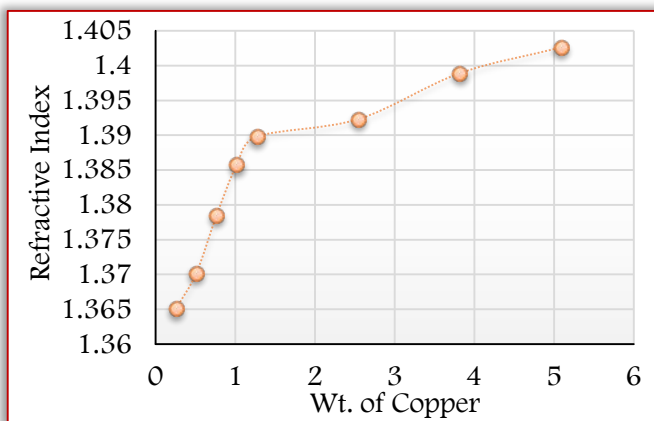


Figure 1: Calibration chart

Table 1 and Figure 1 shows the relation between Weight of copper and Refractive Index. From Figure 1, it is clear that if concentration of copper solution increases Refractive index also increases.

— Experimental procedure

Take 4 conical flasks and add 100 ml water to each of the flask respectively. Label them as 1,2,3,4. Add 5,10,15,20 grams of $\text{CuSO}_4 \cdot 5\text{H}_2\text{O}$ into each flask respectively. When the solution becomes uniform, measure the Refractive Index of solution in each flask using the Refractometer. Now add 1gm of adsorbent (Mango Peel Powder) to each of the flask and keep it in shaker for 20 minutes. After 20 minutes take out the samples and filter the solution using Whitman Filter paper (Grade 1-Particle retention $120\mu\text{m}$). Collect the filtrate and measure Refractive Index. Repeat the same procedure for contact time 40 minutes and 60 minutes by varying adsorbent (MPP) weight i.e., 1gm and 2 gm. The experiments of copper adsorption were performed batch wise [12-13].

RESULTS AND DISCUSSIONS

— Effect of Concentration of copper sulphate solution on % Removal for 1 gram MPP

Table 2 and Figure 2 describes the variation in the percentage removal of copper (II) for 1 gram of adsorbent, MPP with various concentrations. For the contact time of 20 minutes, maximum percentage removal is obtained at 0.15 ppm (63.62%) and minimum removal at 0.2 ppm (18.91%). For 40 minutes contact time, maximum percentage removal is obtained at 0.15 ppm (65.33%) and minimum removal at 0.2 ppm (30.3%).

For 60 minutes contact time, maximum percentage removal is obtained at 0.1ppm (76.89%) and minimum removal at 0.05 ppm (61.65%). Therefore for an adsorbent dosage of 1 gram, maximum removal of copper can be obtained at 60 minutes, which shows that more the contact time; more will be the adsorption capacity.

Table 2: Concentration vs. % Removal for 1 gram MPP

S.No	Concentration	% Removal at 20 mins	% Removal at 40 mins	% Removal at 60 mins
1	0.05	38.1	58.1	61.65
2	0.1	60.2	63.1	77
3	0.15	63.62	65.33	76.89
4	0.2	18.91	30.3	75

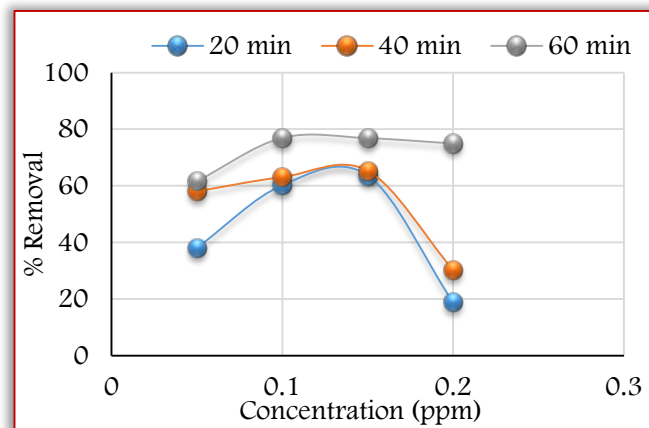


Figure 2: Concentration vs % removal plot for 1 gm MPP

— Effect of Concentration of copper sulphate solution on % Removal for 2 gram MPP.

Table 3 and Figure 3 describes the variation in the percentage removal of copper (II) for 2 gm of adsorbent, MPP with various concentrations. For 20 minutes contact time, maximum percentage removal is obtained at 0.1 ppm (50.99%) and minimum removal at 0.05 ppm (24.27 %).

For 40 minutes contact time, maximum percentage removal is obtained at 0.15 ppm (74.42%) and minimum removal at 0.2 ppm (58.65 %). For 60 minutes contact time, maximum percentage removal

is obtained at 0.05 ppm (78.87%) and minimum removal at 0.2 ppm (71 %). Therefore for an adsorbent dosage of 2 gram, maximum removal of copper can be obtained at 40 minutes.

Table 3: Concentration vs. % Removal for 2 gram MPP

S.No	Concentration	% Removal at 20 mins	% Removal at 40 mins	% Removal at 60 mins
1	0.05	24.27	58.65	78.87
2	0.1	50.99	68	70
3	0.15	28	74.42	75
4	0.2	31	46	71

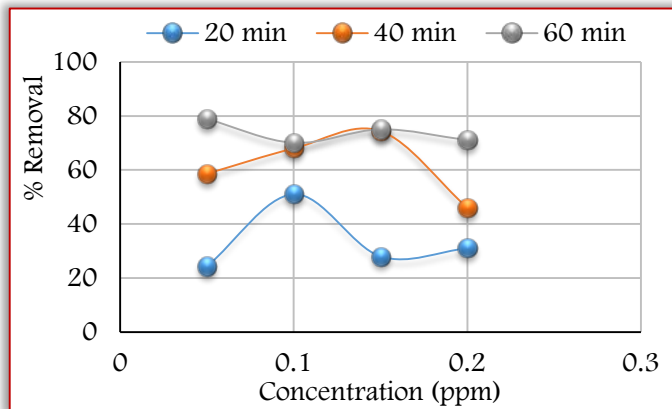


Figure3: Concentration vs % removal plot for 2 gm MPP

CONCLUSIONS

The study shows that adsorption can be used as an efficient method for removal of pollutants from water and thus decontaminating it. However, this process is restricted due to the high cost of the traditional adsorbents like activated carbon.

This study concludes that the removal of heavy metals from water is very important to safeguard society and environment from dangers. This study explored the potential of low cost adsorbent for its ability to adsorb Copper (II). Removal of copper (II) has been studied using surface assimilation process with Mango Peel Powder.

Study can be concluded based on two important factors those are based upon availability of adsorbent (MPP) and time available. If time is considered then the best result can be obtained at a contact time of 40 minutes and concentration of 0.15 ppm for 2 gm of MPP whereas when the availability of adsorbent is considered then the best result can be obtained at contact time of 60 minutes for 1 gm of MPP at concentration of 0.1 ppm.

Acknowledgements:

The authors wish to gratefully acknowledge the support of the Management of MVGRCOE (A), Vizianagaram for carrying out the research work.

References

- [1] Ajmal, MA, Hussain Khan S and Ahmad, A: Role of sawdust in the adsorption of Cu (II) from industrial wastes, *Wat. Res*, 32, 3085-3091, 1998.
- [2] Ajmal, MA, Mohammad, R., Yousuf and Ahmad, A: Adsorption behavior of Cadmium, Zink, Nickel, and Lead from aqueous solution by *Mangifera India Seed Shell*, *India J. Environment Health*, 40,15-26, 1998.
- [3] Anoop Krishnan K., Sreejalekshmi K.G., Vimexen V., Vinu V. Dev: Evaluation of adsorption properties of sulphurised activated carbon for the effective and economically viable removal of Zn(II) from aqueous solutions, *Ecotoxicology and Environmental Safety*, 124, 418-425, 2016.
- [4] ASTM E478 - 08. "Standard Test Methods for Chemical Analysis of Copper Alloys".
- [5] Malkoc, E., and Nuhoglu, Y: Investigations of Nickel (II) Adsorption from Aqueous Solutions Using Tea Factory Waste, *J. Hazardous Materials*, B127, 12-19, 2005.
- [6] Malkoc, E., and Nuhoglu, Y: Fixed bed studies for the sorption of chromium (IV) onto tea factory waste, *Chem. Eng. Sci.*, 61, 4363-4370, 2006.
- [7] Malkoc, E., and Nuhoglu, Y: Adsorption of Ni (II) ions from aqueous solutions using waste of tea factory: adsorption on a fixed-bed column, *J. Hazardous Materials*, B135, 328-236, 2006.
- [8] Malkoc, E., and Nuhoglu, Y: Potential of tea factory waste for chromium (VI) adsorption from aqueous solutions: thermodynamic and kinetic studies, *Sep. Purif. Technol.*, 54, 291-298, 2007.
- [9] Sastry, S.V.A.R. & Sarva Rao, B: Studies on adsorption of Cu (II) using spent tea extract (STE) from industrial wastewater, *i-manager's Journal on Future Engineering & Technology*, 11 (3), 31-35, 2016.
- [10] Sastry, S.V.A.R. & Sarva Rao, B: Determination of adsorption kinetics for removal of copper from wastewater using Spent Tea Extract (STE), *i-manager's Journal on Future Engineering & Technology*, 12 (4), 27-32, 2017.
- [11] Sastry, S.V.A.R. & Anusha, S.A: Studies on continuous adsorption of acetic acid from aqueous solution using rice husk adsorbent, *i-manager's Journal on Future Engineering & Technology*, 14 (1), 42-47, 2018.
- [12] Sastry, S.V.A.R. & Padma D.V: Biosorption of Hexavalent Chromium using Mallet Flower Leaves Powder as adsorbent, *TEST Engineering and Management*, 83 (March/April), 15714- 15729, 2020.
- [13] Sastry, S.V.A.R., Sarva Rao, B & Padma D.V: Studies on Selective Batch Adsorption of Cu(II) and Cr(VI) from aqueous solution, *TEST Engineering and Management*, 83 (May/June), 2020.

Fascicule 3

[July – September]

t o m e

[2020] XIII

ACTA Technica CORVINIENSIS
BULLETIN OF ENGINEERING



ACTA TECHNICA CORVINIENSIS – Bulletin of Engineering

ISSN: 2067-3809

copyright © University POLITEHNICA Timisoara,

Faculty of Engineering Hunedoara,

5, Revolutiei, 331128, Hunedoara, ROMANIA

<http://acta.fih.upt.ro>

¹Mustefa JIBRIL, ²Eliyas Alemayehu TADESE

H2 OPTIMAL AND μ -SYNTHESIS DESIGN OF QUARTER CAR ACTIVE SUSPENSION SYSTEM

¹Department of Electrical & Computer Engineering, Dire Dawa Institute of Technology, Dire Dawa, ETHIOPIA

²Faculty of Electrical & Computer Engineering, Jimma Institute of Technology, Jimma, ETHIOPIA

Abstract: Better journey comfort and controllability of automobile are pursued via car industries with the aid of considering using suspension system which plays a very crucial function in handling and ride comfort characteristics. This paper presents the design of an active suspension of quarter automobile system using robust H2 optimal controller and robust μ -synthesis controller with a second order hydraulic actuator. Parametric uncertainties have been additionally considered to model within the system. Numerical simulation become completed to the designed controllers. Results display that during spite of introducing uncertainties, the designed μ -synthesis controller improves ride consolation and road protecting of the automobile while as compared to the H2 optimal controller.

Keywords: Quarter car active suspension system, H2 optimal controller, μ -synthesis controller

INTRODUCTION

An automobile suspension system is the mechanism that bodily separates the automobile body from the wheels of the car. The cause of suspension system is to enhance the experience comfort, road handling and stability of automobiles. Apple backyard and Well stead have proposed several performance traits to be taken into consideration so one can obtain an excellent suspension system. Suspension includes the system of springs, shock absorbers and linkages that connects a vehicle to its wheels. In other that means, suspension system is a mechanism that bodily separates the car body from the automobile wheel. The principal feature of automobile suspension system is to limit the vertical acceleration transmitted to the passenger which directly affords road consolation.

The fundamental idea of land vehicle transportation has not modified tons inside the previous few many years, although a great deal progress become made in enhancing and optimizing automobile design and era. The quest to continually go quicker, similarly and extra effortlessly, has lead in latest years to the improvement of advanced suspension structures. A progressed suspension system allows a vehicle to attain better speeds over rougher terrain, and results in better handling, in addition to improved trip consolation.

A first step in vehicle suspension design is estimating a preferred spring and damper function, and verifying that characteristic the use of software program simulation. The models used at some point of this step are generally low-order, simple fashions, which hampers short development progress. To predict car response before automobile prototype finishing touch, many researchers have tried to use complex and superior damper fashions to simulate the car's dynamics, however these fashions all be afflicted

by a few disadvantage – it's far both based on empirical statistics, giving no indication of the bodily parameters of the design sought; it could be overly complex, having many parameters and accordingly rendering software impractical; or it can be quick however based totally on the idea that there's no hysteresis in the damping character.

MATHEMATICAL MODELS

— Active Suspension System Mathematical Model

The quarter car active suspension system model is shown in Figure 1.

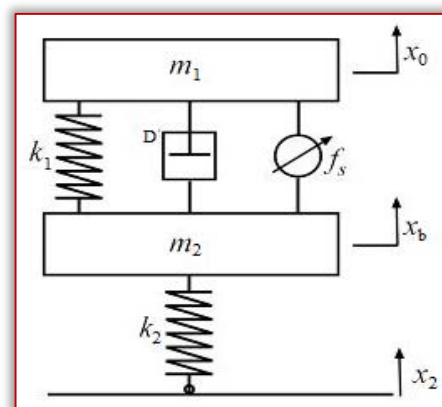


Figure 1: Quarter model of active suspension system
The quarter car active suspension system mathematical model for a two degrees of freedom motion differential equations will be as follow:

$$m_1 \ddot{x}_0(t) + D[\dot{x}_0(t) - \dot{x}_2(t)] + k_1[x_0(t) - x_2(t)] = u \quad (1)$$

$$m_2 \ddot{x}_2(t) - D[\dot{x}_0(t) - \dot{x}_2(t)] + k_1[x_2(t) - x_0(t)] + k_2[x_2(t) - x_1(t)] = -u \quad (2)$$

ROAD PROFILES

— Random Road Profile

The random road disturbance input has a maximum peak of 15 cm and minimum peak of -15 cm as shown in Figure 2.

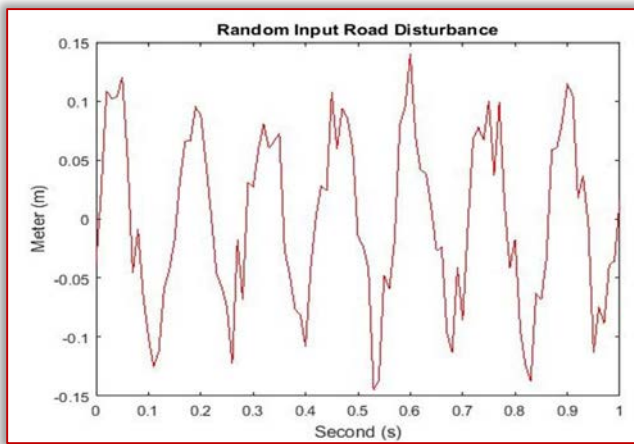


Figure 2: Random road profile

THE PROPOSED CONTROLLER DESIGN

The active suspension system with H2 optimal and μ -synthesis controllers with a second order hydraulic actuator system block diagram is shown in Figure 3.

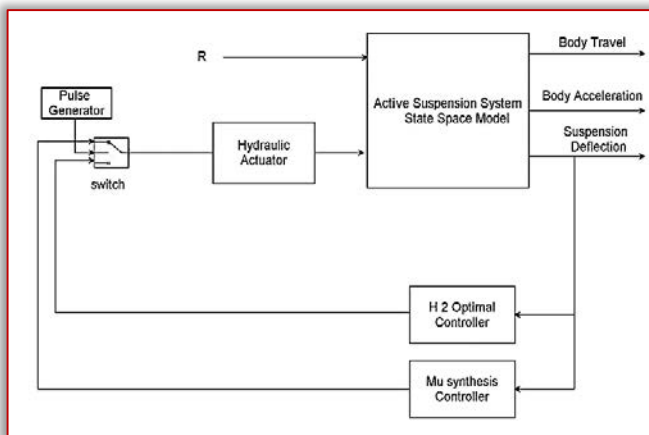


Figure 3: Active suspension system with H2 optimal and μ - synthesis controller's system block diagram

The switching system switch in micro seconds. The hydraulic actuator model is a second order transfer function defined as:

$$actuator = \frac{4s + 23}{s^2 + 26s + 14} \quad (3)$$

RESULT AND DISCUSSION

The quarter car active suspension system parameter values are shown in Table 1.

Table 1: Parameters of quarter vehicle model

Model parameters	symbol	symbol Values
Vehicle body mass	m 1	4550 Kg
Wheel assembly mass	m 2	63 Kg
Suspension stiffness	k 1	18,500 N/m
Tire stiffness	k 2	165,000 N/m
Suspension damping	D	800 N-s/m

—Control Targets Output Specifications

The control targets output specifications of the quarter car active suspension system is shown in Table 2 below.

Table 2. Control targets output specifications

No	Control Targets	Output
1	Body travel	Minimum
2	Body acceleration	Minimum
3	Suspension deflection	Same as Road Profile

—Simulation of a Random Road Disturbance

The body travel, body acceleration and suspension deflection simulation output is shown in Figure 4, Figure 5 and Figure 6 respectively.

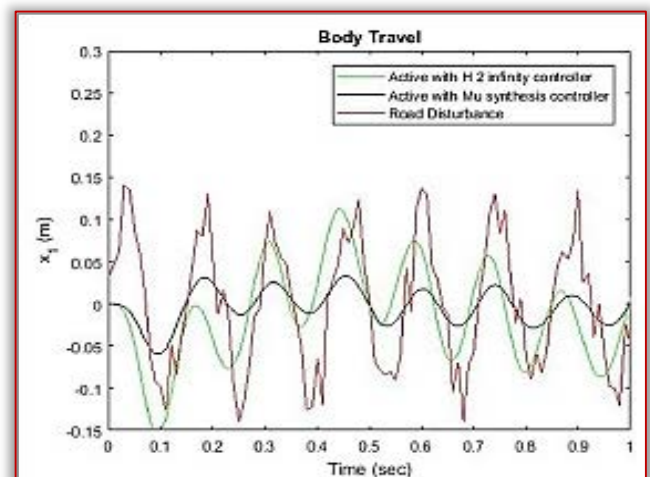


Figure 4: Body travel for random road disturbance

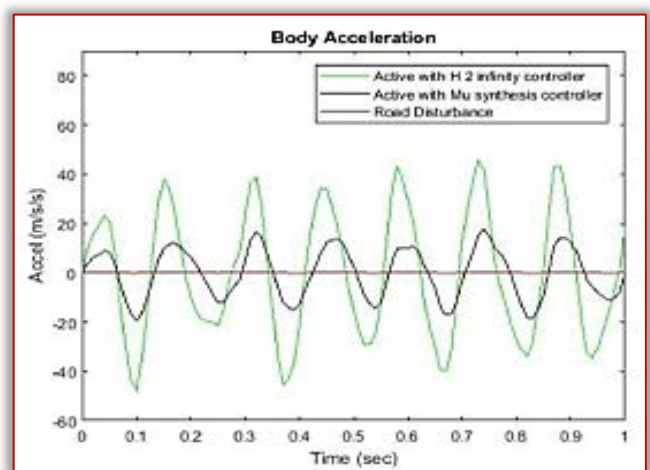


Figure 5: Body acceleration for random road disturbance

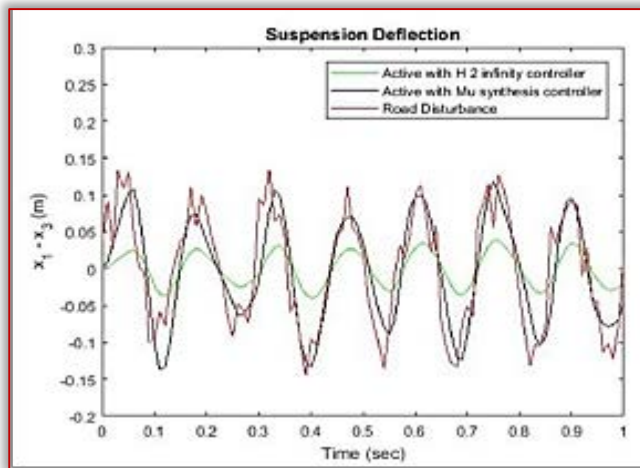


Figure 6: Suspension deflection for random road disturbance

—Numerical Values of the Simulation Outputs

The numerical values of the simulation output for the control targets body travel, body acceleration and suspension deflection is shown in Table 3, Table 4 and Table 5 bellow.

Table 3: Numerical values of the body travel simulation output

No	Systems	Random
1	Road Profile	0.15m
2	H2 Optimal	0.04m
3	μ - synthesis	0.01m

Table 2 shows us the active suspension system with μ - synthesis controller have the minimum body travel amplitude in the random road profile.

Table 3: Numerical values of the body acceleration simulation output

No	Systems	Random
1	Road Profile	5 m/s ²
2	H2 Optimal	40 m/s ²
3	μ - synthesis	20 m/s ²

Table 3 shows us the active suspension system with μ - synthesis controller have the minimum body acceleration amplitude in the random road profile.

Table 4: Numerical values of the suspension deflection simulation output

No	Systems	Random
1	Road Profile	0.14m
2	H2 Optimal	0.04m
3	μ - synthesis	0.14m

Table 4 shows us the active suspension system with μ - synthesis controller have the suspension deflection amplitude the same as the road profile input in the random road profiles.

CONCLUSIONS

The technique turned into advanced to design an active suspension for a passenger vehicle with the aid of designing a controller, which improves overall performance of the system with respect to design desires compared to active suspension system.

Mathematical modeling has been accomplished using a two degree-of-freedom model of the quarter vehicle model for active suspension system considering best vertical movement to evaluate the overall performance of suspension with recognize to various contradicting design goals.

H2 optimal and mu-synthesis controllers design method has been tested for the active suspension system using random road profile. The capability for advanced experience comfort and better road managing using H2 optimal and mu-synthesis controllers design is examined. The objectives of this undertaking were achieved.

Dynamic model for linear quarter car active suspension systems has been formulated and derived for the 2 types of the proposed controllers.

The two proposed controllers are compared and the simulation consequences prove the effectiveness of the provided active suspension system with mu synthesis controller.

References

- [1] Pusadkar et al. "Linear Disturbance Observer Based Sliding Mode Control for Active Suspension Systems with Non-ideal actuator" Journal of Sound and Vibration, p 428-444, 2019.
- [2] Jianjun Meng et al. "Robust Non Fragile H infinity Control of Lateral Semi-active Suspension of Rail Vehicles" Journal of Discrete Dynamics in Nature and Society, p 1-12, 2019.
- [3] Chen.X et al. "Robust H infinity Control Design of an Electromagnetic Actuated Active Suspension Considering the Structure Nonlinearity" Journal of Automobile Engineering, 2018.
- [4] Kuiyang Wang et al. "Static Output Feedback H infinity Control for Active Suspension System with Input Delay and Parameter Uncertainty" Journal of Advances in Mechanical Engineering, 10(7), 2018.
- [5] Pang.H "Adaptive Back Stepping Based Tracking Control Design for Nonlinear Active Suspension System with Parameter Uncertainty and Safety Constraints" ISA Transactions, 2018.
- [6] Pan.H et al."Robust Finite-time Tracking Control for Nonlinear Suspension Systems via Disturbance Compensation" Mechanical System Signal Processing, p 49-61, 2017.
- [7] Yusuf Altun et.al "The Road Disturbance Attenuation for Quarter Car Active Suspension System via a New Static Two Degree of Freedom Design" An

- International Journal of Optimization and Control: Theories & Applications, Vol 7, No 2, 2017.
- [8] Jeng Lang Wu et al. “A Simultaneous Mixed LQR/H infinity Control Approach to the Design of Reliable Active Suspension Controllers” Asian Journal of Control, 2017.
- [9] Liu .et al. “Adaptive Sliding Fault Tolerant Control for Nonlinear Uncertain Active Suspension System” Journal of Franklin Vol. 353, p 180-199, 2016.
- [10] Bhowmik.A et al. “Adaptive Fault Tolerant Control for Active Suspension” IEEE First International Conference on Control, Measurement and Instrumentation, p 386-390, 2016.
- [11] L.C Felix Herran et al. “H2 Control of a One Quarter Semi-active Ground Vehicle Suspension” Journal of Applied Research and Technology, 2016.



ACTA TECHNICA CORVINIENSIS – Bulletin of Engineering
ISSN: 2067-3809
copyright © University POLITEHNICA Timisoara,
Faculty of Engineering Hunedoara,
5, Revolutiei, 331128, Hunedoara, ROMANIA
<http://acta.fih.upt.ro>

¹Tihomir S. LATINOVIC, ²Mladen M. TODIC, ³Dorian NEDELCU, ⁴Cristian P. BARZ

IMPROVING THE SAFETY OF RAILWAY FROM BASIC START-STOP TO THE INTELLIGENT SYSTEM

¹University of Banja Luka, Banja Luka, BOSNIA & HERZEGOVINA

²University of Banja Luka, Banja Luka, BOSNIA & HERZEGOVINA

³„Eftimie Murgu” University of Resita, Department of Materials Engineering, ROMANIA

⁴Universitatea Tehnica Cluj Napoca, Centrul Universitar Nord Baia Mare, ROMANIA

Abstract: Increasing railway safety is the basis of new high-speed railways. To do this, we need automatic locomotive protection in increasing the safety of railway traffic. The basic system used in this is the so-called start / stop automatic protection system type RAS 8385, which consists of a part located on a locomotive and a part located on rails. System has two parts. One is mounted on a locomotive and the other on rails. By contacting the track section and the rolling mode, the locomotive can be stopped if, after contact with the track section, the locomotive has passed faster than it should or had to stop, so the system will automatically lock and shut it down. This system is used to avoid driver errors and reduce its impact on railway safety. The previous start-stop system does not provide complete protection at open crossings, which we have from the moment of the locomotive's exit to its departure at the destination. In the world, and especially in the western Balkans, there are many unmarked crossings or crossings without secure protection against an incoming locomotive other than a warning or light signaling. Then collisions happen with catastrophic consequences. With the help of new intelligent technologies and the above system, it is possible to minimize problems.

Keywords: safety system, railway, intelligent system

INTRODUCTION

Rail is a mode of transport that statistically and practically belongs among the safest and the most efficient modes of transportation. This fact is greatly supported by the continuous development of the system for the management of railway traffic which directly affects its efficiency. The international system for a train control is (ETCS), that is well received in Europe and is expanding to other continents [2]. Teaching, there are also national systems that are generally complementary to ETCS, ie one does not exclude the other. From the beginnings of rail, we have always been a need to develop systems that can control rail traffic. For this purpose, signaling technology is constantly improved, ranging from hand signals to modern technologies. On Figure. 1 is Locomotive upgraded with protection system RAS 8385.



Figure. 1 Locomotive 441-521 with protection system type RAS 8385

All safety railway systems, starting with those used from the beginning of a railway in Europe, down to the most modern, they share the same concept - trains cannot collide if they do not maybe in the same section

of line at the same time [4]. For this reason, the line is divided into sections, also known as blocks. In practice, a train is allowed to occupy only one section. Like on the Figure 2.

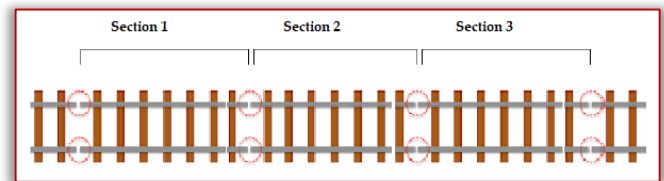


Figure 2. Railroad divided into Sections
Signaling in railway is based on automatic track sections without manual intervention. The section equipped with automatic sections is divided into sections not shorter than the stopping distance of the fastest train running on that section. The function of detecting the presence or passing of a vehicle in a particular compartment may be realized through 2 types of different equipment: [1], [4]

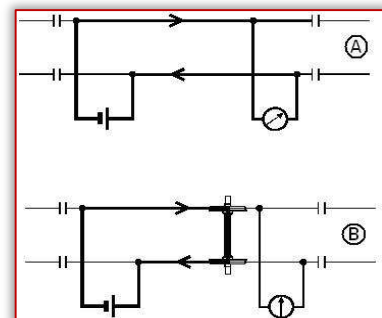


Figure 3. Free (A) and occupied (B) track circuit
An electromagnetic device (relay) realizes the track circuit, an electrical circuit that used as a conductor, the two rails of the track. The transit of a vehicle on

the track causes the electrical contact on the two rails, so the circuit is closed, the relay is characterized by zero current and the block signal is set at danger (or occupied) like on the Figure 3.

On modern railway lines, at the beginning and end of each block section, equipment called an axle counter is installed. The task is to count, discovering all the axles of the vehicle fleet that travel on the track, as well as their driving direction, using two electronic sensor systems on wheels. By comparing the result for the included axes and the result for the counted axes, it is possible to know the status of the track section (free or busy). According to Figure 4, as long as the number of axes of the counted Ak2 (train exiting TS1) is not equal to the number counted Ak1 (train entering TS1), then the track TS1 will be considered "occupied". [4]

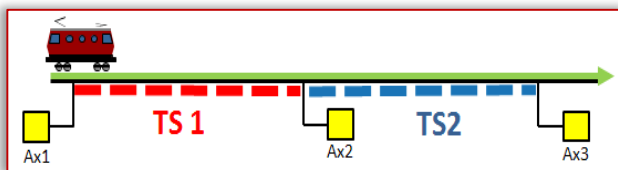


Figure 4. Axle Counters for track occupation detecting
ATP SYSTEMS

ATP Systems from the 80s upgraded rail signaling systems that are used in Europe, for increasing railway safety. The basic idea is to constantly monitor the speed of the train. They're called *ATP* (Automatic Train Protection) systems.

The basic system used in this is the so-called start / stop automatic protection system type RAS 8385, which consists of a part located on a locomotive and a part located on rails. The basic division of the Automatic train protection (ATP) have the point and continuous systems. Figures 5, 6 and 7.



Figure 5. Type LLC0512 ALPRO in direction on the cabin of a train.

ATP system RAS 8385 works on the principle of interaction of resonant circuits. A locomotive ATP device which means a device installed on a traction unit vehicle is configured to transmit or receive inductive balize information by influencing the frequencies of 500 Hz, 1000 Hz, and 2000 Hz.

The actuator, located in the central part of the device, sends a signal that activates pneumatically part of the ATP device and, if necessary, performs forced braking. The same signal is sent at the same time and according to the parts of the ATP device in the steering wheel

where the light and sound signaling indicates the response of the locomotive part of the device or possible forced braking.



Figure 6. Rail balize

Also, this signal is sent to the recorder (located in the cabinet of the central unit of the ATP device) which records the forced braking, ie passing of the locomotive past the prohibited driving signal. On identical the ATP mode responds if the prescribed speed for the default driving mode also occurs, passing a signal with a speed limit signal.



Figure 7. Position of rail balize.

The autostop system with the central device RAS 8385 consists of locomotive and track magnets, as well as signal and control elements in the steering wheel of the vehicle. This system is based on the inductive mode of information transfer from the track part of the device to the part located on the traction vehicle and is designed to increase the safety of railway traffic [7],[8]. The hitchhiker is used for speeds up to 160km / h. [10]

Table 1. Driving mode for different top and restriction speed

Top speed [km/h]	Driving mode	500 Hz	Time control [s]	100Hz	Vigilance [s]
		Restriction speed [km/h]		Restriction speed [km/h]	
140	1	65	20	90	4
100	2	50	26	65	4
80	3	40	24	50	4

When the train is running at normal speed, ie respecting traffic signs, this device does not affect the train running mode [3,5]. Information from the rail Balize is inductively transmitted to the locomotive magnet, and from there to the executive member of the central device.

Then the driver has a certain amount of time to confirm that he has noticed a signal sign, i.e. to confirm his alertness with the vigilance button, and to adjust his speed to the prescribed speed. If these actions are not performed, the air is released in the main brake line, and the train brakes automatically.

INTELLIGENT TRANSPORT SYSTEM (ITS)

Technologies like Global Positioning System (GPS), Satellite Communication, and care used to establish communication between vehicles. Such Intelligent Transport Systems offer a communication platform to facilitate the sharing of information and knowledge within the transportation infrastructure to allow the realization of a range of safety and mobility applications [4].

ITS enables applications across three main categories, with the potential to offer significant social, economic and environmental benefits, namely:

- Safety: ITS safety applications use the communication mechanism within DSRC to create complete situation awareness for vehicles.
- Mobility: ITS mobility applications include travel and route planning, traffic and congestion management including public transport, transport network productivity and reliability enhancement, etc.
- The overall aim of the project was to research, develop, implement and trial (for potential rollout) a DSRC based Intelligent Transport System to improve safety at level crossings. The system aims to reduce and potentially eliminate rail-road crossing accidents by enabling dynamic vehicle-to-vehicle (V2V) and vehicle-to-infrastructure (V2I) communications using DSRC technology. The specific aims within the scope of the project are:
 - Phase 1: To develop an Intelligent Transport System (ITS) simulation platform for rail-road crossings based on 5.9GHz DSRC technology
 - Phase 2: To develop an ITS demonstrator and Proof-of-Concept system
 - Phase 3: To carry-out field trials at level crossing interfaces

Figure 8 illustrates the system architecture of the proposed DSRC based Intelligent Transport System deployed at a level crossing. The system is composed of DSRC enabled roadside units (RSUs) and on-board units (OBUs). The RSUs are placed at locations such as rail-road crossing active signs while the OBUs are installed in road vehicles and trains. [5]

A DSRC based ITS at the level crossing will enable communication between infrastructure nodes and vehicles in the vicinity of the crossing including trains and road vehicles. This communication will enable sharing abundant data between vehicles including basic information such as vehicle size and type, position and motion and other control information such as brake status, throttle, steering angle, etc. Depending on various parameters and conditions, the information can be shared directly using V2V communication or indirectly using V2I communication as presented in Figure 8. The

information will be used by a specialized level crossing safety application to generating warning messages such as advice of an approaching train, an advance indication of a potentially faulty crossing, expected delay at the level crossing, suggestion of alternate routes, etc. The Human-Machine-Interface (HMI) used to communicate safety messages to drivers was developed to not only address the immediate safety requirements but also to promote overall long term behavioral change of drivers towards safety consciousness.

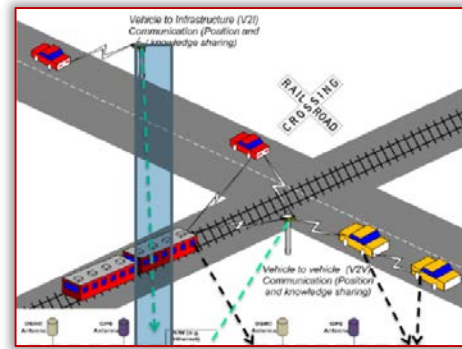


Figure 8. Architecture of Intelligent Transport System [5]
The number of devices we need to manage and communicate will be many times greater than the devices connected to the current Internet. The ratio of communication activated by devices concerning communication activated by humans will also be many times higher like in Figure 9.

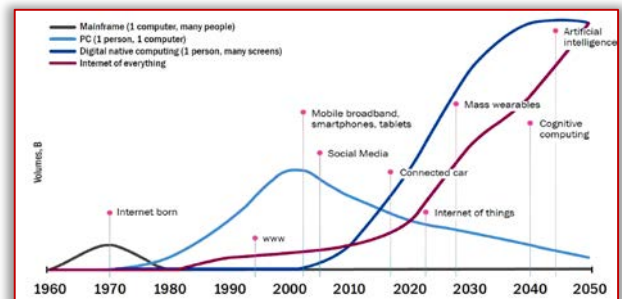


Figure 9. Prediction of the number of digital devices in the future. [6]

Autonomous vehicles have evolved from the technology of the future that was developed in laboratories to the technology that is used and can be seen on the roads like on Figure 10. Test vehicles of companies such as Uber, Waymo, Tesla and Toyota can be seen on the roads and streets of Phoenix, Pittsburgh and Boston. Although there are concerns in America about the safety of autonomous vehicles, due to the last traffic accident in which a pedestrian was killed, the question arises whether autonomous vehicles will be ready for mass access to the roads at all. The answer is yes, but autonomous vehicles will become a reality only when the 5G data network becomes ubiquitous. The current 4G network has quite enough speed if we want to share updated statuses or order a ride, but it cannot give vehicles the

reflexes that people have. Had the capabilities of the 4G network been different, an accident involving an Uber vehicle would surely have been avoided..

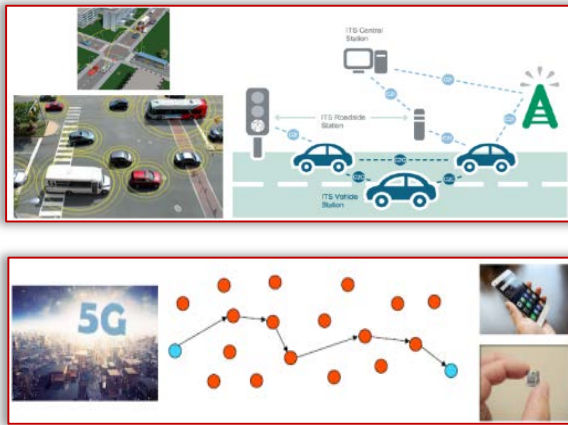


Figure 10. Autonomous vehicles and 5G network to support the development of autonomous and semi-autonomous vehicles

The new 5G network brings with it both autonomous and semi-autonomous vehicles, as well as other technologies, such as virtual reality, smart things, smart apartments, smart guards and artificial intelligence. The 5G network will enable the connection of everything around us in a 1.5 Gb network, and thus the responses, distribution and capacity of the technologies we mentioned earlier. It represents the last part of the connective technological tissue that autonomous vehicles lack, as well as to participate in events and games in real-time. The phone will also run at 1.5 GB and will be a supercomputer with an instinctive connection with other phones [10]

CONCLUSIONS

The paper describes the basic characteristics of hitchhiking devices RAS 8385, and devices for registration of events IRAS 19. Test data were analyzed using IRAS 19. Based on the obtained results, it was concluded that the hitchhiking device RAS 8385 is very effective for increasing railway safety because it can significantly reduce the occurrence of driver errors relevant to safe train running and reduce unwanted outcomes. these errors.

To make the railway system safe and efficient, signaling and train control means are required. They help prevent driver mistakes, monitor their actions, and act as needed to prevent unwanted train collisions. As the technology evolved, the initial mechanical interaction between track and train soon was replaced by permanent magnets and the development of the future most applicable system for train protection in Europe has begun.

The railway management of the region should re-evaluate their approach to monitoring safety and to set priorities for implementing safety enhancement on their respective systems. Desirably, all railway systems of the region should carry out regular safety audits

and risk. The use of a Safety Management System will improve the capability of railway management to identify and prioritize level crossing safety enhancement measures. Existing technologies, such as Global Positioning System (GPS), Satellite Communication, can be employed to establish communication between vehicles. Such Intelligent Transport Systems offer a communication platform to facilitate the sharing of information and knowledge within the transportation infrastructure to allow the realization of a range of safety and mobility applications. Future safety systems are based on the development of a 5G network and connected every transport machine from car to railway machine to machine M2M.

Such a system will be semiautomatic to the automatic car or railway giving the best dose of security for everybody. With 1,5 Gb of download and almost half of upload fastness of 5G network will give us support for any kind of safety systems.

References

- [1] Toš, Z.: Signalizacija u željezničkom prometu, Fakultet prometnih znanosti, Zagreb, 2013.
- [2] Simon F. Ruesche, Jan Steuer, Klaus Jobmann, (2009), Increase of efficiency in wireless train control systems (etcs level 2) by the use of actual packet-oriented transmission concepts, Institute Communications Technology, Hannover (Germany)
- [3] Maurizio Palumbo, Railway Signalling since birth to ERTMS (2013). railwaysignaling.eu, Italy
- [4] J. Singh, A. Desai, F. Acker, S. Ding, S. Prakasamul, A. Rachide, K. Bentley and P. Nelson-Furnell, Cooperative intelligent transport systems to improve safety at level crossing, Centre for Technology Infusion, La Trobe University, Melbourne, Australia, 2012
- [5] J Singh, A Desai, T Spicer, Intelligent system to improve safety at level crossing, Conference On Railway Engineering Wellington, 2010
- [6] Marco Zennaro, Introduction to the internet of things, Abdus Salam International Centre for Theoretical Physic, Trieste, Italy, 2016
- [7] Railway signaling .eu. Downloaded from: <http://www.railwaysignalling.eu/etcs-level> [Accessed Jun 2020]
- [8] Railway signaling .eu. Retrieved from: <http://www.railwaysignalling.eu/wp-content/uploads/2019/10/>
- [9] <https://www.scribd.com/document/361862745/Nordic-Smart-Cities-Carlo-Fischione-short-Low-Res-content/uploads/2019/10>
- [10] <https://altpro.hr/en/product/safety-systems-for-rolling-stock-automatic-train-protection-system-ras-8385-central-device-14>

ACTA TECHNICA CORVINIENSIS – Bulletin of Engineering
ISSN: 2067-3809

copyright © University POLITEHNICA Timisoara,
Faculty of Engineering Hunedoara,
5, Revolutiei, 331128, Hunedoara, ROMANIA
<http://acta.fih.upt.ro>

¹Ancuța N. JURCO, ²Liviu I. SCURTU

GEOMETRICAL DESIGN AND CRASH SIMULATION OF A SHOCK ABSORBER

^{1,2}Technical University of Cluj-Napoca, Faculty of Automotive, Mechatronics & Mechanical Engineering, ROMANIA

Abstract: The safety of the car passengers is an important issue that must be achieved in the structural design of the vehicles. To increase the safety of the passengers, it is intended to design and build the bodywork structure that have a geometry who can reduce the car damage and the passenger's injury in the crash impact. The shock absorber used for automotive structure are intermediate body elements placed between the front bumper and the chassis structure. The study presented on this paper shows the behavior in the case of a frontal impact of a shock absorber structure. In the first part of the paper are presented the latest research and methods used for virtual testing, using finite element methods. Second part of the paper presents the geometrical design and finite element analysis of the proposed shock absorber geometry. Each model is simulated in concordance with the real work condition, with same loading case. Obtained result are analyzed, determining the von Mises stress and displacement.

Keywords: bumper, shock absorber, FEA, solver

INTRODUCTION

In recent years, the rapid development of the automotive industry and required standards regarding the safety of the traffic participants involves the development of new structural parts that can increase the safety in the event of a crash. Current design, simulation and validation techniques improve the comfort and safety of the car passengers. Some of the studies from this research field are presented in the following paragraphs. An extensive study described in eight chapter present the base steps that determine the design, modelling, finite element crash simulation and results interpretation. With the purpose of shock absorber structure optimization for increase the passenger safety are presented various frontal bumper crash scenarios. After simulation, the resulting deformation and the absorbed energy it is observed [7]. The behavior of a chassis structure is crashed from a rigid wall and from a rigid pole at a velocity of 15 m/s. The chassis structure is solved in Radioss solver from both cases. The obtained results show the chassis structure have a better impact behavior of the rigid wall than the case of the rigid pole impact [4]. Another crash analysis that investigates the ways to improve the design of the frontal bumper is presented in [1]. The simulation of the crash is performed at a velocity of 30 m/s. The effect of the thin-walled structure in automotive crashworthiness are studies in [3]. The objective of this study is to optimize a thin-walled structure to attenuate the frontal impact. Are tested five structure models using the explicit finite element method of Ls-Dyna. Praveenkumar present the study of the frontal impact for three different bumpers. The simulation is done at the 17.778 m/s initial speed of the structure and the distance between the bumper and the barrier is 100 mm. The bumper material is an aluminum alloy [2].

FINITE ELEMENT METHOD

Currently the finite element analysis is a numerical simulation method implemented in engineering. In the next paragraphs is presented the base steps that must be follow in order to perform a crash finite element analysis. In figure 1 is presented the flowchart of the crash analysis process [6].

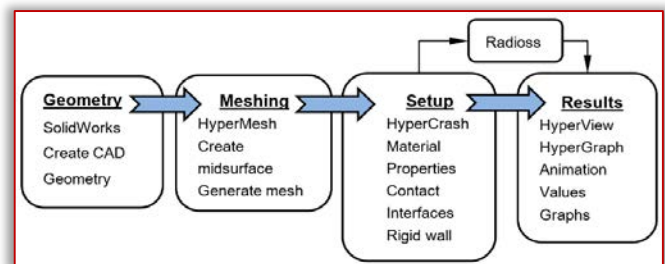


Figure 1 - Flowchart of the crash analysis process

CAD GEOMETRY

The study of the geometry is performed in order to obtain a shock absorber design that have a better performance in case of the frontal crash. The first step of this study is given by the conception and create the CAD model of the shock absorber. In figure 2 is presented the orthogonal and isometric projection of the shock absorber model.

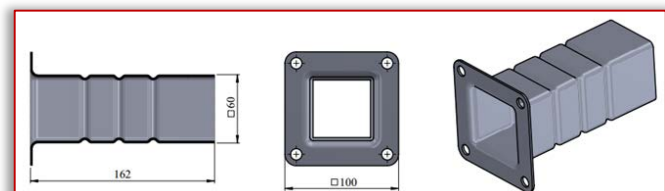


Figure 2 - CAD model of the shock absorber

Using the advanced modelling techniques in SolidWorks [9] software the proposed geometry of the shock absorber is generated. The model is created from a rectangular shape from 60 mm and a 4 mm thickness. The shock absorber geometry is exported from SolidWorks in IGES format.

GEOMETRY DISCRETIZATION

The structure geometry is imported into Hypermesh environment, where is prepared for meshing. After the cleanup surface process, the midsurface of the solid geometry is extracted by using the software commands. Geometry discretization is the fundamental steps required by finite element method and consist in transition from the continue structure to a discrete model with a finite number of points. The surface geometry is meshed automatically according to the pre-determined the quality criterion of the elements.

The property definition, material assigning, contact between surface, imposing the simulation condition and creating rigid elements are done in HyperCrash™. In order to set an imposed velocity of the meshed structure on the rear side of the absorber are created a rigid body element. The mass is attached from the master node in the center of mass of a slave node group. The resulted model is run in Radioss solver and the obtained results are performed in HyperView and HyperGraph [10].

MATERIAL MODEL

The assigned materials from both crash study from the shock absorber are steel and aluminum. The chosen material model from HyperCrash is an elastoplastic material Johnson Cook (Law 2). This material type includes strain rates and the temperature effect.

The mechanical properties of the assigned materials are shown in table 1. In law 2, the material behaves as linear elastic when the equivalent effort is less than yield stress. For high values of the strain, the material's behavior becomes plastic.

Table 1. Mechanical properties of the materials [8]

Steel		Aluminum	
Initial density	7.85e-6 kg/m ³	Initial density	2.7e-6 kg/m ³
Poisson ratio	0.3	Poisson ratio	0.33
Hardening exponent	0.5	Hardening exponent	0.374618
Young modulus	210 GPa	Young modulus	60.04 GPa
Hardening parameter	0.5 GPa	Hardening parameter	0.22313
Failure plastic strain	0.3	Failure plastic strain	0.75

PROCESSING SETUP

To perform a higher accuracy finite element simulation, the shock absorber geometry is fine meshed and it is chosen QEPH shell formulation, which is recommended for crash analysis, and for plastic behavior of the material, five integration points are used.

The finite elements used in this crash simulation study are shell type that have a target length of 2 mm and a thickness of 4 mm. In figure 3 is presented the technique to meshing the symmetric geometry part. In

this case is necessary to mesh just only one quarter of the part.

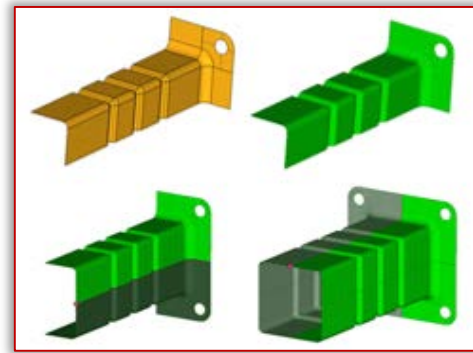


Figure 3 - Steps to create the symmetric mesh

After the quarter FEM model is mirrored from vertical and horizontal plane in order to create the completed model of the shock absorber. The surface contact between the shock absorber and rigid wall is “Type 7” with a Coulomb friction of 0.2. This contact interface is used for the most general types of crash analysis. For imitates the real work condition a mass of 300 kg is attached of shock absorber model. The imposed velocity of the model is 15m/s.

RESULTS

The crash result is presented in figures below for three thickness cases: 4 mm, 1 mm and 0.5 mm for both materials used.

This crash study is done on a graphic workstation, with an Intel Xeon CPU E5-2609v2, 2.5 GHz, and a 32 GB RAM and NVidia Quadro K620 graphical card. In the figure 4 are presented the deformed model of the absorber, vonMises stress and displacement values from a thickness of 4 mm of the steel shock absorber.

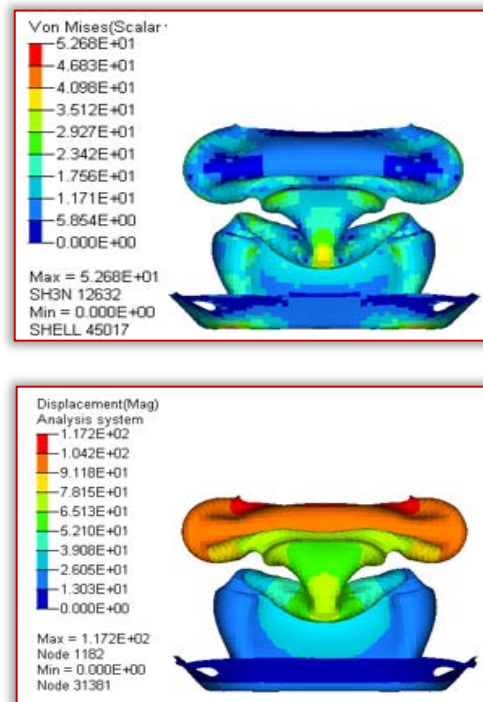


Figure 4 - Stress and displacement for 4 mm thickness of steel absorber

In figure 5 is presented the vonMises stress and displacement values of the aluminium shock absorber with a 4 mm thickness.

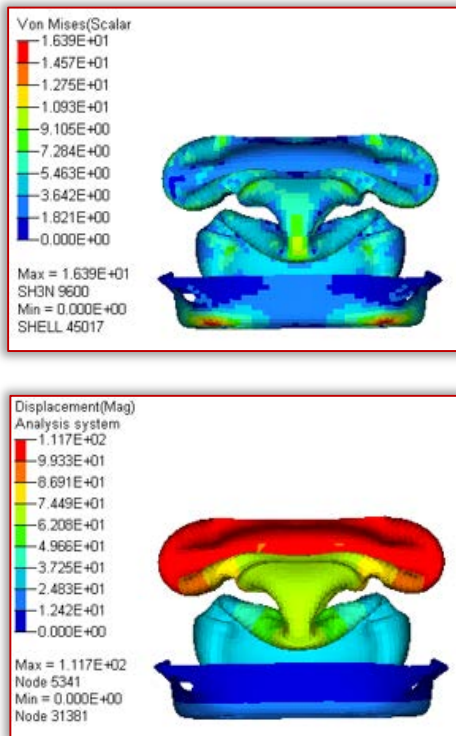


Figure 5 - Stress and displacement for 4 mm thickness of aluminum absorber
The stress and the displacement of the steel shock absorber are presented in figure 6.

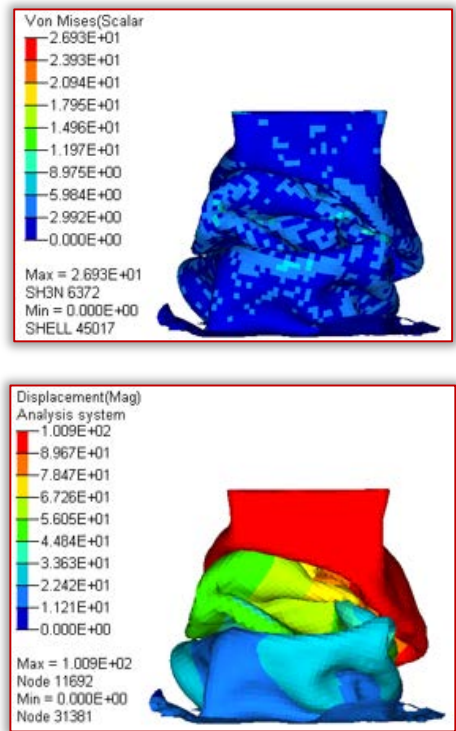


Figure 6 - Stress and displacement for 1 mm thickness of steel absorber
The stress and displacement resulted for an aluminum absorber with a 1 mm thickness are presented in figure 7.

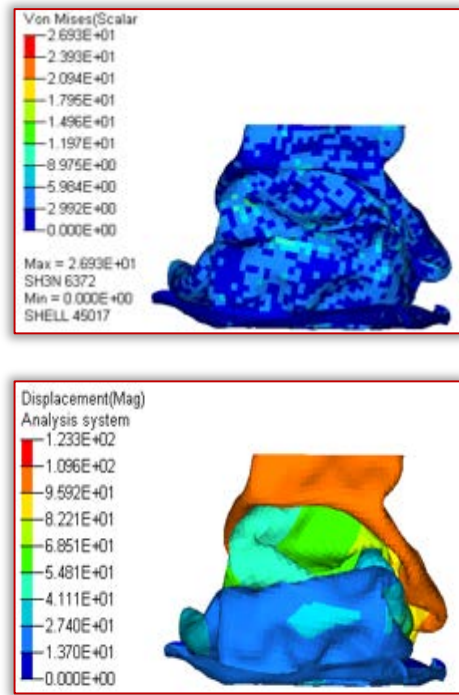


Figure 7 - Stress and displacement for 1 mm thickness of aluminum absorber
In figure 8 the von Mises stress and the displacement resulted for steel absorber are presented. It can be observed that the shock absorber model is totally destroyed.

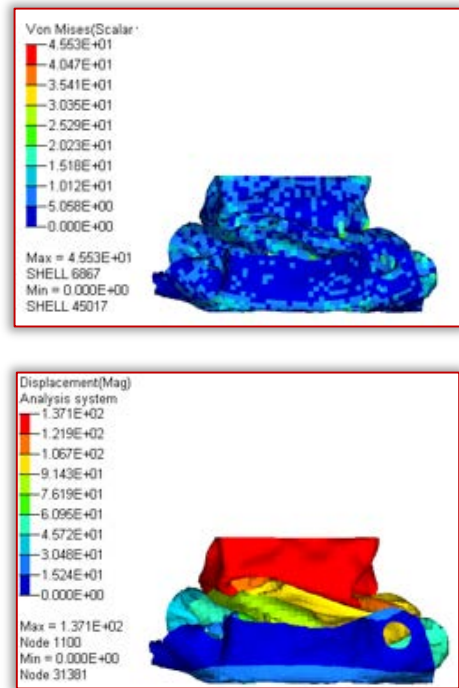


Figure 8 - Stress and displacement for 0.5 mm thickness of steel absorber
In figure 9 are presented the von Mises stress and the displacement of the aluminum shock absorber. The model is totally destroyed.
To a better view a buckling effect of the shock absorber in figure 10 are presented the phase during the crash simulations for a 4 mm from steel.

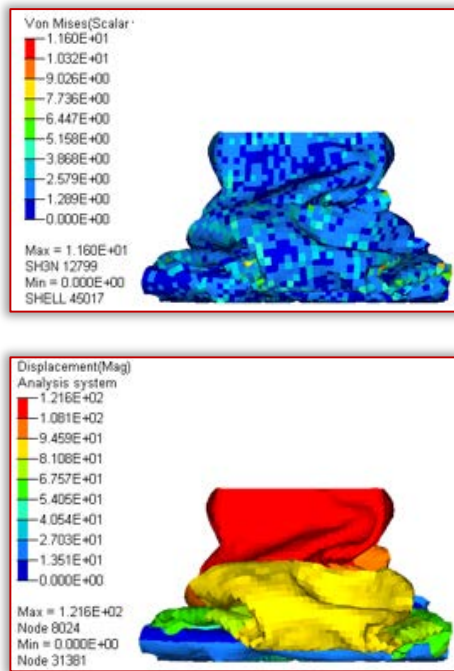


Figure 9 - Stress and displacement for 0.5 mm thickness of aluminum absorber

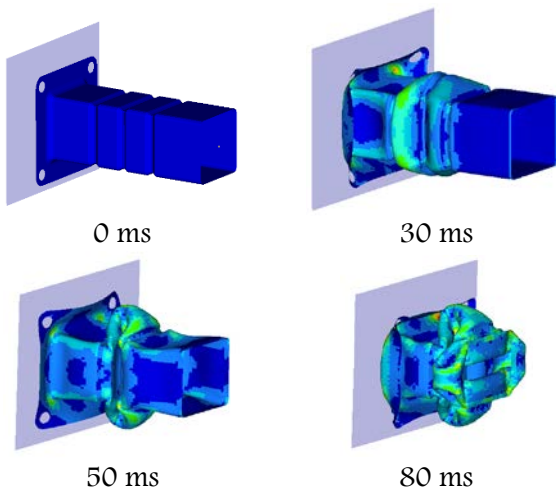


Figure 10 - Buckling effect of the shock absorber during the simulation

CONCLUSIONS

In this paper is present the crash behavior of the shock absorber used in construction of the vehicle's chassis. Are studied two cases of crash collision of a shock absorber from a rigid wall: in the first case, the attenuator is made from steel and the second case, the attenuator is made from aluminum.

During this study are presented all steps in order to create a crash simulation, from the geometrical design until the simulation results. An advantage of using the finite simulation analysis is that depending on the obtained simulation results it is possible to propose the final shape of the analyzed part. The protrusions from the model geometry allow a good axial compression of the model during the crash simulation process. It can be observed that the first simulation case with 4 mm thickness of the absorber

takes over the internal energy better than in the other cases.

Note: This paper is based on the paper presented at ISB-INMA TEH' 2019 International Symposium (Agricultural and Mechanical Engineering), organized by Politehnica University of Bucharest – Faculty of Biotechnical Systems Engineering (ISB), National Institute of Research–Development for Machines and Installations Designed to Agriculture and Food Industry (INMA Bucharest), Romanian Agricultural Mechanical Engineers Society (SIMAR), National Research & Development Institute for Food Bioresources (IBA Bucharest), National Institute for Research and Development in Environmental Protection (INCDPM), Research–Development Institute for Plant Protection (ICDPP), Research and Development Institute for Processing and Marketing of the Horticultural Products (HORTING), Hydraulics and Pneumatics Research Institute (INOE 2000 IHP) and “Food for Life Technological Platform”, in Bucharest, ROMANIA, between 31 October – 1 November, 2019.

References

- [1] Yedukondalu, G., Srinath, A., Suresh Kumar, J., (2015), Crash Analysis of Car Cross Member Bumper Beam, Altair Tehnology Conference, Altair Technology Conference, pp. 1-9, India;
- [2] Praveenkumar, A., Saran, V., Kavi Pradhap, M., (2016). Analysis of Typical Cross-Sectional Bumper Beam, International Journal of Modern Engineering Research, ISSN: 2249-6645, vol. 6(11), pp. 46-50;
- [3] Sahzabi, Balaei, A., Esfahanian, Mohsen. (2017); The Effects of Thin-Walled Structure on Vehicle Occupants' Safety and Vehicle Crashworthiness, International Journal of Automotive Engineering, vol.7(2), pp. 2393-2403;
- [4] Scurtu, I-L., Lupea, I. (2014), Frontal Crash Simulation of a Chassis Frame, Acta Technica Napocensis Series: Applied Mathematics, Mechanics, and Engineering, ISSN: 1221 – 5872, vol. 57(3), pp. 411-414;
- [5] Scurtu I-L., Balcau M-C., Jurco A-N. (2019), Topography Optimization of a Bracket Used for Car Bodywork Reinforcement, Proceedings of the 4th International Congress of Automotive and Transport Engineering (AMMA 2018), Proceedings in Automotive Engineering. Springer, Cham;
- [6] Tiago Miguel Encarnação Nunes, (2017), Multi-objective Design Optimization of a Frontal Crash Energy Absorption System for a Road-safe Vehicle, Thesis to obtain the Master of Science Degree in Aerospace Engineering;
- [7] Vandanapu, Manideep, Kumar., Pandu, Ratnakar, (2015), Design Optimization of Passenger Car Front Bumper, International Journal of Science and Research (IJSR), ISSN (Online): 2319-7064, vol. 4(11), pp. 1411-1417;
- [8] Altair Hyperworks user guide, (2017).
- [9] SolidWorks user guide, (2018).
- [10] Radioss tutorials, (2018).

¹Slobodanka BOLJANOVIĆ, ²Stevan MAKSIMOVIĆ, ³Strain POSAVLJAK

ANALYSIS OF TWO SYMMETRIC CRACKS AT A HOLE UNDER CYCLIC LOADING

¹Mathematical Institute of SASA, Kneza Mihaila 36, Belgrade, SERBIA

²Military Technical Institute Belgrade (VTI), Ratka Resanovića 1, Belgrade, SERBIA

³University of Banja Luka, Faculty of Mechanical Engineering, Banja Luka, BOSNIA & HERZEGOVINA

Abstract: Assessing the failure stability of engineering structures under service loadings by means of relevant crack growth concepts is one of key issues in damage tolerance analysis. Therefore, the behaviour of fatigue damages is theoretically examined through the crack growth rate. This paper describes a straightforward methodology to generate failure resistance under cyclic loading. To explore fatigue behaviour of two through-the-thickness cracks located at a hole, the stress intensity factor and life are estimated by means of developed analytical model. Stress state field is numerically analysed using the finite element method. Through relevant applications predictive capability of estimates is discussed. Relevant failure evaluations are performed in the case of complex-valued functions by employing the Euler's integration method, which is implemented in the software program developed. Whereas the type of cracks examined is taken into account through the stress intensity factor.

Keywords: fatigue resistance, two through-the-thickness cracks, finite element analysis, residual life assessment

INTRODUCTION

Notches play an important role in connections between structural components. Such stress concentrators (holes, cutouts) may often cause the formation of fatigue damages. Therefore, to avoid unexpected failures the reliable computational models have to be developed.

In the literature, extensive theoretical studies have been carried out on the residual strength of open/pin-loaded holes with crack-like damages, which provided adequate experience in exploring of the joints failure. Impellizzeri and Rich [1] have analysed the fatigue behaviour of through-the-thickness crack at a hole employing the weight function method. Mahendra Babu et al. [2] have taken into account the finite element method to evaluate the stress state field of fastener holes with the same crack configuration. Furthermore, to evaluate the stability of pin-loaded hole Liu and Tan [3] have developed a numerical technique by using the boundary element method, whereas Antoni and Gaisne [4] have employed analytical concept. Boljanović and Maksimović [5] have proposed a set of relevant relationships and numerical model for the strength modeling of open/pin-loaded holes under cyclic loading.

This research work analyses the fatigue behaviour of two symmetric cracks located at a hole. The relationship between residual life and crack propagation rate is developed taking into account the effect of stress ratio. Such fracture mechanics-based computational model is verified through experimental observations, and then it is employed for analysing relevant geometrical/loading influences.

CRACK GROWTH EVALUATION

Assessing the failure stability of engineering

structures under service loadings by means of relevant crack growth concepts [4, 5] is one of key issues in damage tolerance analysis. Therefore, the behaviour of fatigue damages (Figure 1) is theoretically examined through the crack growth rate [6] expressed as follows:

$$\frac{da}{dN} = C(e^{\alpha R} \Delta K_I)^m \quad (1)$$

where a is the crack length, C and m are material parameters experimentally obtained, R and ΔK_I denote the stress ratio and the stress intensity factor range, respectively.

In the fatigue analysis herein presented, the residual life is estimated, after integration of the crack growth rate from initial a_0 to final a_f crack lengths, i.e.

$$N = \int_{a_0}^{a_f} \frac{da}{C(e^{\alpha R} \Delta K_I)^m} \quad (2)$$

where N is the number of loading cycles.

Note that relevant failure evaluations are performed in the case of complex-valued functions by employing the Euler's integration method, which is implemented in the software program developed. Whereas the type of cracks examined is taken into account through the stress intensity factor (see section 3).

DRIVING FORCE ANALYSIS UNDER FATIGUE LOADING

According to fracture mechanics the fatigue response of two symmetric cracks (Figure 1) should be estimated by taking into account the stress intensity factor expressed as follows:

$$\Delta K_I = \Delta S f_2 f_{w2} \sqrt{\pi a} \quad (3)$$

where ΔS is the applied stress range.

Since the through-the-thickness cracks are located at a hole such nonlinear stress state conditions are theoretically examined here through the following correction factor [7]:

$$f_2 = 1 - 0.15\lambda + 3.46\lambda^2 - 4.47\lambda^3 + 3.52\lambda^4$$

with

$$\lambda = \frac{1}{1 + \frac{2a}{D}} \quad (4)$$

where D is the diameter of the plate. Further, the interaction between the width and plate hole is taken into account by means of the finite-width correction factor [7] expressed as follows:

$$f_{w2} = \left(\cos\left(\frac{\pi D}{4w}\right) \cos\left(\frac{\pi(D+2a)}{4w}\right) \right)^{-0.5} \quad (5)$$

where w is half of the plate width.

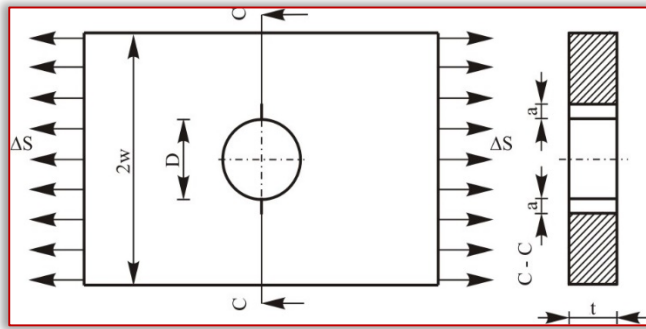


Figure 1. Geometry of the plate with two through-the-thickness cracks

The propagation of fatigue cracks at a hole is also theoretically examined by employing two-dimensional quarter-point singular elements [8] incorporated in the software package MSC/NASTRAN [9]. Relevant applications in which the stress state is evaluated through developed analytical and numerical models are discussed in the next section.

FAILURE ESTIMATION OF FATIGUE DAMAGES AT A HOLE

— RESIDUAL LIFE CALCULATION

The failure analysis presented in this section deals with residual life calculation. Two initial through-the-thickness cracks located at a plate (Figure 1) are subjected to cyclic loading with constant amplitude and the following geometrical/loading parameters are assumed: $a_0 = 1.625$ mm, $w = 60$ mm, $t = 6$ mm, $D = 17.5$ mm, $S_{max} = 69.44$ MPa (with two different stress ratios $R = 0.1$ and 0.3).

The plate is made of 2024 T3 aluminium alloy and the following mechanical and fatigue parameters are adopted: $E = 73.1$ GPa, $\nu = 0.33$, $C = 9.45 \cdot 10^{-11}$, $m = 3$.

The behaviour of fatigue damages are herein assessed employing Eqs. (2)–(5), as it is discussed in previous sections. The evaluated fatigue life, as a function of crack length, are shown in Figure 2a and b in the case of stress ratio equal to $R = 0.1$ and 0.3 , respectively.

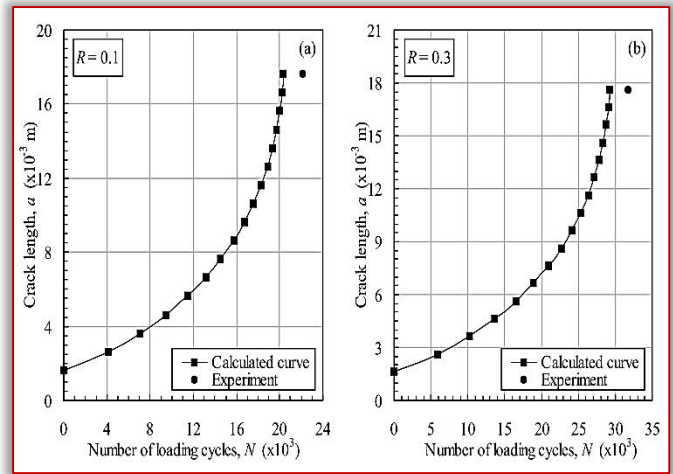


Figure 2. Life estimation for the cyclically loaded plate with two through-the-thickness cracks: (a) $R = 0.1$ and (b) $R = 0.3$.

Furthermore, in Figure 2 the obtained final number of loading cycles and corresponding crack growth lengths are verified through experimental observations. Such comparisons show that relevant fatigue results are in a quite good agreement for the through-the-thickness crack configurations examined

— STRESS STATE ANALYSIS UNDER CYCLIC LOADING

Now the fatigue behaviour of two through-the-thickness cracks (Figure 1) is examined in terms of stress state evaluation. Such crack growth analysis is performed for the plate ($a = 9.53$ mm, $w = 65$ mm, $t = 7$ mm, $D = 16.5$ mm) subjected to maximum stress and stress ratio equal to $S_{max} = 70.33$ MPa and $R = 0$, respectively. For the 2024 T3 aluminium alloy examined here, the same material parameters are adopted as those mentioned in previous section.

The propagation of two through-the-thickness cracks is numerically herein analysed by using the two-dimensional singular finite elements [8], incorporated in the MSC/NASTRAN software package [9]. Actually, by assuming linear-elastic behaviour of material, for appropriate crack lengths the finite element meshes and corresponding stress distributions are evaluated. A representation of the stress distribution ($a = 9.53$ mm) is shown in Figure 3.

Furthermore, the failure mode is estimated through the stress intensity factor by means of Eqs. (3)–(5) and finite element method. Obtained calculations for three crack lengths ($a = 3.47$ mm, 6.25 mm and 9.53 mm) are listed in Table 1. It can be seen that analytical results show quite good correlation to those numerically obtained.

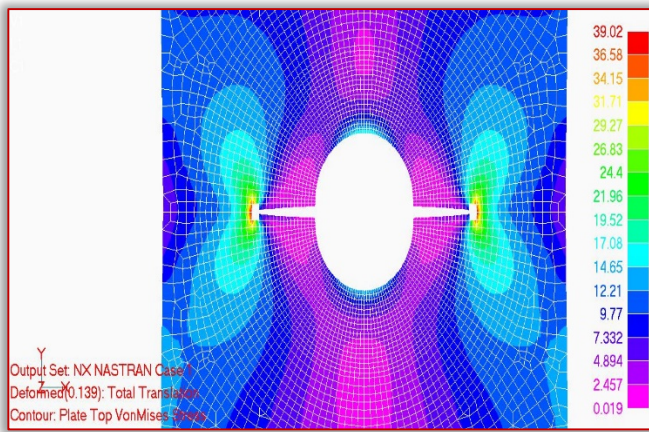


Figure 3. Numerical analysis of two through-the-thickness cracks at a hole

Table 1. Calculated stress intensity factors using analytical model and finite elements

a (mm)	K_{max} (MPam ^{0.5})	
	Analytical	FEM
3.47	15.94	17.89
6.25	18.56	20.17
9.53	21.84	23.86

— EFFECTS OF STRESS RATIO AND HOLE DIAMETER ON THE FATIGUE RESPONSE

The fatigue strength is here investigated taking into account the effects of stress ratio and diameter of the plate (Figure 1). The residual life is evaluated for damaged plates ($a_0 = 2$ mm, $w = 70$ mm, $t = 7$ mm, $S_{max} = 61.22$ MPa), made of 2024 T3 aluminium alloy, in the case of three different stress ratios and diameters: (a) $R = 0.1, 0.25, 0.5$ together with $D = 18$ mm and (b) $D = 19$ mm, 21.85 mm, 24.7 mm, $R = 0.2$, respectively.

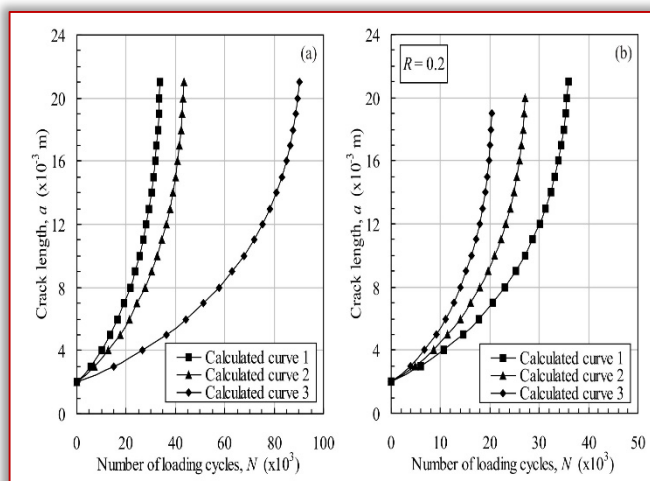


Figure 4. Life estimation for two through-the-thickness cracks at a hole: (a) 1 – $R = 0.1$, 2 – $R = 0.25$, 3 – $R = 0.5$ and (b) 1 – $D = 19$ mm, 2 – $D = 21.85$ mm, 3 – $D = 24.7$ mm.

The failure analysis presented in this section is examined in terms of the stress intensity factor and number of loading cycles (Eqs. (2)–(5)). Relevant life

evaluations, obtained for different stress ratios and diameters of the plate, are shown in Figure 4a and b, respectively. By examining such figures it can be inferred that stress ratio and hole diameter may significantly affect the durability of components with the through-the-thickness cracks at a hole.

CONCLUSIONS

The fatigue degradation is considerable problem in industry which can often cause unexpected catastrophic accidents. Thus, relevant relationships are herein proposed to assess the failure strength of through-the-thickness cracks at a hole taking into account geometrical and loading effects.

Nonlinear stress state field is numerically evaluated by means of quarter-point singular finite elements. Conservative trend of estimates with respect to experimental observations show that developed fracture mechanics based model can be employed for analysing two symmetric trough cracks at a hole.

Acknowledgment

This research work is funded by the Mathematical Institute of the Serbian Academy of Sciences and Arts and the Ministry of Science and Technological Development of Serbia through the project no. OI 174001.

Note:

This paper is based on the paper presented at DEMI 2019 – The 14th International Conference on Accomplishments in Mechanical and Industrial Engineering, organized by Faculty of Mechanical Engineering, University of Banja Luka, BOSNIA & HERZEGOVINA, co-organized by Faculty of Mechanical Engineering, University of Niš, SERBIA, Faculty of Mechanical Engineering Podgorica, University of Montenegro, MONTENEGRO and Faculty of Engineering Hunedoara, University Politehnica Timisoara, ROMANIA, in Banja Luka, BOSNIA & HERZEGOVINA, 24–25 May 2019.

References

- [1] Impellizeri, L.F., Rich, D.L. (1976) Spectrum fatigue crack growth in lugs. In: Fatigue crack growth under spectrum loads. ASTM STP, vol. 598, p. 320–336.
- [2] Mahendra Babu, N.C., Jagadish, T., Ramachandra, K., Sridhara, S.N. (2008) A simplified 3-D finite element simulation of cold expansion of a circular hole to capture through thickness variation of residual stresses. Engineering Failure Analysis, vol. 15, no. 4, p. 339–348.
- [3] Liu, S.B., Tan, C.L. (1994) Two-dimensional boundary element contact mechanics analysis of pin-loaded lugs with single cracks. Engineering Fracture Mechanics, vol. 48, no. 5, p. 711–725.
- [4] Antoni, N., Gaisne, F. (2011) Analytical modelling of static stress analysis of pin-loaded lugs with bush fitting. Applied Mathematical Modelling, vol. 35, no. 1, p. 1–21.

- [5] Boljanović, S., Maksimović, S. (2014) Fatigue crack growth modeling of attachment lugs. International Journal of Fatigue, vol. 58, p. 66–74.
- [6] Zhan, W., Lu, N., Zhang, C. (2014) A new approximate model for the R-ratio effect on fatigue crack growth rate. Engineering Fracture Mechanics, vol. 119, p. 85–96.
- [7] Newman, J.C. Jr. (1976) Predicting failure of specimens with either surface cracks or corner cracks at holes. NASA-TN-D-8244, Hampton: NASA Langley Research Center.
- [8] Barsoum, R.S. (1977) Triangular quarter-point elements as elastic and perfectly-plastic crack tip elements. International Journal for Numerical Methods in Engineering, vol. 11, no 1, p. 85–98.
- [9] MSC/NASTRAN, software code (1994) Theoretical Manuals, the MacNeal-Swendler Corporation, Los Angeles, USA.



ACTA TECHNICA CORVINIENSIS – Bulletin of Engineering
ISSN: 2067–3809

copyright © University POLITEHNICA Timisoara,
Faculty of Engineering Hunedoara,
5, Revolutiei, 331128, Hunedoara, ROMANIA
<http://acta.fih.upt.ro>

¹Milena ĆOSIĆ, ²Slobodanka BOLJANOVIĆ

CHARACTERIZATION OF THE STRUCTURAL CHANGES OF Al18SiCuMg ALLOY DURING THE RHEOCASTING PROCESS

¹University of Belgrade, Institute of Chemistry, Technology and Metallurgy, Njegoševa 12, Belgrade, SERBIA

²Military Technical Institute Belgrade, Ratka Resanovića 1, Belgrade, SERBIA

Abstract: In the present paper, the microstructure evolution of semi-solid metal slurry was investigated. The material was tested by rheocasting route. In order to better estimate the materials behavior, the investigation was performed on three series of samples. The rheocasting was conducted different stirring speed of 500, 1000 and 1500rpm and 0.3 solid fraction, before casting. The microstructure was analysed using an optical and scanning electron microscope. The results show that the relationship between the equivalent diameter of Si and α - Al particles with stirring speed can be well fitted to quadratic or linear equation. The results from this study can also be used to optimize the process and study mechanism of the rheocasting process.

Keywords: semi-solid metal; Al18SiCuMg alloy; rheocasting; microstructure

INTRODUCTION

Hypereutectic Al-18Si alloy is widely used as material with favourable physical and mechanical properties (low thermal expansion coefficient, high wear resistance, excellent castability and low density.

All of these properties makes Al-18Si alloy suitable for automotive and aerospace applications [1,2]. As known that morphology of the various phases presence in alloys (eutectic silicon, primary silicon) affects on the mechanical and cavitation behavior of this alloy.

Si content above the eutectic composition causes formation of coarser Increasing primary Si particles, resulting in deterioration in mechanical properties of Al18Si alloy.

For this reason, the properties of Al18Si can be improved by different techniques such as modification treatment [3,4], rapid solidification processing [5,6] some special techniques such as thixocasting and rheocasting [7,8]. The piston alloy has been mostly used for conventional die-castings but these alloy can be cast by semi-solid metal processing - rheocasting. Semi-solid processing has its many advantages over conventional technologies.

A number of fragmentation theories have been proposed for explain of evolution phases in semisolid casting.

One of these is fragmentation agglomeration theory [7,8,9] . This theory is based on the fragmentation of dendrites into small pieces which will transform into spherical particles. The experimental results based on mentioned theory were also discussed.

In this work, the influence of two processing parameters solid fraction and stirring speed on the microstructure of the rheocast alloy was studied. In addition, the goal was also to investigate the possibilities for application of image analysis in

monitoring of the changes in the samples during rheocast testing.

MATERIAL AND EXPERIMENT

The chemical composition (in wt%) of aluminum silicon alloy used in this work is given in Table 1.

Table 1. Chemical composition
in wt.% of the matrix alloy

Si	Cu	Mg	Ni	Fe	Zn	Mn	Al
18.06	0.80	0.82	0.92	0.7	0.2	0.2	bala.

The alloy was obtained by rheocasting process in the Department of Materials Science "Vinča" Institute. The experimental set-up used in this work consisted of a laboratory electric resistive 2kW furnace (with additional temperature control equipment) and a mixer.

About 450g Al18Si alloy was charged into crucible of the electro-resistance furnace. The matrix alloy was first melted at temperature of 720°C.

After that, the melt was slowly cooled in the solid-liquid temperature range. As soon as the temperature of the melt reached 690°C, the stirrer was immersed into melt. After that the melt was stirred by stirring speed from 500 to 1500 rpm before poured into the mold.

The microstructure changes during mixing were recorded by the SEM (JEOL JSM-5800) and optical microscopy (OM). All of the samples were prepared for metallographic examination in the usual way.

The image analysis was used on the micrographs to determine the equivalent diameter of microstructure features of the samples. For each stirring speed three micrographs were taken from random locations for further analysis.

In order to determine both an equivalent diameter of Si particles and the α -Al particles equation (1) was used. In the expression, in order to calculate the equivalent diameter, A is the diameter of the area

occupied by α - Al particles and Si. The equivalent diameter is calculated as follows:

$$D_{eq} = 2\sqrt{\frac{A}{\pi}} \quad (1)$$

The solid fraction (f_s) can be estimated from the image analysis data using the Eq.(2)

$$f_s = \frac{A_p}{A_m} \times 100 \quad (2)$$

where A_p is the total area of the particles and A_m is the total area of the analyzed micrographs.

EXPERIMENTAL RESULTS

Microstructural characterization of the tested alloys was performed in order to understand the difference in distribution and size of all phases in samples. The changes in appearance of the microstructure samples at 0.3 solid fraction and stirring speeds of 500 -1500 rpm are presented in Figure 1.

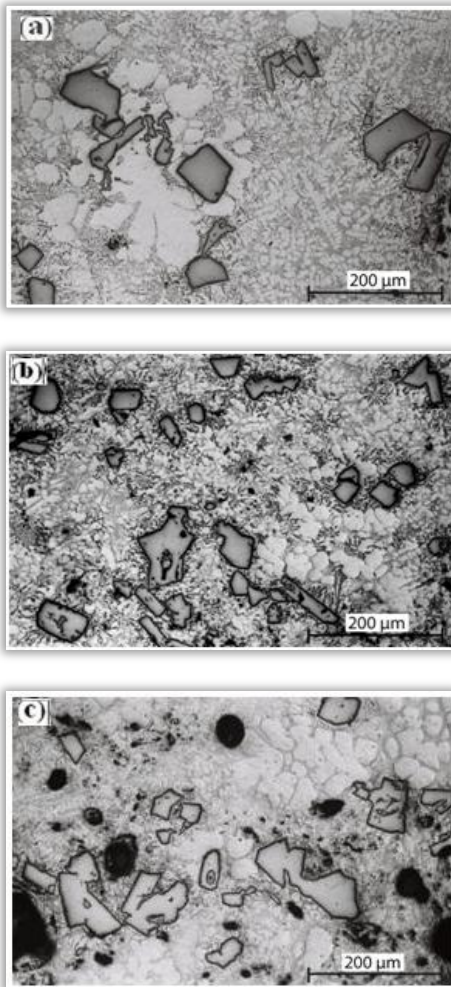


Figure 1. Rheocast microstructures at 0.3 solid fraction and stirring speed of (a) 500 rpm, (b) 1000 rpm and (c) 1500 rpm

The microstructure of the rheocast samples of hypereutectic Al-Si alloy produced with application of different stirring speed during solidification consisted of primary silicon particles and eutectic matrix

(eutectic silicon particles, and eutectic aluminum cells).

Primary Si phase (light gray in the images) in different shapes, from plate-like to polygonal, surrounded by eutectic, where some micro-shrinkage porosity could be detected Figure 1a-c. The image analysis showed that the smallest primary silicon particles found in all samples.

In Figure 1a, there are small primary silicon particles, some of them are connected to each other. These mean that single Si particles grew and their size increased significantly. The congregation phenomenon almost appeared during mixing of melt with stirring speed of 1500rpm (see, Figure 1c)

The effects of stirring speed on the average equivalent diameter of primary Si particles of Al18Si samples are displayed in Figure 2.

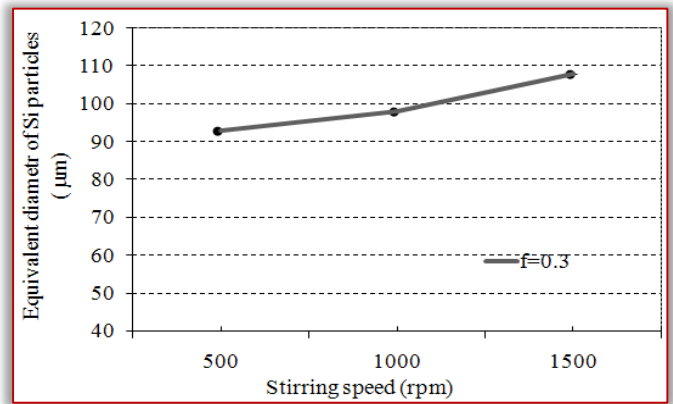


Figure 2. Equivalent diameter of the Si particles at different stirring speed

The data points in Fig 2. may be fitted to the linear equation

$$y = 84.3333 - 0.015 * x \quad (3)$$

where x is the stirring speed. Simulated curve (related to equivalent diameter of Si particles versus stirring speed) for considered conditions is presented in Figure 3.

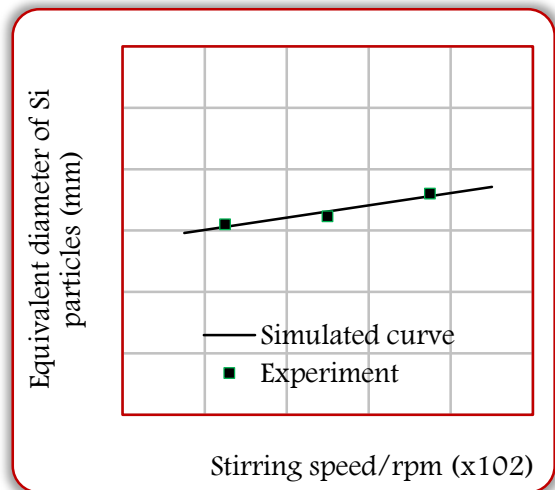


Figure 3. Equivalent diameter of Si particles versus stirring time 1-Linear equation

In Figure 4, the morphology of α -Al phase in microstructure of all samples processed at 0.3 primary solid and various stirring speeds is reported.

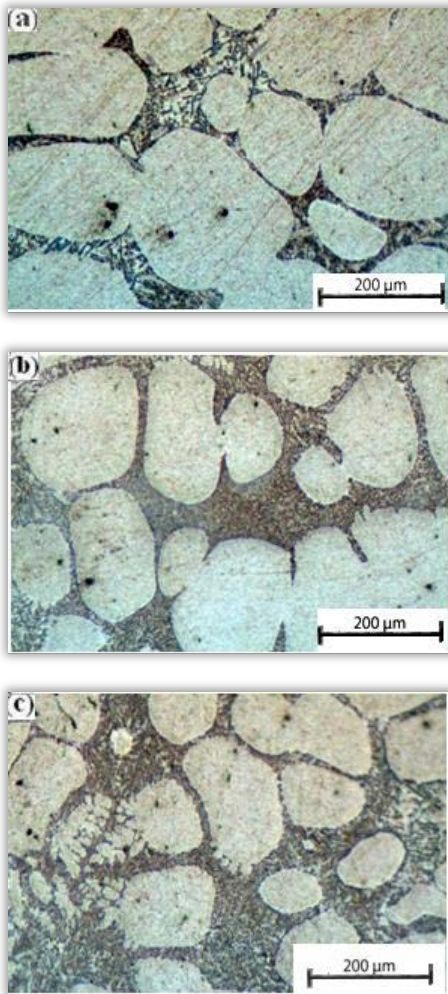


Figure 4. Rheocast microstructures of the α -Al particles. The fragmentation of the dendrite arms into smaller arms occurred during mixing. According to fragmentation - agglomeration mechanism [8,9], an increased in stirring speed produced smaller particles. The change of particles morphology from rosette-like to spherical as clearly shown in Figure 4a-c.

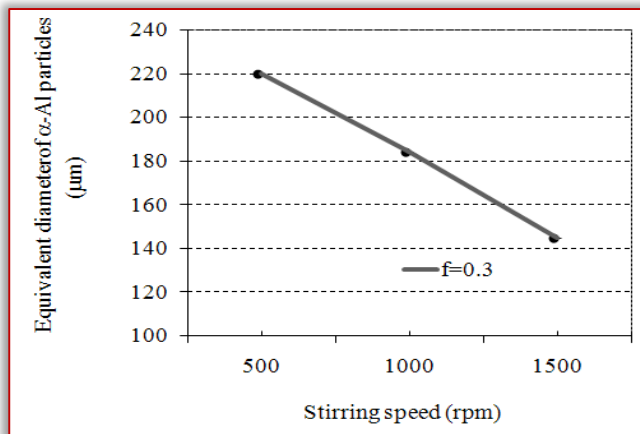


Figure 5. Equivalent diameter of the α -Al particles at different stirring speed

Figure 5 presents the variation of average diameter of the α -Al particles versus stirring speed. The results showed that average diameter decreased slightly first and then decreased as stirring speed further increased.

Moreover, the results of experiment investigations show that the relationship between the equivalent diameter of α -Al particles and the stirring speed can be approximated by a quadratic equation. Function between equivalent diameter and stirring speed (see Figure 5) can be simulated by the following relationship.

$$y = 253 - 0.063 * x - 6 * 10^{-6} * x^2 \quad (4)$$

Simulated curves (related to equivalent diameter versus stirring speed) for considered samples either as linear or quadratic are presented in Figure 3 and Figure 6. All curves are in a good correlation with experimental results in the domain from 500rpm to about 1500rpm. Those relationships can be used as a control of equivalent diameter in the rheocasting condition.

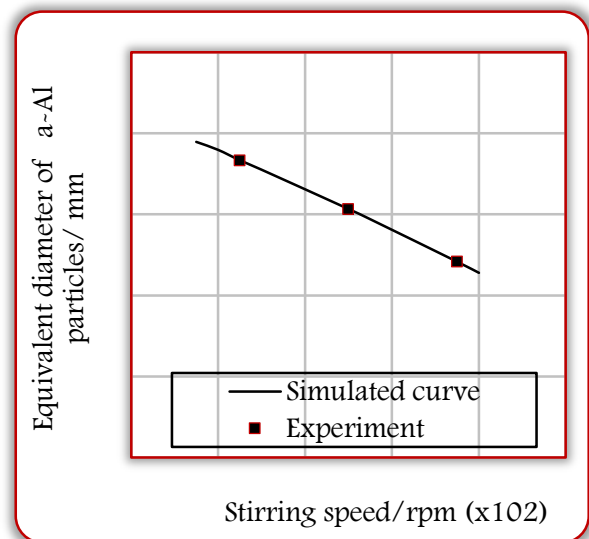


Figure 6. Equivalent diameter of the α -Al particles versus stirring time 1- Quadratic equation

CONCLUSION

In this paper the image analysis was applied to characterize the particle size and distribution of Si and α -Al particles under a given set of rheocasting conditions. The data for the particles size of Si and α -Al, can be described by different equations. In this study, based on experimental results linear and quadratic equations are suggested. Equivalent diameter of Si particles has linear trend with stirring speed while equivalent diameter of α -Al particles has quadratic trend with stirring speed. These equations can be used as a control tool for optimize process and to study the growth mechanism during the rheocasting process.

Note:

This paper is based on the paper presented at DEMI 2019 – The 14th International Conference on Accomplishments in Mechanical and Industrial Engineering, organized by Faculty of Mechanical Engineering, University of Banja Luka, BOSNIA & HERZEGOVINA, co-organized by Faculty of Mechanical Engineering, University of Niš, SERBIA, Faculty of Mechanical Engineering Podgorica, University of Montenegro, MONTENEGRO and Faculty of Engineering Hunedoara, University Politehnica Timisoara, ROMANIA, in Banja Luka, BOSNIA & HERZEGOVINA, 24–25 May 2019.

References

- [1] Robles Hernandez FC., Sokolowski JH.(2009). Thermal Analysis and Microscopical Characterization of Al–Si Hypereutectic Alloys. Journal of Alloys and Compounds, vol.419, p. 180–190.
- [2] Hegde S., Prabhu KN.(2008) Modification of eutectic silicon in Al–Si alloys, Journal of Materials Science, vol.43, no. 9, p.3009-3027, 2008.
- [3] Dahle K., Nogita K., McDonald SD., Dinnis C., Lu L., (2005) Eutectic modification and microstructure development in Al–Si Alloys. Materials Science and Engineering: A. vol. 413–414, p. 243-248.
- [4] Shingu P.,Takamura JI. (1970). Grain-Size Refining of Primary Crystals in Hypereutectic Al-Si and Al-Ge Alloys. Metallurgical Transactions, vol. 1, p. 2339-2340.
- [5] Nogita K., Mcdonald SD., Dahle A. (2004). Eutectic Modification of Al-Si Alloys with Rare Earth Metals. Materials Transactions, vol. 45, no. 2, p. 323-326.
- [6] Kasprzak W., Sahoo M., Sokolowski J., Yamagata H., Kurita H. (2009).The Effect of the Melt Temperature and the Cooling Rate on the Microstructure of the Al-20% Si Alloy Used for Monolithic Engine Blocks. International Journal of Metalcasting, p. 55-72.
- [7] Nafisi, S., Ghomashchi, R.(2006). Grain refining of conventional and semi-solid A356 Al–Si alloy. Journal of Materials Processing Technology, vol.174, p.371–383.
- [8] Nafisi, S., Ghomashchi, R. (2006). Combined grain refining and modification of conventional and rheocast A356 Al–Si alloy. Material Characterization, vol. 57, p.371–385.
- [9] Niroumand B., Xia K. (2000).3D study of the structure of primary crystals in a rheocast Al-Cu alloy. Materials science and Engineering A, vol.283, no.1-2, p.70-75.



ACTA TECHNICA CORVINIENSIS – Bulletin of Engineering
ISSN: 2067-3809

copyright © University POLITEHNICA Timisoara,
Faculty of Engineering Hunedoara,
5, Revolutiei, 331128, Hunedoara, ROMANIA
<http://acta.fih.upt.ro>

¹G.K. GIRISHA, ²S.L. PINJARE

IMPLEMENTATION OF NOVEL ALGORITHM FOR AUDITORY COMPENSATION IN HEARING AIDS USING STFT ALGORITHM

^{1,2}Nitte Meenakshi Institute of Technology, Bangalore, INDIA

Abstract: Audiogram is the graphic record drawn from the results of hearing tests with an audiometer, which charts the threshold of hearing at various frequencies against sound intensity in decibels. This paper presents the work on auditory compensation (also known as audiogram equalizer) implemented with the help of Short Time Fourier Transform (STFT) algorithm. For humans normal hearing ranges from -10dB to 15dB, although 0dB from 250Hz to 8 kHz is reckoned as the average normal hearing. An audiogram is obtained to determine the frequency range the listener is audibly challenged to. STFT algorithm is employed to determine the frequency range of audio signal which is to be selectively amplified as per the audiogram. The present work uses verilog language to implement STFT algorithm. The entire system is developed on Zynq Evaluation and Development Board (Zedboard) using Vivado.

Keywords: Audiogram, STFT, Zedboard

INTRODUCTION

Hearing is one of the important senses which alert us to danger that sometimes may be out of our visual range. Sound is produced upon vibration or back and forth movement. Audio or sound is merely quick movement of air molecules which are caused by vibrations caused by such actions.

The human ear is of three parts: inner ear, middle ear and outer ear. The pinnae are structured to gather sounds from different directions and funnel them into the ear canal. The sound waves are then conveyed onto the middle ear and then the inner ear. Hearing loss or hearing impairment can be partial or total inability to hear, caused by the interruption of audio signals at either or multiple sections of the ear. Certain factors including genetics, aging, infections, exposure to noise, trauma, birth conditions and medications or toxins can invoke hearing loss.

Hearing impairment is categorized into: conductive hearing loss, sensori-neural hearing loss (SNHL) and mixed hearing loss. Conductive hearing loss is caused by the impediment in conveying the sound in its mechanical form through the middle cavity to the inner ear. Sensori-neural hearing loss is due to nerve-related hearing loss. Mixed hearing loss is a combination of the two.

Although there is a wide range of options to treat hearing impairment, hearing aid is one such option in high demand. Hearing aids are sound-amplifying devices designed to increase audibility. Most of the hearing aids cognate similar components such as microphone, amplifier circuitry, miniature loudspeakers and batteries to power the device. Based on the technology used, hearing aids are classified into: Analog and Digital (DSP) hearing aid.

Analog hearing aids operate by amplifying continuous audio waves. Digital hearing aids come with the similar features of programmable analog hearing aid, but convert the audio signal to digital

signal to yield an exact replica of each signal rather than entirely amplifying the signal.

Digital hearing aid like analog hearing aid, has a microphone to convert the analog audio signals to digital form, a microprocessor to amplify and process the digital signal and a miniature loudspeaker to convey audio directly to the ear canal. The signal processing is executed by the microprocessor in real time taking into account of individual user preferences.

Researchers have so far been implementing audiogram equalizer using filter banks for processing audio signal. An array of filters known as analysis filter bank are used to divide the audio signal to different channels based on frequencies. Then an array of amplifier with specific gain is used to amplify signals in each channel.

FIR/IIR filters have been used for implementing filter banks. Filter number and the implementation architectures have a significant impact on system performances, such as computation complexity, area, throughput, and power consumption. Certain signals are confined by the filters based on their frequency values, therefore the filter component values must be selected effectively else required frequencies may be accidentally filtered out.

Digital sequences have smaller signal bandwidth when compared to analog sequences, which puts signal processing time in a significant position among the factors effecting device performance. FFT algorithm operates at a faster pace and since all signals are considered for evaluation no frequency is filtered out, sanctity of the signal is preserved.

This paper shows the implementation of auditory compensation block by selective amplification of audio signal on Zedboard. Zynq-7000 processor is used to perform the processing and amplification of the signal. Zedboard has two 12-bit (each) analog to digital converters (ADC) and an in-built Codec –

ADAU1761 for analog to digital conversion and audio interfacing with the processor respectively.

AUDITORY COMPENSATION

Auditory compensation is the hearing aid's primary functionality to compensate the loss in the hearing level of a patient by amplifying the audio signals depending on the frequency band. The amount of amplification required for an individual is determined by the Audiometry test performed by audiologist.

Each user may have different requirements as per their audiogram results. The audiogram equalizer is one such algorithm which can be used to customize the hearing aid operation. An individual may have attenuated audibility at a particular frequency range, the STFT algorithm is implemented in this paper to identify the frequency range to be processed and then amplified.

— STFT algorithm

STFT also referred to as Short-term Fourier transform is employed to determine the frequency and phase content of a signal over a period of time. The incoming long term audio signal is divided to short terms of equal length and Fourier transform is computed on each of these shorter segments [1].

The discrete STFT is a time-localized spectral transformation based on the discrete Fourier transform (DFT). The DFT coefficients $X(k)$ of a discrete time signal $x(t)$ composed of T samples are calculated according to

$$X(k) = \sum_{t=0}^{T-1} (x(t)e^{-j\frac{2\pi}{T}kt}) , k = 0, \dots, T - 1$$

where k is frequency. The DFT is a frequency localized transformation, the analog frequencies equivalent to normalized frequency are fixed and given by

$$f_k = \frac{k f_s}{T}$$

where $k = 0, 1, 2, 3, \dots, T-1$ and f_s is sampling frequency. The samples of the speech signal are real numbers which makes the DFT to be symmetric.

The STFT can be viewed as a two-dimensional transformation (i.e. frequency and time) which is calculated by splitting the input signal into segments using a sliding time-limited window and then calculating the DFT of each of the segments.

Considering a discrete time input signal, it is segmented into frames according to

$$x_i(r) = w(r) x(r + iD), \quad r = 0, \dots, R - 1$$

where $x_i(r)$ is the windowed i -th frame, r is a local time index, R is the window length, and D is the hop size which represents the number of samples that the sliding window moves between two consecutive frames.

The window lengths of the signal may vary from 8, 16, 32 and so on, and the audio frequency is equally divided among these channels. The frequency range to which the audio signal belongs is determined by the position of maximum magnitude of the complex Fourier sequence.

— Audio Amplification

Audio amplification is the process of making a small signal bigger by a particular factor without affecting other features of the same. An amplifier which amplifies audio of all frequencies by a same factor is called linear amplifier. In this paper a non-linear amplification method is employed, as the user may require different audio intensity at different frequencies.

The user has to undergo an audiogram test to determine his hearing attenuation at various frequencies at both his left and right ear. As per the audiogram result the hearing aid can be configured to amplify the signal to a gain preferred by the user. Each channel represents a particular frequency range and as per the user audiogram result.

METHODOLOGY

The figure 1 presents the novel auditory compensation algorithm using STFT algorithm implemented. The audio signal picked up from the microphone are then converted to digital signals using ADC. The continuous audio signal is divided into smaller segments and STFT is performed on each of these segments. The STFT block finds the FFT of the signal.

The FFT implementation is carried out using butterfly method. After FFT calculations, the Max-Bin block calculates the magnitude of each bin of FFT and results with the index of the bin which has got the maximum magnitude. The index represents the frequency of the audio signal. The amplifier block is used to amplify the real time audio signal based on the frequency determined and the amplification requirement data taken from audiogram to compensate the hearing loss of the patient [2].

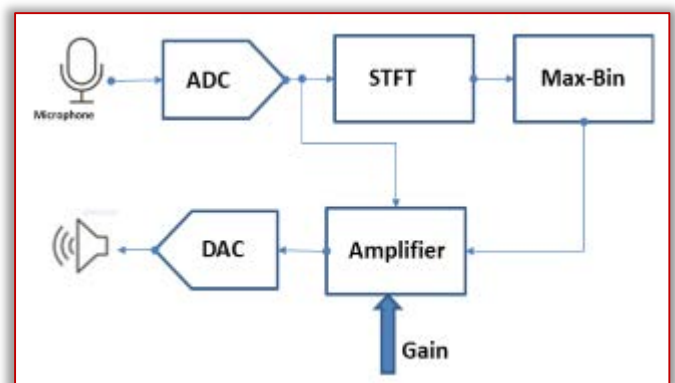


Figure 1: Block diagram of STFT algorithm for Auditory Compensation

- [3] Li M, McAllister H. G, Black N. D, et al, Wavelet-based nonlinear AGC method for hearing aid loudness compensation. IEEE Proceedings-Vision, Image and Signal Processing, vol. 147, pp. 502-507, June 2000
- [4] Vikrant N. P, Krishna Y, Rajashekhar B, et al. Critical-band based compression—an insight into the future of digital hearing aids, Audio, Language and Image Processing, ICALIP 2008. International Conference on. IEEE, pp. 1620-1623, 2008.
- [5] S Hamid Nawab, Thomas F. Quatieri, “Signal Reconstruction from Short-Time Fourier Transform magnitude”, IEEE transactions on acoustics, speech, and signal processing, vol. assp-31, no. 4, August 1983
- [6] Martin Krawczyk and Timo Gerkmann, “STFT Phase Reconstruction in Voiced Speech for an Improved Single-Channel Speech Enhancement”, IEEE transactions on audio, speech, and language processing, vol. 22, no. 12, December 2014
- [7] D. W. Griffin and J. S. Lim, “Signal estimation from modified short-time Fourier transform,” IEEE Trans. Acoust., Speech, Signal Process., vol. 32, no. 2, pp. 236–243, Apr. 1984
- [8] Y. Ephraim and D. Malah, “Speech enhancement using a minimum mean-square error short-time spectral amplitude estimator,” IEEE Trans. Acoust., Speech, Signal Process., vol. 32, no. 6, pp. 1109–1121, Dec, 1984
- [9] R. Crochiere, “A weighted overlap-add method of short-time Fourier analysis/ synthesis,” IEEE Trans. Acoust., Speech, Signal Process., vol. ASSP-28, no. 2, Apr. 1980
- [10] Wang Qing-yun, Zhao Li, Zhao Li-ye, Zou Cairong, A Multichannel Loudness Compensation Method for Digital Hearing Aids, Journal of Electronics & Information Technology, vol. 31, April 2009.
- [11] Y. Lian and Y. Wei, "A Computationally Efficient Non-Uniform FIR Digital Filter Bank for Hearing Aid," IEEE Trans. on Circuits and Systems, vol. 52, December, 2005.
- [12] Ching-Ta Lu and Hsiao-Chuan Wang, "Speech enhancement using robust weighting factors for critical-band-wavelet-packet transform", IEEE International Conference on Acoustics, Speech, and Signal Processing, vol. 1, May 2004.



ACTA TECHNICA CORVINIENSIS – Bulletin of Engineering
ISSN: 2067-3809
copyright © University POLITEHNICA Timisoara,
Faculty of Engineering Hunedoara,
5, Revolutiei, 331128, Hunedoara, ROMANIA
<http://acta.fih.upt.ro>

¹Srinivasa GK GOWDA, ²Sunil JACOB

NETWORK MOBILE TOPOLOGY IMPACT QOS IN MULTI-SERVICE MANET

¹Electronics and Communication Engineering, Jnanavikas Institute of Technology, Bangalore, INDIA

²ECE and Director SCMS Centre for Robotics, SCMS school of Engineering, Kerala, INDIA

Abstract: Mobile Ad-Hoc Network is a set of mobile nodes without infrastructure connectivity. Although the type of data exchanged between MANET QoS knots is significant, multiservice data have not been processed by further previous researches. In this paper, it has suggested an adaptive approach that provides the best delay and output efficiency. It investigated effects of the mobility models and the density of nodes on the performance of On-Demand Distance Vector, AODV routing protocol, using multiservice VBR (MPEG-4) and Constant Bits Rate (CBR) in the first place. Ultimately, in both cases, we compare the performance. Experimentally, we considered Random Waypoint, Random Direction and Mobgen Steady-State as three mobility models. The experimental results indicate that the behaviour of AODV changes depending on the model and the traffic used.

Keywords: AODV, CBR, MANET, QOS, mobility models

INTRODUCTION

The mobile ad-hoc network (MANET) [1] is a self-configuring network of mobile nodes connected to a random topology using wireless connections. The nodes move around freely. The wireless network topology is unpredictable. The limited setup, quick deployment and lack of a central governing body make ad hoc networks ideal for multimedia conferences, construction sites, residential networks and military conflicts [1-3], [2-4].

Mobility models describe the pattern for nodes movement in ad hoc networks. The random nature of these models, as well as their final (computer, tel...) implementation, involves some work in the evaluation of simulation-based routing protocols.

The purpose of the routing protocol is to find the best way to connect two nodes while maintaining a communication QoS. The rapid and unpredictable shift in the topology of the MANET network based on the random mobility of the nodes makes it hard to scan the path.

It is clear that MANET does not guarantee the quality of service, QoS [4] because of the inherently dynamic nature of a mobile ad hoc environment. The performance obviously depends on the routing system and the mobility itself. To guarantee the QoS, it needs to perform deeper assessment studies in order to find the routing protocol and the usability model more suited to an application. The QoS needs some of the output metrics such as throughput, end-to-end delay and jitter. Therefore, several researchers conducted on MANETs' assessment efficiency as a performance analysis of the various routing protocols and the impact of random mobility models on ad hoc networks [5-12].

The rest of this paper is structured as follows: it is shown survey related work in the next section. The problem formulation, followed by the simulation

model used in this analysis, is discussed in section 3. In section 4, it explains simulation. In section 5 addresses the results obtained in this simulation.

RELATED WORK

In [14], Gupta and Kumar developed a random network model for the study of performance scaling on a fixed wireless network; the authors in [14] showed that the performance scaling changes entirely during the time of motion nodes. According to [13,14] the authors in [15] showed that there are three parameters for throughput and delay: hop number, scope, mobility and speed of the node. The authors propose schemes that use the three characteristics to achieve different points in the curve in an optimum manner.

In [16], the authors have shown that different network parameters affect the delay: the probability of channel access, transmission power or distance, load of the network and node density. The agreement pause is the topic of a review by the authors of the paper [17]. The same authors developed an algorithm to achieve optimal delay performance under certain delay conditions. In [9], the experimental results show that the random movement models differ in the efficiency of the AODV routing protocol: Random Waypoint, Random Walk with Reflections and Random Walk with Wrapping.

In [1], the effects of different mobility models on the efficiency of both the (DSR-Reactive) and (DSDV-Proactive protocol) routing protocols were studied. Such four mobility models are Random Waypoint, Team Mobility, Freeway and Manhattan. The study showed that the performance of the mobility models improved.

In [18] with an AODV routing protocol, the performance of the three mobility models: Random WayPoint, Random Walk with Reflections and Random Walk with Wrapping were evaluated. The

results demonstrate that the best Random Waypoint model, with two different scenarios, outperforms the Random Walking Model and Random Direction Model. The results show that the Random Waypoint produces the highest output, whereas the Random Walk Model and Random Direction output falls dramatically over a time period.

The authors of this article [19] present the accomplishments of the Displacement-Sequenced Distance Vector (DSDV) in four separate mobility models: Random Waypoint, RPGM, Gauss Markov and the Manhattan Mobility Model. The findings in this paper show that the DSDV protocol with the RPGM mobility model has improved results with different network load and speed.

Various protocols such as AODV, DSDV, Dynamic Source Routing (DSR) and TORA are compared in [20]. Packet delivery fraction and the end-to-end delivery time according to availability, traffic and network size are the output parameters considered for review. Random Waypoint, Random Walk and Random Directions are the principles of mobility. AODV has been shown to do more than DSDV, TORA and DSR and also with Random Walk and Random Direction models. AODV is recommended to be used under high mobility as it is as effective as protocols DSDV, TORA and DSR.

In [21] the authors were able to evaluate the performance of dynamic source routing (DSR) in multi-service traffic in MANET as a delay.

In [22], the routing problem is proposed in multi-service MANETs as well as the adaptation of the DSR protocol.

The three models of mobility (Random Waypoint, Random Directorate and State of Mobgen-Steady) have been evaluated with CBR traffic in [5] by Random Way Point in low node densities and Mobgen-Steady State with high node density demonstrate the maximum delay.

Nonetheless, Random Way Point achieves optimum performance during the low and high node densities. In paper [6] it is evaluated the AODV protocol's behaviour with the same earlier models of mobility. But this time the analysis is being performed on multi-service (VBR) traffic. The AODV protocol has been adaptive to the type of traffic used. This AODV behaviour change allows this comparative study to be conducted using both traffic forms (CBR) and (VBR).

PROBLEM FORMULATION

It is clear that the QoS maintains a certain level of performance for various applications. The ad hoc network is however used in applications with specific QoS rates. Network traffic is marked as time-sensitive. In this category, we find real-time traffic applications that require a minimum guarantee. This generally works without losing data (e.g. video conferencing)

[23]. Most real-time systems include delay limits to be assured, but these limitations can be slightly exceeded. Most applications in this group can also handle a small amount of packet loss [24]. The second category is data traffic that does not require delays, but it requires a short average delay. The transmission of data requires lossless transmission [23].

The research includes two types of Constant Bit Rate (CBR) and Variable Bit Rate (VBR) traffic. Those technologies produce traffic at a fixed rate in the first class. As far as experience is concerned, certain implementations generate a CBR flow. Many applications produce variable bit rate streams (VBR) in the second class. This traffic affects the amount of information transmitted per unit time (i.e. bit rate). The degree of variance in the bit rate varies from application to application [25].

Among the major challenges of research architectures in ad hoc node density networks, what are the routing protocols and suitable mobility models to use for a given application scenario? To achieve this goal, some work was focused on routing protocol performance assessments and models of mobility as most previous research entered on CBR traffic which is not suited to multimedia VBR applications [26].

This research aims to measure the performance of the AODV Routing Protocol differently and to test the conduct of this protocol by using the CBR and VBR traffic models with various mobility models. It is then proposed an adaptable method that takes advantage of the results and represents the optimum delay and performance. In this way the minimum acceptable delay values assigned to each number of nodes are considered for the optimal delay of the three mobility models. For the optimal performance of three mobility models, the maximum output values are considered for each number of nodes.

This work analysed the effect of the node density on the performance of the AODV routing protocol (end-to-end delay, throughput and packet delivery rate). The three models of mobility are: Random Way Point, Mobgen-Steady State and Random Management.

The VBR traffic is closely consistent with the statistical features of an actual video frame trace created by an MPEG-4 encoder [26]. The traffic stream was regulated by two parameters. The first parameter, the first seed, results in traffic variants. This parameter was kept continuously at 0.4 [25], since all experiments had to use the same traffic trace.

The second parameter, the rate factor has defined the degree of video input scaling up or down while the same sample path and autocorrelation function for the frame size distribution is preserved. The meaning is 0.33 for 40 and 0.25 for 10, 20 and 30 sources [24]. On the basis of [20] the AODV works better than DSDV, TORA and DSR protocols and can be used with high mobility.

The reliability of the performance results is clearly based on the successful selection of the simulation parameters. In mobile ad hoc network simulations, the probability distribution that governs the motion of nodes typically varies over time and converges to a 'state-specific' distribution. Once node speeds and positions are chosen from their constant-state distribution, the output parameters of a given protocol converge to their values as well. In [27], the authors show that it may take more than 1000 seconds of simulation time to achieve stable state [28]. That is why our works take 1200 seconds to simulate.

The ad hoc reactive routing protocol considered Ad hoc on-demand remote routing [20] to be a dynamic on-demand multi-hop routing protocol for mobile ad hoc wireless networks. AODV discovers source routing paths and maintains route cache table case. It is free of loops and uses target sequence numbers. Within AODV a node informs its neighbours by sending "hello messages" constantly at a given interval about its very nature. It helps all nodes to know their neighbours' status, that is, if they have gone down or out of control. A Route Request (RREQ) is used to solve a route to another node in the AODV network.

The receiving node verifies whether it has a path to the specified node. If there is a path, the receiving node answers the question by sending a route response. If there is no path, the receiving node must send a RREQ itself to try to find a route for the requesting node. If the first node does not receive a reply in time, the node will infer that the nodes sought are unavailable. For order to ensure that the route persists, the sender has to keep the route alive by sending packets frequently.

Both nodes along the route are responsible for upstream connections, so the next node is a broken link. This node signals the broken link by sending a downstream error message (RERR) so that users can start looking for a new path.

The mobility model is designed to understand how mobile users move and how their position, movement direction, [35] pause distribution, speed and acceleration change over time. The mobility models are a valid scenario for how people move into, for instance, a meeting or museum.

— Random Way Point (RWP)

Each node is assigned initial location, destination, and speed in this model. The initial location and destination points are selected independently and uniformly in the area where nodes move. The speed is selected uniformly at an interval, regardless of location and destination.

After reaching destination, a new destination is selected from the uniform distribution and a new speed is selected uniformly on [min-speed, max-speed], regardless of previous destinations and speeds.

The node stays at each destination for a specified pause before repeating the process [9,11,26].

— Random Direction (RD)

The Random Direction Mobility Model [36] assigns each node an initial direction, speed and finite travel time. The node then travels in that direction to the simulation area border. The node pauses for a specified time after hitting the simulation limit, selects a different angular direction (between 0 and 180 degrees) and continues.

Random Direction Mobility Model was designed to resolve node clustering in one part of the Random Waypoint Mobility Model simulation area. For the Random Waypoint Mobility Model, this clustering occurs near the simulation area core.

— Mobgen Steady-State (Mbg-SS)

Implementing the RWM model with NS2 testbed [20] begins with a constant pause to the initial location [29,30]. In comparison, the initial positions are uniformly chosen.

With mobgen for NS2[31], another model of RWM in NS2 starts approximately half of the nodes in motion and the second half in pause [32]. For this reason, simulations with setdest take more time to converge with mobgen simulations. If node speeds and positions from their steady-state distribution are chosen, the performance metrics for a given protocol are also convergent to their values.

Therefore, when using setdest or mobgen, the output network will shift systematically as time passes and the calculation of collected results in the conversion cycle is incapable of representing the long term values [33].

The stability model Mobgen-Steady State strengthens the RWP model [27]. In this model, the initial positions and knots speeds from their stationary distributions are selected. Convergence is instant and performance outcomes are trustworthy. The Mobgen-Steady State model code is available to [33].

SIMULATION ENVIRONMENT

To achieve the goal, it needs to investigate how the AODV protocol works when loading nodes increases with specific Mobility Models (Random Waypoint, Random Path, Mobgen Steady-State).

Table 1. Simulation parameters

Parameter	Value
Simulation Time	1600 sec
Number of nodes	10, 20, 30, 40, 50, 60, 70, 80, 90, 100.
Pause Time	0, 10 Sec
Environment Size	2000 m × 2000 m
Traffic Type	Variable Bit Rate (VBR) MPEG-4
Maximum Speeds	20 m/s
Mobility Models	Random Waypoint, Random Direction, Mobgen Steady-State

Network simulator 2.34 NS-2 performed simulations. Using multimedia VBR (MPEG-4) and CBR. Table 1 contains all simulation parameters.

— **Performance Metrics**

For the simulation results, we selected the end-to-end delay and throughput as metrics to measure the efficiency of the different protocols: Average end-to-end latency: the delay of a packet is the time it takes to reach the destination after leaving the source. The total network packet delay is measured by comparing all packets and all destination pairs. The End-to-End TAVG is determined as shown in equation (1):

$$T_{AVG} = \frac{\sum_{i=1}^N (H_r^i - H_t^i)}{N_r} \quad (1)$$

In equation (1), H_t^i emission instant of package i , H_r^i reception instant of package i , N_r the total number of packets received.

Throughput: the ratio of successfully transmitted data per second (2).

$$T = \frac{L-C}{L} Rf(\gamma) \quad (2)$$

In equation (2), $\frac{L-C}{L}$ is the payload transmission rate, R b/s Binary transmission rate, L Packet size, and $f(\gamma)$ is the packet success rate defined as the probability of receiving a packet correctly. This probability is a function of the signal-to-noise ratio (γ).

Packet Delivery Ratio: the ratio of the data packets successfully delivered to the destination.

RESULTS DISCUSSION

This section presents our findings of simulation and performance analysis. Analysis based on comparing the different mobility model metrics that defined in Section 3.

— **Variable Bit Rate (VBR)**

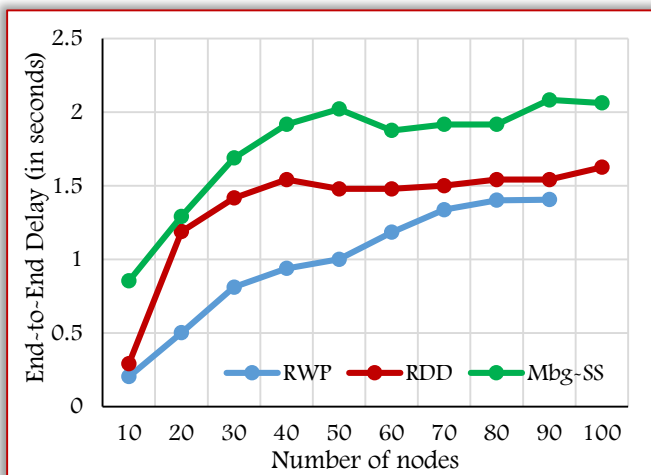


Figure 1. End-to-End Delay vs No. of nodes with VBR

As showing in Figure 1, with AODV, the delay increased. As node density increases.

Once density is important, the delay for the three models is still consistent. With Random Path, AODV takes less time to transmit packets than the other two versions (Random Way Point, Mobgen-ss). On the other hand, Mobgen-ss gives the best performance in terms of delay than Random Way point.

Based on Figure 2, AODV demonstrates higher throughput than both Random Way Point and Mobgen-ss. Also, total node count, the three mobility models are performed. So in the first section, Random Way point produces a high throughput than the Mobgen-ss model, in the second part, Mobgen-ss almost outperforms Random Way point.

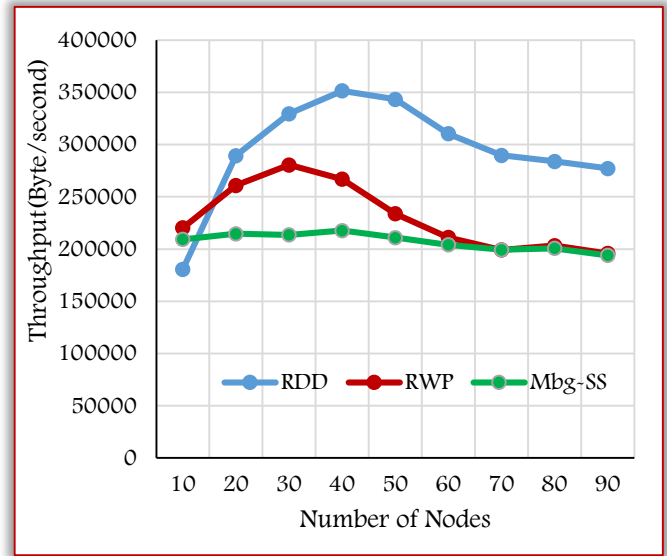


Figure 2. Throughput vs No of nodes with VBR

Figure 3 reveals that, in Random Direction, AODV ensures more packet transfer than Random Way-point and Mobgen-ss. But, for the three mobility models, the packet delivery ratio decreases and is insufficient over all node density.

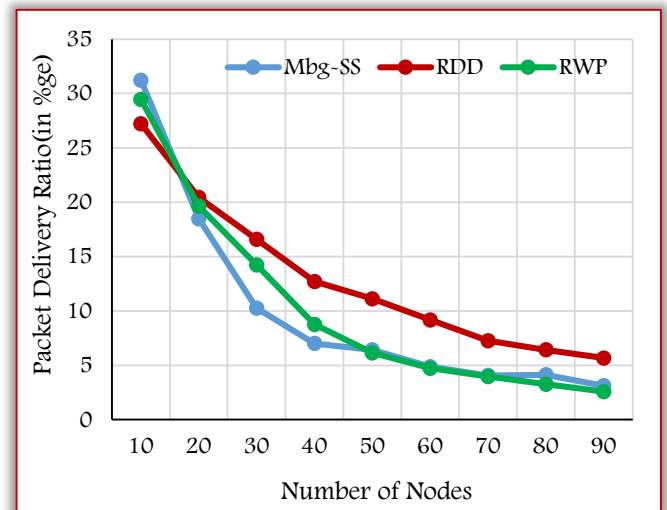


Figure 3. Packet Delivery Ratio vs No. of nodes with VBR

Generally, with AODV and using VBR (MPEG-4) traffic, results (Figures 4-6) suggest using Random Direction in real-time applications with delay limits to be met. It can also be used on applications that tolerate little packet loss.

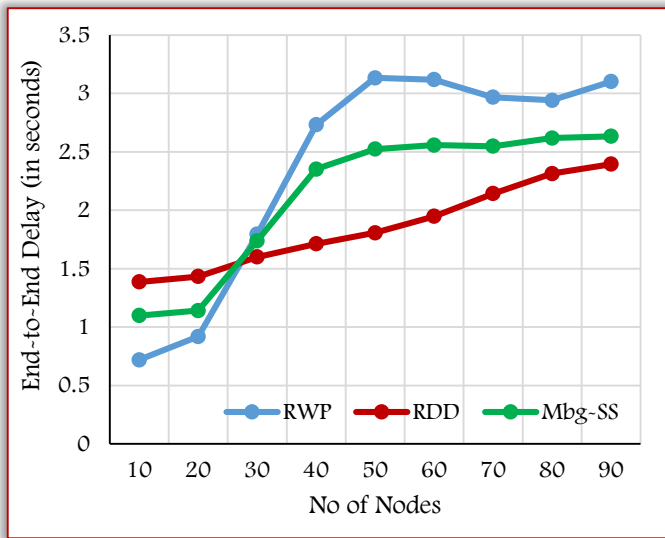


Figure 4. End-to-End Delay vs No. of nodes with CBR

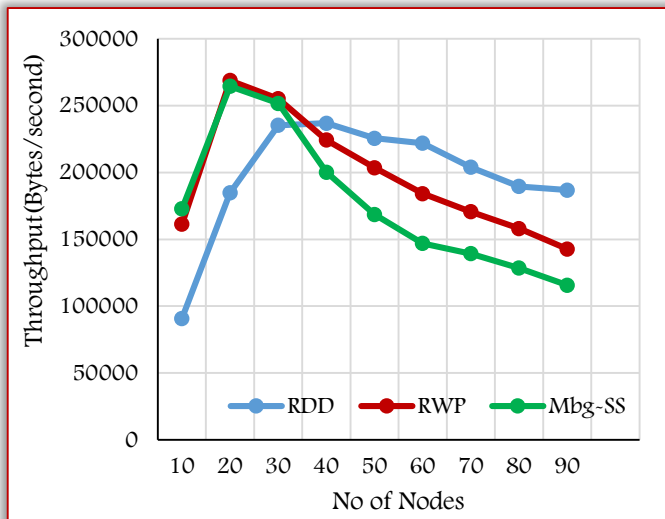


Figure 5. Throughput vs No. of nodes with CBR

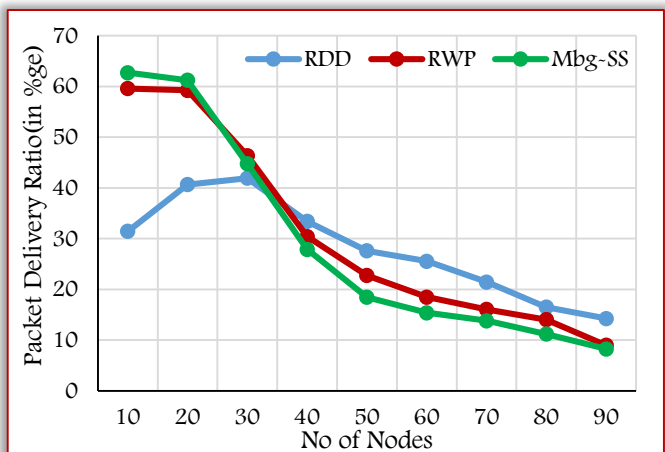


Figure 6. Packet Delivery Ratio vs No. of nodes with CBR

— Constant Bit Rate (CBR)

End-to-end routing protocol is less, constant and consistent when using low node density. In this section, compared to Random Direction and Mobgen-ss mobility models, AODV takes less time to deliver the packets. Once density is high, AODV's behaviors change drastically. End-to-end delay greatly increases. In this part, AODV's delay in Mobgen-ss is less than Random Way point, and high in Random Direction model. AODV performs better in Random Direction than other versatility models.

If we consider only applications that are sensitive to delay, the optimal delay achieved with Random Way Point and heavy density is achieved by Random Direction. So for implementations, the results suggest using Random Way Point on low density and Random Direction on high.

Based on Figure 5 results, AODV with Random Way Point and Mobgen-ss models show higher than Random Direction. After that, AODV's throughput with the three mobility models decreases as node density increases. Nevertheless, with Random Direction, AODV produces better performance of both Random Way Point and Mobgen-ss. On the other hand, considering applications needing a certain amount of throughput, the results suggest using AODV with Random Way Point in low densities and Random Direction mobility model in large densities.

As shown in Figure 6, a higher Packet Delivery Ratio is achieved when using AODV with Random Way Point and Mobgen-ss mobility models. In the Mobility Model Random Direction, AODV performed better in transmitting packet data to destination by increasing node density.

VBR and CBR

That's right. The most common literature mobility model is Random Way Point [29]. This model, with CBR, provides maximum performance in terms of latency, throughput and low-density packet delivery ratio (Figures 4-6).

When moving traffic from CBR to VBR (MPEG-4) on efficiency (end-to-end delay, throughput and packet delivery ratio) on AODV routing protocol, the behavior of AODV changes when using a small node number.

When density is high, AODV (with CBR and VBR traffic) retains the same behavior (Figures 1-6) in terms of delay and Packet Delivery Ratio, excluding throughput. On the other hand, rising node density from low to strong has no effect at AODV protocol behavior in connection with VBR traffic (MPEG-4).

Because the Mobgen Steady State is more realistic than the Random Direction model, the optimal delay is achieved with Random Way Point in small density and with Mobgen Steady State in heavy density. Random Way Point achieves maximum efficiency

over all densities of nodes used, in the case of CBR traffic. On the other hand, in the case of VBR traffic, the optimal delay Figure 1 is similar to that of Mobgen Steady State and with low densities the optimal throughput Figure 2 is obtained by Random Way Point when the high densities used the optimal one are represented by both Random Way Point and Mobgen Steady State.

We therefore encourage the use of the Mobgen Steady State model in applications that are prone to delay (Figures 1 and 4) and that use high node density without considering traffic type (CBR or VBR (MPEG-4)) but for a limited density associated with CBR traffic, we recommend using Random Way Point and Mobgen Steady State for VBR traffic.

On the other hand, if we find applications needing a certain amount of throughput (Figures 2 and 5) and both Random Way Point and Mobgen Steady State are more practical than Random Path, we suggest using the first one mobility model in low node densities without considering the form of traffic (CBR or VBR (MPEG-4)). The Random Way Point will give the best results for the same applications with a CBR traffic when using high knots densities. The Random Way Point will give the best results for the same applications with a CBR traffic when using high knots densities. Inverse with traffic VBR, we suggest using the Mobgen Steady State model with high knots densities.

Eventually, based on VBR variability activity (MPEG-4), Packet Delivery Ratio remains inadequate over all node sizes. That's all three mobility models. AODV protocol can therefore be used on systems tolerating a small amount of packet loss.

CONCLUSIONS AND FUTURE WORK

We presented AODV routing protocol behaviour with multimedia traffic (VBR) and CBR using various mobility models such as Random Way Point, Random Direction and Mobgen Steady State.

For AODV model in combination for CBR traffic, Random Way Point in small density and Mobgen Steady State in heavy density achieve the optimum delay in the first. In the second, Random Way Point achieves optimum throughput.

In the association of AODV model with VBR traffic (MPEG-4), the optimum delay is obtained by Mobgen Steady State. Random Way Point and Mobgen Steady State achieve optimum throughput in the second.

With this process, we hope to help future studies choose parameters. To design the realistic scenarios that more accurately depict real-world applications and QoS.

Another key point in this paper is AODV's actions, with the three versatility mentioned above, depending on the traffic used (CBR or VBR). This activity is affected specifically in low node densities.

One of the most important criteria for promoting real-time communication is delay jitter. In the future, delay jitter metric also needs further analysis.

On the other hand, further analysis should be dedicated to optimizing the Packet Delivery Ratio when using VBR traffic.

References

- [1] D. Bhavyesh, A. Ajith, G. Crina and S. Sugata, "Impact of Node Mobility on MANET Routing Protocols Models," *Journal of Digital Information Management*, Vol. 5, No 1, 2007, pp. 19-24.
- [2] S. Corson and J. Macker, "Mobile Ad Hoc Networking (MANET): Routing Protocol Performance Issues and Evaluation Considerations," RFC, 1999.
- [3] K. Carlo, "Ad Hoc Networking," *Systems Journal*, 1999, pp. 33-40.
- [4] M. Ash and K. Oivind, "Quality of Service in Mobile Ad Hoc Networks: A Survey," *International Journal of Ad Hoc and Ubiquitous Computing*, Vol. 6, No. 2, 2010, pp. 75-98
- [5] M. Amnai, Y. Fakhri and J. Abouchabaka, "Throughput-Delay Optimisation with Adaptive Method in Wireless Ad Hoc Network," *IEEE International Symposium on I/V Communications and Mobile Networks (ISIVC10)*, Rabat, 30 September-2 October 2010, p. 1.
- [6] M. Amnai, Y. Fakhri and J. Abouchabaka, "Evaluation of Impact of Traffic VBR and Mobility on the Performance of AODV Routing Protocols in Mobile Ad Hoc Networks," *IEEE International Conference on Multimedia Computing and Systems (ICMCS'11)*, Ouazazate, 7-9 April 2011.
- [7] M. Amnai, Y. Fakhri and J. Abouchabaka, "Evaluation Analysis of Varying Mobility Models on AODV Protocol of MANETs'," *7èmes JFMM Colloque International Telecom'2011*, Tanger, 16-18 Mars 2011.
- [8] M. A. Rahman, M. S. Islam and A. Talevski, "Performance Measurement of Various Routing Protocols in Ad-hoc Network," *Proceedings of the International MultiConference of Engineers and Computer Scientists 2009 IMECS*, Hong Kong, 18-20 March 2009.
- [9] S. Gowrishankar, T. G. Basavaraju and S. K. Sarkar, "Effect of Random Mobility Models Pattern in Mobile Ad Hoc Networks," *IJCSNS International Journal of Computer Science and Network Security*, Vol. 7 No. 6, 2007, pp. 160-164.
- [10] C. P. Agrawal, O. P. Vyas and M. K. Tiwari, "Evaluating of Varying Mobility Models Network Loads on DSDV Protocol of MANETs," *International Journal on Computer Science and Engineering*, Vol. 1, No. 2, 2009, pp. 40-46.
- [11] B. R. A. Kumar, L. C. Reddy and P. S. Hiremath, "Performance Comparison of Wireless Mobile Ad-Hoc Network Routing Protocols," *IJCSNS International Journal of Computer Science and Network Security*, Vol. 8, No. 6, 2008.
- [12] A. Uchiyama, K. Maeda, T. Umedu, H. Yamaguchi and T. Higashino, "Performance Evaluation of Mobile Wireless Communication and Services with Modeling of Real Environment," *International Journal of Ad*

- Hoc and Ubiquitous Computing, Vol. 2, No. 4, 2007, pp. 239-249
- [13] P. Gupta and P. R. Kumar, "The Capacity of Wireless Networks," IEEE Transactions on Information Theory, Vol. 46, No. 2, 2000, pp. 388-404
- [14] M. Grossglauser and D. Tse, "Mobility Increases the Capacity of Ad Hoc Wireless Networks," IEEE INFOCOM, Anchorage, 2001, pp. 1360-1369.
- [15] A. El-Gamal, J. Mammen, B. Prabhakar and D. Shah, "Throughput-Delay Trade-off in Wireless Networks," IEEE INFOCOM, Hong Kong, 2004.
- [16] S. Narasimhan and S. Kunniyur, "Effect of Network Parameters on Delay in Wireless Ad Hoc Networks," 2nd Annual IEEE Communications Society Conference on Sensor and Ad Hoc Communications and Networks (SECON), Santa Clara, 26-29 September 2005.
- [17] L. Ying, S. C. Yang and R. Srikant, "Optimal Delay-Throughput Trade-offs in Mobile Ad Hoc Networks," IEEE Transactions on Information Theory, Vol. 54, No. 9, 2008, pp. 4119-4143
- [18] M. I. M. Saad and Z. A. Zukarnain, "Performance Analysis of Random-Based Mobility Models in MANET Routing Protocol," European Journal of Scientific Research, Vol. 32, No. 4, 2009, pp. 444-454.
- [19] C. P. Agrawal, et al., "Evaluation of Varying Mobility Models Network Loads on DSDV Protocol of MANETs," International Journal on Computer Science and Engineering, Vol. 1, No. 2, 2009, pp. 40-46.
- [20] M. K. J. Kumar and R. S. Rajesh, "Performance Analysis of MANET Routing Protocols in Different Mobility Models," IJCSNS International Journal of Computer Science and Network Security, Vol. 9, No. 2, 2009.
- [21] R. Beaubrun and B. Molo, "Évaluation du Délai dans un Réseau Mobile Ad Hoc Multi-Services," Canadian Conference on Electrical and Computer Engineering, Niagara Falls, 4-7 May 2008, pp. 000251-000256.
- [22] R. Beaubrun and B. Molo, "Using DSR for Routing Multimedia Traffic in MANETs," International Journal of Computer Networks Communications, Vol. 2, No. 1, 2010.
- [23] J. A. Zubairi, M. A. El-Shaikh and O. Mahmoud, "On Shaping and Handling VBR Traffic in a Diffserv Domain," ATS, Simulation Series, ASTC'01 Conference, Vol. 33, No. 3, 2001, pp. 10-15.
- [24] R. Philip, K. Nahrsted and W.S. Jane, "Scheduling and Buffer Management For Soft-Real-Time Vbr Traffic in Packet-Switched Networks," 21st Annual IEEE International Conference on Local Computer Networks, 1996, pp. 143-152.
- [25] R. Beaubrun and B. Molo, "Using DSR for Routing Multimedia Traffic in MANETs," International Journal of Computer Networks Communications, Vol. 2, No. 1, 2010.
- [26] M. U. Chowdhury, D. Perera and T. Pham, "Performance Comparison of three Wireless Multi-Hop Ah-Hoc Network Routing Protocols When Streaming MPEG-4 Traffic," Proceeding of the 8th International Multi-Topic Conference, 24-26 December 2004, Lahore, pp. 516-521.
- [27] W. Navidi, T. Camp and N. Bauer, "Improving the Accuracy of Random Waypoint Simulations through Steady-State Initialization," 15th International Conference on Modeling and Simulation, 2004, pp. 319-326.
- [28] W. Navidi and T. Camp, "Stationary Distribution for the Random Waypoint Mobility Model," Technical Report MCS-03-04, IEEE Transactions on Mobile Computing, Vol. 3, No. 1, 2004. pp. 99-108
- [29] J. Broch, D. Maltz, D. Johnson, Y. Hu and J. Jetcheva, "Multi-Hop Wireless Ad Hoc Network Routing Protocols," 4th Annual ACM International Conference on Mobile Computing and Networking, 1998, pp. 85-97.
- [30] "Wireless and Mobility Extensions to NS-2," <http://www.monarch.cs.rice.edu/cmu-ns.html>
- [31] "Tutorial for the Network Simulator 'NS'," <http://www.isi.edu/nsnam/ns/tutorial/index.html>
- [32] T. Camp, J. Boleng, B. Williams, L. Wilcox and W. Navidi, "Performance Comparison of Two Location Based Routing Protocols for Ad Hoc Networks," The 21st Annual Joint Conference of the IEEE Computer and Communications Societies, Vol. 3, 2002, pp. 1678-1687
- [33] <http://toilers.min.edu>
- [34] M. Amnai, Y. Fakhri and J. Abouchabaka, "Impact of Mobility on Delay-Throughput Performance in Multi-Service Mobile Ad-Hoc Networks," International Journal of Communications, Network and System Sciences, Vol. 4 No. 6, 2011, pp. 395-402
- [35] DirectMe: A Mobile Phone Algorithm for Direction Detection Alex T. Mariakakis Duke University, ECE/CS 2013 Advisor: Dr. Romit Roy Choudhury
- [36] M. Liu, Y. Wan and F. L. Lewis, "Analysis of the Random Direction Mobility Model with a Sense-and-Avoid Protocol," 2017 IEEE Globecom Workshops (GC Wkshps), Singapore, 2017, pp. 1-6



ACTA TECHNICA CORVINIENSIS – Bulletin of Engineering
ISSN: 2067-3809
copyright © University POLITEHNICA Timisoara,
Faculty of Engineering Hunedoara,
5, Revolutiei, 331128, Hunedoara, ROMANIA
<http://acta.fih.upt.ro>

Fascicule 3

[July – September]

t o m e

[2020] XIII

ACTA Technica **CORVINIENSIS**
BULLETIN OF ENGINEERING



ACTA TECHNICA CORVINIENSIS – Bulletin of Engineering

ISSN: 2067-3809

copyright © University POLITEHNICA Timisoara,

Faculty of Engineering Hunedoara,

5, Revolutiei, 331128, Hunedoara, ROMANIA

<http://acta.fih.upt.ro>

¹Srbislav ALEKSANDROVIĆ, ²Đjordje MILOSAVLJEVIĆ

ACCURACY OF PURE COPPER FLOW CURVES DETERMINATION IN COMPRESSION TESTS

¹Faculty of Engineering, University of Kragujevac, SERBIA

²Cacak, SERBIA

Abstract: Comparison of experimental results obtained in two main compression test methods are presented in this paper. First method is so called Schofman procedure. Second method is near friction free compression test so called Rastegaev procedure, and there is used as referent. Schofman method is attractive with his bright idea of non-experimental grapho-analytical elimination of friction, but experimental part is demanding and often problematic. Performed were Schofman compression test using pure copper samples, and proposed two variation of basic method. In second part of the experiment performed was Rastegaev compression test known as reliable and accurate, and classic compression test with existing of friction. After experimental results comparison and analysis, conclusions made about Schofman method, and especially about proposed corrections of basic procedure.

Keywords: flow curves, compression tests, pure copper

INTRODUCTION

Strain hardening curves or flow curves are the most significant characteristics of metal materials behaviour in the field of plastic deformation. One of the main reasons for that significance is flow curves usage in numerical simulations of forming processes. The accuracy of material data (including flow curves) is an important factor determining the accuracy of simulations.

Strain hardening curves are most often obtained by a tensile test. At the point of onset of necking strain intensity is relatively small. Data after necking is generally obtained by analytical approximation or by simple extrapolation. But, there is another solution – compression tests, suitable especially for bulk forming processes. Exist different methods [1, 2], and unique problem: how minimize influence of friction. One of the classic methods is so called Schofman compression test which is not sufficiently known in the western literature [1]. Essential postulate is inventive idea of friction elimination not by lubrication and experimental procedures but by mathematical extrapolation of proper functions curves. All the other tests are based on different experimental modifications and result corrections [1,2,3,4]. In research centers in Serbia (and former Yugoslavia) well-known is so called Rastegaev compression test [1] (also not sufficiently known in the West), which provide good and usable results.

There are many investigations of compression tests in literature. Some of them are given here. In the paper [3] presented was lead and tin samples compression test without lubrication. Idea was independently determine friction coefficient in ring test and afterwards make corrections of stress-strain curves in appropriate mathematical procedure. In the paper [4] was shown compression test performed with a dumbbell-shaped specimen and closed contact areas.

Authors conclude that it's possible in the tests to estimate large strains (up to 1.5) by suppressing the effects of friction. In the paper [5] given are implementation of numerical procedure called inverse analysis to correct experimentally obtained stress-strain flow curves. Paper [6] gives extensive experimental analysis of 26NiCrMoV 14–5 steel behaviour at higher temperature range (850–1150°C). Beside other techniques, applied was compression test, reached 0.7 strain and determined flow curves, but without experimental and other details. In the paper [7] authors presented was analysis similar to the one gives in paper 6, but with other material (2050 Al–Li alloy) and other temperature range (340–500°C). Used was classic compression test and than made was relatively complicated correction procedure for friction influence elimination.

In this investigation authors was applied classic compression Schofman method on the pure copper samples, with appropriate corrections. Correction effects were estimated by comparing results with separately made reliable Rastegaev test.

EXPERIMENT AND ANALYSIS

Material used in experiment was pure copper (Cu – PHC or CW020A according to EN 13601:2013). It is deoxidated copper intended to electrical industry, process equipment manufacture and other purposes. It has very good formability and high electrical conductivity. Main mechanical properties are given in Table 1.

Table 1. Cu–PHC Mechanical properties

Sign	Temper	Mechanical properties				HV
		R _M N/ mm ²	R _{p02} N/ mm ²	A A5, %	A10, %	
Cu–PHC	R240	240÷300	>180	>14	≥8	65–90

Series of cylindrical samples was prepared for the experimental part of Schofman method (Figure 1). There is in Figure 1 geometry of six samples, but sample with height of 20 mm was abandoned because of unstable compression process. Compression was performed on classic mechanical laboratory testing machine with maximal force of 100 kN. Velocity was 5 mm/min. View of samples and testing machine are given at Figure 1 and Figure 2.

According to Schofman method [1] compression test without lubrication was conducted to strain about 0.7. Force capacity of machine was only limit. After that, collected experimental data were presented in diagram which give dependence of compression stress on strain (Figure 3).

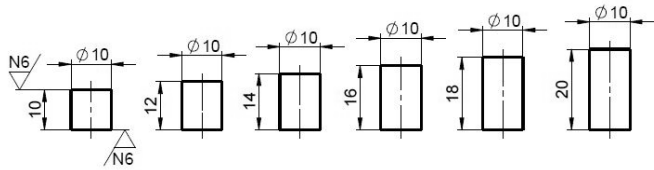


Figure 1. Samples for Schofman test



Figure 2. Testing machine

Diagram stress – sample diameter, sample height ratio need to form based on the data from diagram in Figure 3, at the second stage of Schofman method. Note that in Figure 4 on x-axis given is d_0/h_0 – ratio before deformation, i.e. type of sample.

Through obtained points for strains 0.1 to 0.6 (step 0.1) calculated and drew were extrapolation exponential functions, according to appropriate

mathematical procedure. Points in sections of y-axis and extrapolation curves gives true stress in theoretically low friction condition, i.e. equivalent stress. Note that points for d_0/h_0 – ratio of 0.55 were abandoned (except for minimal 0.1 strain ϵ_1) because of unstable forming (see Figure 1 above).

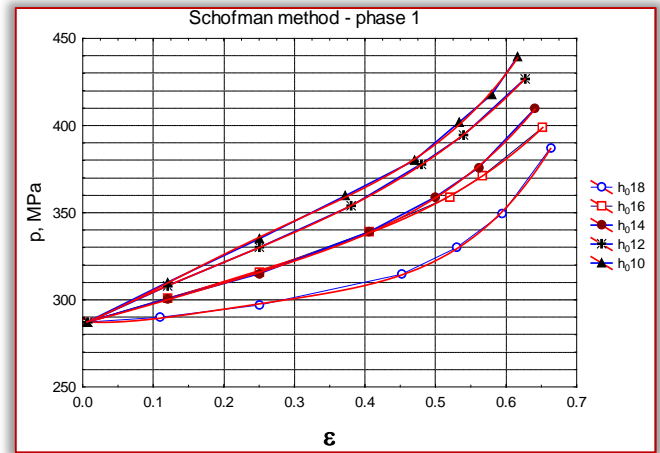


Figure 3. Compression stress – strain diagram

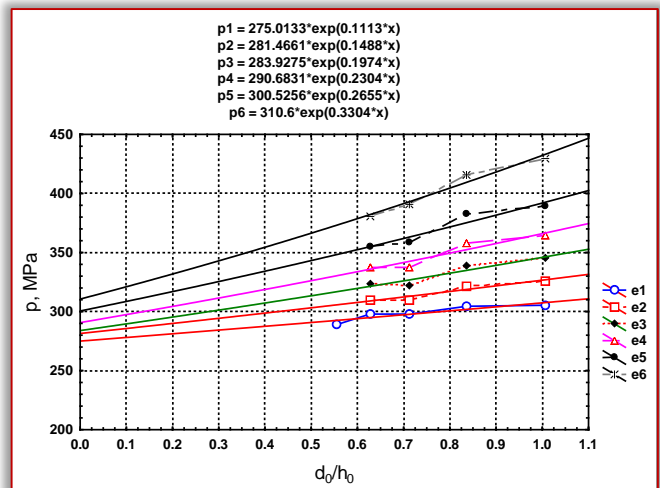


Figure 4. True stress–diameter to height ratio diagram

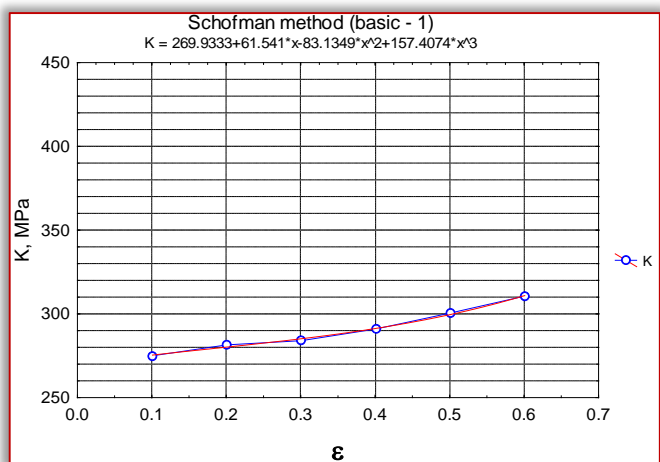


Figure 5. Flow curve–variant 1

Obtained curve (Figure 5) have lower position than can be expected. That was the reason to propose corrected extrapolation, Figure 6. Points for smallest

strain of 0,1 (e1) are most reliable, and for these points calculated was extrapolation function, the same as at Figure 4. Functions for the next strains are equidistant. Flow curve are given in diagram Figure 7, variant 2. Position of the curve K2 is more realistic.

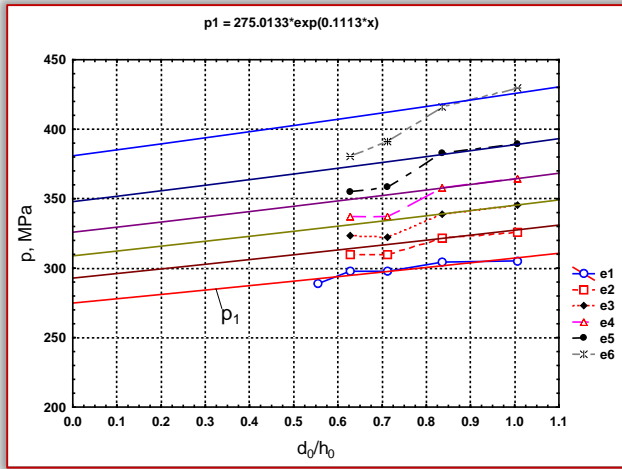


Figure 6. Corrected extrapolation (var. 2)

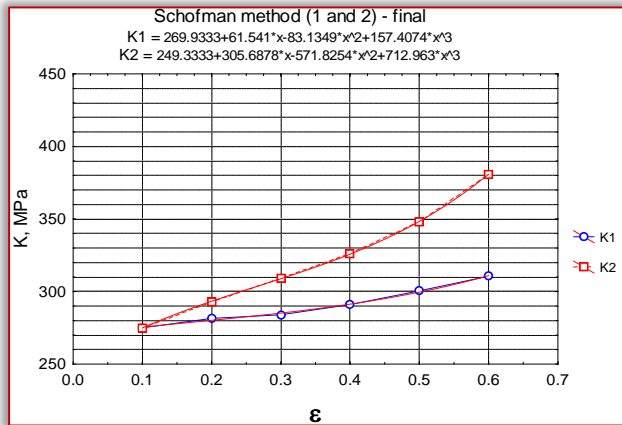


Figure 7. Flow curves (variant 1 and 2)

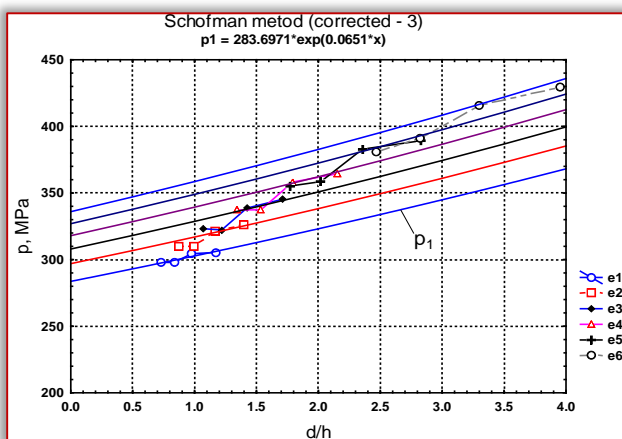


Figure 8. Corrected extrapolation (var. 3)

Variant 3 is second correction and principle is given in Figure 8. Instead of d_0/h_0 there is used value d/h corrected according to realized deformation [1]. Extrapolation functions calculated in the same way as in Figure 6. Flow curve can be seen in Figure 9. Disregarding corrected ratio d/h position of flow curve is relatively low.

For the estimation of obtained flow curves chosen was reliable Rastegaev method [1, 2]. Geometry of special specimen is given at Figure 10, and view at Figure 11. Diameter $d=10$ mm, height $h=12$ mm, $u=0.3$ mm, $t=0.7$ mm. Lubrication was realized with molybdenum disulfide grease.

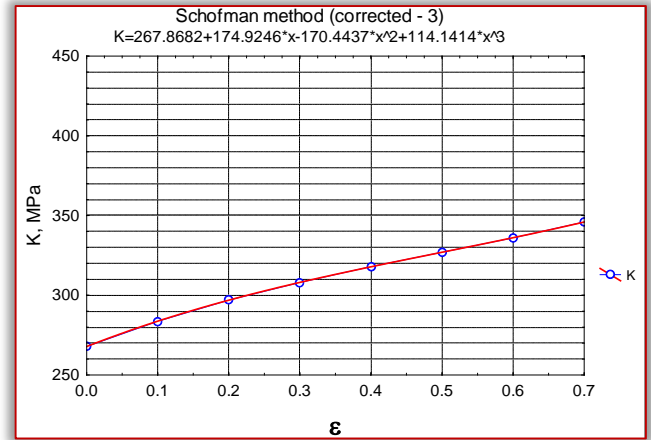


Figure 9. Flow curve-variant 3

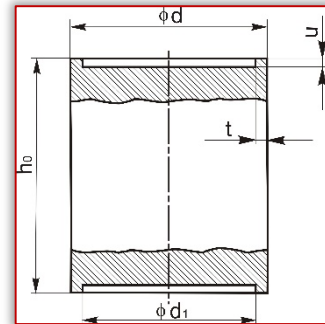


Figure 10. Sample for Rastegaev test



Figure 11. View of Figure 10 sample

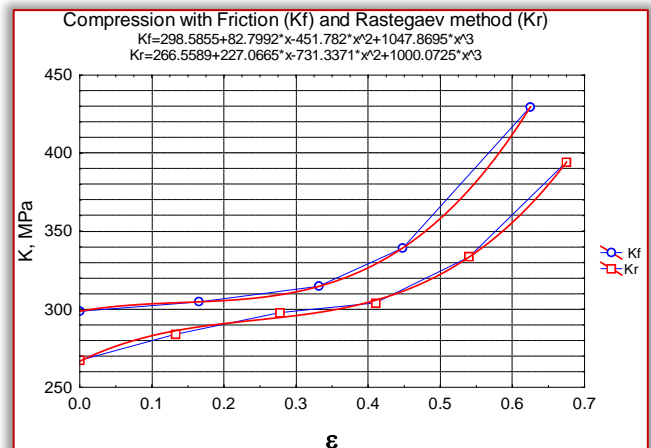


Figure 12. Stress-strain curve with friction (Kf) and Rastegaev flow curve (Kr)

Here, can be seen in Figure 12 effect of Rastegaev reduction of friction. Above stress–strain curve is with and below without friction. Obvious difference between the curves confirms efficiency of Rastegaev method.

Figure 13 shows results comparison of corrected Schofman method (variant 2 and 3) and Rastegaev method which is considered as referent here. Differences are not great and proposed curves are acceptable, but not ideal.

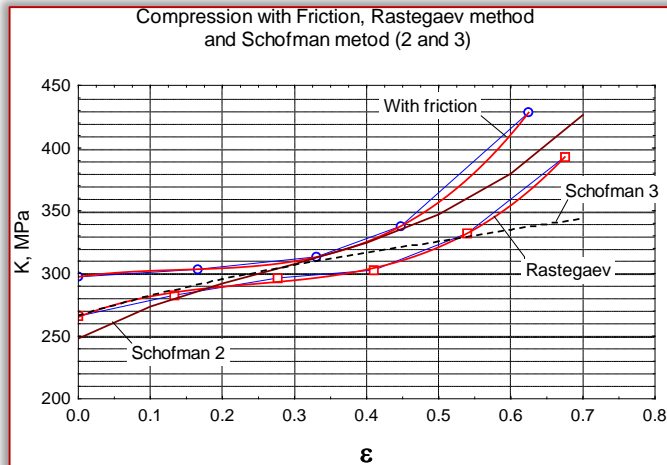


Figure 13. Different flow curves comparison

CONCLUSION

The appropriate corrections in classic Schofman method based on compression test were proposed. Conducted was compression experiment with samples of pure copper (Cu–PHC). Beside experiment for Schofman method, separately was performed compression test with friction, and according to Rastegaev method, with significantly reduced friction. Comparison of the curves with friction and Rastegaev reduction of friction clearly shows effect of that method.

Very sensitive Schofman method gives (in this experiment) lower position of flow curve than can be expected. After correction in grapho–analytical extrapolation procedure obtained more reasonable curves. Estimation of these flow curves were made by comparing with ones obtained in reliable Rastegaev test.

At the end, can be conclude that proposed correction gives acceptable results, but also there is a lot of space for further investigations.

Note:

This paper is based on the paper presented at DEMI 2019 – The 14th International Conference on Accomplishments in Mechanical and Industrial Engineering, organized by Faculty of Mechanical Engineering, University of Banja Luka, BOSNIA & HERZEGOVINA, co–organized by Faculty of Mechanical Engineering, University of Niš, SERBIA, Faculty of Mechanical Engineering Podgorica, University of

Montenegro, MONTENEGRO and Faculty of Engineering Hunedoara, University Politehnica Timisoara, ROMANIA, in Banja Luka, BOSNIA & HERZEGOVINA, 24–25 May 2019.

References

- [1] Marinkovic, V. (1995). Strain hardening of materials in metal forming processes at cold and warm condition, Faculty of Mechanical Engineering, University of Nis.
- [2] Vujovic, V. (1992). Formability, Faculty of Technical Sciences, University of Novi Sad.
- [3] Fereshteh–Sanie F., Fatehi–Sichani F.(2006). An investigation on determination of flow curves at room temperature and under forming conditions, Journal of Materials Processing Technology, no. 177, p. 478–482.
- [4] Usami, M., Oya, T.(2014). Estimation of work–hardening curve for large strain using friction free compression test, Procedia Engineering, no. 81, p.371–376.
- [5] Zhuang X., et. al. (2015). Determination of flow curve and plastic anisotropy of medium/thick metal plate, Journal of Iron and Steel Research International, vol. 22, no. 6, p. 506–512.
- [6] Ebrahimi G.R. et al. (2017). Flow curves, dynamic recrystallization and precipitation in a medium carbon low alloy steel, Vacuum, no. 142, p. 135–145.
- [7] Zhu R., et al. (2018). Flow curve correction and processing map of 2050 Al–Li alloy, Transactions of Nonferrous Materials Society of China, no. 28, p. 404–414.



ACTA TECHNICA CORVINIENSIS – Bulletin of Engineering

ISSN: 2067-3809

copyright © University POLITEHNICA Timisoara,

Faculty of Engineering Hunedoara,

5, Revolutiei, 331128, Hunedoara, ROMANIA

<http://acta.fih.upt.ro>

¹Petar S. DJEKIC, ²Biljana MILUTINOVIC

STUDY OF APPLICATION OF WASTE GLASS POWDER IN VIRGIN RUBBER BLENDS

^{1,2}College of Applied Technical Sciences Niš, Niš, SERBIA

Abstract: One major waste stream emerging as a serious challenge worldwide is glass, despite its ideal properties for recycling and its unsuitability for land filling. Although glass can repeatedly be recycled with no loss of quality, large volumes of glass are ending up in the landfill. If the waste glass could be used as a raw material for some products, a problem could be solved such as concrete, mortars, polymers and so on. This would increase the price of waste glass and, therefore, its interest in recycling of it. One of the ways, that this problem can be solved, is to add waste glass powder (WG powder) to rubber mixture as replacement of silicate filler. The paper presents the possibility of using waste powdered glass as a replacement for silicate filler. In this study different percentages of white waste glass powder, with an average particle size smaller than 63 µm, was added to virgin rubber blends and their influence on the mechanical properties of the rubber mixtures was analyzed. The paper also provides recommendations on the amount of waste glass powder for usage in rubber product. This paper presents a study to replacement of Kaolinite (Al₂Si₂O₅ (OH)₄) with waste glass powder which has SiO₄ as its base. This paper also shows the effect of WG powder on the mechanical properties of the rubber blends

Keywords: waste glass, rubber blends, mechanical

INTRODUCTION

In Serbia, 97% of waste is located at landfills, which is the least economical and environmentally-friendly option for waste management. Austria, for example, recycles that amount of waste, while only three percent ends up at the landfill. Waste glass falls into the category that is least recycled. The reason lies in the fact that the collection costs are very high per ton of collected material goes up to 50 euros per tonne, while the purchase price is barely 10 euros per tonne [1]. Because of the low price of purchase, secondary raw material collectors are not interested in collecting waste glass and recycling centers to buy them.

However, if the waste glass could be used as a raw material for some products, a problem could be solved such as concrete, mortars, polymers and so on [2-5]. This would increase the price of waste glass and, therefore, its interest in recycling of it. One of the ways, that this problem can be solved, is to add waste glass powder (WG powder) to rubber mixture as replacement of silicate filler. This paper presents a study to replacement of Kaolinite (Al₂Si₂O₅ (OH)₄) with waste glass powder which has SiO₄ as its base. This paper also shows the effect of WG powder on the mechanical properties of the rubber blends.

EXPERIMENTAL RESERCH

— Rubber blends

In this paper, the use of white packaging glass is considered. For the purpose of this research, grinding of white glass bottles was done it the Pulversette-FRITISCH 2 mill with porcelain grinding set. After grinding, the shaking of this powder was obtained in a shaker with a set of sieves up to a particle size below 63 µm. After that, the chemical composition was

determined using the Energy-Dispersive X-ray spectroscopy and shown in Table 1.

Table 1. Chemical composition of waste glass powder

Compound	Mass (%)
SiO ₂	71,25
Al ₂ O ₃	1,11
Fe ₂ O ₃	0,77
CaO	8,60
MgO	3,35
SO ₃	0,2
Na ₂ O	12,13
TiO ₂	0,08

After grinding and screening, the waste glass powder (WG powder) was added to a rubber mixture based on SBR rubber. The mixture in which waste glass powder is added is used to make rubber floor coverings. For the purposes of this experiment, the entire amount of chalk was changed with waste glass powder. The composition of the resulting rubber blends is shown in Table 2.

The blends were mixed in a laboratory size two-roll mill at temperature around 80 °C and the mixing time of 15 min. The time and length of the curing process was determined by the Monsanto Rheometer 100S according to ASTM D 2240-93, with the vulcanization time of 15 min, and the vulcanization temperature of 150°C.

Table 2. Composition of rubberblends

Ingredients	Virgin rubber blend (g)	Rubber blend with waste glasse powder (g)	
		50% replacement	100% replacement
Hypren 1502	25500	25500	22500
Regenerated rubber	43500	43500	43500
ZnO	1900	1900	1900
Stearin	770	700	700
TMQ	275	275	275
SOLAR-3	1600	1600	1600
ROF-58	4300	4300	4300
Chalk	48500	48500	48500
Kaolinite	31000	15500	0
WG powder	0	15500	31000

—Mechanical testing

All measurements were performed before and after aging. The aging process was conducted in the aging oven at air atmosphere for the period of 7 days at a temperature of 85 ± 1 °C.

Hardness measurements were performed in accordance with ISO 868-1 [6], using a manual durometer type Shore A. The measurements were carried out 5 times for each sample.

The testing of wear resistance was performed in accordance with ISO 4649 [7] using a Shopper cylindrical device with 5 measurements per sample.

The determination of tensile strength was carried out in accordance with ISO 37 [8] at the Instron testing machines, on dumbbell specimen type "2" of 2 mm in thickness, strained to break. The clamp separation speed was 100 mm/min.

Tear resistance was analyzed in accordance with ISO 34 [9]. Three angular type "A" tubes of 3 mm in thickness were strained to break in the measuring point, where the speed of clamp separation was constant at 500 mm/min.

Scanning electronic microscope and Energy-Dispersive X-ray spectroscopy was performed at JFC-1100E. (JEOL, Japan).

RESULTS AND DISCUSSION

The results of the measurement of the hardness of the samples before and after aging are shown in Figure 1. With the increase in the share of WG powder and the decrease in the proportion of Kaolinite, the hardness is increased, but this increase is not significant. A significant change in hardness occurs when testing aging, which could be expected as the result future vulcanisation.

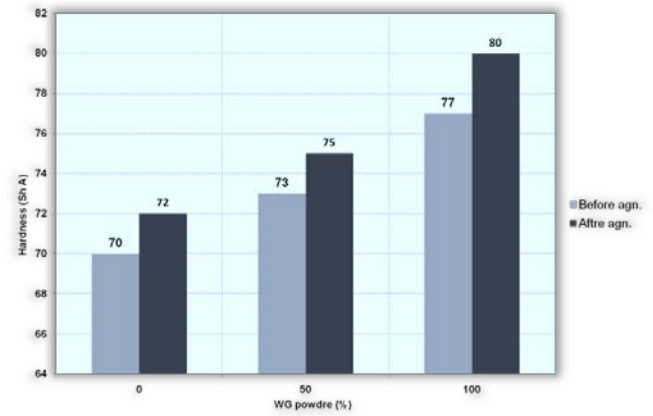


Figure 1. Results of hardness testing

At products such as rubber floor coverings tensile properties (tensile strenght and elocation at brake) do not have high values, ie, the change of this property does not significantly affect at the quality of the product. The results of measuring this property before and after aging are shown in Figure 2.

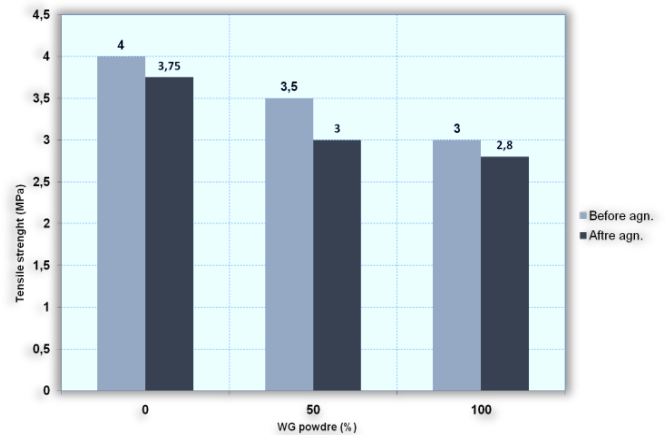


Figure 2. Results of tensile strength of rubber blends

One of the most important properties of the product such as floor coverings is tear strength. It represents a measure of the resistance of the material towards further spread of the crack. Figure 3 shows the results of measuring this property before and after aging.

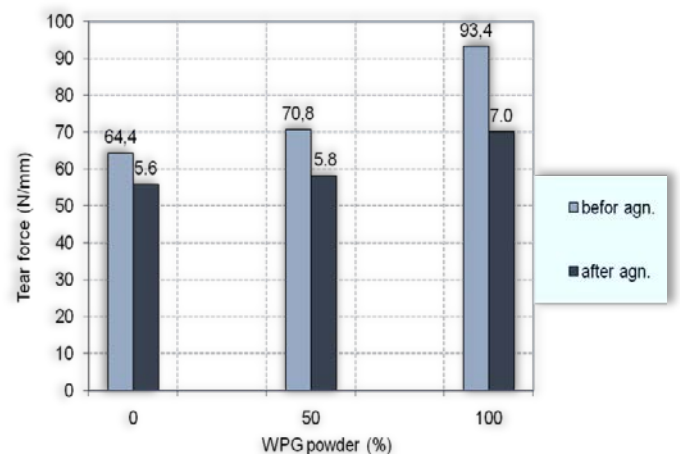


Figure 3. Results of tear resistance testing

Test results for wear resistance are shown in Figure 4. It can be concluded, from the diagram, that WG powder particles have higher effect on this property either before or after aging.

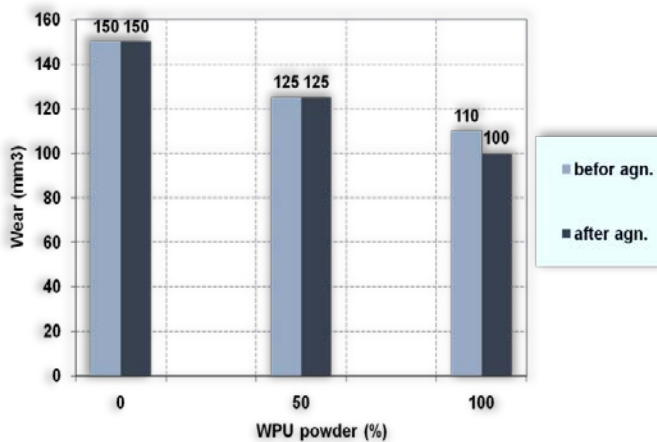


Figure 4. Results of wear resistance test

The appearance and shape of the particles waste glass powder is shown in Figure 5.

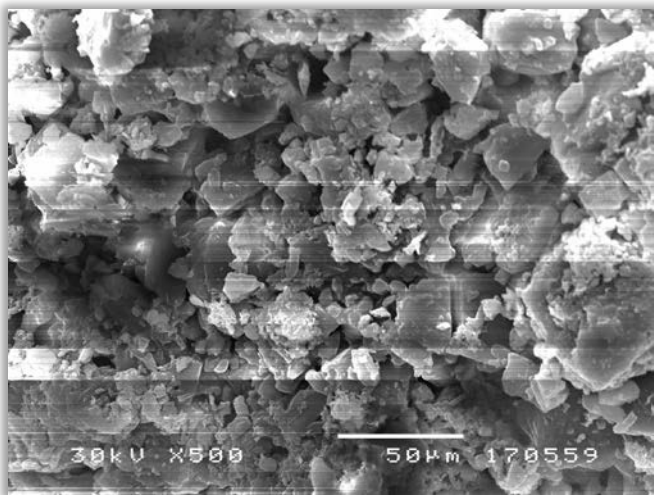


Figure 5. Waste glass powder

Silicate fillers are obtained by precipitation and have small primary particles. These fillers belong to the group of semi-active fillers, which in the case of increased dosage at the rubber increases its elastic properties.

Sodium-aluminum silicate, potassium-aluminum silicate, etc. are used as semi-active fillers. As it can be seen from the results of the examination the impact on hardness and tensile is insignificant.

While the impact on tear strength and wear resistance is significant. This can be assumed that the increased share of SiO_4 has a positive effect on the properties, which has a more pronounced effect of reinforcement. Also, the positive properties of WG powder is transparency, so products can easily be painted.

As SiO_4 is on the seventh place of the Mohs' Scale of hardness and has a pronounced wear resistance, excessive use can lead to accelerated wear and tear of machines and tools so research should be carried out in that direction.

CONCLUSION

Solving of the waste glass problem is a great challenge for a modern society. Because the low purchase price negatively affects on recycling and demand for waste glass as raw material. One way of overcoming the problem is that waste glass is used as a raw material for some products (cements, mortars, polymers, etc.). This paper presents the possibility of usage of WG powder as a substitute for Kaolinite. In doing so, improvements are made in products where the tear strength and wear resistance are the dominant properties such as floor coverings, lower footwear, and so on.

The negative side of the application is reflected in high resilience resistance, as the working machines are damaged. So further research should be carried out in that direction too.

Note:

This paper is based on the paper presented at DEMI 2019 – The 14th International Conference on Accomplishments in Mechanical and Industrial Engineering, organized by Faculty of Mechanical Engineering, University of Banja Luka, BOSNIA & HERZEGOVINA, co-organized by Faculty of Mechanical Engineering, University of Niš, SERBIA, Faculty of Mechanical Engineering Podgorica, University of Montenegro, MONTENEGRO and Faculty of Engineering Hunedoara, University Politehnica Timisoara, ROMANIA, in Banja Luka, BOSNIA & HERZEGOVINA, 24–25 May 2019.

References

- [1] <https://www.tehnologijahrane.com/iz-novina/koje-su-prepreke-u-razvoju-reciklaze-ambalaznog-stakla>
- [2] Lu, J.X., Poon, C.S., (2018.) Use of waste glass in alkali activated cement mortar. *Constr. Build. Mater.* 160, 399-407
- [3] Lu, J.X., Zhan, B.J., Duan, Z.H., Poon, C.S., (2017). Improving the performance of architectural mortar containing 100% recycled glass aggregates by using SCMs. *Constr. Build. Mater.* 153,975-985.
- [4] Balkan e-Waste Management Advocacy Network, Upravljanje e-otpadom u Srbiji, 2010.
- [5] Widmera R., Oswald-Krapf H., Sinha-Khetriwal D., Schnellmann M., Bonia H. (2005). *Global perspectives on e-waste, Environmental Impact Assessment*, vol. 25, p. 436– 458.
- [6] ISO 7619-1:2010. Rubber, vulcanized or thermoplastic -- Determination of indentation hardness -- Part 1: Durometer method (Shore hardness).

- [7] ISO 4649:2010. Rubber, vulcanized or thermoplastic -- Determination of abrasion resistance using a rotating cylindrical drum device.
- [8] ISO 37:2011. Rubber, vulcanized or thermoplastic — Determination of tensile stress-strain properties.
- [9] ISO 34-1:2015. Rubber, vulcanized or thermoplastic -- Determination of tear strength -
- Part 1: Trouser, angle and crescent test pieces.



ACTA TECHNICA CORVINIENSIS – Bulletin of Engineering
ISSN: 2067-3809

copyright © University POLITEHNICA Timisoara,
Faculty of Engineering Hunedoara,
5, Revolutiei, 331128, Hunedoara, ROMANIA
<http://acta.fih.upt.ro/>

¹Meenakshi A. THALOR

ANALYSIS OF DIFFERENT DRIFT DETECTION TECHNIQUES ON DATA STREAM

¹Department of Information Technology, AISSMS Institute of Information Technology, Pune, Maharashtra, INDIA

Abstract: Traditionally, data mining assumes that training and testing dataset are produced from a single, stationary and hidden function. Its means that, the data used at testing time is generated from same function as from training time. In the data stream the above-mentioned assumption is not true that is the source which generates examples at training time need not be the same source which generates examples at testing time. This paper highlights the change of source of data which can be abrupt, gradual, incremental or reoccurring. At the end this paper provides analysis of drift detection methods on abrupt, gradual or incremental drifted data stream.

Keywords: Data Stream, Concept Drift, Drift detection

DATA STREAM CLASSIFICATION

Data stream is continuously arriving sequence of data example available at specific rate, unlimited in size because of that some of data examples are discarded once analyses are done; data examples possess continuously evolving pattern and bustiness as generated from different sources. Traditional data mining approaches is not suitable to data stream because of aforementioned characteristics of data stream. Incremental models [1] are used to handle data stream where the data is fetched at time t rather than retrieving all the data at the beginning of training. Model process each instance with in a constant time and takes only one look on to the data rather than multiple passes. Incremental model makes use of fixed amount of memory for storage and always ready to predict at any time.

Classification helps in decision making by providing the class labels for given data using historical records. Figure 1 shows the classification process on data streams [1] where data chunks $C_1; C_2; C_3; \dots; C_i$ arrive one after one. A data chunk consists of bunch of instances. In two class problem, each chunk contains some class1 instances and some class2 instances.

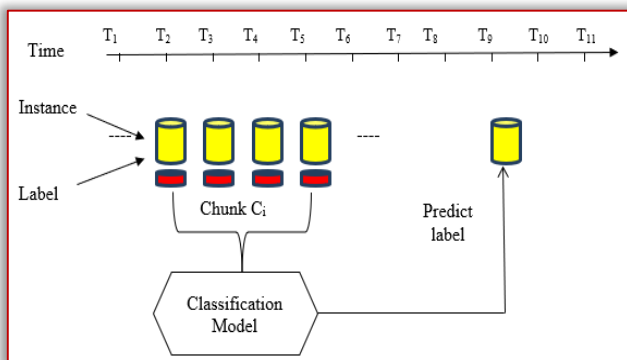


Figure 1: Classification of Data Stream

Suppose $C_1; C_2; C_3; \dots; C_i$ are labeled. At the time stamp T_9 , when an unlabeled chunk C_{m+1} will arrive,

the classification model will provide the class labels of instances available in C_{m+1} on the basis of training data. If the prediction given by classification model for chunk C_{m+1} is correct, the C_{m+1} chunk can join the training set, resulting in more and more availability of training data.

A storage constraint makes it important to carefully select instances which can represent the current distribution. Most studies on data stream mining assume relatively balanced and stable distribution of data in streams. However, most of real time applications involve concept-drifting data streams with unbalanced distributions [2], because of these issues the classification of data stream is a prominent area of research.

Concept Drift

In the data stream, the source which generates examples at training time need not be the same source which generates examples at testing time and this change of source of data is called as concept drift. Thus, data from the previous source may be useless or irrelevant for the current context.

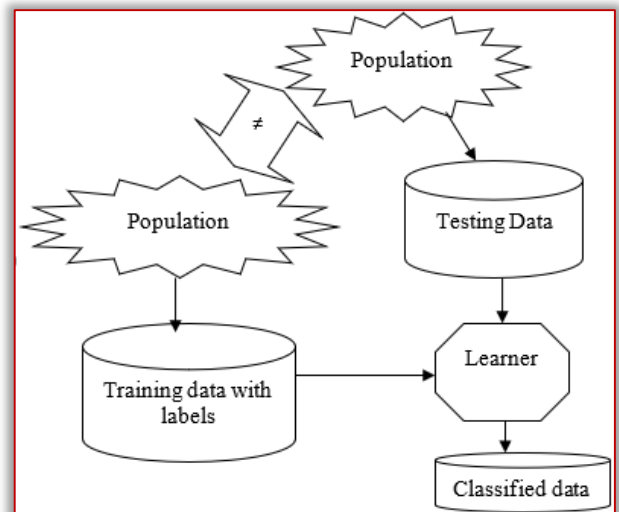


Figure 2: Learning on Non stationary Data Stream

Figure 2 depict the supervise learning on non-stationary data stream where the population data generated at training time is not equivalent to population data at testing time and represented by following equation (1).

$$P_{tr}(Y|X) \neq P_{tst}(Y|X) \text{ and } P_{tr}(X) = P_{tst}(X) \quad (1)$$

The change in source can be categorized in following ways:

SUDDEN CONCEPT CHANGE

In nonstationary data stream, data may be generated from different source, sudden concept change occurs at a point in time when data source changes from one concept to another concept. In figure 3 from timestamp T_2 to T_4 some instances are coming from source S_1 and represented as concept 1 and from timestamp T_5 to T_8 some instances are coming from source S_2 and represented as concept 2. At timestamp T_5 the concepts suddenly change from concepts 1 to concept 2 which is called as concept drift as concept 1 instances are generated by source1 and concept 2 are generated by source 2 and hence their data distribution is different as shown by Mean axis. In order to represent different concepts different colors are used and change of color shows drift occurred.

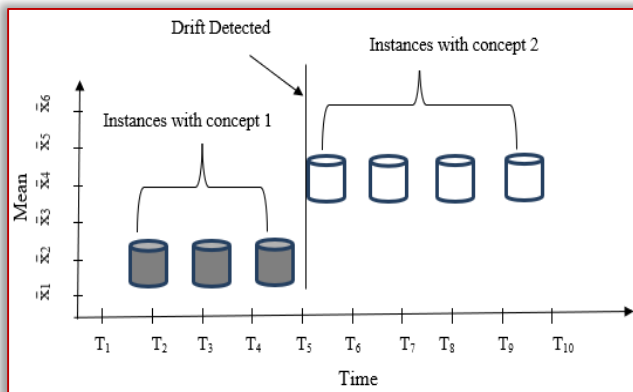


Figure 3: Sudden Concept Change

INCREMENTAL CONCEPT CHANGE

An incremental concept occurs when there are multiple concepts in data stream which are generated from multiple sources and the difference among the multiple sources is very small. In figure 4 concepts are changing as follows:

- Time stamp T_4 : concepts change from concepts 1 to concept 2
- Time stamp T_5 : concepts change from concepts 2 to concept 3
- Time stamp T_7 : concepts change from concepts 3 to concept 4

All these concepts are generated from different sources and hence their data distribution is different as shown by Mean axis.

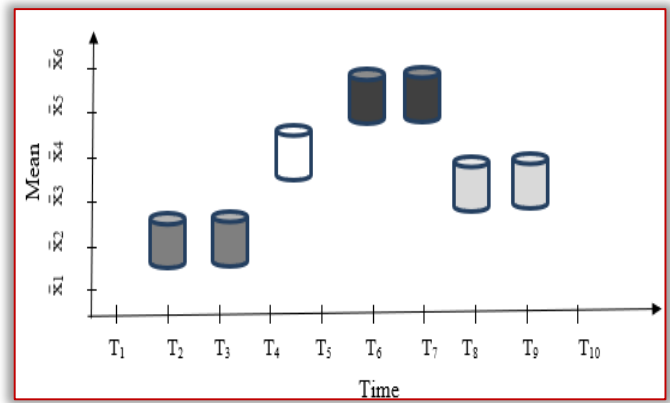


Figure 4: Incremental Concept Change

GRADUAL CONCEPT CHANGE

When two or more data sources generate data after some time stamp, it is called gradual drift. In figure 5 concepts are changing as follows:

- Time stamp T_4 : concepts change from concepts 1 to concept 2
- Time stamp T_5 : concepts change from concepts 2 to concept 1
- Time stamp T_7 : concepts change from concepts 1 to concept 2

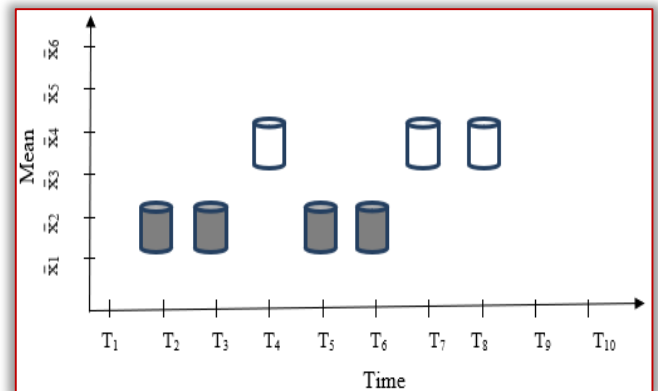


Figure 5: Gradual Concept Change

REOCCURRING CONCEPT CHANGE

Reoccurring concepts occurs when same data is generated over a period of time using different data sources (similar to incremental and gradual drift). It is different from incremental and gradual drift as same sources are used to generate data in near future. In figure 6 concepts are changing as follows:

- Time stamp T_3 : concepts change from concepts 1 to concept 2
- Time stamp T_5 : concepts change from concepts 2 to concept 1
- Time stamp T_7 : concepts change from concepts 1 to concept 2
- Time stamp T_9 : concepts change from concepts 2 to concept 1

This shows a pattern or repeated behavior as concept pattern is reoccurring after some time.

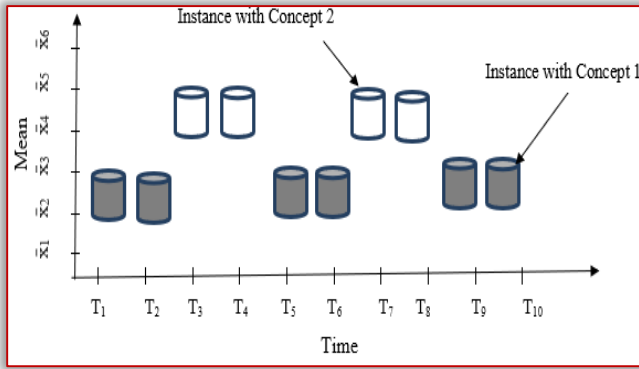


Figure 6: Reoccurring Concept Change

DRIFT DETECTION METHODS

Drift Detection Method (DDM) was introduced by Gama et al. [3] which based on Binomial Distribution. In addition to classification error rate, author defines two levels i.e. the warning level and the alarm level. In time series data, if at i_w the error reaches at the warning level and at i_d it represents the alarm level then it is considered the drift has occurred and drift detector starts the training process with data from i_w . DDM gives better results on data streams which possess sudden drift change because gradually drifts can escape from detector without activating the alarm level.

DDM is further modified as EDDM which was proposed by Baena-Garcia et al. [4] works on distance error rate rather than classification error rate and make use of warning and alarm level thresholds. Once an alarm level is reached, there is need to construct a new model on data from warning level. It make use of a threshold value 30 to search for a concept drift.

ADWIN is ADaptive WINDOWing algorithm proposed by Bifet et al [5] which make use of variable size sliding windows. It uses averaging of elements in the window to detect the drift. The size of window can grow or shrink as and when no drift or change is detected.

HDDM is Hoeffding Drift Detection Methods proposed by by Frias-Blanco et al. [6] where author conducted two tests named as HDDMA-test and HDDMW-test. HDDMA-test compares the moving averages to find the drift and EMWA forgetting scheme [7] is used to weight the moving averages. HDDMA-test and HDDMW-test make use of Hoeffding's inequality [8] to set an upper limit to the level of difference between averages. The weighted moving averages are compared to detect the drift in stream. Results show that HDDM is better to detect abrupt and gradual drifts.

CUSumDM [9] represents Cumulative Sum Detection method which was introduced in Biometrika in year 1954, E.S. Page. It is used for change detection using sequential analysis technique.

Recent drift detection method [10] make use of dynamic dynamic classifier selection in order to detect

drift while [12] consider variety of measure for drift detection in data stream.

EXPERIMENTS AND RESULTS

This paper provides overview of concept drift in data stream by using various drift detection mechanisms. Drift is introduced in synthetic dataset using gradual and sudden generators available in MOA framework. Using synthetic datasets one can analyse how different methods deal with the different types of drift as beginning and end position of drift known in advance.

Total 400000 instances are created and drift is introduced in data stream using SEA generator and hyperplane generator. Experimental results of table 1, table 2 and table 3 are carried out on the abrupt, gradual and incremental drifted data stream respectively using 6 drift detection mechanisms as mention in section 2. Naïve Bayes classifier is used for the learning purpose.

Table 1: Results of Drift detection mechanism on Sudden Drift

Drift detection Method	Accuracy (%)	#drifts detected
DDM	80.67	1
EDDM	80.67	2
CUSumDM	81.06	5
HDDM_A	82.65	2
HDDM_W	84.52	20
ADwin	84.84	10

Table 2: Results of Drift detection mechanism on Gradual Drift

Drift detection Method	Accuracy (%)	#drifts detected
DDM	80.69	1
EDDM	80.68	2
CUSumDM	81.07	3
HDDM_A	81.68	3
HDDM_W	83.72	19
ADwin	83.63	49

Table 3: Results of Drift detection mechanism on Incremental drift

Drift detection Method	Accuracy (%)	#drifts detected
DDM	79.36	1
EDDM	79.36	2
CUSumDM	79.36	1
HDDM_A	79.51	1
HDDM_W	82.11	34
ADwin	82.45	13

Experiment results conclude with following observations that HDDM_W and ADwin detects more drift in data stream with high accuracy whereas DDM, EDDM, CUSumDM and HDDM_A provide approximate similar results. The accuracy can be further enhanced by using ensemble [10][11].

CONCLUSION

The problem of concept drift with its need and type is elaborated in this paper. The several concept drift detection methods like DDM, EDDM, ADWIN, HDDM and CUSumDM and ECDD are discussed with their experimental results.

Results shows that Naïve based classifier provide better accuracy in case of concept change. The accuracy can be further enhanced by using multiple classifiers and results can be shown on different applications.

References

- [1] Thalor, M.A.; Patil, S.T.: Incremental learning on non-stationary data stream using ensemble approach, *International Journal of Electrical and Computer Engineering*, 6(4), 1811–1817 (2016).
- [2] Thalor, M.A.; Patil, S.T.: Learning framework for non-stationary and imbalanced data stream, *International Journal of Engineering and Technology*, 8(5), 1942–1945 (2016).
- [3] Gama, J.; Medas, P.; Castillo, G. and Rodrigues, P.: Learning with Drift Detection, *Lecture Notes in Computer Science*, 3171, 286-295 (2004).
- [4] Baena-Garcia, M.; Campo-Avila, J.; Fidalgo, R.; Bifet, A.; Gavaldua R. and Morales-Bueno R: Early Drift Detection Method, *IWKDD*, 77–86 (2006).
- [5] Bifet, A.: Adaptive Learning and Mining for Data Streams and Frequent Patterns, *Doctoral Thesis*. (2009).
- [6] Frias-Blanco, I.; del Campo-Avila, J.; Ramos-Jimenez, G.; Morales-Bueno, R.; Ortiz-Diaz, A.; Caballero-Mota, Y.: Online and Non-parametric Drift Detection Methods based on Hoeffding's Bounds. *IEEE Transactions on Knowledge and Data Engineering* 27(3), pp. 810–823 (2015)
- [7] Ross, G. J., Adams, N. M., Tasoulis, D. K., Hand, D. J.: Exponentially Weighted Moving Average Charts for Detecting Concept Drift. *Pattern Recognition Letters*, 33(2), pp. 191–198 (2012)
- [8] Hoeffding, W.: Probability Inequalities for Sums of Bounded Random Variables. *American Statistical Association* 58 (301), pp. 13–30 (1963)
- [9] Granjon, P.: The CuSum algorithm-a small review (2013).
- [10] Pinage, F.A., Santos, E.M., & Gama, J.: A drift detection method based on dynamic classifier selection. *Data Mining and Knowledge Discovery*, 34, 50-74 (2019).
- [11] Mahdi, O.A., Pardede, E., Ali, N., & Cao, J.: Diversity measure as a new drift detection method in data streaming. *Knowl. Based Syst.*, 191, 105227(2020).
- [12] Thalor, M.A.; Patil, S.T.: Review of ensemble-based classification algorithms for nonstationary and imbalanced data. *IOSR Journal of Computer Engineering*, 16(1), 103–107(2014).
- [13] Thalor, M.A.; Patil, S.T.: Learning on high frequency stock market data using misclassified instances in ensemble. *International Journal of Advanced Computer Science and Applications*, 7(5):283–288 (2016).



ACTA TECHNICA CORVINIENSIS – Bulletin of Engineering
ISSN: 2067-3809
copyright © University POLITEHNICA Timisoara,
Faculty of Engineering Hunedoara,
5, Revolutiei, 331128, Hunedoara, ROMANIA
<http://acta.fih.upt.ro>

¹Nikola PETROVIĆ, ²Bojan KRSTIĆ, ³Jelena PETROVIĆ

EVALUATION OF FREIGHT TRANSPORT MODES BASED ON EXTERNAL COSTS

¹University of Niš, Faculty of Mechanical Engineering, Aleksandra Medvedeva 14, Niš, SERBIA

²University of Niš, Faculty of Economics, 11 Kralja Aleksandra Ujedinitelja street, Niš, SERBIA

³University of Niš, Faculty of Sciences and Mathematics, Višegradska 33, Niš, SERBIA

Abstract: External costs represent the costs which are incurred by activities of company or person whereby they are borne by someone not involved in those activities. The purpose of this paper is a comparative analysis of negative external costs arising from the realization of freight road, rail and inland waterway transport. The main goal of this paper is to quantify the external costs caused by different modes of freight transport, based on the characteristics of the transport means and the characteristics of the goods being transported, as well as the length of the goods transport. The implemented methodology is a unique tool by which it is possible to redirect users towards transport modes that are more acceptable from the aspect of sustainability.

Keywords: modes of transport, external costs, internalization

INTRODUCTION

Transport plays an important role in economic and social development of every country as well as in the development of global market [1]. But, every mode of transport has positive and negative effects on society. Transport results in negative external effects such as emissions, noise, congestion and infrastructural wear and tear [2].

In the EU, external costs of transport (road, rail and IWW (inland waterway)) are recorded in the amount of EUR 571 billion without congestion and EUR 841 billion, including congestion. The results of research in EU indicate on the main factors of external costs: accidents (29% of external effects), congestion (27%), air pollution (14%), climate (14%), noise (7%), well-to-tank (5%) and habitat damage (4%) [3].

In contrast to the positive effects, negative effects, i.e. costs of the negative effects of transport do not bear directly those who caused them but they are falling at the expense of the Society. The Society submits external costs in order to increase public health capacity in order to protect endangered plant and animal species and to rehabilitate the social environment. As a consequence of this, there are making wrong decisions in the transport market, as well as inefficient use of available resources and loss of well-being. In order to prevent this is done internalisation of external costs.

The internalisation of external costs through market-based instruments is generally regarded as an effective way to limit the negative effects of transport. The principle of internalisation of external costs involves adding external costs to the individual cost of pollutants. The internalisation of external costs affecting the price increase of the product pollutants and the reduction in demand for their products. Pollution prevention is more profitable than pollution control, and waste minimization, recycling and reuse

are more profitable than disposal and control of waste.

In order to make internalisation of external costs, it is necessary to estimate external costs in the transport sector. Starting from 2004, several research projects and models have been implemented in Europe to define and evaluate external costs in the transport sector [4]. Among the most important are: HEATCO (Developing Harmonised European Approaches for Transport Costing and Project Assessment, 6th Framework Programme), CAFE CBA (Clean Air for Europe Programme, Cost Benefit Analysis of Air Quality), TREMOVE policy assessment model, ASSET (ASsessing SENSitiveness to Transport) GRACE (Generalisation of Research on Accounts and Cost Estimation, 6th Framework Programme).

Some results of these projects are summarized in the IMPACT project in 2008 from which it emerged Handbook on estimation of external costs in the transport sector [5]. Updating the latest date related to external costs is provided in the Update of the Handbook on External Costs of Transport [6]. On the basis of manuals it is possible to calculate unit costs of pollutants in the form of €/tonne which take into account the negative consequences of traffic functioning such as: harmful impact on human health (mortality, morbidity), the impact of emissions of harmful substances on facilities and materials, negative impact on the biosphere, a detrimental effect on biodiversity and ecosystems, impact on the generation of greenhouse gases.

Updated study External transport costs in the EU shows that average external transport costs for road are much higher than for rail. Per passenger kilometer costs of cars are about four times higher than in rail transport. The situation is similar to freight transport. Since the dominant cost categories are accidents and emissions (climate change and air pollution), special

attention will be given to them in the paper. The purpose of this paper is the quantification and analysis of the external costs of freight transport. The aim of the paper is to conduct a comparative analysis of external costs of road, rail and IWW freight transport, from air pollution, accidents and climate change.

METHODOLOGY – QUANTIFICATION OF EXTERNAL EFFECTS

— Air pollution

Air pollution caused by traffic activities leads to different types of external costs. The most important external costs are health costs due to cardiovascular and respiratory diseases caused by air pollutants. The most important air pollutants related to traffic are particles (PM₁₀, PM_{2.5}), Nitrogen Oxides (NO_x), Sulfur Dioxide (SO₂), Volatile organic compounds (VOC) and Ozone (O₃) as indirect pollutants.

For road transport, the most important impact on costs are emission standards for vehicles which again, partly depend on the age of the vehicle. The emissions of road vehicles, then, depend on vehicle speed, fuel type and fuel combustion technology and exhaust gas treatment technologies, load factors, vehicle size, type of drive and geographical location of the road. The quantification of external cost of pollutant emissions in road transport when transporting goods can be carried out depending on a particular category of vehicle and its emission class, i.e. euro standards. The costs of air pollution depend on the area through which a particular vehicle carries out the transport of goods. Costs are expressed in €c per vehicle–kilometer. The highest cost of air pollution are recorded for passing through city zone while the lowest cost of air pollution are recorded on highway [6].

The key cost impacts for rail transport are: vehicle speed, load factors, a combination of power generation plants and the geographical location of plant installations. Calculating air pollution costs involve the use of linear functions and calculations that are included in the top–down model, also linear functions, marginal costs of air pollution are approximately equal to the average cost of air pollution. External costs of air pollution from road, rail and IWW transport can be calculated on the basis of the form:

$$C_m = \sum_{c,i} (V_{k_{m,c,i}} \cdot MC_{m,c,i}) \quad (1)$$

where:

C = Air pollution costs per trip (€/trip),
V_k = Vehicle kilometres (vkm/trip),
MC = External marginal air pollution costs,
i = Type of infrastructure (urban road, interurban road, motorway),
c = Country,
m = Mode.

— Accidents

Accident externalities represents the most important external costs of road transport [7]. These social costs include the costs of material damage, administrative costs, treatment costs, production losses and non–material costs (shortening life expectancy, suffering, pain, sadness, etc.) [8].

The most important impacts on costs in road transport, in addition to mileage, vehicle speed, road type, the characteristics of the driver (such as driver behavior, experience, speed), the volume and speed of traffic, time of day (day / night) and interact with weather conditions, the level of infrastructure maintenance, the degree of utilization of the capacity of the infrastructure, and the level of segregation of road traffic lanes.

The following form can be used to calculate the cost of traffic accidents in road transport [9]:

$$C_m = \sum_{c,i} (V_{k_{m,c,i}} \cdot MC_{m,c,i}) \quad (2)$$

where:

C = Accident costs per trip (€/trip),
V_k = Vehicle kilometres (vkm/trip),
MC = External marginal accident costs,
i = Type of infrastructure (urban road, interurban road, motorway),
c = Country,
m = Mode.

According to German statistics, the share of fatal HGV (Heavy goods vehicle) accidents on highways is 50% of all fatal HGV accidents, which is very high compared to other countries. Combined with traffic flow data, this gives a marginal value in the case of an accident for highways that are higher than for other types of roads. In the original data in Switzerland, the share of motorway accidents was only 20% [6].

The main impacts on rail transport costs are traffic volumes, weather conditions, maintenance levels and level of segregation between systems, especially between road and rail transport and between different types of trains. To calculate the cost of accidents in railway transport can use the form [9]:

$$C_m = \sum_{c,i} (V_{k_{m,c}} \cdot MC_{m,c}) \quad (3)$$

where:

C = Accident costs per trip (€/trip),
V_k = Vehicle kilometres (vkm/trip),
MC = External marginal accident costs,
c = Country,
m = Mode.

In the rail and IWW transport sectors of the EU, accidents are much less common than in road transport. Therefore, the cost estimation of accidents must be based on the average number of accidents in the past few years. The latest estimates of this type have been carried out [8] and according to them, the

average cost of accidents of freight rail transport is 0.2 € per 1000 vkm. All incident costs can be considered as external, because the marginal costs are equal to average costs [6].

For inland waterways and maritime transport, information about accident costs is completely lacking. However, the number of casualties in water transport is considered insignificant [8].

— Climate change

The main effects of the greenhouse gases in relation to transport are Carbon dioxide (CO₂), Methane (CH₄) and Nitrogen oxide (N₂O). These emissions contribute to global warming by acting with different effects such as sea level rise, impact on agriculture (due to changes in temperature and precipitation), health effects (increased heat stress, expansion areas vulnerable to parasites and increase disease devolution e.g., malaria, etc., ecosystems and biodiversity, increasing extreme weather effects, etc. The general approach to estimating average costs caused by climate change for different transport modes consists of four steps [8]:

- ≡ Estimation of total GHG emissions per vehicle type by country,
- ≡ Calculate the total CO₂ equivalent of GHG emissions using the Global Warming Potentials.
- ≡ Multiplication of total tons of CO₂ equivalent of GHG emissions with an external cost factor expressed in €/tonne to estimate the total external costs associated with global warming per country. Due to the global impact on the damage caused by global warming, the same cost factor can be applied in all countries.
- ≡ Calculate the average climate change costs (per tkm/pkm) by dividing the total costs per vehicle type per country by the number of tkm/pkm per country.

As for the external costs of air pollution as well as for the external costs of climate change, marginal costs are equal to average costs. Marginal costs of climate change for different types of vehicles and transport modes can be calculated by multiplying the emission factors.

RESULT OF RESEACH – EXEMPLARY TRANSPORT LINK BUDAPEST – FRANKFURT AM MAIN

This paper presents the calculation of external costs (air pollution, accidents and climate change) caused by different modes of transport (road, rail, IWW) between the ports of HUBUD Budapest and DEFRA Frankfurt am Main. The assumed cargo that is being transported is 20 TEU (Twenty-foot equivalent unit) containers. Transport is considered for the following vehicle categories:

- ≡ Truck (Rigid HGV), Gross vehicle weight 24–40t, Emission class Euro V,
- ≡ Short train, Train weight 500t, electrified and diesel,

≡ Euro ship container 0–1500t.

The distances for each mode of transport through a particular country are given in Table 1.

Table 1. The length of the routes of different transport modes through a particular country

	Road	Rail	IWW
Hungary	177,91	182,08 (electrified) 5,27 (diesel)	–
Austria	328,52	360,67 (electrified)	–
Germany	453,87	450,61 (electrified)	–
Total (km)	960,30	998,63	1268,80

Based on the above procedures, the adopted characteristics of the transport vehicles and using the updated data from [6] and [8], the following results were obtained (table 2).

Table 2. External costs of air pollution, accidents and climate change in €

	Air pollution	Accidents	Climate change	External costs
Road	1351	2302	593	4246
Rail	79	132	167	378
IWW	267	0	330	597

From the standpoint of external costs, it can be concluded that the railway mode of transport is the best for the transport of 20TEU containers between Budapest and Frankfurt am Main, because it causing the least air pollution, accidents and climate change. If the containers were transported by road, rail and IWW, the external costs would amount to EUR 4246, 378 and 597 respectively.

Based on the comparing transport modes, external freight costs for road transport are about 11 times higher than rail transport and about 7 times higher than IWW transport.

CONCLUSIONS

The transport system allows the functioning of the world economy at all levels, but it also causes a series of direct and indirect effects, which from the standpoint of human society can be judged also and negatively. The consideration and quantification of these effects were the first step of the economists to model alternative development scenarios and their costs, to be later transferred to their internalization in the short and medium-term policy. During previous research conducted is understood that the cost of transport includes not only what the state or users pay for transport services, but they include a much wider set of cost.

According to statistics, the dominant categories of external costs are costs incurred by traffic accidents, climate change costs and air pollution costs.

A comparative analysis of the representative negative external costs which arise from the realization of freight road, rail and IWW transport should influence on redirecting of users or decision makers to an

acceptable mode of transport. An example of transporting 20 TEU containers and quantifying the use of three transport modes shows that external costs are the highest use of trucks while at least external costs are caused by the rail.

When choosing a particular mode of transport for the transport of goods is necessary to consider, as far as possible, all costs and not only the cost of transport services.

Note:

This paper is based on the paper presented at DEMI 2019 – The 14th International Conference on Accomplishments in Mechanical and Industrial Engineering, organized by Faculty of Mechanical Engineering, University of Banja Luka, BOSNIA & HERZEGOVINA, co-organized by Faculty of Mechanical Engineering, University of Niš, SERBIA, Faculty of Mechanical Engineering Podgorica, University of Montenegro, MONTENEGRO and Faculty of Engineering Hunedoara, University Politehnica Timisoara, ROMANIA, in Banja Luka, BOSNIA & HERZEGOVINA, 24–25 May 2019.

References

- [1] Petro, F., Konečný, V. (2017). Calculation of emissions from transport services and their use for the internalisation of external costs in road transport, *Procedia Engineering*, vol. 192, p. 677–682.
- [2] Ljungberg, A. (2016). Marginal cost-pricing in the Swedish transport sector – An efficient and sustainable way of funding local and regional public transport in the future? *Research in Transport Economics*, vol. 59, p. 159–166.
- [3] Essen, H., Infrastructure Charging and Internalisation of Transport Externalities. <https://ec.europa.eu/transport>, accessed on 2019–04–11.
- [4] Ivković, I. (2012). Research of performances of the Compressed Natural Gas powered bus in terms of safety and environmental influence, Doctoral Dissertation, University of Belgrade, Faculty of Transport and Traffic Engineering.
- [5] Maibach, M., Schreyer, C., Sutter, D., Essen, H.P., Boon, B.H., Smokers, R., Schroten, A., Doll, C., Pawlowska, B., Bak, M. (2008). Handbook on estimation of external costs in the transport sector – Produced within the study Internalisation Measures and Policies for All external Cost of Transport (IMPACT), CE Delft.
- [6] Korzhenevych, A., Dehnen, N., Bröcker, J., Holtkamp, M., Meier, H., Gibson, G., Varma, A., Cox, V. (2014). Update of the Handbook on External Costs of Transport, European Commission – DG Mobility and Transport, Ricardo –AEA, Issue 1.
- [7] Dementyeva, M., Koster, P.R., Verhoef, E. T. (2015). Regulation of road accident externalities when insurance companies have market power, *Journal of Urban Economics*, vol. 86, p. 1–8.

- [8] Essen, H., Schroten, A., Otten, M., Sutter, D., Schreyer, C., Zandonella, C., Maibach, M., Doll, C. (2011). External Costs of Transport in Europe – Update Study for 2008, CE Delft, Delft.
- [9] Schroten, A., Essen, H., Anthes, R. (2011). External Cost Calculator, Methodology report, CE Delft, Delft.



ACTA TECHNICA CORVINIENSIS – Bulletin of Engineering
ISSN: 2067–3809
copyright © University POLITEHNICA Timisoara,
Faculty of Engineering Hunedoara,
5, Revolutiei, 331128, Hunedoara, ROMANIA
<http://acta.fih.upt.ro>

¹Stefan ĐURIĆ, ²Bogdan NEDIĆ, ³Slobodan MALBAŠIĆ, ⁴Jelena BARALIĆ

APPLICATION OF NEW TECHNOLOGIES FOR DEMILITARIZATION ORDNANCE IN ORDER TO PROTECT ENVIRONMENT

^{1,2}Faculty of Engineering University of Kragujevac, Sestre Janjić 6, 34000 Kragujevac, SERBIA

³Ministry of Defence Republic of Serbia, Bircaninova 5, 11 000 Belgrade, SERBIA

⁴Faculty of Technical Science University of Kragujevac, Svetog Save 65, 32000 Čačak, SERBIA

Abstract: Demilitarization of the explosive ordnance using the conventional methods, which are most common, results in significant environmental pollution. In the demilitarization process and destroying explosive ordnance, toxic particles of heavy metals and chemical compounds of explosive substances from ordnance that are being processed, are being released in the environment. Current research shows that conventional methods pollute up to ten times more than modern methods of destruction. The paper discusses the application of unconventional processing methods in order to develop new technologies for the explosive ordnance disposal (EOD) in order to improve the environmental aspects of this process. Experimental tests have shown the positive results of abrasive water jet application in the process of cutting the projectile shell, which, in addition to reducing the harmful effects on the environment, raises the level of safety and productivity of the entire process of work.

Keywords: demilitarization, contamination, environment, unconventional methods, abrasive water jet

INTRODUCTION

Demilitarization of explosive ordnance (EO) is a complex process that includes a series of operations that are divided into several phases. The EO can be delaborated or destroyed for a number of reasons, the most frequent ones being the decommissioning of outdated items, then the EO damaged during transportation, natural disasters, poor storage conditions, etc. Special emphasis is placed on ordnance articles that are destroyed that have previously suffered severe damage due to incidents or accidents (unexploded ordnance). These resources in the given situations are most often destroyed on the spot as they are caught [1].

The ordnance demilitarization process represents the process of translating ordnance into the state in which asset can no longer perform its basic function for which it is intended [2]. During the life cycle of ordnance, complex physical–chemical reactions occur within the device, which increases the risk of unintentional initiation and the occurrence of damage [2, 3]. The demilitarization process is an integral part of the ordnance lifecycle, which aims to include this requirement as a basic requirement at an early stage of development [4].

The STANAG 4518 standard defines that during its development, ordnance is to envisage its delaboration process [5]. Although this standard provides guidance, they do not, however, include everything necessary for the demilitarization process. Considering the demilitarization process in the development phase, ordnance should provide [6]:

- easy disassembly of subassemblies and elements of ordnance,
- easy access and removal of EM,

— processed materials and components can be reused,

— minimizing the use of specialized tools,

— process automation and reduced human resources.

After the events of the 1990s, especially after the NATO bombing in 1999, a large number of ordnance remained to be destroyed on the territory of the Republic of Serbia. These EO are very expensive, dangerous and, on the other hand, useless to store, which necessitates their demilitarization. In addition to solving its own problems with the large number of ordnance, there is room and ability to solve the problem of explosive ordnance on a global level. With the application of new technologies, harmonized with European regulations and legal regulations, it is possible to position itself in the market as a leader in the process of EOD.

The paper presents new technologies in the field of nonconventional processing methods, with a special focus on the application of the material cutting method using the abrasive water jet.

ECOLOGICAL ASPECTS OF ORDNANCE DEMILITARIZATION BY THE APPLICATION OF CLASSICAL METHODS

The classic demilitarization procedures of EO in practice are still the most common, regardless of the large number of limiting factors regarding legal regulations. The focus is on the safety of people and the work environment, which is addressed by applying various preventive methods of protection. Note, that danger lasts directly during the preparation of the process, during the duration of the process, and a certain time interval after the demilitarization process. Second, but considerably more harmful, bearing in mind the lasting consequences are the

environmental aspects of the demilitarization process [2, 6]. The classic methods of the EO demilitarization are divided:

1. open detonation,
2. open burning,
3. detonation in the detonation chamber,
4. contained burn,
5. permanent disposal of EO.

The way of selecting the method to be applied to the demilitarization process depends on several EO parameters:

- physical condition of EO,
- amount of EO,
- legislation and norms,
- available capacities and resources,
- technological options and capacities.

Classical methods such as open detonation and open burning are applied in cases where there is no available technology for the ordnance operation in some other way (Figure 1). These methods are completely unacceptable because they pollute the environment and leave lasting consequences. The environment is contaminated, heavy metals are released, which flow through the soil into submersible water systems or are released into an atmosphere where they can no longer be controlled [2, 7].



Figure 1 Contamination of the environment during the processing EO

Chemical elements such as Pb, Sb, Ba and toxic gases found in combustion products such as hydrochloric, carbon monoxide, nitrogen monoxide, nitrogen dioxide and hydrogen cyanide are easily get in and retain in soil and underground waters [2]. Table 1 shows the emission of toxic gases through the

equivalent NO₂ that pollute the air in the demilitarization process.

Table 1. Emission of the particles that pollute air expressed through NO₂ equivalent

Demilitarization method	Process emissions (gram NEQ per kg MEM)
Open burning	285
Open detonation	141
Closed detonation	14
Rotary clin	25

Based on the data presented in Table 1, none of the listed methods meets the requirements of the European Environmental Standards [8].

The paper [2] provides an overview and analysis of the impact of ordnance hazardous ingredients on the environment and on human health. The development of new demilitarization technologies is an absolute priority in terms of research, in order to improve the process, from the aspect of protection, safety and productivity, and enable further demilitarization of the remaining and newly produced ordnance [7].

APPLICATION OF NEW TECHNOLOGIES IN THE DEPARTMENT OF DEMILITARIZATION ORDNANCE

In the process of implementing new technologies, priority is to decrease the level of pollution and release of toxic substances into the environment during the EO demilitarization process. Methods on which a large number of research and experimental investigations are carried out are [6, 9]:

- projectile delaboration using Abrasive Water JET (AWJ) technology,
- projectile delaboration using Water Jet Washout (WJW) technology.

The use of AWJ technology is used in cases of complete EO processing. The technology is based on the cutting of the missile shell transversely in relation to the axis of rotation of the projectile (Figure 2a). In the process of delaboration, there is a permanent disturbance of the geometry of the projectile shell and waste in the form of steel is used in the recycling process as a secondary raw material [7].



Figure 2. Delaboration of projectile by applying AWJ technology

In order to reduce the risk, the process can be entirely underwater. Although there is no thermal change in

the structure of the material in the cutting process, the friction of the particles of the explosives can lead to the self-initiation process, which is why it is desirable to process the cutting process in water (Figure 2b). In this way, the level of risk and the possibility of self-initiation process are reduced.

After cutting the shell, the next phase involves the removal of explosive filling from the casing, which can be further recycled and reused in the process of the laboratory. AWJ technology also enables the operation of large-scale caliber missiles (Figure 3a), as well as the deployment of rocket engines (Figure 3b), which is not possible with conventional methods.

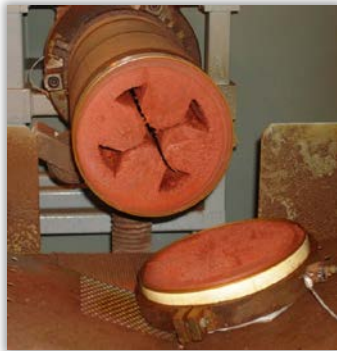


Figure 3. Delaboration of rocket engines and high caliber projectile by applying AWJ technology

Delaboration of projectile using WJW technology is based on the principle of high-pressure explosive loading (Figure 4). Unlike AWJ technology, in the WJW process there is no physical destruction of the missile shell. In this way, it is possible to re-use the missile shell.

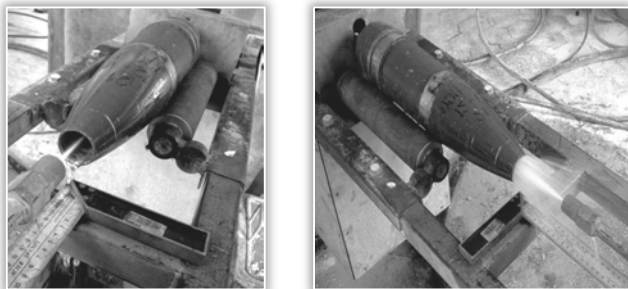


Figure 4. Delaboration of projectile by applying WJW technology

The water used in the delaboration process (AWJ, WJW) during the process is contaminated, but is

filtered in the re-process. At the end of the elaboration process, the water is permanently disposed of and treated as wastewater [6].

Laboratory for Cutting metal and tribology at the Faculty of Engineering Sciences in Kragujevac, in cooperation with The Technical Overhaul Institute Kragujevac and The Technical Overhaul Institute Cacak, carried out experimental tests of the process of cutting the projectiles of the caliber 100 and 105 mm.



Figure 5 Display of the 100 mm caliber projectiles when cutting using AWJ

The process of cutting the projectile shell proceeded continuously, with the sample fixed to the work table, while the nozzle was translaterally moving without changing the height of the nozzle in relation to the work table (Figure 5). In the paper [7] results are shown, the cutting parameters and the entire process are analyzed, which determines the possibility of using AWJ technology in the EOD.

CONCLUSION

The paper presents new technologies in the field of nonconventional metal treatment processes. The implementation and application of these technologies in the EO process of delaboration should lead to a significant improvement in the environmental aspects of the EO demilitarization process and partially or completely replace the classical procedures. Classical practices are, from the ecological point of view, completely unacceptable, and in addition they are economically unsuitable, as are high-risk processes. Using AWJ and WJW technology, a significantly larger selection is provided and it extends the ability to delaborate EO of different types and calibers. In this way, beside environmental aspects, efficiency in terms of recycling and reengineering of materials is achieved. Materials and procedures for projectile casing or explosive mixtures and their laboratory technology are one of the most technologically demanding processes. With the application of new technology of delaboration, with overhaul and recycling, the lifetime of expensive elements that are an integral part of the EO system is prolonged and enables them to be reused.

Acknowledgement

This publication was also supported by the Ministry of Education, Science and Technological Development of Serbia, project TR35034 "The research of modern non-

conventional technologies application in manufacturing companies with the aim of increasing efficiency of use, product quality, reduce of costs and save energy and materials".

Note:

This paper is based on the paper presented at DEMI 2019 – The 14th International Conference on Accomplishments in Mechanical and Industrial Engineering, organized by Faculty of Mechanical Engineering, University of Banja Luka, BOSNIA & HERZEGOVINA, co-organized by Faculty of Mechanical Engineering, University of Niš, SERBIA, Faculty of Mechanical Engineering Podgorica, University of Montenegro, MONTENEGRO and Faculty of Engineering Hunedoara, University Politehnica Timisoara, ROMANIA, in Banja Luka, BOSNIA & HERZEGOVINA, 24–25 May 2019.

REFERENCES

- [1] Bogdanov, J. (2015) Poznavanje ubojnih sredstava, 1st. edition. Medija centar „Odbrana“.
- [2] Jeremić, R. (2012) Ekološki aspekti procesa demilitarizacije i uništavanja ubojnih sredstava. Vojnotehnički glasnik, vol. 60, no. 1, pp. 284–298.
- [3] Alverbro, A., Björklund, A., Finnveden, G., Hochschorner, E., Hägvall, J (2009) A life cycle assessment of destruction of ammunition, Journal of Hazardous Materials, vol. 170, no. 2–3, pp. 1101–1109.
- [4] Mescavage, G (2009). Demilitarization as a systems engineering requirement. 44th Annual Gun & Missile Systems Conference & Exhibition, 6–9 April 2009, Kansas City, USA.
- [5] NATO Standardization agency (NSA), NATO Standardization agreement: Safe disposal of munitions, design principles and requirements, and safety assessment, STANAG 4518, 2001.
- [6] Poulin, I. (2010) Literature review on demilitarization of munitions, Document prepared for the RIGHTTAC Technology Demonstration Project, Defence Research and Development Canada.
- [7] Đurić, S., Nedić, B., Baralić, J., Bogdanov, J., Miljković, A. (2018) Researching the possibility of applying abrasive waterjet in projectile disassembly process, 8th International Scientific Conference on Defensive Technologies OTEH 2018 Conference Proceedings, pp. 200–204.
- [8] Duijm, N.J., Markert, F (2002) Assessment of technologies for disposing explosive waste, Journal of Hazardous Materials, vol. 90, no. 1, pp. 137–153.
- [9] Wilkinson, J., Watt, D. (2006) Review of demilitarization and disposal techniques for munitions and related materials, Document prepared for the MSIAC member nations, Munitions Safety Information Analysis Center.



ACTA TECHNICA CORVINIENSIS – Bulletin of Engineering
ISSN: 2067–3809
copyright © University POLITEHNICA Timisoara,
Faculty of Engineering Hunedoara,
5, Revolutiei, 331128, Hunedoara, ROMANIA
<http://acta.fih.upt.ro>

¹Babatope Abimbola OLUFEMI, ²Rachael Aniedi ESSIEN

PRODUCTION OF BIOLUBRICANTS FROM NEEM SEED OIL CATALYZED BY CALCIUM OXIDE FROM SNAIL SHELL

¹Department of Chemical and Petroleum Engineering, University of Lagos, Akoka, Lagos, NIGERIA

Abstract: Biolubricants was produced from neem seed oil with methanol by transesterification using calcium oxide as catalyst. Snail shells were utilized as a source of calcium oxide (CaO) in catalyzing the transesterification reaction to produce the methyl ester biolubricant. The heterogeneous catalyst was prepared by calcination method. Experimental results showed that the maximum yield of the methyl ester was 96.7 % obtained at a methanol-oil ratio of 6:1, catalyst of 6 wt.% and a reaction time of 5 hours. Major lubricating properties of the synthesized neem biolubricant such as viscosities at 40°C and at 100°C, viscosity index and pour point were analyzed and found to have values of 54.87 cSt, 6.64 cSt, 136.43 and – 9°C respectively. The biolubricant produced is comparable to other plant based biolubricant and the International Standards Organisation Viscosity Grade 46 (ISO VG 46) commercial standards for light and industrial gear applications.

Keywords: Neem seed oil, heterogeneous catalyst, transesterification, biolubricant, snail shell

INTRODUCTION

Environmental concerns associated with the use of petroleum-based products in various industries, such as forestry, farming and mining to mention a few have led to increased interest in the use of environmentally friendly substitutes. Growing environmental concerns are providing the incentive for increasing the demand and usage of plant oils in lubricants for many applications. The nature of vegetable oil, that is, easily renewable, biodegradable and non-toxic makes it the best alternative to mineral oil in the production of lubricants (Syaima et al., 2014).

Today, the constant use of petroleum-based products and other non-renewable assets are depleting the world's natural resources (Schneider, 2006). Biolubricant production is necessary to serve as a substitute lubricant to supplement or replace conventional lubricants due its numerous advantages such as renewability, biodegradability and lower gaseous emission profile (Bilal, et al., 2013).

It has been recounted that finding the other alternatives sources of feedstock and catalyst is of great interest in biolubricants production (Ghafar et al., 2019). Banu et al., (2018), Bahadur et al., (2015), Thangaraj et al., (2014), Muthu et al., (2010), Woma et al., (2019) among others also stressed the importance of neem seed oil as a viable source of material. According to Idris et al., (2018), neem oil can successfully serve as a lubricant, based on the lubricant properties it displayed for both light automotive systems and heavy automotive system. It has been observed that biolubricants are biodegradable and release less carbon and greenhouse gases compared to petroleum-based lubricants according to Hossain et al., (2018). According to Damjanovic et al., (2016), from an environmental point of view, the advantages of using vegetable oil as compared to conventional mineral oils are expressed

as non-toxicity, bio-degradability, renewability, good lubricity, high flash point and viscosity index, low volatility, savings and conservation of non-renewable resources. Others are less dependence on non-renewable resources, reduced emissions of greenhouse gases and increased agricultural production.

Heikal et al., (2017) reported that even though biolubricants are priced twice as high as conventional petroleum lubricants, various industries are investing in research and development programs toward increasing the oil recovery from seeds, reducing the costs of processes and exploring niche application areas. In the continuous activity for sourcing for better biolubricants, it had been reported that chemical modification of vegetable oils causes improved thermooxidative stability, thereby allowing their use in a wider range of operating conditions (Cecila et al., 2020).

Towards the production of suitable and accepted biolubricants, Hassan et al., (2019) reported that the increasing prices of crude oil, depletion of crude oil reserves in the world, and global concern in protecting the environment from pollution have renewed interest in developing and using environment-friendly lubricants derived from alternative sources.

According to Suresha et al., (2020), neem oil has promising benefits in all fields. As a result, neem oil was explored with tribological properties as biolubricant, by exploring the role of graphene nanoplatelets (GNPs) in neem oil as it affects viscosity, friction and wear as well as on seizure load which are important factors that accounts for the right selection of the appropriate lubricant in different sliding components of food processing machines.

Various researchers have contributed towards perfecting the suitability of biolubricants for various

domestic and industrial purposes over the years. Bilal et al., (2013) studied the feasibility of producing biolubricant from *Jatropha* oil by conducting chemical modifications on the *Jatropha* crude oil. The modification involved improving some of the lubricating properties of the *Jatropha* crude oil.

The physicochemical properties of *Jatropha* biolubricant were also compared with a certain standard properties of lubricants. It was found that the biolubricant produced is comparable to the ISO VG 46 commercial standards for light and industrial gears applications and other plant based biolubricants. Bokade and Yadav (2007) presented a reaction for the preparation of alkyl esters by transesterification process. They produced methyl/ethyl/propyl fatty acid esters called biodiesels, octyl fatty acid ester called biolubricants, which comprises contacting fatty acid glycerides / triglycerides with or without free fatty acids of vegetable oil with alcohols in the presence of a solid heteropolyacids catalyst which is substantially insoluble in the reaction mixture under reaction conditions.

From the study, optimized heteropolyacids (10%TPA) supported on clay was observed to be the best, stable, free fatty acid tolerable catalyst for the transesterification of edible and non-edible oil with lower and higher alcohol to get biodiesel and biolubricants.

The importance of sustainable development based on renewable and environmentally friendly products in the production of biolubricants was also presented by Soufi et al., (2018). They observed that biolubricants that are mainly produced by chemical modification of vegetable oils are sustainable products for biorefineries and the future of lubricant industries.

Biofuels and biolubricants production for industrial application from some common oil as feed stock was considered by Abdalla (2018). Studies on lanthanum and zinc (10-30 mol%) incorporated Mg-Al hydrotalcites for transesterification of soybean oil with methanol and n-octanol to produce biodiesel and biolubricant was presented by Rahul et al., (2011). They observed that the catalyst with 20 mol% of lanthanum showed a soybean oil conversion of 100% and biodiesel yield of 95% at 423 K in 4 hours. Basicity also affected catalyst activity.

Economical and safe ways to improve the properties of biolubricants, such as increasing their poor oxidative stability and decreasing high pour points, among others was presented by Salimon et al., (2010). They concluded that plant bio-based oils are an important part of new strategies, policies, and subsidies, which aid in the reduction of the dependence on mineral oil and other nonrenewable sources.

Betiku et al, (2017) worked on two-step conversion of neem (*azadirachta indica*) seed oil into fatty methyl esters using a heterogeneous biomass-based catalyst from cocoa pod husk. Their results confirmed that neem seed oil methyl ester (NSOME), which conformed to ASTM D6751 and EN 14214 standards, was produced at an optimum yield of 99.3 wt % using a methanol/oil ratio of 0.73 (v/v), catalyst amount of 0.65 wt%, and reaction time of 57 min while maintaining a constant reaction temperature of 65 °C. The transesterification of neem seed oil using a two step acid-base transesterification method using H₂SO₄ and NaOH had been reported with results that conformed to American Standard Testing Method (ASTM D6751), European Standard and Ghana Standard Authority (Abdul-Wahab and Takase, 2019).

According to Tanwar et al., (2013), neem oil has the highest potential and production among the available wild oils for neem oil methyl ester (NOME) production in India. About 75-80% oil potential is available in surplus which could be harnessed. This is a promising future for biolubricants production from neem oil. In addition, neem seed which contain 25%-45% oil on dry matter basis which is a non edible oil was used in transesterification reactions (Sathya and Manivannan, 2013).

Chauhan (2015) reported the experimental analysis of neem oil by transesterification and partial hydrogenation with better lubricity properties. Chan et al., (2018) added that in terms of the tribological aspect, a good biolubricant base stock can be made by optimizing two characteristics, which are the stability and adhesiveness of its generated tribofilm within the lubricating conditions. These could be met provided that the viscosity range of the lubricant and the lubrication regime are suitable and tally with the application requirements.

Tribological additives may then be added to further improve the base stock. In a recent study, it was proved that the production of different biolubricants having suitable chemical and rheological properties fitted to be used as commercialized industrial lubricants (Attia et al., 2020).

Catalyst is a fundamental requirement for biodiesel production, the choice of catalyst has always resulted into certain level of differences in the course of producing methyl esters (Singh et al., 2006). Difficulties with using homogeneous catalysts centre on their sensitivity to free fatty acid (FFA) and water in the source oil (Ma and Hanna, 1999). Heterogeneous catalysts are promising for the transesterification reaction of vegetable oils to produce methyl esters and have been studied intensively over the years. Unlike the homogeneous catalysts, heterogeneous catalysts can be easily separated from reaction mixture and reused for many

times (Omotoso and Akinsanoye, 2015). Non-conventional catalysts are natural or biological materials that can serve as heterogeneous catalysts. These include egg shells, waste shells of mollusk, industrial egg shell wastes, carbonate rocks, oyster shell, crab shells, chicken shells, duck shells, quail egg shells, laterites and lots more (Nakano et al., 2003). Most of these are wastes generated in various nations; they can serve as cheap source of catalysts that are employable in biofuel and biolubricants production. This will lead to the reduction of cost, waste recycling and clean environment, thereby enhancing waste to wealth (Omotoso and Akinsanoye, 2015).

This study was carried out with the objective of extracting oil from neem seed and chemically modifying the crude oil using calcium oxide from snail shell to produce synthetic ester biolubricant. The physico-chemical properties of neem biolubricant produced were compared with standard properties of lubricants. The parameters effecting on the transesterification such as methanol-oil ratio, catalyst ratio and reaction time were optimized.

EXPERIMENTAL

— Materials

The materials and reagents used in carrying out the research are as follows: crude neem oil, anhydrous methanol and orthorosphoric acid.

The instruments and equipment used in carrying out the study are: beakers (50-500 ml), burettes (50 ml), conical flasks, glass funnels, pH meter, retort stand and clamps, measuring cylinders (50-1000 ml), furnace, oven, electronic weighing balance, water bath, magnetic stirrer, heating mantle and the Gas Chromatography Mass Spectroscopy (GCMS) instrument.

— Preparation of Catalyst

The CaO catalyst was prepared from waste snail shells by calcination method. The snail shells were washed using distilled water and sun dried. Then the solid catalysts was crushed and calcined in the furnace at 800°C for 1 hour. After cooling, the resultant solid product was ground, sieved and kept in air tight sample bottles.

The sample bottles were kept in the desiccator to prevent air contact. The catalyst was activated by impregnation of a known quality of the powdered sample using orthorosphoric acid as the impregnation agent. Impregnation ratio of 15 g of activation agent to 5 g of the calcined snail shells was mixed. This mixture was stirred for 30 minutes, until a paste was formed and was allowed to stand for 24 hours.

The activated substrate was filtered using a filter paper. The mixture was washed by pouring distilled water gradually over the filter paper containing the sample while the filter paper was placed over a conical flask. The pH of the filtrate was checked

regularly using a pH meter until the pH was within the range 6 – 8. The activated substrate was then dried in an oven at 105°C for 10 minutes.

— Biolubricant Synthesis

Trans-esterification reactions were performed in a water bath. The oil was heated at 55°C for 5 minutes in a heating mantle to evaporate water and other volatile impurities.

The trans-esterification process parameters such as amount of catalyst, methanol to oil ratio and reaction time were varied to attain maximum methyl ester conversion. This was achieved by stirring a mixture of oil and catalyst (6%, 8% and 10% of the weight of the oil) with a magnetic stirrer, then, adding a designated amount of methanol (6:1, 8:1 and 10:1 mole ratio of methanol to oil). Each experiment was allowed to continue at 65°C at variable reaction time (3, 4 and 5 hours).

After the reaction was completed, the mixture was allowed to cool down and filtered to remove the catalyst. After, the mixture was poured into a separating funnel and allowed to stand for 24 hours to separate layers clearly.

— Characterization of Neem Biolubricant

According to ISO VG 46, the properties of the crude oil which are pertinent to lubricity are the viscosities at 40°C, 100°C, viscosity index and the pour point. The synthesized biolubricant was characterized for these physico-chemical properties.

» Viscosity

The viscosity was measured at two different temperatures of 40°C and 100°C respectively. A proper viscometer spindle was chosen. The sample was transferred to a beaker large enough to hold the viscometer spindle. The beaker was placed on a heating mantle which was set to a desired temperature, while the temperature of the sample was raised. The temperature of the sample was checked using a thermometer.

When the desired temperature was reached, the sample was then removed from the heat source and the viscosity was recorded. The spindle was attached to the upper coupling by holding it between the thumb and forefinger while cautiously rotating the spindle counter clockwise. The knob was set to the minimum speed which includes the centipoise range of the material to be tested.

The uppermost number on the knob indicates the revolutions per minute (rpm). The spindle was immersed into the sample up to the middle of the identification in the shaft. The viscometer was turned on and allowed to run until a constant reading was obtained.

» Viscosity Index

The viscosity index is an empirical number. Its value was determined using the values obtained from

viscosity. The viscosity index was determined using ISO VG index calculator.

» **Pour Point**

The pour point is the lowest temperature at which a liquid is still able to pour. A quantity of 5 ml of oil was drawn into a capillary tube tied to a thermometer, placed in a 250 ml beaker containing distilled water and immersed together in a water bath for controlled heating. The temperature at which the oil begins to move downwards due to its weight is the pour point.

— **Statistical Analysis**

The methodology involved optimizing neem biolubricant production using statistical analysis with MATLAB® R2014a The MathWorks Inc. (1994–2020) software.

The optimization of neem biolubricant production via transesterification process was designed using full factorial design. The effects of variables such as the methanol-oil ratio, catalyst ratio and reaction time, on the biolubricant yield was determined in order to find out the optimum conditions required for neem biolubricant production.

RESULTS AND DISCUSSION

— **Interaction between variables**

Figures 1–3 represent the interaction between the three variables; methanol-oil ratio, catalyst ratio and reaction time. The maximum point on these figures indicates a well-defined optimum condition for the variables.

In Figure 1, high biolubricant yield was favored by high catalyst ratio and high methanol-oil ratio. Similarly in Figure 2, high biolubricant yield was also favored by high reaction time and high methanol-oil ratio. Also in Figure 3, high biolubricant yield was favored by high catalyst, high reaction time and high methanol-oil ratio. However, in Figure 3, the catalyst proportion of 6 wt% favored the oil yield than others.

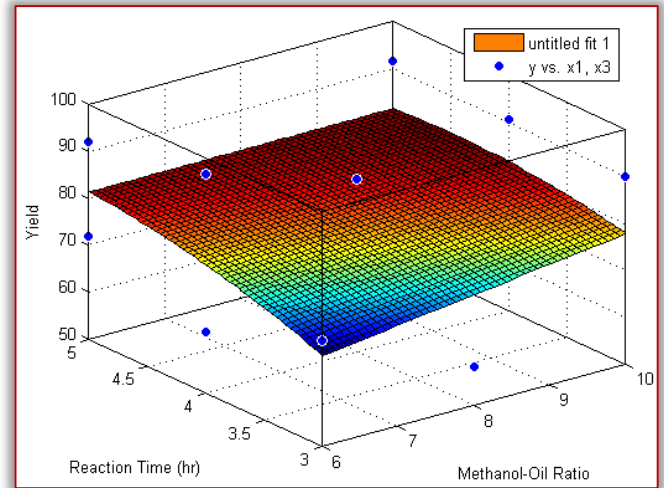


Figure 2: A plot showing the interaction between reaction time and methanol-oil ratio on biolubricant yield

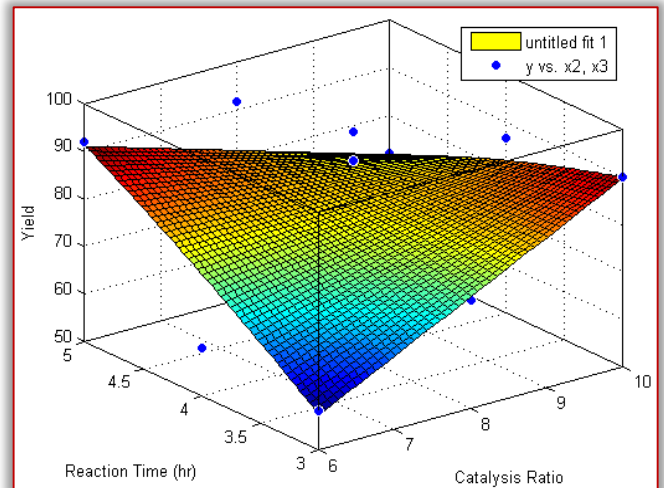


Figure 3: A plot showing the interaction between reaction time and catalyst ratio on biolubricant yield

— **Optimization of Parameters**

Statistical analysis was used for the optimization of parameters. The model equation based on the coded values (X_1 , X_2 and X_3 as methanol to oil ratio, catalyst concentration and reaction time respectively) for the yield of biolubricant from neem oil is expressed in Equation (1) as follows:

$$Y = \beta_1X_1 + \beta_2X_2 + \beta_3X_3 + \beta_{11}X_1^2 + \beta_{22}X_2^2 + \beta_{33}X_3^2 + \beta_{12}X_1X_2 + \beta_{13}X_1X_3 + \beta_{23}X_2X_3 \quad (1)$$

The β_i and β_{ij} are constants, where i and j are positive numbers 1, 2 or 3.

The result of this statistical analysis generated optimum values at methanol-oil ratio of 6:1, catalyst concentration of 6 wt% and reaction time of 5 hours. The optimized biolubricant yield of 96.7% was produced at a methanol-oil ratio of 6:1, catalyst amount of 6 wt. % and reaction time of 5 hours.

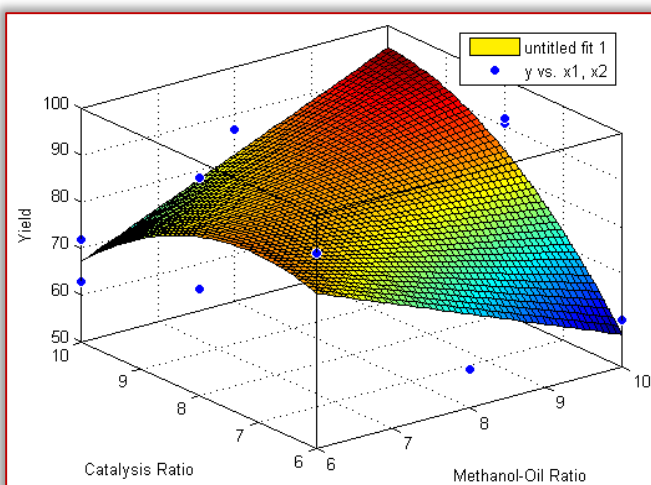


Figure 1: A plot showing the interaction between catalyst ratio and methanol-oil ratio on biolubricant yield

Thus, it showed that the statistical values and the experimental values are in agreement. Therefore, the effect of reaction conditions, which yielded a conversion of 96.7%, were methanol-oil ratio 6:1, catalyst concentration 6 wt. % and reaction time of 5 hours.

— **Determination of Physico-Chemical Properties**

The ISO VG 46 is one of the grades requirements based on the viscosity range of lubricants, and is one of the two grades that represents over 80% of all lubricants utilized (Lauer, 1995). Requirements for such applications are viscosities at 40 and 100 °C, viscosity index and pour point.

Table 1: Physico-chemical Properties of Synthesized Biolubricant in Comparison with ISO VG 46 and Petroleum Based Lubricants

Properties	Neem Bio lubricant	ISO VG 46	Petroleum based Lubricant
Viscosity at 40 °C (cSt)	54.87	> 41.4	10.801
Viscosity at 100 °C (cSt)	6.64	> 4.1	3.136
Viscosity Index	136.43	> 90	165.4
Pour Point	-9	< - 10	- 9

The viscosities of the biolubricant at 40 and 100 °C are very important lubricity properties. They are useful in determining the fluidity of the lubricant at low and high temperatures. They also show the thermal stability of the lubricant. The viscosity of the synthesized neem biolubricant meets the requirement of the ISO VG 46 since its viscosities are within the standard range presented in Table 1.

Viscosity index shows the characteristics of the lubricant viscosities when temperature changes are applied. The viscosity index obtained for the neem biolubricant was 136.43 and it is comparable to other plant based biolubricant. The high viscosity index of the biolubricant is an indication that changes in viscosities at higher temperatures are going to be minimal. The higher the viscosity index, the more preferable is the lubricant.

Pour point is the lowest temperature at which oil flows. Pour point is crucial for oils that must flow at low temperatures. It is one of the critical properties which determines the performance of lubricants. The pour point of the synthesized neem biolubricant obtained was – 9 °C, which is also comparable to the pour point value of other petroleum based oil.

— **GCMS ANALYSIS**

Synthesized neem biolubricant was selected for GCMS analysis based on its high lubricity properties. To

identify the fatty acid composition of the synthesized neem biolubricant, the gas chromatography coupled with mass spectrometry (GCMS) analysis was used.

Table 2 presents the composition of the synthesized biolubricant produced from the neem oil as extracted from the obtained various peaks of the GCMS used. The table showed that the produced biolubricant consists principally of the fatty acid methyl esters of oleic, palmitic and stearate acids, hence confirming a high quality product.

The values are represented as the relative percentage area from the sum of all identified peaks. Also from Table 2, methyl-9-octadecanoate (methyl oleicate) has the highest percentage. It can also be observed that traces of other methyl esters are present in the composition of the produced biolubricant.

Table 2: Fatty Acid Composition of Synthesized Neem Biolubricant

S/ No	Name of Compound	Number of Carbon	Value of Compound (%)	Retention Time (Minutes)
1	Methyl-hexadecanoate (Methyl palmitate)	C17	56.35	11.33.
2	Methyl-9-octadecanoate (Methyl oleicate)	C19	100	13.307
3	Methyl-octadecanoate (Methyl stearate)	C19	43.33	13.517
4	Hexa-decanonoic acid (Palmitic acid)	C16	4.97	13.787
5	9-octadecanoic acid (Oleic acid)	C18	83.73	14.136
6	Methyl 18-methyl-nonadecanoate	C21	4.88	15.690
7	Diisooctyl-phthalate	C24	6.74	18.891
8	9-hexylheptadecane	C26	5.22	21.708

Figure 4 is the chromatogram of the biolubricant synthesized from neem oil, many minor and major peaks were observed between retention time of 11 minutes to 22 minutes.

The chromatogram showed three considerable peaks at 11.33, 13.307 and 13.517 minutes and minor peaks with retention time of 13.787, 14.136, 15.690, 18.891 and 21.708 minutes. These peaks are due to the esters of fatty acids and methanol since neem oil is a mixture of various fatty acids.

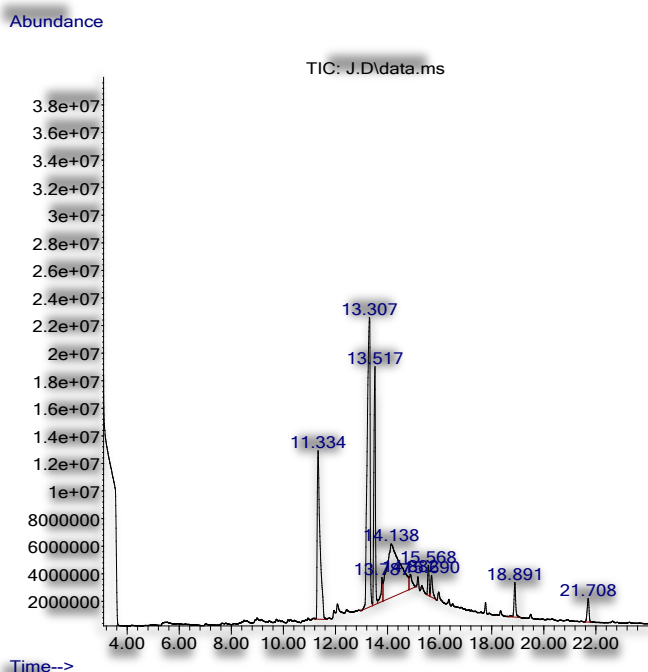


Figure 4: Chromatogram of Methyl Ester of Neem Oil

The peaks of 13.787 and 14.136 minutes indicated unreacted fatty acids. The peak of retention time 18.891 minutes indicated the chemical modification of oil due to either dimerization or condensation reaction of present fatty acids.

The peak at 21.708 minutes was as a result of degradation of fatty acids to alkanols which was promoted by the presence of calcium carbonate from snail shells. The product suggested a beta cleavage of the fatty acid caused by thermal catalytic effects of the carbonates.

CONCLUSION

Neem oil was extracted from neem seeds and chemically modified via trans-esterification using snail shell as a natural source for the production of the catalyst. The catalyst was derived from CaCO_3 in the snail shells which was converted to CaO after calcination at a temperature of 800°C for 1 hour. The optimum conditions yielded a conversion of 96.7% for a methanol-oil ratio of 6:1, catalyst concentration of 6 wt. % and a reaction time of 5 hours.

The method of using snail shells as catalyst source reduced the cost of catalyst and was environmentally friendly. Hence, it could be used in large scale industrial process of bio lubricant production, making the process affordable and ecologically benign.

Major lubricating properties of synthesized neem biolubricant analyzed and compared with standards specified by ISO VG 46 showed good agreement. Hence, the synthesized neem biolubricant can preferably serve as a substitute for petroleum based lubricants in light and industrial gear applications. Other natural sources of calcium oxide is recommended as catalyst in the production of biolubricants.

References

- [1] Abdalla B. K., Biofuels and Bio Lubricants Production for Industrial Application, The Sudanese Experience, SciEnvironm, Volume 1(2), pp. 39-41, 2018.
- [2] Abdul – Wahab, T and Takase, M. A., Biodiesel Production from Neem (*Azadirachta Indica*) Seed Oil, International Journal of Innovative Research and Development, Vol 8, Issue 8, pp. 33-40, 2019.
- [3] Attia, N. K., El-Mekki, S. A., Elardy, O. A., and Abdelkader, E. A. Chemical and rheological assessment of produced biolubricants from different vegetable oils. Fuel, 271, 117578, pp. 1-6, 2020.
- [4] Bahadur S., Goyal P. and Sudhakar K., Ultrasonic Assisted Transesterification of Neem Oil for Biodiesel Production, Energy Sources, Part A: Recovery, Utilization, and Environmental Effects, 37:17, pp. 1921-1927, 2015.
- [5] Banu, H. D., Shallangwa, T. B., Innocent, J., Thomas, O. M., Hitler, L. and Sadia, A., Biodiesel Production from Neem Seed (*Azadirachta indica*) Oil Using Calcium Oxide as Heterogeneous Catalyst, J Phys Chem Biophys, Vol. 8, Issue 2, pp. 1-3, 2018.
- [6] Betiku, E, Etim A. O., Perea, O. and Ojumu, T. V., Two-Step Conversion of Neem (*Azadirachta indica*) Seed Oil into Fatty Methyl Esters Using a Heterogeneous Biomass-Based Catalyst: An Example of Cocoa Pod Husk, Energy and Fuels, 31(6), pp. 6182-9193, 2017.
- [7] Bilal S, Mohammed-Dabo I. A, Nuhu M, Kasim, S. A, Almustapha I. H and Yamusa Y. A., Production of biolubricant from *Jatropha curcas* seed oil, Journal of Chemical Engineering and Materials Science, Vol. 4(6), pp. 72-79, 2013.
- [8] Bokade V. V and Yadav G. D., Synthesis of bio-diesel and bio-lubricant by transesterification of vegetable oil with lower and higher alcohols over heteropolyacids supported by clay (k-10), Trans IChemE, Part B, Process Safety and Environmental Protection, 2007, 85(B5), pp 372–377, 2007.
- [9] Cecilia, J. A., Ballesteros Plata, D., Alves Saboya, R. M., Tavares de Luna, F. M., Cavalcante, C. L., and Rodriguez-Castellón, E., An Overview of the Biolubricant Production Process: Challenges and Future Perspectives. Processes, 8(3), 257, pp. 1-24, 2020.
- [10] Chan, C. H., Tang, S. W., Mohd, N. K., Lim, W. H., Yeong, S. K., and Idris, Z., Tribological behavior of biolubricant base stocks and additives, Renewable and Sustainable Energy Reviews, 93, pp. 145-157, 2018.
- [11] Chauhan P. S., Study of neem oil as a source of biolubricant, VIVECHAN, International Journal of Research, Vol 6, Issue 1, pg. 62-69, 2015.
- [12] Damjanović, N., Davidović, Z., and Spasojević-Šantić, T. Ecological and economical aspects of use of biolubricants and conventional lubricants, Goriva i maziva: časopis za tribologiju, tehniku podmazivanja i primjenu tekućih i plinovitih goriva i inženjerstvo izgaranja, 55(3), pp. 188-199, 2016.
- [13] Ghafar, F., Sapawe, N., Jemain, E. D., Alikasturi, A. S., and Masripan, N., Study on The Potential of Waste Cockerle Shell Derived Calcium Oxide for Biolubricant

- Production, Materials Today: Proceedings, 19, pp. 1346-1353, 2019.
- [14] Hassan, A. F., Taiseer Hassan, M., & Youssif, A. A., Production of Bio Lubricant from Jojoba Oil, International Journal of Engineering Innovation & Research, Volume 8, Issue 4, pp. 146-153, 2019.
- [15] Heikal, E. K., Elmelawy, M. S., Khalil, S. A., and Elbasuny, N. M., Manufacturing of environment friendly biolubricants from vegetable oils, Egyptian Journal of Petroleum, 26(1), pp. 53-59, 2017.
- [16] Hossain, M. A., Iqbal, M. A. M., Julkapli, N. M., San Kong, P., Ching, J. J., and Lee, H. V., Development of catalyst complexes for upgrading biomass into ester-based biolubricants for automotive applications: a review, RSC advances, 8(10), pp. 5559-5577, 2018.
- [17] Idris, M. N., Usman, M., and Igbafe, I. A., Experimental Studies on Neem Seed (*Azadirachta Indica*) as a Possible Engineering Lubricating Fluid, International Journal of Agriculture and Earth Science, 4(2), pp. 25-34, 2018.
- [18] Lauer, D. A., Gear oil classification and specification, Journal of chemistry and technology, 441 – 458, 1995.
- [19] Ma F. & Hanna M.A., Biodiesel production: a review, Bio-resource Technology: 70:1- 15, 1999.
- [20] Muthu, H., SathyaSelvabala, V., Varathachary, T. K., Kirupha Selvaraj, D., Nandagopal, J., and Subramanian, S., Synthesis of biodiesel from neem oil using sulfated zirconia via tranesterification, Brazilian Journal of Chemical Engineering, 27(4), pp. 601-608, 2010.
- [21] Nakano T., Ikawa N. I, and Ozimek L, Chemical composition of chicken egg shell and shell membranes. Poultry Science, 82(3), pp. 510-514, 2003.
- [22] Omotoso, M. A and Akinsanoye, O. A., (2015), A review of biodiesel generation from non-edible seed oils using non-conventional heterogenous catalysts, Journal of Petroleum Technology and Alternative fuels. Vol.6 (1), pp. 1- 12.
- [23] Rahul R., Satyarathi, A. K., and Srinivas D., Lanthanum and zinc incorporated hydrotalcites as solid base catalysts for biodiesel and biolubricant production, Indian Journal of Chemistry, Vol 50 A, pp. 1017-1025, 2011.
- [24] Salimon J., Salih N. and Yousif E., Biolubricants: Raw materials, chemical modifications and environmental benefits, Eur. J. Lipid Sci. Technol. 112(5), pp. 519–530, 2010.
- [25] Sathya T. and Manivannan A., Biodiesel production from neem oil using two step transesterification, International Journal of Engineering Research and Applications, Vol. 3, Issue 3, pp.488-492, 2013.
- [26] Schneider M.P.. Plant-oil-based lubricants and hydraulic fluids. J Sci. Food Agr; 86(12): 1769 – 1780, 2006.
- [27] Singh, B.A., He J., Thompson J.V.. Process optimization of biodiesel production using alkaline catalysts applied engineering in agriculture. American Society of Agricultural and Biological Engineers. ISSN 0883 – 8542. 22(4) 597–600, 2006.
- [28] Soufi M. D., Ghobadian. B., Atashgaran, M., Mousavi, S. M., and Najafi, G., Biolubricant production from edible and novel indigenous vegetable oils: mainstream methodology, and prospects and challenges in Iran, Biofuels, Bioprod. Bioref, pp. 1-12, 2018.
- [29] Suresha, B., Hemanth, G., Rakesh, A., and Adarsh, K. M., Tribological Behaviour of Neem Oil with and without Graphene Nanoplatelets Using Four-Ball Tester. Advances in Tribology, Volume 2020, Article ID 1984931, pp. 1-11, 2020.
- [30] Syaima M.T.S., Zamratul M.I.M., Noor I.M. and Rifdi W.M.W.T., Development of bio-lubricant from *Jatropha curcas* oils. Int. J. Res. Chem. Metal Civil Eng.; 1 (1), 2014.
- [31] Tanwar D, Ajayta, Sharma D, Mathur Y. P., Production And Characterization of Neem Oil Methyl Ester, International Journal of Engineering Research & Technology (IJERT), Vol. 2 Issue 5, pp. 1896-1903, 2013.
- [32] Thangaraj B., Ramachandran K. B. and Raj S. P., Homogeneous Catalytic Transesterification of Renewable *Azadirachta indica* (Neem) Oil and Its Derivatives to Biodiesel Fuel via Acid/Alkaline Esterification Processes, International Journal of Renewable Energy & Biofuels, Vol. 2014, pp. 1-12, 2014.
- [33] Woma, T. Y., Lawal, S. A., Abdulrahman, A. S., Olutoye M. A., and Ojapah M. M., Vegetable Oil Based Lubricants: Challenges and Prospects, Tribology Online, 14(2), pp. 60-70, 2019.



ACTA TECHNICA CORVINIENSIS – Bulletin of Engineering
ISSN: 2067-3809
copyright © University POLITEHNICA Timisoara,
Faculty of Engineering Hunedoara,
5, Revolutiei, 331128, Hunedoara, ROMANIA
<http://acta.fih.upt.ro>

Fascicule 3

[July – September]

t o m e

[2020] XIII

ACTA Technica **CORVINIENSIS**
BULLETIN OF ENGINEERING



ACTA TECHNICA CORVINIENSIS – Bulletin of Engineering

ISSN: 2067-3809

copyright © University POLITEHNICA Timisoara,

Faculty of Engineering Hunedoara,

5, Revolutiei, 331128, Hunedoara, ROMANIA

<http://acta.fih.upt.ro>

¹Susarla Venkata Ananta Rama SASTRY

STUDIES ON ADSORPTION OF ACETIC ACID FROM AQUEOUS SOLUTION BY USING LEAVES OF MANILKARA ZAPOTA

¹Department of Chemical Engineering, MVGR College of Engineering (A), Vizianagaram, Andhra Pradesh, INDIA

Abstract: One of the serious environmental problems is the existence of acetic acid in industrial wastewaters. Very small concentration change of acetic acid present in water can drastically change health problems of both humans and animals. Over the last decade researchers have turned their attention in cheaper adsorbents. This paper studies about the effective use of the leaves of Manilkara Zapota (commonly known as Sapota) as biosorbent for removal of acetic acid. The effects of various parameters such as time of contact, adsorbent dosage and initial concentration are done experimentally using a batch process. Amongst them acetic acid also plays a crucial role. So this research is carried out and the data has been evaluated using Freundlich adsorption isotherm model. This paper discusses about the effect of different parameters on adsorption such as adsorbent dosages, initial concentration and contact time at room temperature.

Keywords: adsorbent dosage, adsorption, initial concentration, Manilkara Zapota, Saponin

INTRODUCTION

Environmental pollution is one of the biggest problems faced in this present era. It has exponentially increased over the decade. One of the serious environmental problems is the existence of acetic acid in industrial wastewaters. Very small concentration change of acetic acid present in water can drastically change health problems of both humans and animals [1–3]. Acetic acid is considered a volatile organic compound. Acetic acid is used in the synthesis of vitamins, antibiotics, cosmetics, dyes, insecticides, photographic chemicals, plastics, pharmaceuticals and hormones [4–6].

Over the last decade researchers have turned their attention in cheaper adsorbents. There were many adsorbents used for removal of acetic acid. Few of them are alloy surface (Au/Pd), activated carbon obtained from maize cobs, coconut shell activated charcoal, date seeds activated carbon, activated carbon from rice husk and waste wood, activated carbon from *Jatropha curcas* seed coat and fruit pericarp [7–9].

The purpose of this study is to explore the application of activated carbon obtained from leaves of Manilkara Zapota. Sapodilla or sapota (*Manilkara zapota*) is commonly known as chiku in our country. It has a ripened fruit which is sweet, malty flavor. But its raw one is hard to touch as it contains high amounts of saponin. Compounds extracted from the leaves have anti-diabetic, antioxidant, anti-inflammatory, controls b.p and hypocholesterolemic properties (Figure 1).

This paper discusses about the effect of different parameters on adsorption such as adsorbent dosages, initial concentration and contact time at room temperature.



Figure 1: Sapota Leaves

The objectives of the study are:

- ≡ To check the suitability of leaves of Manilkara Zapota to remove Acetic acid from wastewater.
- ≡ To perform batch experiments for studying the effect of initial concentration, adsorbent dosage and contact time of acetic acid solution on the removal of acetic acid.
- ≡ To test the suitability of Freundlich isotherm for the adsorption of Acetic acid.

MATERIALS AND METHODS:

The adsorbate used is Acetic acid. The solvent used is distilled water. The adsorbent used is Activated carbon obtained from leaves of Manilkara Zapota.

—Preparation of adsorbate

Acetic acid solutions were prepared by diluting the requisite amount of acetic acid with water to obtain the adsorbate solutions of different initial concentrations. Fresh solutions were prepared daily before starting the experiments. We have taken 5, 10, 15, 20, 25 ml of these solutions to conduct our experiments [10–11].

—Preparation of adsorbent

The raw material used for preparation of the adsorbent was collected from MVGR College of Engineering (A), Vizianagram district, Andhra Pradesh, India.

The following procedure was adopted for adsorbent preparation [12]:

- ≡ The leaves of Manilkara Zapota were collected from campus of MVGR College of Engineering (A), Vizianagaram, Andhra Pradesh, India.
- ≡ These leaves were washed with normal tap water and dried in sun light until the weight of the leaves became constant.
- ≡ Then these leaves were powdered in ultra-fine grinders and screened through BSS sieves (100,150, 240 mesh), maintaining the average particle size in the range of 100 to 240 mesh.
- ≡ The adsorbent thus obtained is stored in closed (airtight) glass bottles for its subsequent use.

—Experimental procedure

This experiment was conducted in a batch process. Five glass conical flasks were used for the experiment. The five glass flasks were added with different concentrations of acetic acid solution. After that they were titrated against standardized sodium hydroxide of 3N. After that the samples of activated carbon (obtained from leaves of Manilkara Zapota) with identified weight were positioned into each of the flask. The flasks with acetic acid and activated carbon contents are thoroughly agitated in a shaker.

For equal mixing the shaker was kept at constant speed throughout the experiment. After that the sample was filtered using a filter paper. After that we added distilled water again to the filtrate as it was found to be in maroon red in color.

After that, it is titrated using the 3N standardized NaOH solution. The experiment was conducted under different parameters and the data so obtained was able to determine the adsorption capacity of the respective adsorbent [12–13].

The respective procedure is done with the change in initial concentrations, adsorbent dosage and time of contact.

RESULTS AND DISCUSSION

—Effects of initial concentration

The concentration of the active sites of the adsorbent plays an important role in attracting the Acetic acid

from the solution. The effect of initial concentration on the rate of adsorption is shown in the Figure 2.

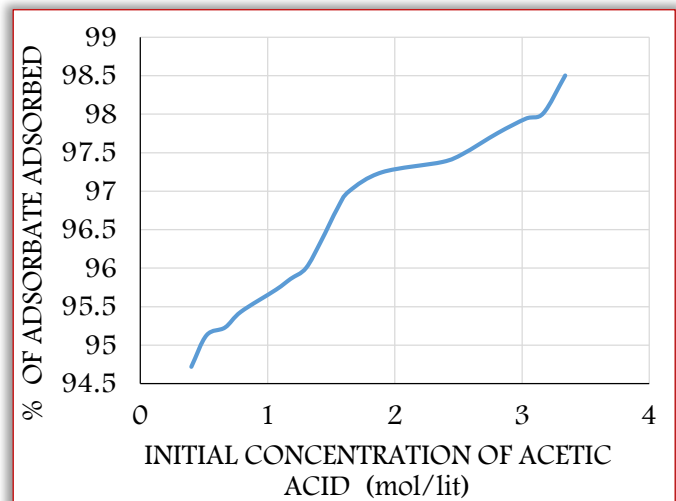


Figure 2: Effect of Initial Concentration on % of adsorbent adsorbed

It is also observed that % removal of acetic acid increases with the increase in the initial concentration. Rate of adsorption also increases with the increase in initial concentration as depicted in Figure 2.

—Effects of adsorbent dosage

The effect of % removal of adsorbate on adsorbent dosage is shown in the Figure 3. From this Figure it is observed that as adsorbent dosage increased, the % removal of acetic acid also increased.

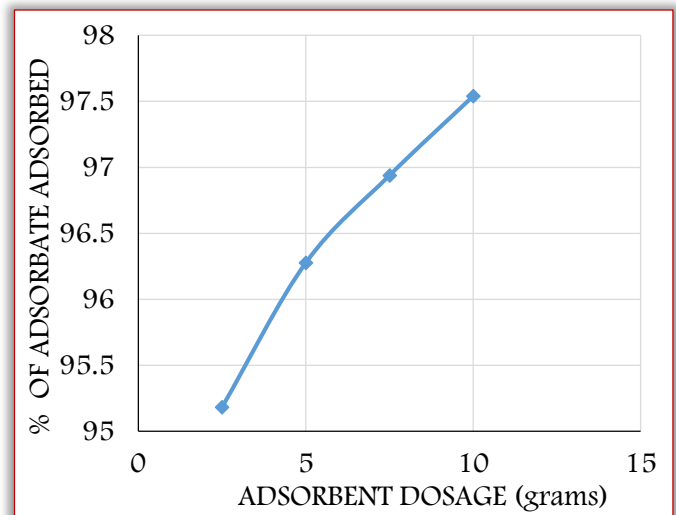


Figure 3: Effect of adsorption dosage on acetic acid adsorption

—Effect of contact time

In an adsorption experiment, contact time parameter plays a crucial role. Experiments were performed at three different times at a temperature of 28 to 30 °C. Figure 4 represents the variation of % of adsorbate adsorbed with change in the contact time.

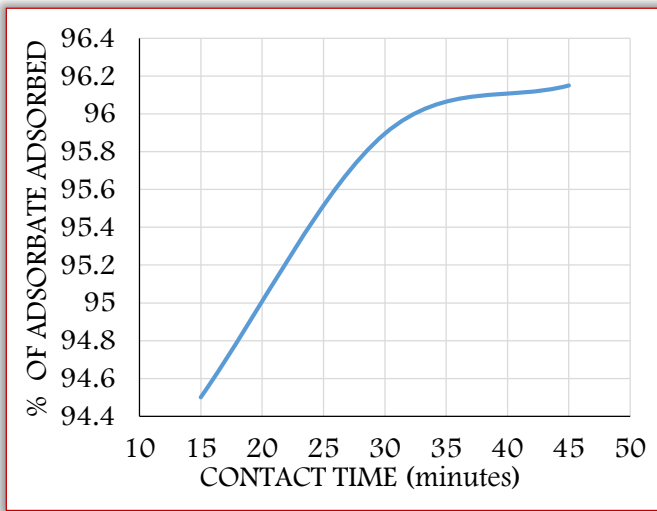


Figure 4: Effect of contact time on % of Adsorbate adsorbed

— Freundlich Adsorption Isotherm

The Freundlich isotherm can be written as:

$$\log q_e = \log K_f + (1/n) \log C_e$$

where:

- » K_f and n are characteristics of the adsorbate–adsorbent system, which identify the capacity of adsorption.
- » $1/n$ is a function of the strength of the adsorbate for a given adsorbate–adsorbent system.
- » K_f and n are obtained by fitting the present experimental data on q_e and C_e for Cr(VI) in accordance with above Freundlich adsorption isotherm equation.

If $n = 1$ then partition between the 2 phases (solute in the solution and the solid adsorbent) are independent of the concentration.

$1/n$ gives the slope of above equation.

If $1/n$ is > 1 (or $n < 1$) indicates that the adsorption between adsorbent and solute is favorable [12].

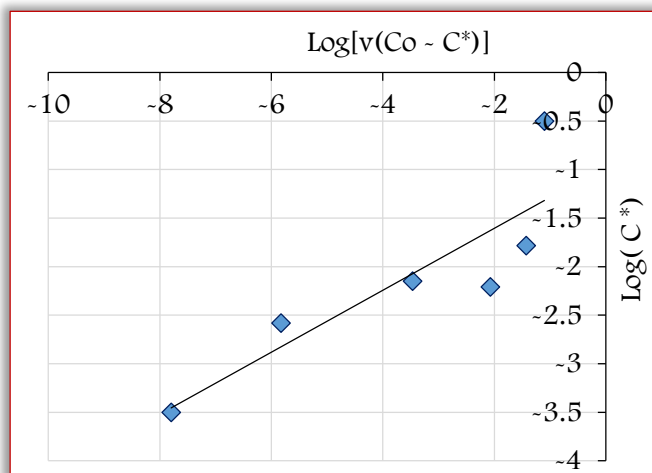


Figure 5: Freundlich Adsorption Isotherm

The equilibrium data for the removal of acetic acid by adsorption with the leaves of Manilkara Zapota at

30°C were verified using the Freundlich isotherms. Figure 5 confirms that adsorption for the current study logically follows the Freundlich adsorption pattern and 1st order kinetics.

CONCLUSIONS

The study shows that adsorption can be used as an efficient method for removal of pollutants from water and thus decontaminating it. However, this process is restricted due to the high cost of the traditional adsorbents like activated carbon. This study explored the potential of low cost adsorbent for its ability to adsorb the acetic acid for the marketable use because of its being widely available and efficient. The adsorption of acetic acid on activated carbon (obtained from leaves of Manilkara Zapota) from water was considered to investigate the adsorption potential of the respective adsorbent. The results showed that leaves of Manilkara Zapota can be used as a cheap, good and accepted adsorbent for the recovery of Acetic acid from the aqueous solutions.

The entire experiment was summarized and the results are jotted down as follows:

- The adsorption increases with an increase in adsorbent dosage.
- The experimental adsorption data logically follows the Freundlich adsorption isotherm.
- The % removal of acetic acid increases with the increase in initial concentration of acetic acid.
- This adsorbent could also replace the presently used adsorbents for the removal of acetic acid and can be categorized under low cost adsorbents.
- While carrying out the experiment, highest acetic acid adsorption of about 98.1% is achieved.

Acknowledgements:

The authors wish to gratefully acknowledge the support of the Management of MVGRCOE (A), Vizianagaram for carrying out the research work.

References:

- [1] Ajmal, MA, Hussain Khan S and Ahmad, A: Role of sawdust in the adsorption of Cu (II) from industrial wastes, *Wat. Res.*, 32, 3085–3091, 1998.
- [2] Ajmal, MA, Mohammad, R., Yousuf and Ahmad, A: Adsorption behavior of Cadmium, Zink, Nickel, and Lead from aqueous solution by Mangifera India Seed Shell, *India J. Environment Health*, 40, 15–26, 1998.
- [3] Anoop Krishnan K., Sreejalekshmi K.G., Vimexen V., Vinu V. Dev: Evaluation of adsorption properties of sulphurised activated carbon for the effective and economically viable removal of Zn(II) from aqueous solutions, *Ecotoxicology and Environmental Safety*, 124, 418–425, 2016.
- [4] ASTM E478 – 08. “Standard Test Methods for Chemical Analysis of Copper Alloys”.
- [5] Malkoc, E., and Nuhoglu, Y: Investigations of Nickel (II) Adsorption from Aqueous Solutions Using Tea

- Factory Waste, J. Hazardous Materials, B127, 12–19, 2005.
- [6] Malkoc, E., and Nuhoglu, Y: Fixed bed studies for the sorption of chromium (IV) onto tea factory waste, Chem. Eng. Sci., 61, 4363–4370, 2006.
- [7] Malkoc, E., and Nuhoglu, Y: Adsorption of Ni (II) ions from aqueous solutions using waste of tea factory: adsorption on a fixed-bed column, J. Hazardous Materials, B135, 328–236, 2006.
- [8] Malkoc, E., and Nuhoglu, Y: Potential of tea factory waste for chromium (VI) adsorption from aqueous solutions: thermodynamic and kinetic studies, Sep. Purif. Technol., 54, 291–298, 2007.
- [9] Sastry, S.V.A.R. & Sarva Rao, B: Studies on adsorption of Cu (II) using spent tea extract (STE) from industrial wastewater, i-manager’s Journal on Future Engineering & Technology, 11 (3), 31–35, 2016.
- [10] Sastry, S.V.A.R. & Sarva Rao, B: Determination of adsorption kinetics for removal of copper from wastewater using Spent Tea Extract (STE), i-manager’s Journal on Future Engineering & Technology, 12 (4), 27–32, 2017.
- [11] Sastry, S.V.A.R. & Anusha, S.A: Studies on continuous adsorption of acetic acid from aqueous solution using rice husk adsorbent, i-manager’s Journal on Future Engineering & Technology, 14 (1), 42–47, 2018.
- [12] Sastry, S.V.A.R. & Padma D.V: Biosorption of Hexavalent Chromium using Mallet Flower Leaves Powder as adsorbent, TEST Engineering and Management, 83 (March/April), 15714–15729, 2020.
- [13] Sastry, S.V.A.R., Sarva Rao, B & Padma D.V: Studies on Selective Batch Adsorption of Cu(II) and Cr(VI) from aqueous solution, TEST Engineering and Management, 83 (May/June), 2020.



ACTA TECHNICA CORVINIENSIS – Bulletin of Engineering
ISSN: 2067–3809
copyright © University POLITEHNICA Timisoara,
Faculty of Engineering Hunedoara,
5, Revolutiei, 331128, Hunedoara, ROMANIA
<http://acta.fih.upt.ro>

¹Mladen TODIC, ²Ostoja MILETIC, ³Said PAŠALIĆ

ZONE OF THE STRESS AND OF THE STRAINS WHEN BENDING LAMINAR COMPOSITES

^{1,2}University of Banja Luka, Faculty of Mechanical Engineering, Banja Luka, BOSNIA & HERZEGOVINA

³University of Bihac, Faculty of Technical Engineering in Bihac, Bihac, BOSNIA & HERZEGOVINA

Abstract: Spreading stress–strain zone at bending or profiling of laminar composite is in function: layer material characteristic, geometric layer size, parameters at deformation layered composites and deformation degree. The mechanical properties of the layered material significantly affect the position and intensity of the voltage–deformation zone and the way of making the laminar composite. If the mechanical properties of the layers are significantly different, the stress zone deformation defines the material of the layer with higher mechanical properties. This paper deals with the case when the mechanical properties of the layers are very similar. Stress of the states can be simulated with program packages that are related to areas, ie possible of the stress–strain states area. One of these software is ANZIS. In this program, simulation of the position of the two–layer laminar composite with Cu–Al layers was performed. The simulation was performed by force bending in the middle of the work pieces

Keywords: laminated composites, bending, stress zone, deformation zone

INTRODUCTION

Composite materials are largely used in science and technology. The technologies of getting these materials are becoming more and more perfect. Known technologies for obtaining laminar composites are: rolling, explosive affixture and gluing. Their technological processing into semi–products and products requires reliable processes that will not lead to the appearance of micro–cracks at the layer boundary and in the layers themselves which can later propagate in realistic conditions of application due to dynamic loads, which can lead to destruction of the system in which they are applied. Prior to bending or profiling of composite layers it is very important to know the position of the layers in relation to the radius of bending and profiling and their mechanical and geometric sizes. In order to gain access to product–making technology, which will not result in the emergence of crack in the composite layers, degradation of layer thickness and micro–crack formation [1,2]. The zones of the stress and of the strain intensity is exactly dependent on the above parameters and the degree of deformation [3].

STRESS–STRAIN ZONES AT BENDING OF THE LAMINAR COMPOSITES

When bending the composite laminar materials, report is triaxial stress and strain state, Figure 1. Since of the bending non–monoton process is very important to know: the geometric prametri layers, the mechanical characteristics of the layer material, the position of the layers in relation to the bending radius and the degree of deformation [4]. These parameters affect the stretching and pressure zones at the cross section of the profile, their size and the degree of deformation at which the destruction will not occur.

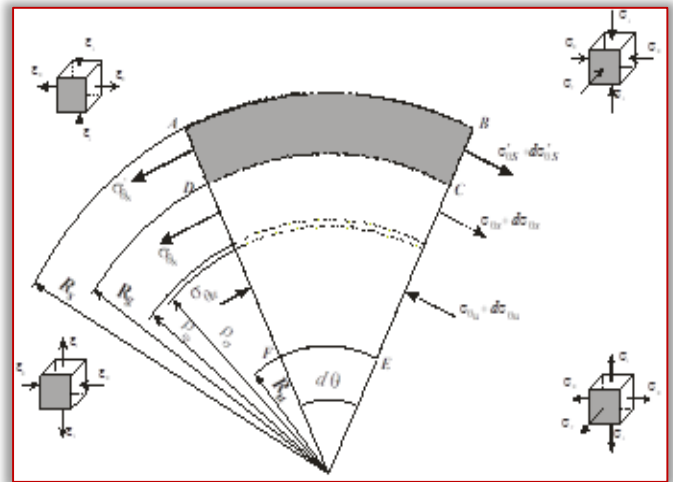


Figure 1. Scheme of stress and strain state at the bending of the two–layered composite, R_s – radius of bending the outer surface, R_g – radius of bending on the boundary of the layers, R_u – radius of bending of the inner surface, R_n – radius of neutral surface (lines) deformation, R_σ – radius of the neutral surface (lines) of the stress, σ_θ – tangential of the stress, σ_r – radial of the stress, σ_s – longitudinal stress in the direction or radius of bending, ϵ_θ – tangential of the strain, ϵ_r – radials of the deformation and ϵ_s – longitudinals of the deformation

When bending single–layer or multilayer materials, the stress and deformation state in work piece can be brought in:

- » elastic of the area
- » elastic–plastic, and
- » plastic of the area.

Stress of the states can be simulated with program packages that are related to areas, ie possible of the

stress–strain states area. One of these software is ANZIS. In this program, simulation of the position of the two–layer laminar composite with Cu–Al layers was performed. The simulation was performed by force bending in the middle of the work pieces, which is resting be on two supports, Figure 2. Copper thickness 3.2 mm and Al 3.5 mm. When is the copper layer on the concave (upper) side, ie. to the deformed force, the neutral line stress distance is 2.9 mm from the concave surface. When in this position Al then is the neutral line spaced 3.75 mm.

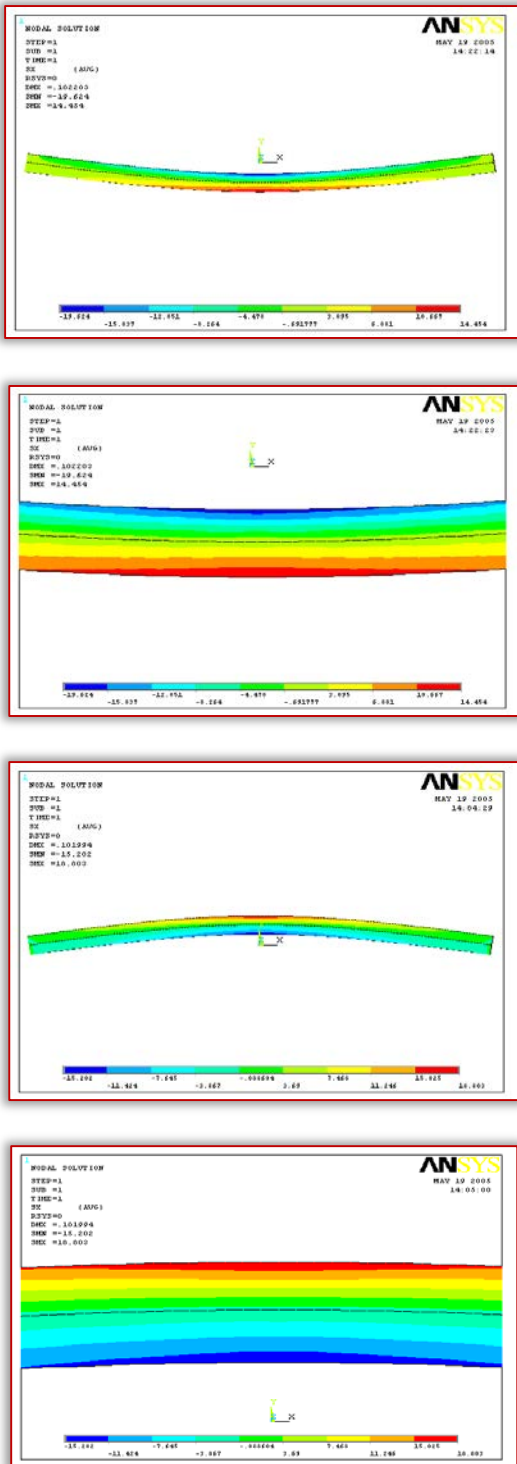


Figure 2. Double layer laminar composite, Cu–Al

For determine the radius of neutral deformation surface ρ_φ , it is necessary to know the size of the outer (R_s) and inner (R_u) radius of bending, on the basis of which the radius of the neutral layer (surface) of deformation can be determined by the expression

$$\rho_\varphi = \frac{R_s^2 - R_u^2}{2s_u} \quad (1)$$

where: s_u –the thickness of the work pieces of the two–layer composite

The deformation state on the convex (outer) and concave (inner) surface is determined by expressions

$$\varphi_{is} = \frac{2}{\sqrt{3}} \ln \frac{R_s}{\rho_\varphi} \quad (2)$$

$$\varphi_{iu} = \frac{2}{\sqrt{3}} \ln \frac{\rho_\varphi}{R_u} \quad (3)$$

After determining the radius of the neutral layer of deformation, knowing the size flowing limits of the material can be determined the boundary between elastic and plastic zone. After that, the stress of the per throughout laminate composite can be determined.

The tangential stresses in the compression zone are determined by the expression

$$\sigma_{\theta u} = -\frac{2}{\sqrt{3}} \left(\sigma_i + \frac{\sigma_{iu} \varphi_{\theta u} - \sigma_i \varphi_{\theta i}}{n+1} \right) \quad (3)$$

$$\sigma_i = A \left(\ln \frac{\rho_\varphi}{r} \right)^n$$

Radial stress are determined by expression

$$\sigma_{ru} = -\frac{2}{\sqrt{3}} \frac{\sigma_{iu} \varepsilon_{\theta u} - \sigma_i \varepsilon_{\theta i}}{n+1} \quad (4)$$

The intensity of deformation on the convex surface is determined by equality

$$\varphi_{is} = \frac{2}{\sqrt{3}} \ln \frac{R_s}{\rho_\varphi} \quad (5)$$

The intensity of deformation on concave surface is determined by equality

$$\varphi_{iu} = \frac{2}{\sqrt{3}} \ln \frac{\rho_\varphi}{R_u} \quad (6)$$

EXPERIMENTAL DETERMINATION OF THE POSITION OF NEUTRAL SURFACE

Experimental determination of the neutral deformation surface position can be determined by the method of parallel lines, and the degree of deformation on the convex concave side by the application of the circles mesh or squares network

[5]. It is therefore necessary to apply the line to the side surfaces of the work pieces, and the circles on the surface of the deformation work pieces [6,7].

The optimal distance between the lines is about one millimeter, and can be less. Detection of line position change during deformation is possible by using a three-dimensional camera or after deformation by recording the geometric size of the lines and circles by means of a microscope. By processing the positions, comes position of the neutral deformation surface is reached in the multilayer composites and deformations on the convex and concave sides of the contour. The neutral deformation layer does not change its length during bending deformation but only changes the curvature, which is the result of the bending radius [8].

Depending on the change in the position of the applied lines at the sides, the comes is to the neutral deformation surface is reached. Mathematical dependency can be expressed through the following

$$s_{n\phi} = \frac{(l-l')}{(l''-l')}s \quad (6)$$

where are:

$s_{n\phi}$, mm – the distance of the neutral surface of deformation from the inner surface of the workpiece
 l , mm – the initial spacing of the parallel lines applied to the workpiece ,
 l' , mm – the spacing of parallel lines on the inner side of the workpiece ,
 l'' , mm – the spacing of parallel lines on the outside side of the workpiece,
 s , mm – workpiece thickness.

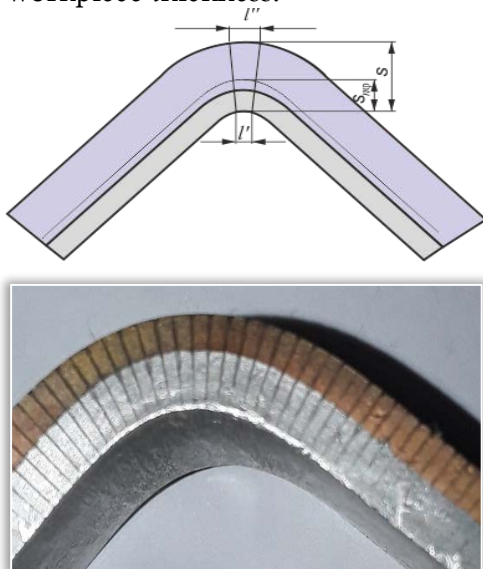


Figure 4. Geometrical size of the position and spacing of the parallel lines applied to the lateral surface and their position after the deformation of the Cu–Al Line on the surface of the piece and the workpiece at the bending of the two – layer laminar composite (layered material), Figure 4.

In Table 2, given on the neutral position of the deformation surface of the two–layer composite Cu–Al is calculated, the radius on the tool $r = 6$ mm

Table 2. Position of neutral deformation surface

Workpiece	Angle of the bending in the first and second phase	Layer on the convex side of the workpiece	Distance of neutral surface from concave surface, mm
1	52° 10'	Al	2.00
	89° 03'		1.735
2	50° 14'	Cu	3.611
	89° 50'		3.204

After deformation, the thickness of the aluminum layer was increased when this layer was on the concave side and thinning when it was on the convex side, Figure 5.



Figure 5. The layers of the laminar double–composites after bending force and their deformation after the experiment was performed in two bending cycles

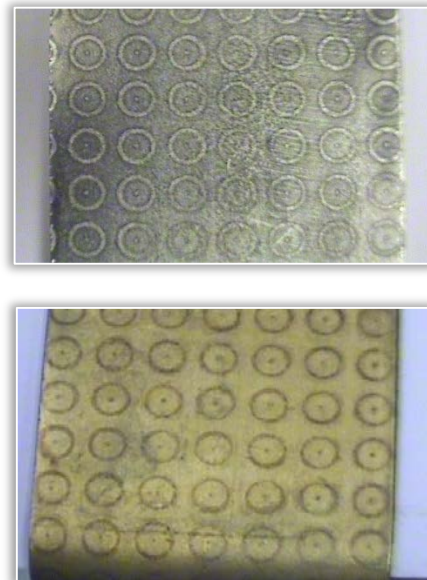


Figure 6. Circles on Layer Al surface 99.0 (left image) and on the surface of the Cu 99.9 layer (right)

On the surface of the two – layer laminated composite, a network of circles was introduced to determine the intensity of deformation on these surfaces, Figure 6. The intensity of deformation on the convex and concave sides is given in Figures 7 and 8.

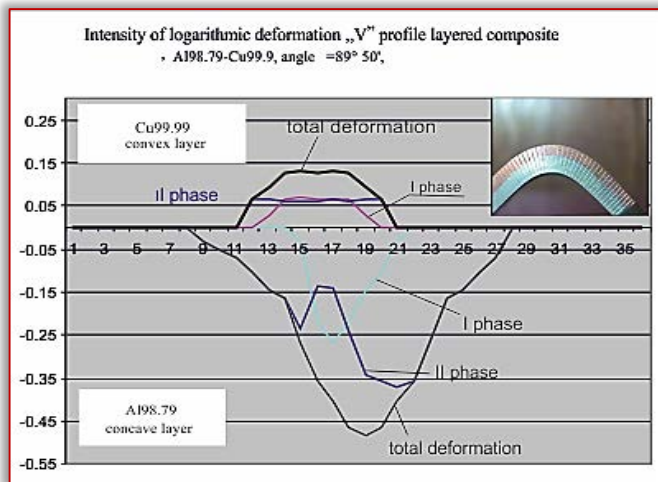


Figure 7. Intensity of deformation on the concave and convex surface of the two-layer laminar composite Cu–Al at bending of the radius tool $r = 6$ mm (Cu convex zone)

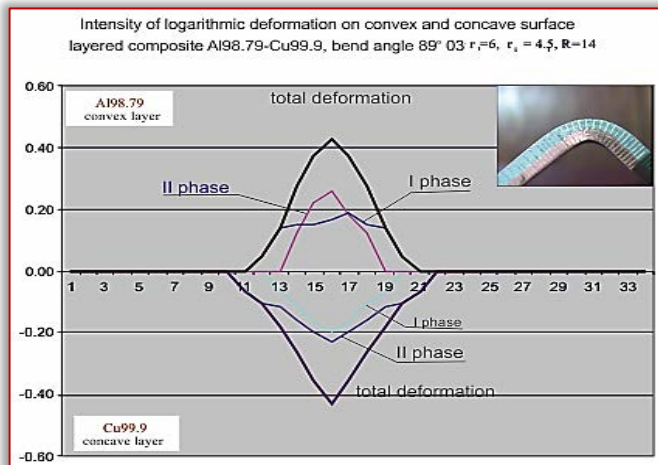


Figure 8. Intensity of deformation on the concave and convex surface of the two-layer laminar composite Cu–Al at bending of the radius tool $r = 6$ mm (Al convex zone)

CONCLUSION

Theoretical and experimental research of the deformation intensity when the bending of the two-layer composite, where he is aluminum layer (thickness 3.5 mm) and copper (thickness 3.2 mm) show that very important mechanical and geometric sizes are essential on the concave side. They directly affect boundary deformability if they are approximately the same. The study shows that the aluminum layer determines the maximum deformability limit, regardless of whether it is on a concave or convex side, an intense thickening or thinning of this layer is present.

Note:

This paper is based on the paper presented at DEMI 2019 – The 14th International Conference on Accomplishments in Mechanical and Industrial Engineering, organized by Faculty of Mechanical Engineering, University of Banja Luka, BOSNIA & HERZEGOVINA, co-organized by Faculty of Mechanical Engineering, University of Niš, SERBIA, Faculty of Mechanical Engineering Podgorica, University

of Montenegro, MONTENEGRO and Faculty of Engineering Hunedoara, University Politehnica Timisoara, ROMANIA, in Banja Luka, BOSNIA & HERZEGOVINA, 24–25 May 2019.

References

- [1] M. Todić, O. Miletić, M. Stefanović, 2005: Position of neutral areas of intensity of stress and deformations at two layer composite materials, *Jurnal for Technology of plasticity*, Vol. 30, Number 1/2, Novi Sad, 2005, p. 109–118
- [2] Jennifer R. Mawdsley, Desiderio Kovar, and John W. Halloran.2000, *Fracture Behavior of Alumina/Monazite Multilayer Laminates*. J. Am. Ceram. Soc., 83, Materials Science and Engineering Department, University of Michigan, Ann Arbor, Michigan
- [3] Ryutaro Hino, Yoshihiro Goto, Fusahito Yoshida, 2003, Springback of sheet metal laminates in draw-bending, *Journal of Materials Processing Technology* 139, p. 341–347.
- [4] Mladen Todic. 2006, Položaj neutralnih površina napona i deformacija kod slojevitih kompozitnih materijala , doktorska disertacija , Mašinski fakultet Banja Luka.
- [5] Groover, M.P. (2007). *Fundamentals of Modern Manufacturing*. John Wiley & Sons, Hoboken. Note that the title of the book is italicized.
- [6] M. Todić, O. Miletić, T. Latinović: Višeslojni materijali za elastične (odskočne) pločice, termobimetali, V Međunarodno savjetovanje o dostignućima elektro i mašinske industrije, DEMI 2003., Banja Luka, 2003., str. 697–703
- [7] M. Todić, O Miletić: Bifurkacija slojeva kod dvoslojnih kompozitnih materijala, XXXI Savjetovanje proizvodnog mašinstva Srbije i Crne Gore sa međunarodnim učesćem, Kragujevac 19–21 septembar 2006., str. 263–269
- [8] M. Todić, O. Miletić: Signifikance of geometrical and mechanical parameters on delamination to the bending composites with two layers, *Internacional Conference on Innovative Technology in Design, Manufacturing and Production, IN-TECH 2010*, Prague, Czech Republic, 2010, p. 507–511



ACTA TECHNICA CORVINIENSIS – Bulletin of Engineering
ISSN: 2067-3809

copyright © University POLITEHNICA Timisoara,
Faculty of Engineering Hunedoara,
5, Revolutiei, 331128, Hunedoara, ROMANIA
<http://acta.fih.upt.ro>

¹Victor Viorel SAFTA, ¹Bianca-Ştefania ZĂBAVĂ, ²Viviana CIUCĂ

HIGH EFFICIENCY GAS HEATING SYSTEMS – A REVIEW

¹University Politehnica of Bucuresti, Department of Biotechnical Systems, Bucharest, ROMANIA

²National Society "Pasteur Institute" S.A. Bucharest, ROMANIA

Abstract: This paper reviews modern versions of high efficiency gas heating systems, presenting operating principles and constructive structures, and highlighting the benefits of their use both in terms of thermal efficiency and in terms of regarding the reduction of pollutant emissions into the atmosphere. This issue is of a particular importance for the implementation of viable solutions for ensuring the thermal energy in rural households in our country, where natural gas is available.

Keywords: gas heating systems, high thermal efficiency, low pollutant emissions

INTRODUCTION

The use of natural gas to heating systems from rural households, where available, is particularly profitable for the benefits it offers both from an economic and environmental points of view.

From an economic point of view, the burning of natural gas for the production of thermal energy is the cheapest process compared to the burning of other conventional fuels. Figure 1 shows the results of a study made in March 2015, in United Kingdom of Great Britain, regarding the cost of the producing of 1 kWh of heat through different thermal energy production processes.

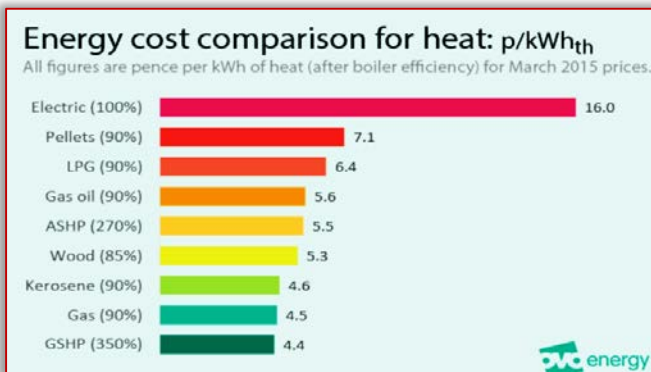


Figure 1 – The cost of producing 1 kWh of thermal energy by different heat production processes [10]

In terms of emissions to the atmosphere, gas burning produces the smallest amount of fine particles compared to the amounts of particles produced by combustion of the other conventional fuels (Figure 2). Also, the carbon footprint resulting from the burning of natural gas is the smallest compared to those resulting from the combustion of the other categories of conventional fuels (Figure 3). Both situations are particularly favourable from the point of view of environmental protection.

Modern heating systems based on the burning of natural gas can be divided into two main categories, namely: indoor air heating systems with furnaces and boiler heating systems with boiler and radiator network.

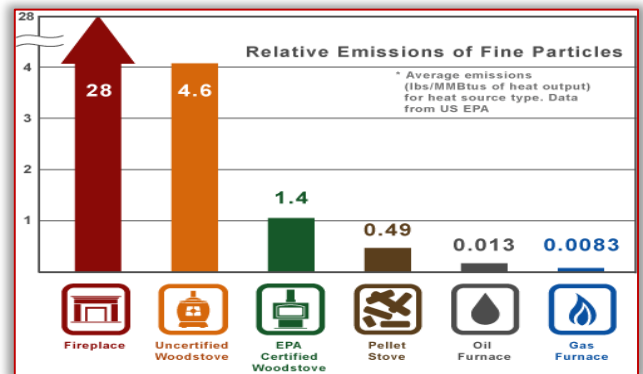


Figure 2 – Solid suspensions emissions produced by different conventional fuels burning [3]

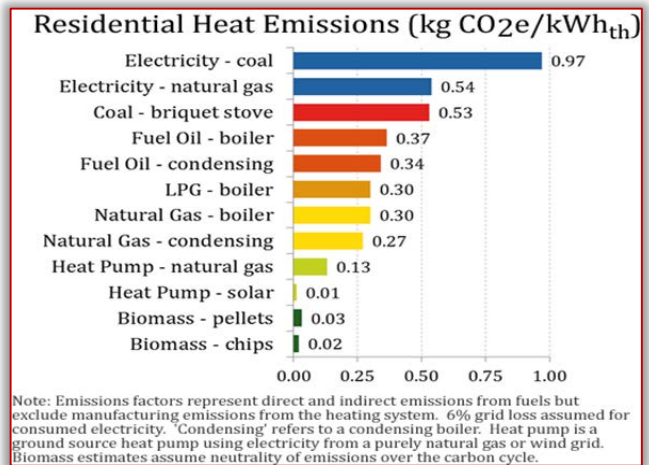


Figure 3 – The carbon footprints produced by different conventional fuels burning [11]

INDOOR AIR HEATING SYSTEMS WITH FURNACES

Currently, modern indoor air heating systems can be classified according to the following criteria: the air circulation mode through the furnace heating system and the transmission efficiency of the thermal energy produced by combustion of the natural gas to the air flow through the furnace heating system.

It should be noted that the efficiency of a heating system with furnace or boiler is measured by annual fuel efficiency (AFUE). Thus, an AFUE of 90% means that 90% of the fuel energy becomes heating energy

for home, and 10% escapes out through the vent pipe and through the heating system jacket [6].

According to the air circulation mode through the furnace heating system there are furnace heating systems with free air circulation (by convection) and furnace heating systems with forced air circulation.

The free air circulation heating systems are characterized by constructive simplicity, reduced operating and maintenance costs and reduced thermal energy transmission efficiency (55–65% AFUE to the oldest up to 70% AFUE to the modern ones) [7].

An example of such a modern heating system is shown in the scheme from Figure 4 where it is observed that the gas burner is mounted in a combustion chamber located directly on the outside wall of the home, provided with combustion air intake duct and exhaust fumes. In direct contact with combustion chamber is placed an air circulation channel through which the indoor air enters and heats.

The circulation through the air heating channel is made by convection as follows: the cold indoor air is admitted through the bottom entrance of the channel, contacts the wall of the combustion chamber and increases its temperature, and due to the fact that its density is decreasing, it rises and is discharged through a distributor on the top of the channel, like warm air producing the heating of the room.

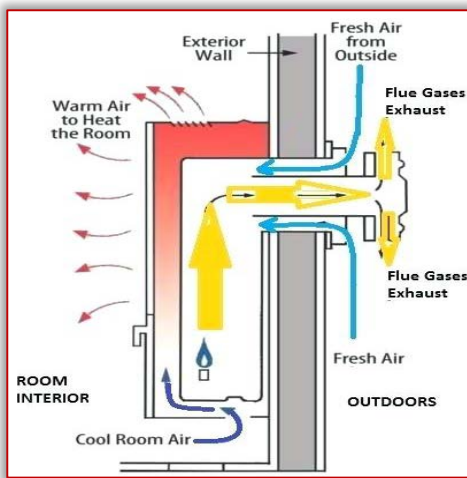


Figure 4 – Heating system with convective air circulation [4]

This heating system is characterized by a very simple construction, easy operation and maintenance, and due to the positioning of the pipes for air intake for gas combustion and flue gas discharge, the efficiency of transmitting thermal energy to the indoor air is satisfactory.

The forced-air heating systems are more complex and more sophisticated in terms of exploitation and maintenance but are also more efficient in terms of transmitting thermal energy to the air that needs to be heated.

Thus, from the point of view of the efficiency of transmitting thermal energy to the air to be heated, forced-air heating systems can be classified into three categories, namely: conventional forced-air heating systems, mid-efficiency forced-air heating systems and high efficiency forced-air heating systems.

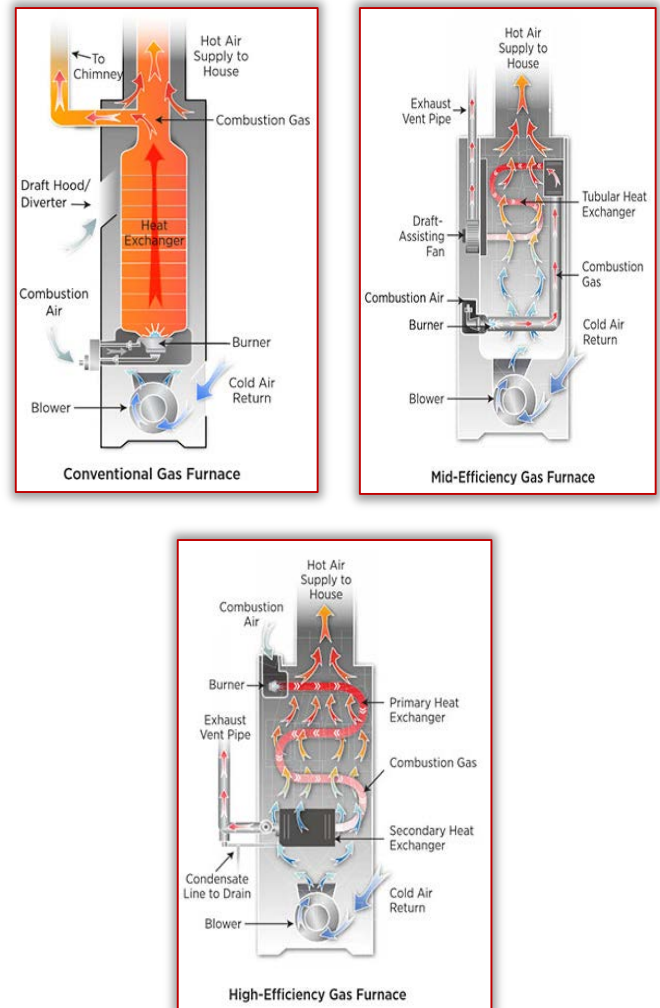


Figure 5 – Principal schemes of forced-air heating systems [7]

Conventional forced-air heating systems (Figure 5a) are the classical heating systems where the in-room air to be heated is introduced into the system through its lower part by means of a fan/exhauster and brought into contact with the wall of the combustion chamber where the gases are burnt, increasing its temperature and then being discharged to the room through a distributor placed on the top of the system. This type of system has 56–72% AFUE efficiency, with the best performing at 78% AFUE.

Mid-efficiency forced-air heating systems (Figure 5b) are the heating systems in which the in-room air to be heated is circulated through the system via a fan/exhauster taking up the energy of the flue gas by means of a tubular heat exchanger placed in their flow direction. It is mentioned that in order for the heat transfer to be as efficient as possible, an auxiliary fan/exhauster is provided in the system to uniform

the flue gas flow through the heat exchanger tube. This type of systems have increased efficiency of 80–82% AFUE.

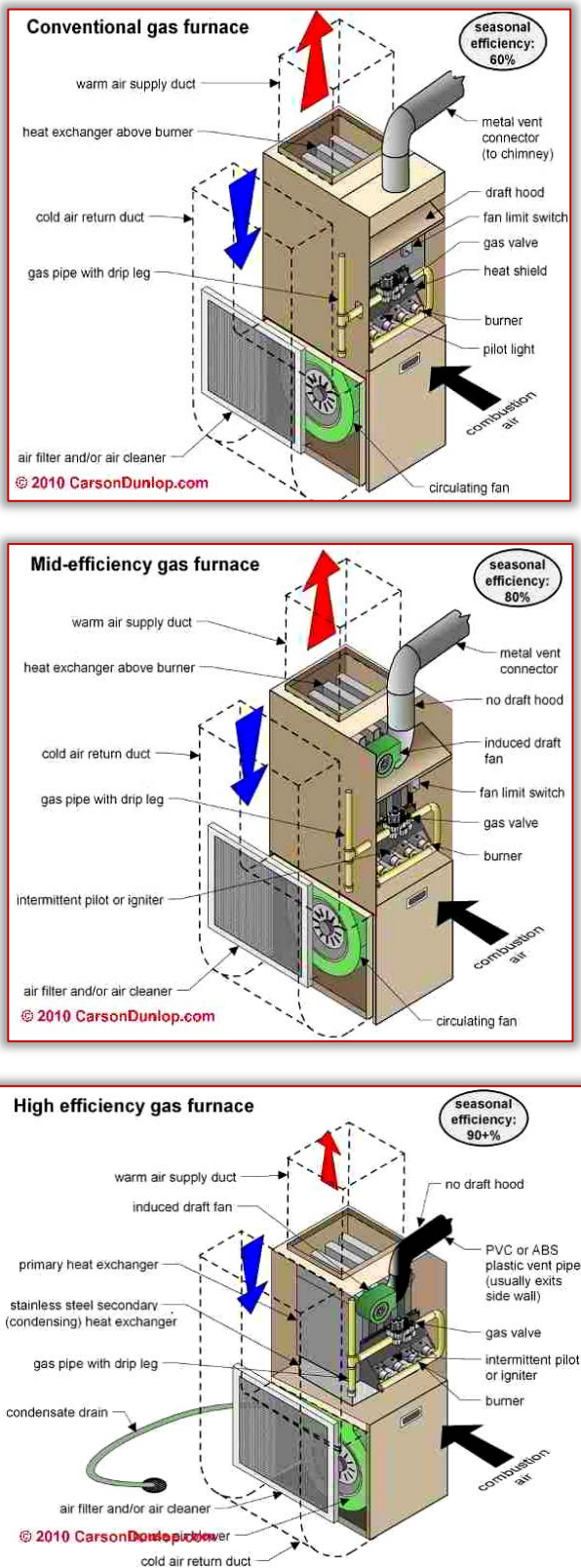


Figure 6 – Constructive structures of forced-air heating systems [8]

High efficiency forced-air heating systems (Figure 5c) are the heating systems to which the in-room air to be heated is circulated through the system by means of a fan/exhauster, taking the energy of the flue gas

through a tubular heat exchanger, similar to that of the mid-efficiency systems. In addition, because during the gas burning process, approx. 12% of the heat energy is taken up by the water vapours in form of latent heat, a secondary heat exchanger is introduced into the system to recover this heat energy by condensing the water vapours from the flue gas stream. In this way, to this type of heating systems the efficiency increases considerably to 90–98% AFUE.

On the basis of these considerations, it is mentioned that the high efficiency forced-air heating systems are called condensing air heating systems, while the mid-efficiency forced-air heating systems are called non-condensing air heating systems.

Figure 6 shows the constructive structures of forced-air heating systems. Thus, in Figure 6 up left, is shown the constructive structure of a conventional air-forced heating system, in Figure 6 up right, is shown the constructive structure of a non-condensing air-forced heating system, and in Figure 6, down, is shown the constructive structure of a condensing air-forced heating system.

At present, in Europe and the United States, the most widely used air heating systems are the condensing and non-condensing air heating systems, which have replaced conventional classic heating systems, with the tendency of imposing the high efficiency condensing air heating systems.

By comparing the condensing and non-condensing air heating systems, it can be argued that condensing air heating systems have the following advantages: much higher efficiency, thereby ensuring a substantially reducing of the long-term operating costs, low flue gas temperature (about 55°C, compared to 180°C for the non-condensing systems), very low heat loss in combustion exhaust and significantly reduced CO₂ emissions. The disadvantages of condensing air heating systems are as follows: higher investment and installation costs, corrosion problems arise because the produced condensate is acidic, high maintenance costs and relatively low reliability [5].

BOILER HEATING SYSTEMS WITH RADIATOR NETWORK

Boiler heating systems with radiator networks (see Figure 7) are commonly used as household heating appliances and have the important advantage of providing in addition the necessary domestic hot water.

Constructively, the structure of a boiler heating systems consist of a boiler, a radiator network and a hot water supply system. At present, two large boiler heating systems are offered on the market, differentiated by the efficiency of the boiler, namely: conventional heating systems fitted with classic boiler and high efficiency heating systems with condensing boiler.

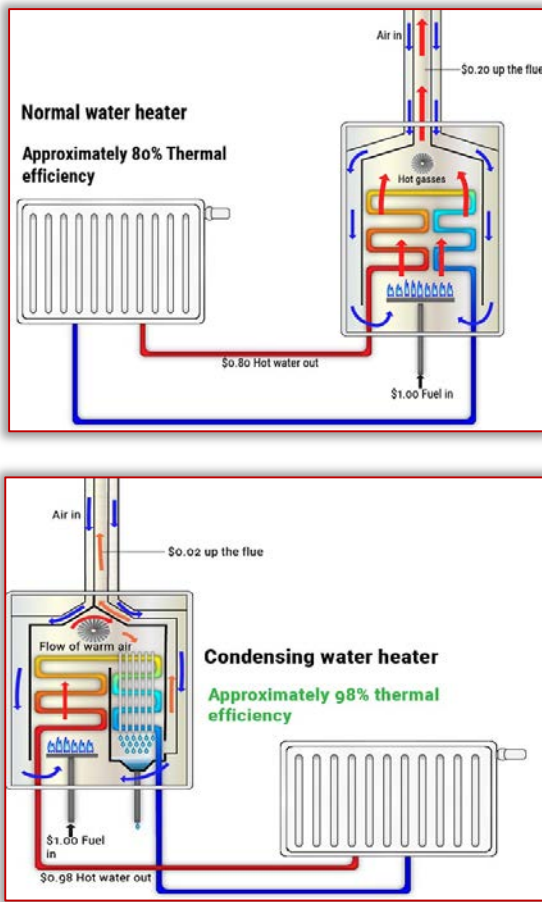


Figure 7 – Principles of heating systems with boilers and radiators network [9]

The fundamental difference between conventional boilers and condensing boilers is that the use the residual heat of the flue gases to preheat the cold return water entering in the boiler. This makes the efficiency of 55–65% AFUE of conventional boilers or 75–78% AFUE of modern non–condensing boilers to increase to 90–99% AFUE in condensing boilers [9].

These outstanding performances of the condensing boilers are mainly achieved by introducing an supplementary heat exchanger, in addition to the heat exchanger for water heating, which transfers the residual heat of the flue gas to return water entering the boiler. The schematic diagram of Figure 8 shows the essential operating differences between a non–condensing boiler and a condensing boiler.

The Figure 9 shows the constructive structure a condensing boiler heating system.

Analyzing comparatively condensing boilers with non–condensing boilers it can be said that the advantages and disadvantages of the condensing boilers are similar to those of the condensing and non–condensing air heating systems. However, it can be mentioned, that the price of high–efficiency boiler systems is at least twice as high as the price of conventional boiler heaters, while the cost of high–efficiency air heating systems is only 30–40% higher than that of a conventional air heating systems [2].

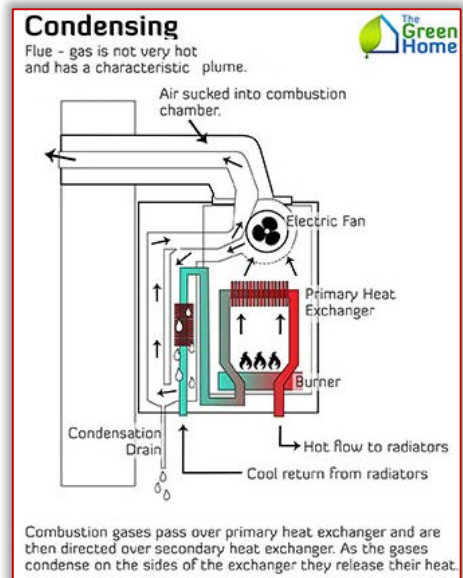
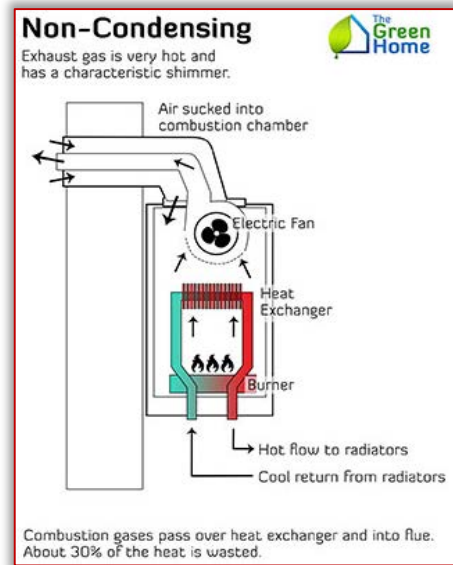


Figure 8 – The essential differences between a non–condensing boiler and a condensing boiler [1]

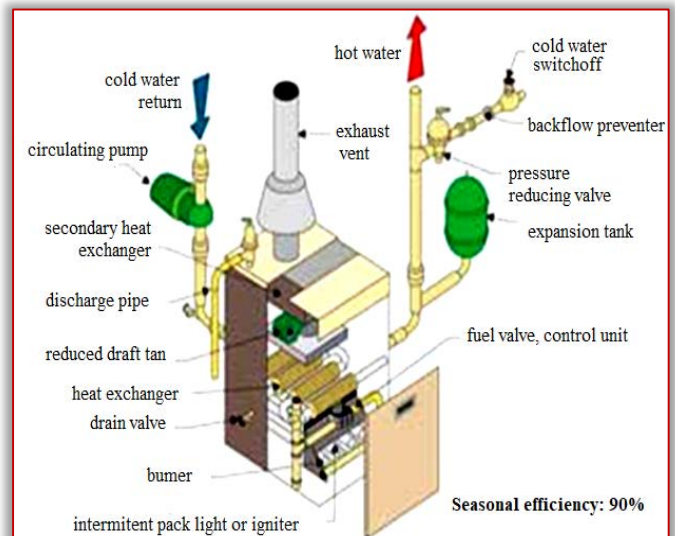


Figure 9 – The constructive structure of a condensing boiler [2]

CONCLUSION

In this paper are presented variants of modern gas heating systems of household, presenting the operating principles, constructive structures and highlighting the benefits of their use in terms of thermal efficiency and in terms of reducing pollutant emissions into the atmosphere. It is can be mentioned that both for the air–heating systems, as well as for the heating systems with the boiler there were created and realized various modern variants with high efficiency, between 90–99% AFUE, which in Europe and the United States tend to increasingly replace conventional gas heating systems.

The problem of introducing modern high efficiency gas heating systems is very important because it constitutes a viable and extremely valuable solutions for ensuring the thermal energy in households in our country rural areas, where natural gas is available.

Note:

This paper is based on the paper presented at ISB–INMA TEH' 2019 International Symposium (Agricultural and Mechanical Engineering), organized by Politehnica University of Bucharest – Faculty of Biotechnical Systems Engineering (ISB), National Institute of Research–Development for Machines and Installations Designed to Agriculture and Food Industry (INMA Bucharest), Romanian Agricultural Mechanical Engineers Society (SIMAR), National Research & Development Institute for Food Bioresources (IBA Bucharest), National Institute for Research and Development in Environmental Protection (INCDPM), Research–Development Institute for Plant Protection (ICDPP), Research and Development Institute for Processing and Marketing of the Horticultural Products (HORTING), Hydraulics and Pneumatics Research Institute (INOE 2000 IHP) and “Food for Life Technological Platform”, in Bucharest, ROMANIA, between 31 October – 1 November, 2019.

References

- [1] ***AGS Heating and Plumbing, (2019), <http://www.agsheating.ie/index.php/gas-plumbing-heating-services-dublin/condensing-explain-3>
- [2] *** American Society of Home Inspectors, (2019), <http://www.ashireporter.org/HomeInspection/Articles/High-Efficiency-Boilers/14731>
- [3] *** EPA Burn Wise, (2019), <https://www.slideshare.net/mheeke/epa-burn-wise>
- [4] *** Furnace Heating System, (2019), <http://romandou.info/furnace-heating-system>
- [5] *** GreenMatch, (2015), <https://www.greenmatch.co.uk/blog/2015/10/condensing-vs-non-condensing-boilers>
- [6] *** GOODMAN, Air Conditioning and Heating, (2019), <https://www.goodmanmfg.com/resources/hvac-learning-center/before-you-buy/is-a-high-efficiency-furnace-right-for-me>
- [7] ***Heating and Air Conditioning St. Louis by Galmiche & Sons, (2019), <https://www.galmicheandsons.com/hvac-blog/what-is-a-high-efficiency-condensing-furnace>

- [8] *** InspectAPedia, Encyclopedia of Building & Environmental Inspection, Testing, Diagnosis, Repair., (2019), https://inspectapedia.com/heat/Condensing_Boilers_Furnaces.php
- [9] ***Ke Kelit, (2019), <https://www.kekelit.co.nz/heat-source-central-heating>
- [10] ***OVO Energy, (2019), <https://www.ovoenergy.com/guides/energy-guides/heating-costsgas-vs-oil-vs-electric-storage-heaters.html>
- [11] *** Word Enery Council, Comparison of Energy System using Life Cyle Assesment (2014), <https://permies.com/wiki/carbon-footprint-heat>



ACTA TECHNICA CORVINIENSIS – Bulletin of Engineering
ISSN: 2067–3809

copyright © University POLITEHNICA Timisoara,
Faculty of Engineering Hunedoara,
5, Revolutiei, 331128, Hunedoara, ROMANIA
<http://acta.fih.upt.ro>

Fascicule 3

[July – September]

t o m e

[2020] XIII

ACTA Technica **CORVINIENSIS**
BULLETIN OF ENGINEERING



ACTA TECHNICA CORVINIENSIS – Bulletin of Engineering
ISSN: 2067-3809
copyright © University POLITEHNICA Timisoara,
Faculty of Engineering Hunedoara,
5, Revolutiei, 331128, Hunedoara, ROMANIA
<http://acta.fih.upt.ro>

¹Iulia GĂGEANU, ¹Petru CÂRDEI, ²Gheorghe VOICU

EXPERIMENTAL RESEARCHES ON THE EVOLUTION OF THE LENGTH OF FIR TREE SAWDUST PELLETS

¹National Institute of Research – Development for Machines and Installations Designed to Agriculture and Food Industry – INMA Bucharest, ROMANIA

²University Politehnica of Bucharest, ROMANIA

Abstract: The paper presents the results obtained from the experimental researches conducted for tracking and monitoring the evolution of the length of fir tree pellets obtained using an experimental single pellet installation. The changes in pellet length represents an important quality parameter for biomass pellets used as biofuels. The evolution of pellet length was monitored for a period of 91 days and the results showed a strong connection between the changes in length or disintegration (rupture) of pellets and some of the input parameters characteristic for the raw material used. The results obtained in this paper offer an understanding on the factors affecting pellet quality and their durability in time.

Keywords: biomass sawdust, compression, pellet length

INTRODUCTION

The evaluation of the performances of the products obtained in a technological process represents an important stage for the appreciation of the applied technology and at the same time, for its improvement or even optimization. In general, in this stage we analyze the quality (output) parameters of the system that models the technological process, depending on the input and command parameters of the same system, (Cardei et al., 2019). The analysis is performed on the experimental data obtained in observations for pellets obtained for each combination of input and control parameters used in the 243 experiments conducted for each of the dies used (straight circular cylindrical dies), 8 and 10 mm diameter die (Gageanu et al., 2019). The observation in time was limited to the measurement of the length of the pellets.

According to the systemic model of the technological process of obtaining pellets from fir tree sawdust, the quality assessment of pellets could be made by following the evolution of four quality parameters in time: the length, the density, the moisture and the volume of the pellets. The fifth parameter of output and quality, the energy consumed per unit mass of the pellets, is a parameter of mechanical and economic character, which is considered in separate optimization calculations. Out of these qualitative parameters, we focused on tracking the behavior of pellet length over time. The density of pellets was examined as a qualitative parameter at when exiting from the working process, as well as moisture and the other qualitative parameters.

Obviously, there are other interesting features from a qualitative point of view: the variation in time and especially with the storage conditions, the calorific power, the external and internal appearance regarding cracks or breakages, etc.

The globalized importance of biofuels has led to the emergence of a huge volume of specialized literature dedicated to their manufacture, conservation and exploitation, (Marian G., 2016; Berkesy et al., 2012). In addition to a specific vocabulary, there has also been dense legislation in the field of biofuel manufacture and exploitation, (Marian G., 2016).

An analysis of quality parameters for pellets used as biofuels is given, for example, in (Berkesy et al., 2012). The quality indicators considered were taken from the standard EN ISO 17225–2. The pellets studied in this article belong to class A1, according to ISO 17225–2, table 1. In (Berkesy et al., 2012), a series of standards were used to analyze the quality parameters: moisture, bulk density, ash, calorific power. The use of European standards on a large scale in the quantitative evaluation of pellets for biofuels are also illustrated in (Marian et al., 2011), where specific quality requirements for pellets from different categories are listed and the authors examine a wide range of pellets with different compositions (energy willow, acacia, straw and mixtures).

A similar approach to the quality problem of biofuels from different biomass sources is presented in (Gaber et al., 2014), where quality assurance systems and quality control measures for these product categories are presented. The role of quality control of raw materials is emphasized in order to obtain superior qualities for the final products. It also addresses a large category of wood chips: fir, beech, birch, etc. The authors give a precise and very dense terminology, whose respect is necessary for facilitating the dialogue between specialists in the current era.

(Smaga et al.) also deal with the description of the qualitative parameters of some biofuels, taking into account in particular the calorific power, the humidity and the sulfur content, as well as the amount of ash

resulting by combustion. Values of these parameters are given for mowed grass, weeds, walnuts, pistachios, miscanthus, Jerusalem artichokes, sawdust, etc.

The relation between the quality of the raw material and the quality of the finished product of biofuels is also addressed by (Gillespie et al., 2013), in the sense of prediction, which we also try to achieve in our researches dedicated to fir wood pellets. Specifications and references to specialized literature on pellet characterization, from the physical point of view (including mechanical qualities) and chemically, but also thermally, are also conducted by (Hernandez et al., 2017). Calculation formulas for some mechanical properties, for the gross calorific value, etc. as well as the statistical qualitative characterization of some batches of pellets, are presented in (Artemio et al., 2018). Besides the technical aspect of pellets manufacturing and their use, the economic aspect is a very important one, a reference work through the concrete data being represented by (Purohit & Chaturvedi, 2016). The profitability of acquiring raw materials, but also the optimum time of storage for sale (therefore having a controlled production), are very important aspects for the production of biofuels from vegetable waste.

A large technical–economic study of wood pellet production technologies was conducted by (Sjoding et al., 2013). In addition, because, in fact, time does not destroy the stored pellets, but the storage and handling conditions (temperature, moisture, pressure, mechanical shocks, etc.), there are works that are especially concerned with the storage phase of the pellet life (Stelte W., 2013).

Directly interested in the production of wood biomass pellets, the producers have a wide range of indications for the production process. These indications, in general, are normal to be compared with the conclusions of experimental results. An interesting source in this regard is (<http://www.lidapelletmill.com/newsshow-Factors-that-affect-the-pellet-quality-219-93-1.html>).

MATERIALS AND METHODS

In order to determine the long–term durability of pellets obtained from the experiments conducted, each pellet sample was allowed to cool and was then individually introduced in a closed bag, the sample number and the values of the control and control parameters being noted. The bags were stored in a single layer in boxes, at a temperature of 20–25 °C, an air moisture of max 75%, and a pressure between 86–106 kPa.

Samples were measured using electronic callipers with a measuring range between 0–100 mm, 0.01 mm resolutions, 0.03 precision, action roller and depth rod.



Figure 1 – Detail during measurements

The measurements were performed over a period of 91 days, performing a measurement every 7 days, thus resulting in a total of 14 measurements for each pellet sample. For the pellets that have broken during the 91 days of performing measurements, the value 0 was recorded beginning with the moment of breakage.



Figure 2 – Examples of broken pellets (in the first day – up, and in the day they broke – down)

RESULTS

— Pellet length variation in time

The variation of the length of the pellets in time, from exiting the formation process (the initial zero time), to the last day of tracking their evolution, is an important parameter to give a global picture of the tendencies of stabilization of the pellets. In figure 3 are presented the evolution time curves for five of the two hundred and forty–three curves in the database.

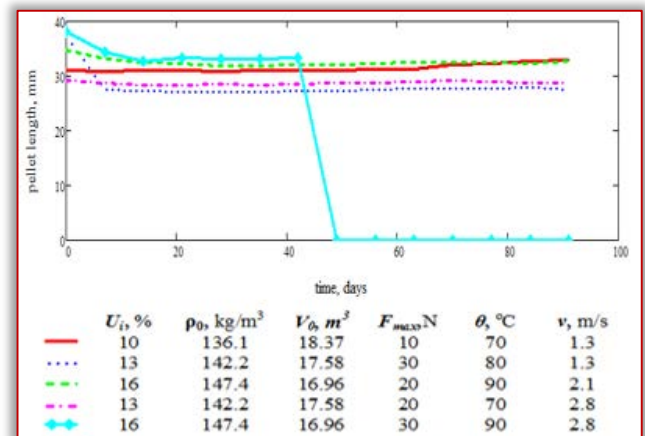


Figure 3 – Variation in time of the length of some pellets whose production data are provided in the caption

It is observed that most curves show a decrease in length (a longitudinal contraction) in the first 10 days, after which some have a weak tendency to decrease or increase towards the end of the tracking period. The curves remain bordered in the range of 25 – 40 mm.

Figure 3 shows a single exception from this behavior, the curve that according to the graph reaches zero length, in the formal sense established by the experimenter for the pellets that disintegrate during the tracking period. As a result, some of the pellets lose their consistency and become unusable.

— **Observation on pellets that disintegrate completely during the tracking period**

In this paragraph, we will try to characterize the causes that lead to the failure of pellets in the post-formation stage that is, after leaving the compression process. Specifically, we try to find the main possible causes for the failure of the pellets (disintegration or irreversible deformations that make the pellets unusable for the proposed purpose).

By applying a simple algorithm for counting the failures, in the batch of pellets from the experiments conducted using the 10 mm diameter die, we found 25 pellets that became unusable during the 91 days during which their behavior was tracked. Comparing to the number of 243 pellets, a failure rate of 10.288% results.

This percentage can be used to estimate the durability of the batch of manufactured pellets (without considering the durability determination in accordance with European norms, leading to an estimated durability value of 89.72%. In general, the durability values for marketable batches of pellets are higher than 96.5%. Considering the experimental production mode and the non-standardized estimation method for durability, we consider that a satisfactory approximation has been made.

Table 1. Repartition of broken pellets in the 91 days after production, on the cases used for obtaining them (according to the input and command parameters used)

Initial moisture, %	10	13	16
Number of broken pellets	1	0	24
Raw material density, kg/m ³	136.1	142.2	147.4
Number of broken pellets	1	0	24
Initial raw material volume, cm ³	16.9	17.58	18.37
Number of broken pellets	24	0	1
Maximum compression force, kN	10	20	30
Number of broken pellets	10	8	7
Temperature, °C	70	80	90
Number of broken pellets	5	9	11
Pelleting speed, mm/s	1.3	2.1	2.8
Number of broken pellets	6	3	16

The analysis of table 1 shows that the moisture of the raw material, its density and volume produce the phenomenon of disintegration of pellets in time. The maximum moisture and density and the minimum volume of raw materials are the most likely causes of pellet disintegration because 24 of the 25 cases of disintegrated pellets were formed under these conditions. The maximum pressing force, the piston advancement speed (pelleting speed) and the die temperature do not seem to greatly influence the behaviour of pellets after they are obtained.

A graphical representation of the occurrence of pellet failures depending on raw material moisture and relative density is given in Figure 4.

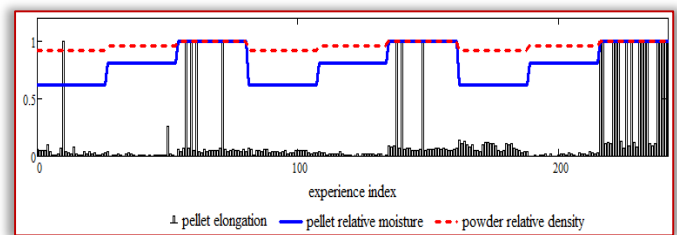


Figure 4 – Elongation variation of pellets obtained depending on raw material moisture and relative density for the 243 experiments conducted

CONCLUSIONS

Tracking the evolution of the physical characteristics of pellets over time is a mandatory test for estimating their quality. These tests have been standardized for several years and include the characterization of mechanical properties, caloric power, moisture, etc. The study whose results are presented in this paper only deals with the evolution in time of one of the dimensions that define the geometry of the pellets obtained from fir tree sawdust.

An important conclusion is that the high moisture of the raw material leads to a high moisture of the pellets, which causes most of the pellets to disintegrate. In the same situation is the density of the raw material. Its growth leads to pellets with higher density, but which can disintegrate more easily.

Another important conclusion is that not the direct time is the one leading to pellet depreciation after production, but the evolution in time of physical storage and transport parameters.

Acknowledgement

This work was supported by a grant of the Romanian Research and Innovation Ministry, through Programme 1 – Development of the national research–development system, subprogramme 1.2 – Institutional performance – Projects for financing excellence in RDI, contract no. 16PFE.

Note:

This paper is based on the paper presented at ISB–INMA TEH' 2019 International Symposium (Agricultural and Mechanical Engineering), organized by Politehnica University of Bucharest – Faculty of Biotechnical Systems Engineering (ISB), National Institute of Research–Development for Machines and Installations Designed to

Agriculture and Food Industry (INMA Bucharest), Romanian Agricultural Mechanical Engineers Society (SIMAR), National Research & Development Institute for Food Bioresources (IBA Bucharest), National Institute for Research and Development in Environmental Protection (INCDPM), Research-Development Institute for Plant Protection (ICDPP), Research and Development Institute for Processing and Marketing of the Horticultural Products (HORTING), Hydraulics and Pneumatics Research Institute (INOE 2000 IHP) and “Food for Life Technological Platform”, in Bucharest, ROMANIA, between 31 October – 1 November, 2019.

References

- [1] Artemio C.P., Maginot N.H., Serafin C.U., Rahim F.P., Guadalupe R.Q.J., Fermin C.M., (2018), Physical, mechanical and energy characterization of wood pellets obtained from three common tropical species. PeerJ 6:e5504; DOI 10.7717/peerj.5504;
- [2] Berkesy L., Begea M., Berkesy C., Crăciun M., Suci L., (2012), Qualitative aspects regarding biomass destined for heating, Ecotera, no. 30, 2012, pp. 64–71
- [3] Cardei P., Gageanu I., Matache M. (2019), Researches on the systemic structuring and statistical modelling of biomass pelleting processes
- [4] Gaber M., Handlos M., Metschina Ch. (2014), Biomass manual. Quality assurance systems and quality control measures, Ik landwirtschaftskammer steiermark, Waldverband, steiermark gmbh, Graz;
- [5] Gageanu I., Cardei P., Matache M., Voicu Gh. (2019), Description of the experimental data of the pelleting process using elementary statistics, Proceedings of the Sixth International Conference “Research People and Actual Tasks on Multidisciplinary Sciences”, 12–15 June 2019, Lozenec, Bulgaria, pp. 436–444;
- [6] Gillespie G.D., Everard C. D., Fagan C.C., McDonell K.P. (2013), Prediction of quality parameters of biomass pellets from proximate and ultimate analysis, Fuel, vol. 111, pp.771–777;
- [7] Hernandez, L.C., Forero, C.A., Sierra, F.E., (2017), Biomass Densification: a Review of the Current State-of-the-Art of the Pellet Market and Analysis of New Research Trends, TECCIENCIA, Vol. 12 No. 23, pp. 81–92
- [8] Marian G., (2016), Solid biofuels, production and properties. Manual for the use of solid biofuel producers., Bons Offices, Chisinau;
- [9] Marian G., Gudima A., Muntean A., Gorobet V, Pavlenco A. (2011), Straw pellets, pros and cons, CZU 662.636.3, State Agrarian University in Moldova;
- [10] Smaga M., Wielgosinski G., Kochanski A., Korczak K. (2018), Biomass as a major component of pellets, Acta Innovations, no. 26, pp. 81–92;
- [11] Purohit P., Chaturvedi V. (2016), Techno-economic Assessment of Biomass Pellets for Power Generation in India, CEEW Working Paper;
- [12] Sjoding D., Kanoa E., Jensen P. (2013), Developing a Wood Pellet/Densified Biomass Industry in Washington State: Opportunities and Challenges Technical Assessment, Washington State University, Extention Energy Program;
- [13] Stelte W. (2012), Guideline: Storage and Handling of Wood Pellets, Report, Danish Technological Institute;
- [14] <http://www.lidapelletmill.com/newsshow-Factors-that-affect-the-pellet-quality-219-93-1.html>



ACTA TECHNICA CORVINIENSIS – Bulletin of Engineering
ISSN: 2067-3809
copyright © University POLITEHNICA Timisoara,
Faculty of Engineering Hunedoara,
5, Revolutiei, 331128, Hunedoara, ROMANIA
<http://acta.fih.upt.ro>

¹Sakshi SINGH, ²Suresh KUMAR

THE TIMES OF CYBER ATTACKS

^{1,2}Department of Computer Science Engineering, AIACTR, Delhi, INDIA

Abstract: Cyber security's importance is on the rise. Our world relies on technologies more than ever before. Government, military, organizations, financial institutions, universities and other businesses collect, process and store a large amount of information on computers. This trend is growing faster every day. As computers become a major source of information, they need to be protected. Every day a new type of cyber-attack came into an act which makes digital data more vulnerable day by day. Cyber security is the practice of ensuring the integrity, confidentiality, and availability (ICA) of information. It requires a broad variety of resources to secure networks, computers, services and data against threats or non-authorized entry, which encompasses best practices for risk control techniques and technologies. In this paper, we will address generations of cyber-attacks, attacker strategy, and biggest cyber -attacks in India. The statistical data of cyber-attacks and security will be discussed. The paper will also clarify emerging concepts of information technology and potential protection developments. In this article, intelligent protection strategies will be clarified to secure information from multiple intruders.

Keywords: confidential data, cyber-attacks, cybercrimes, cyber security, defense, hackers

INTRODUCTION

Cyber protection requires technologies, processes and acts to prevent interference, intrusion or unwanted access to networks, equipment, facilities and documents. This involves data storage. It may also be considered protection in the area of information technology. It is important, as states, businesses, and financial institutions and medical organizations gather, process and store data on computers and other tools without precedent. Sensitive details, be it intellectual possession, financial records, personal information or some other records category that could have adverse impacts on unwanted entry or disclosure, may be a major part of this database.

The corporation that transmits sensitive data through networks and other instruments in the market sense determines the discipline of information management, and the processes that are used to administer and retain it.

As cyber threats are increasing in scale and scope, businesses and institutions, in particular those responsible for safeguarding public protection, health and financial data, have to take action to secure their confidential details for company and workers. Cybercrime is one of the world's largest and one of the biggest risks to any organization.

The impact on society is reflected in the numbers. Cyber protection firms estimate the worldwide expense of cybercrime to \$6 trillion by 2021 [1]. This reflects the largest global capital transition in history, threatens opportunities for creativity and production and would be more lucrative than the entire international trade in all big illegal substances.

The cost estimates of damage are based on historical statistics of cybercrime including recent year-over-year growth, a dramatic rise in the hostile nation-state and gangs-hacking activities, and a greater

cyber-attack surface by 2021. Cybercrimes involve harm, devastation, burglary, stealing of profitability, intellectual property, burglary of personal and financial data, embezzlement, fraud, normal-term post-attack intrusion, forensic analysis, repair and erase hacked and reputational abuse.

India, with over 560 million internet users, ranks just behind China, is the second largest online platform in the world. According to Internet and Mobile Association of India (IAMAI) [1,2], more than 600 million internet users are projected in India by 2021. In 2015 just 17% of Indians were able to use the internet. There were 483 million internet users in India in 2018. In 2023, 666.4 million internet users will be registered, according to the study [3]. It will lift the figure. Because of its untapped potential, India is the world's second largest online sector. The bulk of internet users in India are cell phones internet users who allow the most practical alternatives to the costly hardware that desktops and networks require. As of 2016, India's mobile Internet usage figures is 320.57 million and Indian Internet users estimated 492.68 million by 2022. 390.9 million users were able to navigate the internet via cell phone in 2018. The number will hit 500.9 million internet users in 2023 [3]. This amount is anticipated.

The paper is structured as follows: Section II covers the annual statistical data about cyber-attacks and the expenses spent on them. Section III defines various cyber-attack generations with examples over the last few decades. Section IV explains the biggest cyber-attacks that took place in India. Section V explains how cybercrimes flourish in future and estimated investment on them. Section VI describes how future technologies should be developed with inbuilt security. Section VII suggests some smart security solutions that will help to tackle future

cybercrimes and economic losses done by them to the nation. Section VIII describes the conclusion.

LITERATURE REVIEW

Any significant violation of information security will collapse and destroy the credibility of an entire organization. Cybersecurity risks are not just a problem of major corporations, such as banks, software firms, and state departments, but also the obligation of any other citizen involved with their records. The rate of cyber-crimes is increasing day by day and therefore the analysis of information security statistics and patterns in past years is necessary for us to understand the diabolistic and illegal forms in which data abuses arise and take steps to be secured.

» 2017

For cybercrimes, 2017 was a high year. The number of cyber-safe accidents has almost doubled from 2016 according to the Online Confidence Alliance [4]. This huge spike, from approximately 82,000 accidents in 2016 to approximately 160,000 in 2017, has been credited in the "2017 Cyber Report" [5]. The eye-catching figures of cybercrime in 2017 were further helped by high-profile ransomware attacks like WannaCry and NotPetya. The estimated expense of a violation was \$3,62 million in 2017, according to the Ponemon Institute and IBM's 2017 "Expense of Data Breaching Report" [6].

The most troubling evidence cited in this study were that, with the implementation of public management practices such as patching apps and performing phishing instruction, 93% of accidents may have been stopped. Although 52% of infringements culminated in "real hacking," 15% were induced by lack of safety devices, 11% were triggered by inadequate internal danger control and 8% by phishing, respectively [5].

» 2018

The biggest DDoS attack ever reported was endured by GitHub [7] in 2018. The assault culminated in 1.3 terabits of GitHub traffic for a second. A team of security experts from Security Research Labs took to the Hack in the Box security conference to reveal their project: two years in the reverse engineering phase of the operating systems of Android phones, which showed that some handset makers withhold security fixes from users.

With fines of up to 20 million [8] or up to 4% of the annual worldwide turnover for those companies caught mishandling user data, GDPR promised to usher in a new age for the processing of personal data.

» 2019

In 2019, the cyber technology industry grew by 8.7% and the money invested on data management, rules and data privacy law enforcement tools was \$124 billion (Weekly computer) [9,10]. Around 94% of

targeted emails use the payload or malware root to add harmful data. 91% of cyber-attacks start with a "spear-phishing" text, an increasingly popular type of phishing that allows more precise and personal use of knowledge regarding a target (Be4Know) [11]. Billions of dollars of damage is triggered by cybercrimes, as per analysis by Juniper, the figure reached \$2 trillion by 2019 [12].

CYBER-ATTACK GENERATIONS

- # The Ist Generation: In the late 1980s, hackers mounted virus attacks on standalone PCs, typically propagated via disks. The affected private users and companies contributed to the creation of anti-virus (AV) products focused on signature info. Examples of first-generation assaults are:
 - » Elk Cloner (1982): the first computer virus in the world.
 - » Brain (1986): booting attack.
- # The IInd Generation: In the mid-1990s, quickly expanding worm attacks emerged straight from the omnipresent Internet, which forced businesses to build a firewall at the infrastructure's periphery to keep the bad people out. Examples of IInd generation attacks include:
 - » The Morris Worm (1988): One of the first computer worms, leading to the US first felony conviction under the Computer Fraud and Abuse Act.
 - » Melissa (1999): A mass mailing macro virus.
- # The IIIrd Generation: During the first years of the new century, criminals began exploiting bugs during software that could impact the businesses exploiting them. That is also about the period when the purpose of the offender switches from appreciation to remuneration. Initially, the botnet was used, particularly for the spam distribution. This attack generation contributes to the creation of IDS systems, which soon incorporated correction capability and became Intrusion prevention systems. Signatures were already based on IDS / IPS. Examples of assaults from the third century include:
 - » ILOVEYOU (2000): A worm infecting tens of millions of Windows machines.
 - » SQL Slammer (2003): Denial of service on 75,000 hosts.
- # The IV Generation: During the early part of the last decade, there were no signs of the emergence in targeted attacks. During a conversation on the absence of clear evidence regarding weapons of mass destruction, citizens were prompted to follow the word "hidden unknowns" invented by then American defence secretary Donald Rumsfeld. Malware application consistency increases and the

first rootkit starts to pop up. Types of threats from the fourth generation include:

- » Stuxnet (2005-10): State-sponsored development, targeting SCADA systems in critical infrastructure, including the Iranian nuclear program.
 - » The Target Breach (2013): Not a virus or worm, but a targeted attack on the clothing retailer. The details of 40- 70 million credit cards stolen, 110 million people's personal information breached.
 - » The DYN Attack (2016): Not a virus or worm, but a massive distributed denial of service (DDOS) attack on the major DNS provider.
- # The Vth Generation: A wide-ranging mega-attacks funded by the government began in 2017 so that several businesses may execute them. Cybercrime has its internet and escrow networks. There's a busy null-day market. Examples of assaults from the Vth wave are:
- » WannaCry (2017): Major ransomware attack affecting 200,000 computers across 150 countries.
 - » Petya and NotPetya (2016-17): Variance of ransomware used against machines across Europe.

BIGGEST CYBER-ATTACKS IN INDIA

≡ SIM Swap Fraud

In August 2018, Navi Mumbai arrested two men for cybercrime. They participated in fraudulent practices with regard to the money transfer from the accounts of a variety of people, unlawfully collecting details on the SIM card. This fraudsters obtained details from citizens and prevented the usage of false documents on their SIM cards. They had to transfer four Indian Rupees out of different accounts successfully. We also went to access a few corporations' profiles [13].

≡ Cyber Attack on Cosmos Bank

The Cosmos Bank's Pune branch was targeted in August 2018 by a brazen cyber assault, which saw the loss of almost 94 Crores rupees. By breaching the Cosmos Bank's computer, In Hong Kong, Hackers cleaned out and passed the funds to a trust. The lawsuit was put before Cosmos Bank with a Pune court of cyber assault.

Hackers hacked into the bank's ATM network and stole many details from owners of visas and debit cards. The assault did not go against the cohesive banking solution of Cosmos Bank. The deposits and balance sheets remain unchanged and have little impact on the financial statements of the owner. The switching process was built to function as the node of communication between the payment portals and the bank's central banking solution.

The malware assault on the switching network created many false alerts that verified many external demands for visas and debit cards. In 28 nations, there were 14,000 sales, more than 450 tickets. 400 cards and 2,800 transactions were used at the state

level. This was the first malware assault to break up the link between the payment gateway and the Indian bank [13].

≡ ATM System Hacked in Kolkata

Fraudsters pirated in July 2018 and wiped off almost 20 lakh rupees of different banks' accounts on ATM servers at Canara Branch. More than 50 people were killed and over 300 ATM customers were accused of providing account data in India.

Hackers used skimming machine on ATMs to capture debit cardholders' data to execute a minimum purchase of INR 10,000 and an INR cap of 40,000. Two people who collaborated for a foreign group used skimming operations to collect bank data were arrested on 5 August 2018 in New Delhi [13].

≡ Websites Hacked

Between April 2017 and January 2018, more than 22,000 websites have been compromised. The Indian Cyber Emergency Response Team's figures indicate that over 493 pages, including 114 government-owned websites, were compromised with malware spreads.

The attacks were to gather information about users on the network infrastructure and device data [13].

FUTURE OF CYBER-ATTACKS

The cybercrime industry has risen with the economic growth of at least \$1.5 trillion annually. It is projected to hit \$300 billion by 2024 for the cyber-security sector.

In 2021, it is estimated that 70% of all purchases for crypto-currencies would be for illicit activity. Cyber-crime costs are estimated at 6 trillion dollars globally by 2021 for corporations and organizations. The loss reported being 20 billion dollars in Ransomware worldwide. An organization's total cybercriminal loss is projected to be 13 million dollars annually [14,15]. In the near-decade, there are a variety of big cyber threats.

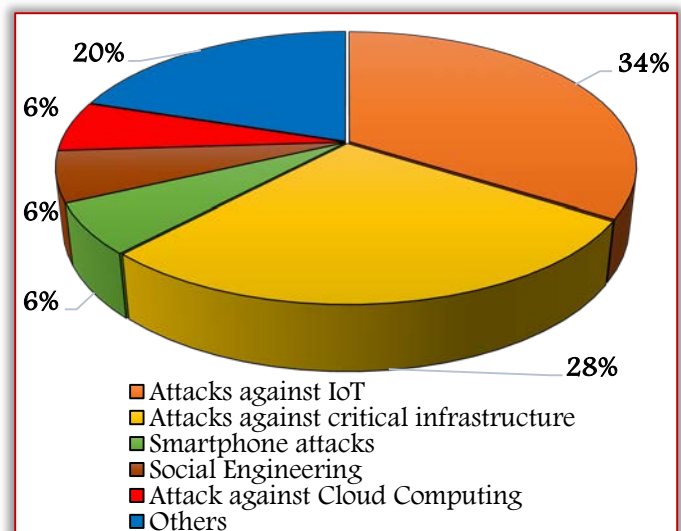


Figure 1. Major cyber-attacks by 2025

Attacks against IoT would be 34%. A maximum of 98% of IoT computer traffic is authenticated, exposing network data that is sensitive and private. 28% of sensitive infrastructure threats and 20% of devices would be targeted [14]. Using a smartphone and other media, attackers attempted to pass on confidential details to citizens. Such assaults are recognized as virtual infrastructure and will carry 6% of assaults in the future.

There are also ongoing advances in cloud infrastructure, which have several bugs that cyber attackers or malicious insiders may use.

DESIGNING FUTURE TECHNOLOGY WITH SECURITY

The design of future technologies must provide security. Adding protection afterwards is not enough or viable anymore. Innovation in defence will have more efficient and insightful approaches to face threats. For cooperation and advancement of adoptions, networks and safety requirements must be available. Throughout the design and implementation of their goods, security and protection suppliers must be assured. To avoid compromise and render safety clear to the user, goods and services must be solid. For both parties and systems in the digital world, encryption needs to secure data while it is accessible or used.

organizations. The cybercriminals and hacktivists will try to utilize cyber-technology to transmit their message and raise revenue and violence in the tribunal.

To order to contend with cyber threats and to secure records, particular information defence platforms and technology would need to be more mature and more complex. Defence systems need to be linked in such a way that they may function in real-time. Human will not be able to handle all information attacks so in future the dependency on AI will increase. Also, there is a need to cultivate next generation and advanced cyber experts who will know how to drive and develop those systems. We need a stronger protection approach to secure our infrastructure, technologies and knowledge.

For now, hacking has become the number one cause of the intrusion, accompanied by ransomware, intruder and outsider agents and unintentional violations. The number of attacks which lead to device failure and data loss continues to grow. Tougher privacy and other legislation related to cybercrime will be implemented to determine and prosecute criminals and avoid cyber-attacks.

This is claimed that what hackers and criminals would be seeking would decide the future of information protection. And it will mostly be the health-related information and also the wealth like credit card and other financial information. For these regions, data defence should then be stronger because the information is the most valuable commodity.

The security departments have traditionally been focused on on-site applications but now Azure, cloud with AWS, and SaaS software can be included, causing other critical details to be compromised or breached. Capable computer frameworks must be implemented that can track, identify and handle cyber-attacks and deter them in real-time.

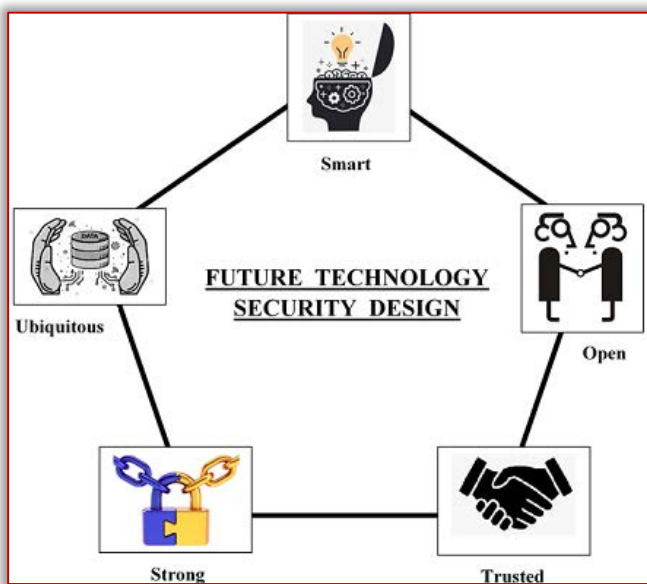


Figure 2. Future Technology security design

SMART SECURITY SOLUTIONS

Today, all our critical systems are interconnected and computer-driven. The digital and Internet of Things (IoT), Artificial Intelligence (AI) and Big Data and cloud storage etc. would be more relevant to day-to-day tasks and decisions. Such tools have a significant impact on their degree of weakness, relations and complexities.

In the future, cyber-attack based technology for Protection and Offensive can be built by

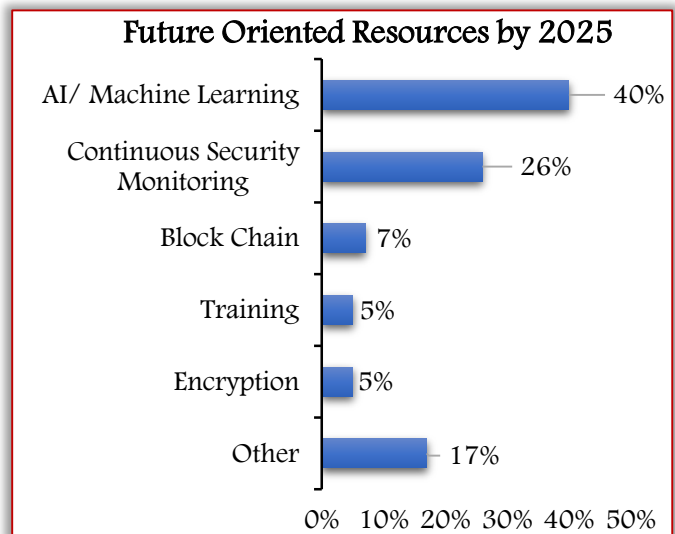


Figure 3. Resources that are used for security purpose in future [14]

CONCLUSION

The defense of our classified documents, personally identifying details (PIIs), secure health records (PHIs), financial knowledge, intellectual property, technology and computer networks against intrusion and undermining attempts by offenders and opponents is an essential part in cybersecurity.

Cyber threats from every organization's level can arrive. It was becoming really important to warn people about social manipulation schemes like phishing and more sophisticated computer security threats, such as ransomware (such as WannaCry, NotPetya). In this article, we have discussed the drastic increase in the number of internet users in the last few years with the biggest cyber-attacks that took place in India.

The generations of various cyber-attacks give us a clear view of how cyber-attacks technologies upgraded from the very beginning. We have also discussed how cyber-attacks will affect us economically in the upcoming future and counter technologies to overcome all those cyber-attacks. Smart security solutions are suggested to tackle them.

References

- [1] Indian Internet 2019, <https://cms.iamai.in/Content/ResearchPapers/d3654bcc-002f-4fc7-ab39-e1fbeb00005d.pdf>
- [2] <https://economictimes.indiatimes.com/tech/internet/india-has-second-highest-number-of-internet-users-after-china-report/articleshow/71311705.cms?from=mdr>
- [3] Cyber Security, https://niti.gov.in/sites/default/files/201907/CyberSecurityConclaveAtVigyanBhavanDelhi_1.pdf
- [4] <https://www.internetsociety.org/news/press-releases/2019/internet-societys-online-trust-alliance-reports-cyber-incidents-cost-45b-in-2018/>
- [5] 2017 Cybercrime Report, <https://cybersecurityventures.com/2015-wp/wp-content/uploads/2017/10/2017-Cybercrime-Report.pdf>
- [6] 2017 Cost of Data Breach Study, <https://www.ibm.com/downloads/cas/ZYKLN2E3>
- [7] <https://www.wired.com/story/github-ddos-memcached/>
- [8] <https://privacy.net/cybersecurity-statistics/>
- [9] <https://www.gartner.com/en/newsroom/press-releases/2018-08-15-gartner-forecasts-worldwide-information-security-spending-to-exceed-124-billion-in-2019>
- [10] <https://www.computerweekly.com/>
- [11] <https://www.knowbe4.com/>
- [12] <https://www.juniperresearch.com/document-library/white-papers/the-future-of-cybercrime-white-paper>
- [13] <https://www.kratikal.com/blog/5-biggest-cyber-attacks-in-india/>
- [14] <https://www.radarservices.com/resources/study2025/>

- [15] CYBERSECURITY FUTURES 2025 INSIGHTS AND FINDINGS, <https://cltc.berkeley.edu/wp-content/uploads/2019/02/Cybersecurity-Futures-2025-Insights-and-Findings.pdf>



ACTA TECHNICA CORVINIENSIS – Bulletin of Engineering
ISSN: 2067-3809
copyright © University POLITEHNICA Timisoara,
Faculty of Engineering Hunedoara,
5, Revolutiei, 331128, Hunedoara, ROMANIA
<http://acta.fih.upt.ro>

Fascicule 3

[July – September]

t o m e

[2020] XIII

ACTA Technica CORVINIENSIS
BULLETIN OF ENGINEERING



ACTA TECHNICA CORVINIENSIS – Bulletin of Engineering
ISSN: 2067-3809
copyright © University POLITEHNICA Timisoara,
Faculty of Engineering Hunedoara,
5, Revolutiei, 331128, Hunedoara, ROMANIA
<http://acta.fih.upt.ro>

MANUSCRIPT PREPARATION – GENERAL GUIDELINES

Manuscripts submitted for consideration to **ACTA TECHNICA CORVINIENSIS – Bulletin of Engineering** must conform to the following requirements that will facilitate preparation of the article for publication. These instructions are written in a form that satisfies all of the formatting requirements for the author manuscript. Please use them as a template in preparing your manuscript. Authors must take special care to follow these instructions concerning margins.

INVITATION

We are looking forward to a fruitful collaboration and we welcome you to publish in our **ACTA TECHNICA CORVINIENSIS – Bulletin of Engineering**. You are invited to contribute review or research papers as well as opinion in the fields of science and technology including engineering. We accept contributions (full papers) in the fields of applied sciences and technology including all branches of engineering and management.

ACTA TECHNICA CORVINIENSIS – Bulletin of Engineering publishes invited review papers covering the full spectrum of engineering and management. The reviews, both experimental and theoretical, provide general background information as well as a critical assessment on topics in a state of flux. We are primarily interested in those contributions which bring new insights, and papers will be selected on the basis of the importance of the new knowledge they provide.

Submission of a paper implies that the work described has not been published previously (except in the form of an abstract or as part of a published lecture or academic thesis) that it is not under consideration for publication elsewhere. It is not accepted to submit materials which in any way violate copyrights of third persons or law rights. An author is fully responsible ethically and legally for breaking given conditions or misleading the Editor or the Publisher.

ACTA TECHNICA CORVINIENSIS – Bulletin of Engineering is an international and interdisciplinary journal which reports on scientific and technical contributions. Every year, in four online issues (**fascicules 1–4**), **ACTA TECHNICA CORVINIENSIS – Bulletin of Engineering [e-ISSN: 2067-3809]** publishes a series of reviews covering the most exciting and developing areas of engineering. Each issue contains papers reviewed by international researchers who are experts in their fields. The result is a journal that gives the scientists and engineers the opportunity to keep informed of all the current developments in their own, and related, areas of research, ensuring the new ideas across an increasingly the interdisciplinary field. Topical reviews in materials science and engineering, each including:

- surveys of work accomplished to date
- current trends in research and applications
- future prospects.

As an open-access journal **ACTA TECHNICA CORVINIENSIS – Bulletin of Engineering** will serve the

whole engineering research community, offering a stimulating combination of the following:

- Research Papers – concise, high impact original research articles,
- Scientific Papers – concise, high impact original theoretical articles,
- Perspectives – commissioned commentaries highlighting the impact and wider implications of research appearing in the journal.

ACTA TECHNICA CORVINIENSIS – Bulletin of Engineering encourages the submission of comments on papers published particularly in our journal. The journal publishes articles focused on topics of current interest within the scope of the journal and coordinated by invited guest editors. Interested authors are invited to contact one of the Editors for further details.

BASIC MANUSCRIPT REQUIREMENTS

The basic instructions and manuscript requirements are simple:

- Manuscript shall be formatted for an A4 size page.
- The all margins of page (top, bottom, left, and right) shall be 20 mm.
- The text shall have both the left and right margins justified.
- Single-spaced text, tables, and references, written with 11 or 12-point Georgia or Times New Roman typeface.
- No Line numbering on any pages and no page numbers.
- Manuscript length must not exceed 15 pages (including text and references).
- Number of the figures and tables combined must not exceed 20.
- Manuscripts that exceed these guidelines will be subject to reductions in length.

The original of the technical paper will be sent through e-mail as attached document (*.doc, Windows 95 or higher). Manuscripts should be submitted to e-mail: redactie@fih.upt.ro, with mention “for **ACTA TECHNICA CORVINIENSIS**”.

STRUCTURE

The manuscript should be organized in the following order: Title of the paper, Authors' names and affiliation, Abstract, Key Words, Introduction, Body of the paper (in sequential headings), Discussion & Results, Conclusion or Concluding Remarks, Acknowledgements (where applicable), References, and Appendices (where applicable).

THE TITLE

The title is centered on the page and is CAPITALIZED AND SET IN BOLDFACE (font size 14 pt). It should adequately describe the content of the paper. An abbreviated title of less than 60 characters (including spaces) should also be suggested. Maximum length of title: 20 words.

AUTHOR'S NAME AND AFFILIATION

The author's name(s) follows the title and is also centered on the page (font size 11 pt). A blank line is required between the title and the author's name(s). Last names should be spelled out in full and succeeded by author's initials. The author's affiliation (in font size 11 pt) is provided below. Phone and fax numbers do not appear.

ABSTRACT

State the paper's purpose, methods or procedures presentation, new results, and conclusions are presented. A nonmathematical abstract, not exceeding 200 words, is required for all papers. It should be an abbreviated, accurate presentation of the contents of the paper. It should contain sufficient information to enable readers to decide whether they should obtain and read the entire paper. Do not cite references in the abstract.

KEY WORDS

The author should provide a list of three to five key words that clearly describe the subject matter of the paper.

TEXT LAYOUT

The manuscript must be typed single spacing. Use extra line spacing between equations, illustrations, figures and tables. The body of the text should be prepared using Georgia or Times New Roman. The font size used for preparation of the manuscript must be 11 or 12 points. The first paragraph following a heading should not be indented. The following paragraphs must be indented 10 mm. Note that there is no line spacing between paragraphs unless a subheading is used. Symbols for physical quantities in the text should be written in italics. Conclude the text with a summary or conclusion section. Spell out all initials, acronyms, or abbreviations (not units of measure) at first use. Put the initials or abbreviation in parentheses after the spelled-out version. The manuscript must be writing in the third person (“the author concludes...”).

FIGURES AND TABLES

Figures (diagrams and photographs) should be numbered consecutively using Arabic numbers. They should be placed in the text soon after the point where they are referenced. Figures should be centered in a column and should have a figure caption placed underneath. Captions should be centered in the column, in the format “Figure 1” and are in upper and lower case letters.

When referring to a figure in the body of the text, the abbreviation “Figure” is used. Illustrations must be submitted in digital format, with a good resolution.

Table captions appear centered above the table in upper and lower case letters.

When referring to a table in the text, “Table” with the proper number is used. Captions should be centered in the column, in the format “Table 1” and are in upper and lower case letters. Tables are numbered consecutively and independently of any figures. All figures and tables must be incorporated into the text.

EQUATIONS & MATHEMATICAL EXPRESSIONS

Place equations on separate lines, centered, and numbered in parentheses at the right margin. Equation numbers should appear in parentheses and be numbered consecutively. All equation numbers must appear on the right-hand side of the equation and should be referred to within the text.

CONCLUSIONS

A conclusion section must be included and should indicate clearly the advantages, limitations and possible applications of the paper. Discuss about future work.

Acknowledgements

An acknowledgement section may be presented after the conclusion, if desired. Individuals or units other than authors who were of direct help in the work could be acknowledged by a brief statement following the text. The acknowledgment should give essential credits, but its length should be kept to a minimum; word count should be <100 words.

References

References should be listed together at the end of the paper in alphabetical order by author's surname. List of references indent 10 mm from the second line of each references. Personal communications and unpublished data are not acceptable references.

- *Journal Papers*: Surname 1, Initials; Surname 2, Initials and Surname 3, Initials: Title, Journal Name, volume (number), pages, year.
- *Books*: Surname 1, Initials and Surname 2, Initials: Title, Edition (if existent), Place of publication, Publisher, year.
- *Proceedings Papers*: Surname 1, Initials; Surname 2, Initials and Surname 3, Initials: Paper title, Proceedings title, pages, year.



ACTA TECHNICA CORVINIENSIS – Bulletin of Engineering
ISSN: 2067-3809

copyright © University POLITEHNICA Timisoara,
Faculty of Engineering Hunedoara,
5, Revolutiei, 331128, Hunedoara, ROMANIA

<http://acta.fih.upt.ro>

INDEXES & DATABASES

We are very pleased to inform that our international scientific journal **ACTA TECHNICA CORVINIENSIS – Bulletin of Engineering** completed its 12 years of publication successfully [2008–2019, Tome I–XII].

In a very short period the **ACTA TECHNICA CORVINIENSIS – Bulletin of Engineering** has acquired global presence and scholars from all over the world have taken it with great enthusiasm.

We are extremely grateful and heartily acknowledge the kind of support and encouragement from all contributors and all collaborators!

ACTA TECHNICA CORVINIENSIS – Bulletin of Engineering is accredited and ranked in the “B+” CATEGORY Journal by **CNCIS – The National University Research Council’s Classification of Romanian Journals**, position no. 940 (<http://cncis.gov.ro/>).

ACTA TECHNICA CORVINIENSIS – Bulletin of Engineering is a part of the **ROAD, the Directory of Open Access scholarly Resources** (<http://road.issn.org/>).

ACTA TECHNICA CORVINIENSIS – Bulletin of Engineering is also indexed in the digital libraries of the following world’s universities and research centers:

WorldCat – the world’s largest library catalog

<https://www.worldcat.org/>

National Library of Australia

<http://trove.nla.gov.au/>

University Library of Regensburg – GIGA German Institute of Global and Area Studies

<http://opac.giga-hamburg.de/ezb/>

Simon Fraser University – Electronic Journals Library

<http://cufts2.lib.sfu.ca/>

University of Wisconsin – Madison Libraries

<http://library.wisc.edu/>

University of Toronto Libraries

<http://search.library.utoronto.ca/>

The University of Queensland

<https://www.library.uq.edu.au/>

The New York Public Library

<http://nypl.bibliocommons.com/>

State Library of New South Wales

<http://library.sl.nsw.gov.au/>

University of Alberta Libraries – University of Alberta

<http://www.library.ualberta.ca/>

The University of Hong Kong Libraries

<http://sunzi.lib.hku.hk/>

The University Library – The University of California

<http://harvest.lib.ucdavis.edu/>

ACTA TECHNICA CORVINIENSIS – Bulletin of Engineering is indexed, abstracted and covered in the world-known bibliographical databases and directories including:

INDEX COPERNICUS – JOURNAL MASTER LIST

<http://journals.indexcopernicus.com/>

GENAMICS/JOURNALSEEK Database

<http://journalseek.net/>

DOAJ – Directory of Open Access Journals

<http://www.doaj.org/>

EVISA Database

<http://www.speciation.net/>

CHEMICAL ABSTRACTS SERVICE (CAS)

<http://www.cas.org/>

EBSCO Publishing

<http://www.ebscohost.com/>

GOOGLE SCHOLAR

<http://scholar.google.com>

SCIRUS – Elsevier

<http://www.scirus.com/>

ULRICHWeb – Global serials directory

<http://ulrichweb.serialssolutions.com>

getCITED

<http://www.getcited.org>

BASE – Bielefeld Academic Search Engine

<http://www.base-search.net>

Electronic Journals Library

<http://rzblx1.uni-regensburg.de>

Open J-Gate

<http://www.openj-gate.com>

ProQUEST Research Library

<http://www.proquest.com>

Directory of Research Journals Indexing

<http://www.drji.org/>

Directory Indexing of International Research Journals

<http://www.citefactor.org/>



ACTA TECHNICA CORVINIENSIS – Bulletin of Engineering

ISSN: 2067-3809

copyright © University POLITEHNICA Timisoara,

Faculty of Engineering Hunedoara,

5, Revolutiei, 331128, Hunedoara, ROMANIA

<http://acta.fih.upt.ro>



copyright © University POLITEHNICA Timisoara,
Faculty of Engineering Hunedoara,
5, Revolutiei, 331128, Hunedoara, ROMANIA

<http://acta.fih.upt.ro>